

Mécanismes de corrosion d'aciers revêtus par AlSi(ZnMg)

Cyril Nicard

▶ **To cite this version:**

Cyril Nicard. Mécanismes de corrosion d'aciers revêtus par AlSi(ZnMg). Autre. Université Paris sciences et lettres, 2018. Français. NNT : 2018PSLEC006 . tel-02535302

HAL Id: tel-02535302
https://pastel.hal.science/tel-02535302

Submitted on 7 Apr 2020

HAL is a multi-disciplinary open access archive for the deposit and dissemination of scientific research documents, whether they are published or not. The documents may come from teaching and research institutions in France or abroad, or from public or private research centers.

L'archive ouverte pluridisciplinaire **HAL**, est destinée au dépôt et à la diffusion de documents scientifiques de niveau recherche, publiés ou non, émanant des établissements d'enseignement et de recherche français ou étrangers, des laboratoires publics ou privés.

PSL UNIVERSITÉ PARIS

THÈSE DE DOCTORAT
DE L'UNIVERSITÉ PSL

Préparée à L'Ecole Nationale Supérieure de Chimie de Paris (ENSCP)

Mécanismes de corrosion d'aciers revêtus par AlSi(ZnMg)

Soutenue par
Cyril NICARD
Le 04 10 2018

Ecole doctorale n° 388
Ecole doctorale Chimie Physique et Chimie Analytique de Paris

Spécialité
Chimie Physique

Composition du jury :

Armelle, RINGUEDE IRCP, ENSCP, France	*Président*
Bernard, NORMAND INSA de Lyon, France	*Rapporteur*
Tomáš, PROSEK University of Chemistry and Technology of Prague, République Tchèque	*Rapporteur*
Christine, BLANC CIRIMAT–ENSIACET– INP, France	*Examinateur*
Christian, ALLELY ArcelorMittal Research, France	*Examinateur*
Polina, VOLOVITCH IRCP, ENSCP, France	*Directeur de thèse*

Chimie Paris ParisTech | PSL

Corrosion mechanisms of AlSi(ZnMg) coated steel

« La maturité de l'homme est d'avoir retrouvé le sérieux qu'on avait au jeu quand on était enfant. »

La Horde du Contrevent (2004)

A.Damasio

Acknowledgement – Remerciements

Ces trois années de thèse m'auront vu grandir humainement et scientifiquement. Rétrospectivement, je me rends compte que je dois cette réussite à un très grand nombre de personnes dont je ne pourrai pas faire la liste exhaustive. Je vais cependant profiter de ces quelques lignes pour remercier ceux que j'ai pu côtoyer.

Tout d'abord je remercie mes encadrants directs : Polina Volovitch, ma directrice de thèse et Christian Allély, mon responsable industriel, pour la bienveillance de leur supervision, de leur conseil et de leur enseignement tout au long de ces trois ans. Ce fut un plaisir de présenter le résultat de mes travaux aux membres de mon jury, Bernard Normand, Tomáš Prosek, Christine Blanc et Armelle Ringuede que je remercie pour l'intérêt qu'ils ont porté dans l'examen et l'évaluation de mon manuscrit. Merci également à Jan Stoulil et Vaclav Sefl pour leur importante contribution dans le second chapitre.

Je remercie Michel Babbit, Danielle Quentin, Jacques André Petitjean, Natalie Fournier et Julie Lanoé pour l'opportunité qu'ils m'ont donnée de travailler au sein du centre de recherche d'ArcelorMittal à Maizières-lès-Metz. Je remercie tout particulièrement Astrid Grégoire, Aymeric Corbel et Charifa Riani pour leur assistance tout au long de mon travail dans l'équipe mais aussi tous les autres membres du service « Surface and Coating » (et la liste est longue) pour leur gentillesse, la bonne ambiance et la richesse des discussions. Merci aussi a toutes ces personnes avec qui j'ai pu sympathiser hors du service : Arthur, Aude, Audrey, Coralie, Grégory(s), Hervé, Jan , Joris, Kevin, Lou, Nico(s), Mallory, Maxime, Rémi, Romain(s), Sandra et Vincent, mais aussi tous les stagiaires qui étaient autant de rencontres formidables.

La majeure partie de mon temps s'est effectuée à Metz et la vie y a été agréable grâce à toutes ces personnes. J'ai aussi passé une partie de mon temps au sein de l'institut de recherche de Chimie-Paritech. Je remercie à l'occasion Michel Mortier, Hervé Willaime, Michel Cassir et Armelle Ringede pour la chance qui m'a été donnée d'intégrer l'équipe Interface Electrochimie et Energie. Un énorme merci à Aurélie, Armelle, Thomas et Virginie pour leur aide et leur soutien au moment de la rédaction. Merci à Abdelilah, Alina, Amandine, Andrey, Diego, Dmitri, Ersan, Haitam, Kevin, Manelle, Marie-Hélène, Mélisande, Moussa, Oumaïma, Simon, Slava, Valérie, Xuijie pour les moments de rire. Bien que je n'aie pas souvent été au laboratoire pendant la thèse, vous m'avez fait me sentir comme partie intégrante de l'équipe.

Merci à Perrine, ma sœur presque siamoise de bureau et de thèse avec qui j'ai beaucoup, beaucoup ri et c'était pour le mieux. Merci Audrey et Benjamin, pour tous ces bons moments

passés autour d'une crêpe et/ou d'un cidre. Merci Junsoo et Thomas, les meilleurs des meilleurs. Merci Matthieu, mon coach spirituel et physique, pour ces séances de musculation et ces parties endiablées d'Armada.

Merci aux autres amis avec qui j'ai pu partager des moments ressourçants ou qui sont venu mettre l'ambiance à Metz et mettre à mal mes stocks. Merci au Vivian's et à son personnel d'avoir rempli leur rôle à merveille. Merci aussi à Thomas et Julie pour m'avoir aidé dans mes relectures bien qu'à l'autre bout du monde.

Merci à mes grands-parents qui m'ont approvisionné par la poste ou directement, je leur dois un moral directement proportionnel au contenu de mon frigo. Merci à mes parents et plus généralement à ma famille qui m'ont soutenu et cru en moi. Merci à mon frère et ma sœur qui ont toujours joué avec moi de bon cœur. Merci Véronique pour m'avoir accueilli, et merci Mathilde, mon cœur, pour tout. Pour finir je te remercie toi qui as lu, lis ou liras tout ou partie de ce document.

Merci à tous pour cette aventure humaine et scientifique,

Cyril Nicard

Décembre 2018

Table of Content

Table of Content ix
List of Tables xiii
List of Figures xv
List of acronyms and abbreviations xxi
Introduction ..... - 1 -
Context of the PhD ..... - 1 -
Structure of the PhD ..... - 3 -
Chapter I – State of the art ..... - 9 -
1 Aluminum based coatings: process and microstructure ..... - 9 -
2 Effect of alloying on Al microstructure ..... - 12 -
3 Corrosion of Al - based materials ..... - 17 -
4 Effect of precipitates and intermetallic phases on Al reactivity ..... - 24 -
5 Atmospheric corrosion of Al and Zn based coatings for steel and role of corrosion products ..... - 29 -
6 Layered double hydroxides ..... - 34 -
7 Conclusions of Chapter 1 ..... - 36 -
Chapter II – Experimental ..... - 47 -
1 Materials ..... - 47 -
2 Accelerated corrosion tests ..... - 48 -
3 Corrosion product removal and dissolution rates determination ..... - 49 -
4 Phases identification ..... - 50 -
5 Inductive Coupled Plasma Optical Emission Spectrometry (ICP-OES) and Atomic Emission SpectroElectroChemistry (AESEC) ..... - 51 -
6 Electrochemical experiments ..... - 52 -
Chapter III - Effect of Zn and Mg alloying on microstructure and anticorrosion mechanisms of AlSi based coatings for high strength steel ..... - 61 -
Abstract ..... - 61 -
1 Introduction ..... - 62 -
2 Experimental ..... - 63 -
3 Results ..... - 66 -
4 Discussion ..... - 78 -
5 Conclusions ..... - 81 -
Acknowledgements ..... - 82 -

Chapter IV – Electrochemical reactivity of Al(Zn), Al_3FeSi_2 and Mg_2Si phases and its consequence for corrosion mechanisms of AlSi(Zn,Mg) coated steel ..... - 91 -
Abstract ..... - 91 -
1 Introduction ..... - 92 -
2 Experimental ..... - 93 -
3 Results ..... - 97 -
4 Discussion ..... - 107 -
5 Conclusions ..... - 109 -
Acknowledgements ..... - 110 -
Graphical Abstract ..... - 111 -
Chapter V – Role of corrosion products in corrosion mechanisms of AlSi(ZnMg) coated high strength steel ..... - 119 -
Abstract ..... - 119 -
1 Introduction ..... - 120 -
2 Experimental ..... - 121 -
3 Results ..... - 124 -
4 Discussion ..... - 133 -
5 Conclusions ..... - 135 -
Acknowledgements ..... - 136 -
Graphical Abstract ..... - 137 -
Chapter VI – Conclusion and Perspectives ..... - 143 -
Perspectives ..... - 149 -
Appendix 153
1 Schematic representation of hot dip process for high strength steel 153
2 Samples positions (a) and recommended evolution of temperature, humidity and salt spray periods (b) during accelerated corrosion test VDA 233-102. 154
3 Principles of AESEC 155
4 Homemade electrochemical cell used in galvanic coupling experiments for pure phases 156
5 Binary phases diagrams Al-Zn, Al-Si, and sections of ternary phase diagrams Al-Si-Mg and Al-Si-Zn 157
6 X-ray diffraction spectra of the synthetic pure phases 159
7 XPS spectra of the reference metallic Si phase and formed by heat treatment SiO_2 160
8 Solubility diagram of AlZnMg 160
RESUME 165
Introduction 165

1 Etat de l’art 167

2 Expérimental..... 170

3 L’effet de l’ajout de Zn et de Mg sur la microstructure et les mécanismes de corrosion des aciers haute résistance revêtus par AlSi. 173

4 Couplage galvanique et dissolution sélective des phases pures dans les revêtements anticorrosion AlSi(ZnMg) pour les aciers haute résistance..... 177

5 Effet protecteur des produits de corrosion des revêtements anticorrosion AlSi(ZnMg) pour les aciers haute résistance. 180

6 Conclusions et perspectives..... 184

List of Tables

Chapter I
Table 1 : Composition of wrought Al alloys (from [13,14]) ..... - 13 -
Table 2 : Mass percentage of β-(Zn) phase depending on Zn content. (from [16]) ..... - 13 -
Table 3 : Preferentially formed phases for highly alloyed Al [13-18] ..... - 16 -
Table 4 : Identified phases in Al-based coatings (stch = stoichiometric quantity) [18-24] ..... - 17 -
Table 5 : Free enthalpies of formation for aluminum products (in water) ..... - 18 -
Table 6 : Typical composition of activators for Al anodes (data from [16,18,-]) ..... - 22 -
Table 7 : Corrosion potential of selected intermetallics in ASTM G69 solution. ..... - 24 -
Table 8 : Phases expected in AlSiZnMg coatings and their corrosion potential in ASTM G69 electrolyte (data from [13,29,48]) ..... - 24 -
Chapter II
Table 1 : Phases weight composition and suppliers. ..... - 48 -
Chapter III
Table 1 : Summary information about studied AlSi(Zn,Mg) coatings on high strength steel. Types of material, number of tested compositions, composition range, number of cycles in accelerated corrosion test VDA 233-102 at which the red rust appears for the first time and measured corrosion potential in 0.1 M NaCl aqueous solution with initial pH 7 are presented. ..... - 63 -
Table 2 : Main phases detected in AlSi(Zn,Mg) coatings: labels used for Figs. 1–3, chemical compositions and expected corrosion potentials, E, in unbuffered 0.1 M NaCl aqueous solution. ..... - 66 -
Table 3 : Mass balance for different coatings: total (T), soluble (S) and insoluble (I) weight loss after 6 cycles of the accelerated test. T values were obtained from weight measurements before the test and after the test and corrosion products removal. The error in T values because of the dissolution of uncorroded coating in nitric acid can reach 1.51 $g.m^{-2}$. S and I were calculated from the ICP-OES analysis of the lixiviate collected under each sample during corrosion test and the ICP-OES analysis of the solution obtained by the removal of insoluble corrosion products in nitric acid (see text for details). ..... - 71 -
Table 4 : Enrichment or depletion of soluble and insoluble corrosion products by Al, Si, Zn and Mg after 12 cycles of VDA 233-102 test of unscratched AlSi(Zn,Mg) coatings. The coefficients of selectivity, K_{sel} (X), were calculated as a fraction of the element X (X = Al, Mg, Si or Zn) present in the lsolution (water or nitric acid for soluble and insoluble components respectively), normalized by the content of X in the coating. The values of $K_{sel}(X) > 1$ are in bold, these values indicate that the corresponding product (soluble or insoluble) is enriched by the element X, while the values of $K_{sel}(X) < 1$ correspond to the depletion of X. $K_{sel}(X) = 1$ for a congruent oxidation or dissolution of X. ..... - 73 -
Table 5 : Corrosion products identified on AlSi(Zn,Mg) coated steel by XRD and Raman spectroscopy. ..... - 75 -
Table 6 : Chemical composition determined from EDS analysis of platelets shown in Fig. 9f. ..... - 77 -
Chapter IV
Table 1 : Phases weight and molar compositions and suppliers. ..... - 94 -
Table 2 : Corrosion potential of the studied phases (Ecorr / V vs. SCE) measured in different electrolytes as indicated and color code associated with each phase for schematic presentation of the phases. ..... - 98 -
Table 3 : Galvanic current ($\mu A.cm^{-2}$) measured on Al and Al(Zn) phases when coupled with different Si, Fe or Mg containg phases in 0.172 M NaCl aqueous solution (initial pH 7). ..... - 100 -
Chapter V
Table 1 : Potential and current evolution on AlSiZn and AlSiZnMg coated steels during electrochemical tests described in Fig. 4. ..... - 127 -
Table 2 : . Corrosion products identified by XRD. ..... - 129 -
RESUME
Tableau 1 : Phases préférentiellement formées en fonction des éléments en présence (Al > 60 %m.) 169

Tableau 2 : Phases identifiées dans des revêtements à base d'Aluminium (stch = stœchiométrie) 169

List of Figures

Chapter I
Figure 1 : Commercialized hot dip coating for steel (Numbers in wt. %) (from [1,2]) - 9 -
Figure 2 : Hot dip process and coating system drawing (from [3]) - 10 -
Figure 3 : Cross-sectional SEM views of aluminized steel sheets which were hot dipped in pure Al (A) and AlSi9 (B) at 800 °C. Intermetallic phase between coating and steel. (from [6]) - 11 -
Figure 4 : SEM images and EDS analysis of present phase for an Al15Zn62Mg17Si6 alloy. (from [21]) - 15 -
Figure 5 : E-pH diagram for pure Al at 25 ˚C in aqueous solution (adapted from Pourbaix 1974). The lines (a) and (b) correspond to water stability and its decomposed product. (from []) - 18 -
Figure 6 : Illustration of commonly accepted corrosion mechanisms for Al alloys (from [28]) - 20 -
Figure 7 : Alloying elements influence on the dissolution potential of aluminum alloys in ASTM G69. (from [29]) - 20 -
Figure 8 : Anode efficiency and operating potentials of the Al-Zn alloys with different Zn content. (from [16]) Legend: ♦ potential and ● efficiency - 21 -
Figure 9: Polarization curves of Zn, Al and Zn_2Mg at pH ranging from 7 to 10 in NaCl 5wt. % (from [43]). - 25 -
Figure 10 : Schematic mechanism of local corrosion around a Si particle (from [46]). - 26 -
Figure 11 : Localized corrosion mechanisms of Mg_2Si in Al and AlMg matrix (from [50]). - 27 -
Figure 12 : SEM observation and potentiodynamic polarization curves in 0.1 M NaCl solution of Aluminum-Silicon coating different layers obtained by the electrochemical micro-cell positioned in the GDOES sputter craters (from [51]). - 28 -
Figure 13 : SEM image and EDS spectra in the corroded zone at the interface between the coating and the substrate (the area of analysis is indicated). The sample was corroded in accelerated tests. Gold (Au) a 20 nm gold layer was sputtered on the surface before SEM observation in order to avoid the charging of the non-conductive corrosion product surface (from [12]). - 30 -
Figure 14 : XRD spectra of different corrosion products collected from the surface of the corroded coatings after 168 h exposure to NSS test according toEN ISO 9227: (a) Galvalume® coating, (b) G–0.5Mg coating, (c) G–1.5Mg coating, (d) G–2.5Mg coating (from [19]). - 31 -
Figure 15 : Morphologies of different corroded coating surfaces after dissolving corrosion products with 10wt. % ammonium persulphate solution: (a) Galvalume coating, (b) G– 0.5Mg coating, (c) G–1.5Mg coating and (d) G–2.5Mg coating (from [19]). etc. - 32 -
Figure 16 : Typical morphology (SEM–FEG) of ZnO electrodeposited from the solution in absence (a) and in presence (b) Mg^{2+} in comparison with the morphology of ZnO formed by the corrosion of Zn–Mg coating after 70 cycles of ECC1 test (c) (from [54)]. - 33 -
Figure 17 : Graph of permeability test on different corrosion products. (from [60]) - 35 -
Chapter II
Figure 1 : Temperature and humidity variation during a one-week single cycle of the VDA 233-102 test. (from [7]) - 49 -
Figure 2 : Local Electrochemical Impedance Spectroscopy (LEIS) explanatory diagram. - 53 -
Figure 3 : Scanning Vibrating Electrode Technique (SVET) explanatory diagram. - 54 -
Chapter III
Figure 1 : Typical X-ray diffraction spectra of AlSi, AlSiZn and AlSiZnMg coated steels. The identified phases and related labels are listed in Tab. 2. - 66 -
Figure 2 : Typical secondary electron images and corresponding EDS elemental maps of cross sections and surfaces of the (a) AlSi, (b) AlSiZn, (c) AlSiZnMg coated steels with high Si content. The proposed phase attribution is shown using the phase labels listed in Table 2. - 67 -
Figure 3 : Phases distribution in AlSiZnMg coated steel with low Si content and Mg to Si weight ratio (a) Mg:Si = 0.5, and (b) Mg:Si = 1. The phase attribution is shown using the labels listed in Tab. 2. - 68 -

Figure 4 : Electrochemical behaviour of studied coatings in unbuffered 1 wt. % NaCl solution with initial pH 7. a) Open circuit potential (E) evolution vs time for AlSi, AlSiZn and AlSiZnMg coated steels as indicated. b)–c) Cathodic and anodic polarization curves (log current (J) vs potential E) for AlSi (curve 1), AlSiZn (curve 2) and AlSiZnMg (curves 3,4) coated steels. The polarization curves 1–3 were recorded after the open circuit potential stabilization for all phases (1 h of immersion). For comparison the polarization curve 4 shows the initial behaviour of AlSiZnMg coating before the potential stabilization (after 10 min of immersion). Polarization directions are indicated by arrows. ..... - 69 -
Figure 5 : Typical surface appearance of AlSi, AlSiZn and AlSiZnMg coated steels before (initial) and after several cycles of accelerated corrosion test VDA 233-102 (as indicated)..... - 70 -
Figure 6 : Evolution of the quantity of soluble Al, Si, Zn and Mg in the solution collected with cycling in accelerated corrosion test VDA 233-102 for (a) AlSi, (b) AlSiZn and (c) AlSiZnMg coatings. For each chemical element the total dissolved mass is normalized by the sample surface area, msol / g.m^{-2}. ..... - 72 -
Figure 7 : (a) X-ray diffraction spectra and (b–c) Raman spectra of AlSiZn and AlSiZnMg coatings after 12 cycles of accelerated corrosion test VDA 233-102. Raman spectra recorded in the scratch (b) and on the coating (c–d) are shown. The identified phases and related labels are listed in Tables 2 and 5. ..... - 74 -
Figure 8 : EDS maps showing corrosion products distribution after 12 cycles of the VDA 233-102 test in the cross sections of unscratched (a) AlSi, (b) AlSiZn and (c) AlSiZnMg coated steels with high Si content. O distribution permits to distinguish corrosion products from non-corroded areas while Al, Si and Mg distributions help to identify the phases. General view and more resolved images are shown. ..... - 76 -
Figure 9 : Distribution of corrosion products near the scratch of (a, c, e) AlSiZn and (b, d, f) AlSiZnMg coated steels after 6 cycles of VDA 233-102 test. General top view of the scratch (a, b) and the morphology of corrosion products inside the scratch (c, d) are shown from the top by secondary electron images, the element distribution in the cross section is shown using EDS mapping (c, d). ..... - 77 -
Figure 10 : Schematic representation of proposed corrosion and protection mechanisms in (a) AlSiZn and (b) AlSiZnMg coated steel in the presence of the defect going up to the steel. Step 1. Coating dissolution and sacrificial effect. For AlSiZn two types of mirogalvanic coupling are proposed - “sacrificial” coupling protecting steel and “lost” current used in micro galvanic coupling with Si because Si potential (60.5 V vs. SCE) is close to potential of steel and cathodic versus AlZn. Step 2. Precipitation (and partial modification) of corrosion products due to pH increase and drying. Step 3. Dissolution of Zn and Al containing corrosion products from AlSiZn at advanced stages of corrosion because of continuous pH increase. This step is absent when corrosion products contain Mg^{2+} because of their high pH stability (for instance $Mg(OH)_2$ formation in place of dissolution of LDH resulting in a skin effect). As a result, Mg is expected to extend both, the coating life (and hence a sacrificial protection) and the barrier effect of corrosion products in the scratch. ..... - 81 -
Chapter IV
Figure 1 : Typical polarization curves of (a) Al, Fe, Al(Zn) solid solution, and (b) Mg_2Si, SiO_2, Si, Al_3FeSi_2 in NaCl 0,172 M (1 wt. %) aqueous solution at pH 7. ..... - 99 -
Figure 2 : (a) Open circuit potential of pure aluminum in NaCl 0.172 M or $ZnCl_2$ 0.086 M aqueous solution at pH 5 to 7 (adjusted with NaOH 1 M aqueous solution). (b) Simulated predominant Al/Zn containing species formed in an aqueous solution with 0.172 M NaCl , 0.086 M $ZnCl_2$, 0.001 M $AlCl_3$ (Hydra Medusa). Smk = simonkolleite.- 100 -
Figure 3 : Evolution of the potentials measured in coupling experiments between the substrate steel and the phases relevant for the AlSi(Zn,Mg) coating. Coupled phases: (a) Fe-Al, (b) Fe-Al(Zn32), (c) Si-Fe and (d) Al_3FeSi_2-Fe in 0.172 M NaCl aqueous solution. Coupling tests consisted of 6 h cycles, each cycle consisted of 30 minutes of the OCP measurement on two uncoupled phases followed by 5 hours and 30 minutes of galvanic coupling). .... - 101 -
Figure 4 : Evolution of the potentials measured on phases relevant for intrinsic microgalvanic coupling in AlSi(Zn,Mg) coating during coupling tests. Coupled phases: (a) Si-Al, (b) Si-Al(Zn32), (c) Al_3FeSi_2-Al, (d) Al_3FeSi_2-Al(Zn32), (e) Mg_2Si-Al and (f) Mg_2Si Al(Zn32) in 0.172 M NaCl aqueous solution. Coupling tests consisted of 6 h cycles, each cycle consisted of 30 minutes of the OCP measurement on two uncoupled phases followed by 5 hours and 30 minuts of galvanic coupling). ..... - 102 -
Figure 5 : ATR spectra of uncorroded and corroded Mg_2Si. ..... - 103 -

Figure 6 : Evolution of potential measured on 2 phases during coupling tests for (a) SiO2-Al and (b) SiO2-Al(Zn32) in NaCl 0.172 M aqueous solution. (c) Galvanic current of Si containing phases and Al or Al(Zn32) in NaCl 0.172 M aqueous solution. ..... - 104 -
Figure 7 : Calculated from AESEC data elemental dissolution currents J_x (X=Al, Si, Mg and Zn as indicated) for dissolution of (a) Al(Zn32), (b) Mg_2Si, (c) Zn_2Mg in 0.172 M NaCl aqueous solution as a function of the imposed current J_e=100, 200, 500 and 1000 µA.cm^{-2}. ..... - 105 -
Figure 8 : Effect of pH on the elemental dissolution currents Jx (x=Al, Zn, Mg, and Si) for (a) Al(Zn32), (b) Mg_2Si, (c) Zn_2Mg dissolving inn 0.172 M NaCl aqueous solution with different pH under imposed anodic current of 500 µA.cm^{-2}. ..... - 107 -
Figure 9 : Microstructural scheme of (a) AlSi, (b) AlSiZn and (c) AlSiZnMg with color scale depending on phase potential in NaCl 0.172 M aqueous solution. Color scale is described in Tab. 2. ..... - 108 -
Figure 10 : (a) Phases sorted by corrosion potential in NaCl 1 wt. 1 % aqueous solution from Si (-0,170 V vs. SCE) to Mg_2Si (-1,35 V vs. SCE). (b) Microstructural scheme of AlSi, AlSiZn and AlSiZnMg with color scale. (c) Galvanic coupling potential evolution of Al-Si, Al(Zn32)-Si, Al-Mg_2Si, Al(Zn)-Mg_2Si, SiO_2-Al and SiO_2-Al(Zn) in NaCl 1 wt. 1 % aqueous solution. ..... - 111 -

Chapter V

Figure 1 : Typical example of in-situ optical images of immersed cut edges of (a) AlSi, (b) AlSiZn, (c) AlSiZnMg after 48h immersion in 1 wt. % NaCl aqueous solution at initial pH 7. ..... - 124 -
Figure 2 : Secondary Electron Images of (a,b) AlSiZn and (c,d) AlSiZnMg coatings cut edges after 48h immersion in 1 wt. % NaCl aqueous solution at initial pH 7. Images (a,c) show general appearance of the cut edges before and after corrosion while (b,d) illustrate the morphology of corrosion products formed on the steel (in the center of the cut edge). Zones corresponding to the resin (zone 0), coating (zone 1) and the intermetallic layer (zone 2) are schematically limited by dash lines. ..... - 125 -
Figure 3 : EDS Spectra (normalized on oxygen peak) of corrosion products detected on cut edges, the collation of PC1-2 is shown in Fig. 2 and the location of PC 3-5 is shown in Fig,10. Considering elemental composition, some corrosion products are proposed. ..... - 126 -
Figure 4 : (a) Potential and (b) current evolution at OCP and under cathodic polarization in 1 wt. % NaCl ..... - 126 -
Figure 5 : Secondary Electron mages of (a,b,c) AlSiZn and (d,e,f) AlSiZnMg during electrochemical sequence described in figure 4. (a, d) are before the test, (b, e) at the end of stage II (7 h) and (c, f) at the end of stage III (19 h)..... - 128 -
Figure 6 : XRD spectra for AlSi, AlSiZn, AlSiZnMg and AlSiMg coated steel after the complete electrochemical sequence (Cu) Ka. The peak identification is shown using the labels listed in Tab. 2. ..... - 129 -
Figure 7 : Impedance modulus as a function of applied frequency for (b) AlSiZn (c) AlSiZnMg at different stage of the electrochemical sequence described in fig. 4. ..... - 130 -
Figure 8 : Admittance cartography of (a) AlSiZn (b) AlSiZnMg during electrochemical sequences presented in Fig. 7. (a,b) are taken at stage I, III and VI. ..... - 131 -
Figure 9 : SVET cartography of (a) AlSi, (b)AlSiZn and (c) AlSiZnMg scratched coating at different times in NaCl 100 mg.L^{-1}. ..... - 132 -
Figure 10 : Secondary electron images and corresponding EDS elemental of (a,b) AlSiZn, (c,d) AlSiZnMg scratched coated steels surface. (a,b) are located at scratch right edges while (b,d) are focused in the scratch (on substrate steel). ..... - 133 -
Figure 11 : (a) Typical cut edges appearance of AlSi, AlSiZn, AlSiZnMg coatings after 48h immersion in 1 wt. % NaCl aqueous solution at initial pH7. (b) Secondary Electron Images of AlSiZn and AlSiZnMg coatings cut edges after 48h immersion in 1 wt. % NaCl aqueous solution at initial pH7. 0: Resin; 1: Coating; 2: Intermetallic. ..... - 137 -

Chapter VI

Figure 1 : Elemental distribution obtained from EDS maps showing corrosion product distribution after 12 cycles of VDA 233-102 test in the cross sections of unscratched (a) AlSi, (b) AlSiZn and (c) AlSiZnMg coated steels with high Si content. O distribution permits to distinguish corrosion products from non-corroded areas while Al, Si and Mg distributions help to identify the phases. General view and more resolved images are shown. ..... - 144 -

Figure 2 : (a) Phases ranked by corrosion potential in 1 wt. % NaCl aqueous solution from Si (-0,170 V vs. SCE) to Mg_2Si (-1,35 V vs. SCE). (b) Schematic phase distribution in the coating microstructure for AlSi, AlSiZn and AlSiZnMg with the color scale indicating relative corrosion potential – more red color indicates more anodic behavior. (c) Evolution of galvanic coupling potentials for Si containing phases coupled with Al or Al(Zn32) in 1 wt. % NaCl aqueous solution which explains the benefits of Mg alloying. ..... - 146 -
Figure 3 : Schematic representation of proposed corrosion and protection mechanisms in (a) AlSiZn and (b) AlSiZnMg coated steel in the presence of the defect going up to the steel. Step 1. Coating dissolution and sacrificial effect. For AlSiZn two types of mirogalvanic coupling are proposed - “sacrificial” coupling protecting steel and “lost” current used in micro galvanic coupling with Si because Si potential (60.5 V vs. SCE) is close to potential of steel and cathodic versus AlZn. Step 2. Precipitation (and partial modification) of corrosion products due to pH increase and drying. Step 3. Dissolution of Zn and Al containing corrosion products from AlSiZn at advanced stages of corrosion because of continuous pH increase. This step is absent when corrosion products contain Mg2+ because of their high pH stability (for instance Mg(OH)2 formation in place of dissolution of LDH resulting in a skin effect). As a result, Mg is expected to extend both, the coating life (and hence a sacrificial protection) and the barrier effect of corrosion products in the scratch. ..... - 147 -
Figure 4 : SVET cartography of (a) AlSi, (b) AlSiZn and (c) AlSiZnMg scratched coating at different times of immersion in 100 $mg.L^{-1}$ NaCl solution. ..... - 148 -

RESUME

Figure 1 : Revêtements anticorrosion à base d’aluminium (Al-based) ou de zinc (Zn-based) utilisés dans l’industrie (Compositions données en pourcentage massique) 168
Figure 2 : Electrochimie des revêtements étudiés dans une solution aqueuse de NaCl 1 % massique (pH initial 7). a) Evolution du potentiel en circuit ouvert (E) en fonction du temps pour les aciers revêtus par AlSi, AlSiZn et AlSiZnMg. b) Courbes de polarisation cathodique et anodique (courant logarithmique I en fonction du potentiel E) d’acier revêtus par AlSi (courbe 1), AlSiZn (courbe 2) et AlSiZnMg (courbes 3,4) AlSiZnMg après 1 h d'immersion (courbes 1-3) à 10 min d'immersion (courbe 4). Le sens de la polarisation est indiqué par des flèches. 174
Figure 3 : Cartes EDS montrant la distribution des produits de corrosion après 12 cycles de test VDA 233-102 dans les tranches d’aciers revêtus par (a) AlSi, (b) AlSiZn et (c) AlSiZnMg. 175
Figure 4 : Distribution des produits de corrosion à proximité de la rayure réalisée sur des aciers revêtus par (a, c, e) AlSiZn et (b, d, f) AlSiZnMg après 6 cycles de test VDA 233-102. La vue générale de dessus de la rayure et la morphologie des produits de corrosion à l'intérieur de la rayure sont montrées par imagerie d'électrons secondaires, la distribution des éléments dans la tranche est montrée en ajoutant la cartographie élémentaire en EDS..... 176
Figure 5 : Courbes de polarisation de (a) solution solide Al (Zn), Al, Fe et (b) Mg2Si, SiO2, Si, Al3FeSi2 dans une solution aqueuse de NaCl 0,172 M (1 % massique). 178
Figure 6 (a) Potentiel en circuit ouvert de l'aluminium pur en fonction du temps dans une solution aqueuse de NaCl 0,172 M ou $ZnCl_2$ 0,086 M à pH 5 à 7 (ajusté avec une solution aqueuse de NaOH 1 M). (b) Espèce prédominante simulée contenant Al / Zn 179
Figure 7 : Potentiels libres de phases pures pendant les essais de couplage pour (a) SiO_2-Al et (b) SiO_2-Al (Zn32) dans une solution aqueuse de NaCl 0,172 M. (c) Courant de couplage entre les phases contenant du silicium et Al ou Al (Zn32) dans une solution aqueuse de NaCl 0,172 M. 180
Figure 8 : Les images électroniques secondaires d’arrêtes coupées d’aciers revêtus d’ (a) AlSiZn et (b) AlSiZnMg après 48h d'immersion dans une solution aqueuse NaCl 1 % massique à pH initial 7. 0: résine; 1: Revêtement; 2: Intermétallique. 181
Figure 9 : Cartographie par électrode vibrante en continu d’aciers revêtus par (a) AlSi (b) AlSiZn et (c) AlSiZnMg (rayés) dans NaCl 100 $mg.L^{-1}$. 182
Figure 10 : Imagerie d'électrons secondaires et élémentaires EDS correspondant pour des aciers revêtus par (a) AlSiZn, (b) AlSiZnMg (rayés). 1: À l'intérieur de la rayure; 2: En dehors de la rayure. 183
Figure 11 : (a) Phases triées par potentiel de corrosion dans une solution aqueuse de NaCl 1 % massique. De Si en vert clair (-0,170 V vs. SCE) à Mg_2Si en violet (-1,35 V vs. SCE). (b) Schéma des microstructures de AlSi, AlSiZn et

AlSiZnMg avec échelle de couleur. (c) Courant de couplage galvanique entre Si et Al ou Al(Zn32) dans une solution de NaCl 1 % massique. 185
Figure 12 : Représentation schématique des mécanismes de corrosion et de protection proposés dans le cas d'aciers revêtus par (a) AlSiZn et (b) AlSiZnMg en présence du défaut allant jusqu'à l'acier. 186
Figure 13 : (a) Aspect des arêtes de coupe typiques des revêtements AlSi, AlSiZn, AlSiZnMg après 48h d'immersion dans une solution aqueuse de NaCl 1 % en masse à pH initial 7. (b) Imagerie en électrons secondaires de bord coupés d'aciers revêtus par AlSiZn et AlSiZnMg après 48h d'immersion dans une solution aqueuse de NaCl 1 % en masse à pH initial 7. 0: résine; 1: Revêtement; 2: Intermétallique. 187

List of acronyms and abbreviations

Abbreviation:	Meaning:
AESEC	Atomic Emission SpectroElectroChemistry
AlSi	Aluminum based coating with Si content up to 9 wt. %
ASTM G69	American Society for Testing and Materials standard number G69 defining the measurement of corrosion potential in aqueous solutions containing 58.5 g/l of NaCl and 9 ml/l of a 30 wt. % H_2O_2.
EDS	Energy Dispersive Spectroscopy
FEG	Field Emission Gun
GDOES	Glow Discharge Optical Emission Spectroscopy
GI steel	Hot Deep Galvanized steel
ICP OES	Inductively Coupled Plasma Optical Emission Spectroscopy
LDH	Layered Double Hydroxide
LME	Liquid Metal Embrittlement
OCP	Open Circuit Potential
PVD	Physical Vapor Deposition
REACH	Registration, Evaluation, Authorization and Restriction of Chemicals
SCE	Saturated Calomel Electrode
SEM	Scanning Electron Microscopy
SNMS	Secondary Neutral Mass Spectrometry
TEM	Transmission Electron Microscopy
VDA	Verband der Automobil Industrie – "Association of Automobile Industry" (in German)
VOC	Volatile Organic Compound
XPS	X-ray Photoelectron Spectroscopy
XRD	X-Ray Diffraction
ZnAlMg	Zinc-aluminum-magnesium coating for steel typically containing 1.5-11 wt. % of Al and 0.5-6 wt. % of Mg
ZHC	Zinc hydroxycarbonate (simonkolleite), $Zn_5(OH)_8Cl_2$
wt. %	Weight Percent
at. %	Atomic Percent

Introduction

Context of the PhD

For nearly 10 years, the top priority of automotive industry has been to reduce the vehicles weight in order to reduce carbon emissions while maintaining a high level of the passenger's safety. To meet this demand, new high strength steel grades, able to undergo high mechanical stresses even if they have reduced thickness, have been developed. Nowadays, two families of steel meet these criteria. The first one is composed of steels for cold stamping applications with very high mechanical resistance (tensile strength greater than 1000 MPa, typically 1600 MPa and more). The second family regroups steels for hot stamping. One of the most used from these steels is 22MnB5 grade (tensile strength 1500 MPa) which does not create spring back after hot forming. The new high strength steel grades are commercialized with a metallic coating to protect them against corrosion. Zinc (Zn) and zinc alloys have been used for many years in automotive industry as protective coatings for steel. However, for high strength steels, the use of zinc has a drawback because low melting temperature of zinc can contribute to Liquid Metal Embrittlement (LME) of the substrate after heat treatment.

Aluminum (Al) is used as an alternative material in anticorrosion coatings for high strength steel. Today, AluSi® coating (AlSi containing 9 at. % of Si) is one of the most widely used solution selected by Arcelor Mittal for hot stamping since the melting point of AlSi is 200°C higher than the melting point of zinc which permits to avoid cracking problems. Moreover, Al also protects steel surface from corrosion and oxidation during austenitizing thermal treatment. Still, compared to zinc based coatings, AlSi has several disadvantages: little or no sacrificial protection and susceptibility to localized corrosion (pitting). Zn and Mg alloying of AlSi-based coating was recently proposed in Arcelor Mittal to improve anticorrosion performance (patent is submitted). To optimize these new AlSi(ZnMg) coatings the understanding of their reactivity during corrosion and in particular the role played by each alloying elements is primordial.

In this context, the present PhD aims to identify the elementary steps and to understand corrosion mechanisms of AlSi based coatings with Zn and/or Mg alloying and in particular:

- To determine the effects of the alloying elements on the phase composition and the microstructure of the resulting coating;

- To understand the electrochemical characteristics of the new phases composing the coating and to correlate the phase composition and spatial distribution (microstructure) with the electrochemical response of the coating;

- To characterize the behavior of these new coatings in accelerated corrosion tests, measuring weight loss, identifying selective dissolution of phases and the nature of formed corrosion products;

- To correlate stability of specific corrosion products with the coating microstructure, considering selective dissolution of the phases and the nature of the corrosive environment;

- To understand the impact of the electrochemical reactivity of the individual phases and their combinations, of the coating microstructure and of the chemistry of formed corrosion products on the intrinsic reactivity of the coatings and its sacrificial and self-healing capacity.

To achieve these objectives, we combined accelerated corrosion tests in climatic chambers and electrochemical tests on model coatings and pure phases. The coatings microstructure and spatial distribution of corrosion products before and after accelerated corrosion tests or electrochemical tests where observed using Scanning Electron Microscopy (SEM) and Energy Dispersive Spectroscopy (EDS). Raman spectroscopy and X-ray diffraction (XRD) were additionally used to identify metallic phases, their preferential consumption and formed corrosion products. Pure phases identified in the coatings microstructure were synthesized in partnership with the Technical University of Prague Technica 5 (J. Stoulil and V. Self). The electrochemistry of these was tested in order to understand the contribution of the individual phases in general corrosion mechanisms. Galvanic coupling experiments in different combinations of these phases and/or Mn22 substrate were conducted to explore possible micro galvanic coupling in the coatings and evaluate its relative importance in corrosion mechanisms. Finally, artificial damage (scratch down to steel) was made in the new coatings and sacrificial capacity of the new coatings and the impact of corrosion products on coatings reactivity were verified by local electrochemical techniques: Local Electrochemical Impedance Spectroscopy (LEIS), Local Electrochemical Impedance Mapping (LEIM) and Scanning Vibrating Electrode Technics (SVET).

Structure of the PhD

This PhD is organized in **three parts** and **six chapters**.

The first part regroups the introduction, the first chapter which describes the state of the art relevant for formulation of AlSi metallic coatings with Zn and Mg alloying, and the second chapter explaining the experimental strategy. The first chapter details the relevant information found in the literature about the microstructure and corrosion resistance of aluminum coatings, aluminum alloys and aluminum anode materials. The electrochemical properties of some selected systems, the proposed corrosion mechanisms and formed corrosion products are described. The literature review served also to select the pure phases possible in AlSiZnMg coatings on steel in order to produce these pure phases for mechanistic studies. The second chapter, "Experimental", summarizes the techniques and methodology used in the work: accelerated corrosion tests used to test coated steels, surface analysis technics, used to observe corroded profiles and identify solid phases, as well as solution analysis technics and electrochemical set up used in the work.

The second part, composing the core of this work, consist of three technical chapters presented as three publications. The objective of those chapters is to answer to the questions asked in introduction.

The third chapter, "Effect of Zn and Mg alloying on microstructure and anticorrosion mechanisms of AlSi based coatings for high strength steel", is focused on the microstructural analysis of AlSi(ZnMg) coatings and the morphology and intensity of corrosion attack in accelerated corrosion tests. First mechanisms of corrosion are proposed.

The fourth chapter, "Electrochemical behavior of Al(Zn), Al_3FeSi_2 and Mg_2Si phases and its consequence for corrosion mechanisms of AlSi(Zn,Mg) coated steel" presents the electrochemical behavior of the pure phases and their combinations for the phases identified in the previous chapter. A particular attention is made for selective dissolutions and galvanic coupling experiments. The mechanisms by which individual phases contribute to the reactivity are discussed.

The fifth chapter, "Role of corrosion products in corrosion mechanisms of AlSi(ZnMg) coated high strength steel", evaluates the effect of corrosion products formed on AlSi(ZnMg) coatings on the steel protection in case of the contact of coated and uncoated steel surfaces. The effect of alloying on the steel protection at cut edges and in artificial scratches going down to steel in AlSiZn and AlSiZnMg coated steels is studied by immersion tests, local electrochemical technics and surface characterization. The mechanisms explaining the correlation between the

coating composition, the composition of corrosion products and the protection of naked steel are proposed.

The last part of the document is short, it presents the general conclusions brought by the thesis, summarizes anticorrosion mechanisms of AlSi(ZnMg) coatings for high strength steel and the perspectives of the study.

Several appendices give some details useful for the reader like binary and ternary phase diagrams, design of specific experiments or technics, etc.

Chapter I

State of the Art

Chapter I – State of the art

This chapter review the literature about the microstructure of Al based materials and the effect of alloying on the microstructure and corrosion resistance, which was used as a basis for the coating development and the methodology selected in the PhD. One should note that because the result chapters are prepared as papers for submission in scientific journals, each chapter also presents a short literature review focused on the paper subject.

1 Aluminum based coatings: process and microstructure

1.1 Aluminum based coatings developments

Aluminum based anticorrosion coatings for steel have been developed as an alternative to zinc based coatings. Aluminum based coatings are relatively new but aluminum has been used in zinc based coatings for decades as an alloying element. Figure 1 [1,2] shows the time evolution in development of commercial Zn-based and Al-based coatings used in automotive industry. The number after each element represents the weight content (wt. %) of the alloying elements.

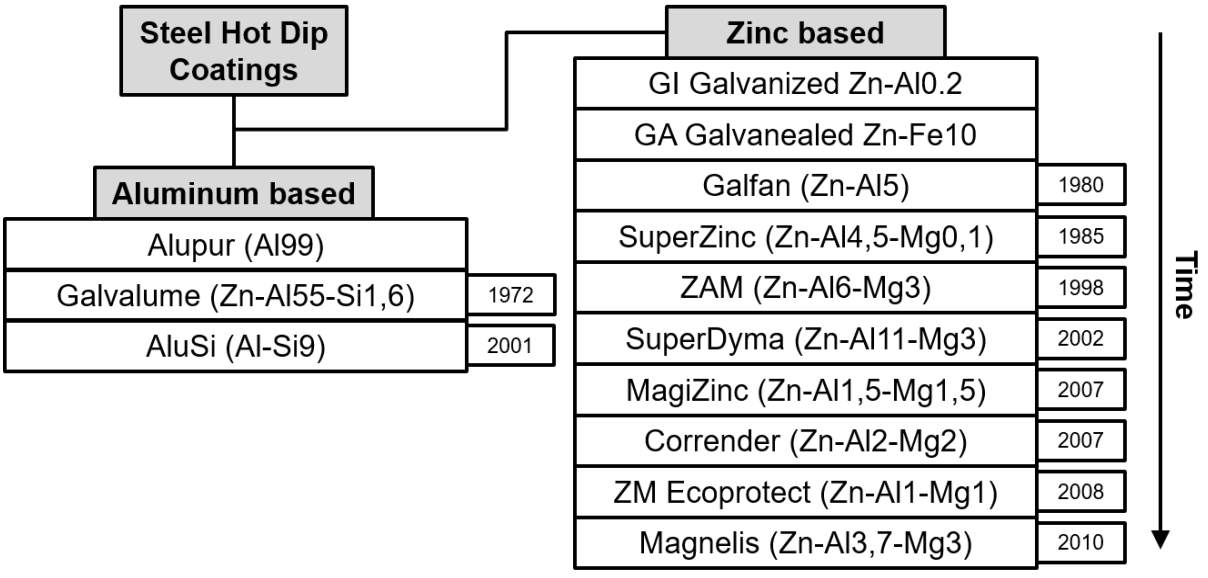


Figure 1 : Commercialized hot dip coating for steel (Numbers in wt. %) (from [1,2])

Metallic coatings to protect steel in automotive industry are mainly deposited by continuous hot dip process [3] (Figure 2 & Appendix 1). The steel strip is dipped in a bath of

molten metal (aluminum-based) in order to obtain a metallic coating on both sides of the substrate. The line speed is typically in the order of 100 m/min.

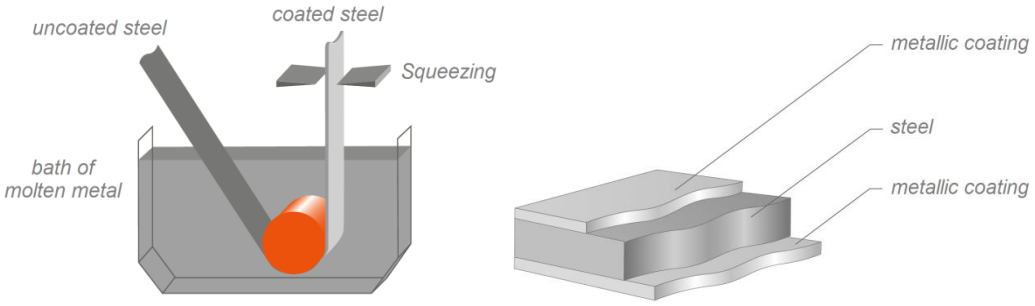


Figure 2 : Hot dip process and coating system drawing (from [3]).

Other fabrication processes are used or in developments, like electrodeposition [4], cold spray, hot spray, arc spray [5], spin coating [5], slurry coating and PVD but majority of protective coatings for steel in automotive industry are still made by a classic hot dip process. The service properties of coatings depend on their microstructure: the nature of the phases, their amount and their distribution. In order to obtain a desired microstructure, the bath composition, bath temperature and the dipping time are controlled.

1.2 Microstructure of Al(Si) coatings

1.2.1 Aluminum coatings

Non-alloyed aluminum (Alupur®) coatings on steel are formed by immersion of the steel coil in an aluminum bath at around 700 °C [6]. These coatings are composed of an Al matrix, and an intermetallic at the coatings-steel interface. Indeed, because of the high process temperature, iron diffuses through the coating and creates a thick and brittle Al-Fe intermetallic layer with the thickness increasing with the bath temperature [6]. This intermetallic is undesired because of its mechanical and electrochemical properties. O.A Fasuba et al [5] demonstrated that Al coatings deposited by arc spray have compact microstructures and very thin intermetallic layer but are not acceptable in terms of corrosion resistance because of its high sensitivity to pitting. Aluminum electrodeposition gives very homogeneous and dense monophasic face centered cubic (fcc) Al coatings and the intermetallic between them and the underlying steel is almost non-existent. Nevertheless, organic or molten salt baths are required for these processes, which makes them very harmful for the environment and too complex to

be adapted at an industrial scale for continuous coating lines with high speed deposition rates [6,7].

To summarize, **high purity aluminum (more than 99.9 wt. %) shows very good corrosion performances [4] but this level of purity cannot be reached by usual hot dip techniques because of the iron accumulation in the bath.**

1.2.2 Al(Si) coatings

In order to improve the hot dip aluminum coating microstructure, Si is added to the bath to limit Fe diffusion and reduce the growth of the intermetallic [6]. 9 wt. % of Si usually added to the aluminum bath to obtain Al-Si eutectic composition and lower melting temperature. In the final coating microstructure $AlFeSi$ intermetallic phase is created instead of Fe_2Al_5 in pure Al (Figure 3).

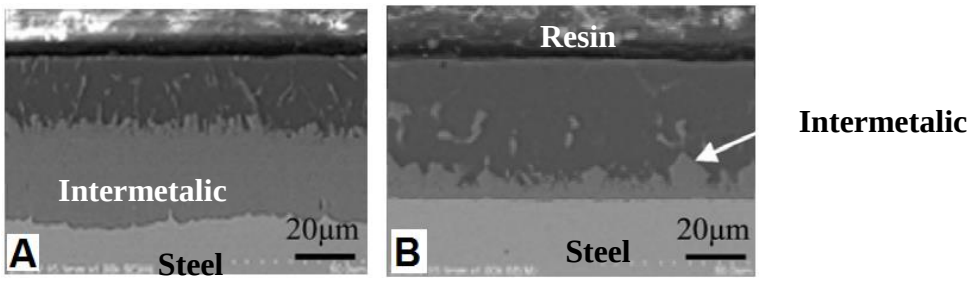


Figure 3 : Cross-sectional SEM views of aluminized steel sheets which were hot dipped in pure Al (A) and AlSi9 (B) at 800 °C. Intermetallic phase between coating and steel. (from [6])

In similar conditions, the intermetallic layer 25 µm thick is formed for pure Al coating and 3-4 µm thick for AlSi9. For ternary Al-Fe-Si systems [8], the amount of formed $AlFeSi$ phases increases with the process temperature. After hot dip, the coating is composed of an $AlFeSi$ intermetallic layer at the interface with the steel, and an Al-rich phase with pure Si needles. Takata et al. [9] proposed a mechanism explaining the variation of the thickness by the variation of the kinetics of the intermetallic growth. The authors concluded that ***AlFeSi*** **intermetallic** is more continuous and better **limits the diffusion of** ***Fe*** than the $AlFe$ particles formed without Si **resulting in thinner intermetallic layer** after hot dip process.

Addition of Si also results in high fraction of metallic Si needles inside the coating. Si morphology can be refined by Sr alloying which is an important issue to avoid micro galvanic corrosion [10].

1.2.3 AluSi® for hot stamping

For high strength steel, the fabrication process can also contain a supplementary hot stamping step. During this step, steel coil is heated at around 900°C during 5-10 min to obtain an austenitic microstructure; then the blanks are hot formed and cooled in a tool to obtain the targeted martensitic microstructure. This is the so called hot stamping process which is used in automotive industry [11]. After hot stamping process, AluSi has a layered microstructure [12]. The iron diffusion is more pronounced than in hot dip step, AlFe and AlFeSi intermetallic close to τ5 and τ6 intermetallic are formed. Intermetallic phases formed in AluSi® (8.7 at. % of Si) are generally close to **τ5 and τ6 intermetallic composition. These phases are inevitable and their impact of the corrosion mechanisms of AlSi coated steel is not yet completely understood.**

2 Effect of alloying on Al microstructure

In order to modify the microstructure and create new phases with different mechanical or electrochemical properties various alloying elements can be used. Huge amount of the literature about the effect of alloying elements on the microstructure of aluminum alloys but also aluminum anodes and some aluminum based coatings is accumulated, this section will provide only essential information relevant for our study.

2.1 Aluminum alloys

Al wrought alloys are mainly used in aeronautic industry and are classified in series from 1000 to 8000 depending on alloying elements. Table 1 shows the content of principal alloying elements and the nature of formed intermetallics [13-15]. The alloying elements can be distributed in the alloy in two different ways. When the alloying elements are in small amounts and soluble in aluminum matrix, they form a fcc solid solution in Al. Otherwise, their presence result in formation of the inclusions of the second phase which will generally concentrate at grain boundaries. Al-Fe intermetallics generally comes from fabrication process while Mn, Mg, Cu, Zn and Si are intentionally added to improve the mechanical properties of the alloys but at the same time, they modify the anticorrosion properties. The 6000 series alloys are known to be resistant especially in atmospheric conditions.

Table 1 : Composition of wrought Al alloys (from [13,14])

Series	Alloying Element wt. % [14]	Inclusions [13]
1000	No intentional, Fe by fabrication process	Al_3Fe, Al_6Fe
2000	Cu (2-6 %)	Al_2Cu
3000	Mn (0,5-1.5 %)	$AlMnFe$,Al_6Mn
4000	Si (0,8-1,7 %)	Si
5000	Mg (0,5-5 %)	$AlMg_2$,$AlMg_5$
6000	Si, Mg (0.2-1.5 %)	$AlFeSi$,Mg_2Si
7000	Zn, Mg (1-7 %)	$MgZn_2$

2.2 Aluminum anode materials

Aluminum alloys are used as anode materials to protect steel structures exposed to sea water (bridge, underground structures). The aim of a sacrificial anode is to protect a selected material from corrosion by coupling it with the anode material which will corrode preferentially. The way aluminum is made sacrificial in these anodes can be interesting to modify AlSi coating and make it sacrificial for steel. In the majority of anode materials described in the literature, Zn is added to Al to decrease the free corrosion potential. The phase diagram of Al-Zn system is given in **Appendix 5**. For a composition Al-4.5 wt. % of Zn, the corrosion potential of the alloy is -0.95 V vs. SCE (saturated calomel electrode) [16]. β-(Zn rich) phase (Table 2) forms in Al alloys with Zn content more than 4.5 wt. % and this active phase drives the corrosion [17] in these alloys. In practice, for Al anodes the Zn concentration is usually kept in the range 0.1 - 4.5 wt. % [18] in order to avoid β-(Zn) formation and microgalvanic coupling.

Zn in the alloy /wt %	β phase /%
20	3.08
40	24.83
60	54.62
80	67.43

Table 2 : Mass percentage of β-(Zn) phase depending on Zn content. (from [16])

In aluminum anodes, a third element is generally added to Al-Zn alloys such as Hg, Sn, or In, to increase the efficiency of the anode. These elements are called activators and are generally soluble in the Al fcc matrix.

2.3 Microstructure of aluminum based coatings

2.3.1 Galvalume® coatings

Galvalume® coatings are mainly used in construction industry. These coatings contain 43.4 wt. % of Zn and 1.6 wt. % of Si and are formed by hot dip process. They are very resistant to atmospheric corrosion but they offer a less efficient cathodic protection to steel in atmospheres with low chloride contents than zinc. To improve it, addition of small quantities of Mg (from 0 to 2.5 wt. %) in Galvalume® was proposed [19]. Without Mg alloying, Galvalume is composed of Al rich dendrites, Zn rich interdendrites and Si particles. The addition of 1.5 wt. % of magnesium creates a Zn-Zn_2Mg eutectic in the inter-dendrites. Above 2.5 wt. % of Mg, all inter-dendrites at the surface are composed by Zn_2Mg (Figure 4).

Wei Liu [20] determined fractions of different phases in the Zn - Al (50 wt. %) -Si (1.6 wt. %) coatings (very close to the Galvalume® coating composition) as a function of the amount of Mg and demonstrated that Mg combined with Zn to form Zn_2Mg but also with Si to form Mg_2Si intermetallic.

The stability of AlSiZnMg quaternary system was experimentally and theoretically studied by Qian Li [21], in Zn rich domain (50 wt. %-70 wt. %). For a composition of Al15Zn62Mg17Si6 (here and later the numbers after the element indicate the weight fraction of the element in the coating) Mg_2Si, Zn_2Mg and Si precipitates where also detected.

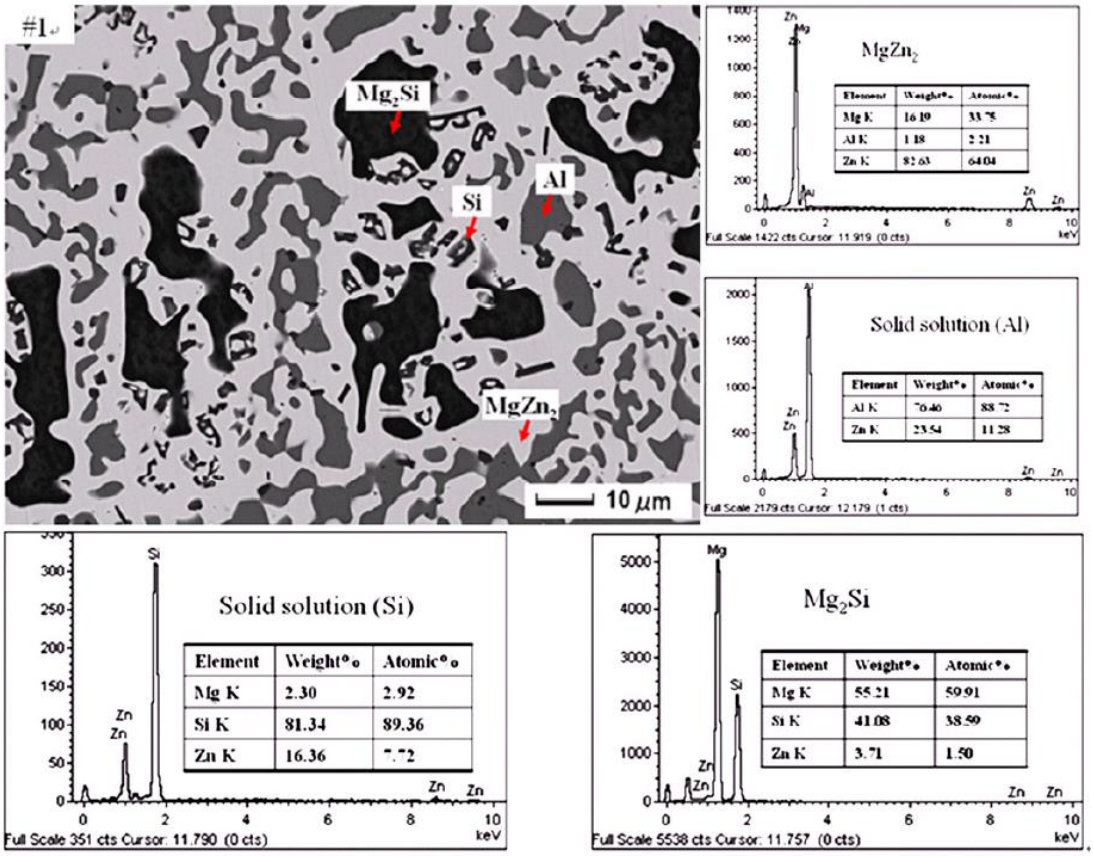


Figure 4 : SEM images and EDS analysis of present phase for an Al15Zn62Mg17Si6 alloy. (from [21])

2.3.2 Hot dip Al-Mg-Mn coatings

Al-rich coatings with Mg and Mn alloying were tested by Debabrata Pradhan and al. [22]. The composition was based on the Al alloys of 3000 and 5000 series. Mg content was chosen below 3.5 wt. % to eliminate the risk of the precipitation of the electrochemically active Al_3Mg_2 - β phase at the grain boundaries. The latest increases the susceptibility to inter-granular attack and inter-granular stress corrosion cracking. Similarly, Mn content was selected below the eutectic composition of 1.82 wt. % to exclude Al_6Mn-β phase precipitation. The formation of AlMg and AlMn phases should be avoided because these phases have a very low potential and can generate local galvanic coupling. The surface composition was homogeneous (Al solid solution). The Mn was concentrated as solid solution in the AlFe intermetallic phase. The thickness of the coating depended on the dipping time, being 45 µm thick for 10 s, 60 µm for 20 s and 70 µm for 30 s of deep process.

2.3.3 Physical Vapor Deposition (PVD) AlSiMg and AlZn coatings

Several examples of Al-rich coatings deposed by PVD can be found in the literature. In the publication of Yoshihiko Kyo [23] an Al11.8Mg3.3Si coating was obtained by thermal treatment at 778 K for 2 hours. In this material Mg and Si were dissolved in Al matrix and Mg_2Si intermetallic was also precipitated.

In another publication A. Perez [24] deposited by PVD several AlZn coatings with different Zn content and concluded that at Zn contents less than 10 at. % a single Al solid solution with pyramidal shape morphology is obtained. For compositions above 10 at. % of Zn the coating was biphasic and nodular shaped.

2.4 Microstructure of alloyed Al

In the solid solution domain of aluminum, the solubility of abundant alloying elements can be classed from the most soluble to the least soluble alloying element as following [13-18]:

Zn>Mg>Mn>Cu>Si

Table 3 summarizes the major phases which could appear in the binary and ternary systems reviewed in this chapter with more than 60 wt. % of Al but the content of the second and third element higher than the limit of the solubility in Al matrix. The proportion and repartition of the phases depend on the composition and the fabrication process and is not named in the table.

Table 3 : Preferentially formed phases for highly alloyed Al [13-18]

Phases	**Preferentially formed phases**
Al	Al
Al+Si	Al , Si
Al+Zn	(Al) , $Al-Zn$ *binary*
Al+Mg	$AlMg_2$, $AlMg_5$
Al+Fe	Al_3Fe, Al_6Fe
Al+Fe+Si	$Al_xFe_ySi_z$ *intermettalics*
Al+Si+Zn	(Al) , Si
Al+Si+Mg	Al + Mg_2Si

Some of the listed phases cannot however be formed in hot dip process and other Fe containing phases can be formed. The phases identified in Al-based coatings of different compositions on steel are presented in Table 4. To sum up, different **new phases can be formed**

by Al alloying by Zn and Mg: Zn can be soluble in Al matrix and depending on elemental compostionMg_2Si, Zn_2Mg can precipitate. The spatial distribution of these phases in aluminum based coatings and the effect of the new phases on corrosion mechanisms need to be understood.

Table 4 : Identified phases in Al-based coatings (stch = stoichiometric quantity) [18-24]

Coating composition wt. %	Preferentially formed phases
Al	Al, Al_3Fe, Al_6Fe
AlSi	$Al\ , Si,\ Al_xFe_ySi_z$ *(τ5 & τ 6)*
AlZnMg	$Al\ , Zn_2Mg, Al_3Fe,\ Al_6Fe$
AlSiZn (Zn<10 %)	$(Al)\ , Si,\ Al_xFe_ySi_z$ *(τ 5 & τ 6)*
AlSiZn(Zn>10 %)	$(Al)\ , Al-Zn$ *binary,* $Si\ Al_xFe_ySi_z$ *(τ 5 & τ 6)*
AlSiMg (Mg<Mg_2Si stch)	$Al, Si, Mg_2Si, Al_xFe_ySi_z$ *(τ 5 & τ 6)*
AlSiMg(Mg>Mg_2Si stch)	$Al, Si, Mg_2Si, AlMg_2,\ Al_xFe_ySi_z$ *(τ 5 & τ 6)*

3 Corrosion of Al - based materials

Al is usually covered by a thin dielectric barrier layer of the oxide [14]. It makes the open circuit potential (OCP) of Al and its alloys very close to the OCP of steel. In sea water and more generally chloride rich environments the real OCP difference between Fe and Al is less than 150 mV, whereas it is more than 400 mV between Fe and Zn. This explains why Zn and not Al is generally used to protect steel against corrosion.

If sacrificial protection by Al alloys is aimed, the understanding and the control of properties and the formation conditions of passive films are fundamental.

3.1 Passive film formation

Aluminum spontaneously oxidizes in nearly all environments containing oxygen (air, water …). The free energy of this reaction (1) is about –1675 kJ [25]. The oxide is formed within a millisecond under a few millibars of oxygen pressure.

$$2Al + \frac{3}{2}O_2 \rightarrow Al_2O_3 \qquad (1)$$

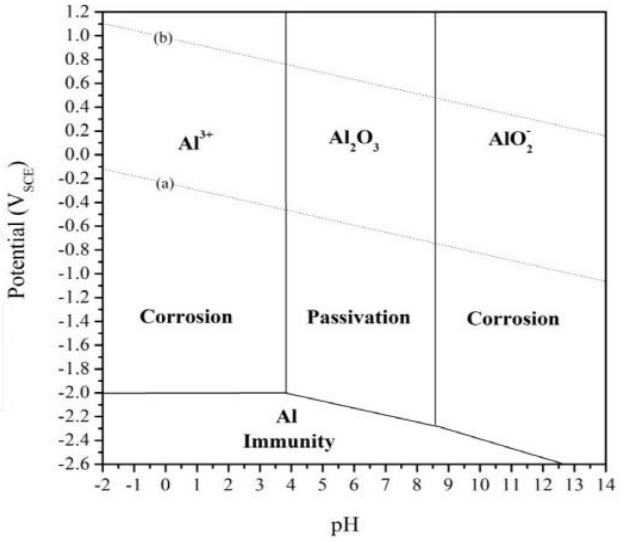
The Al_2O_3 layer is amorphous, and its thickness is generally between 4 and 10 nanometers [26]. It creates a separation between the bare metal and the environment, preventing the oxidation reaction to go further in the material. In aqueous media, this oxide layer can be destabilized by hydroxide ions to forming soluble aluminates:

$$Al_2O_3 + 3H_2O + 2OH^- \rightarrow 2Al(OH)_4 \qquad (2)$$

Depassivated metallic Al is immediately oxidized by the electrochemical reaction:

$$2Al + 6OH^- \rightarrow Al_2O_3 + 6e^- + 3H_2O \qquad (3)$$

From the Pourbaix diagram shown in Figure 5, it can be seen that the Al oxide is stable in the pH range from 4 to 9. At pH lower than 4 or higher than 9, Al_2O_3. Al which is recognized as a very protective metal in neutral pH conditions may rapidly corrode in acidic or alkaline environments.



(a) $H_2 \leftrightarrow 2H^+ + 2e^-$

$$H_2O \leftrightarrow \frac{1}{2}O_2 + 2H^+ + 2e^-$$

Figure 5 : E-pH diagram for pure Al at 25 ˚C in aqueous solution (adapted from Pourbaix 1974). The lines (a) and (b) correspond to water stability and its decomposed product. (from [27])

3.2 Passive film stability

In solution or in humid atmosphere the Al_2O_3 layer is progressively hydrated. Thermodynamically, the most stable product is boehmite with a ΔG of formation as high as -1825.4 kJ (Table 5) [26].

Table 5 : Free enthalpies of formation for aluminum products (in water)

Species	ΔG°/KJ mol-1
Al^{3+}	-485
$Al(OH)_4^-$ (aq)	-1297.8
$Al(OH)^{2+}$ (aq)	-694.1
OH^- (aq)	-694.1
H_2O	-237.2
$Al(OH)_3$ amorphe ($Al_2O_3.3H_2O$)	-1137.6
$Al(OH)_3$ Gibbsite ($Al_2O_3.3H_2O$)	-1154.9
Al_2O_3.H2O Boehmite	-1825.4

Equilibrium between the hydrated porous external layer and the compact amorphous oxide is achieved when the hydrated layer is thick enough to prevent H_2O diffusion.

Coated steels for automobile industry are used and tested in atmospheric condition, exposed to humidity and/or corrosive electrolytes, the formation of the passive layer on Al is inevitable and it efficiently protects Al from corrosion. In the absence of the defects in Al coating, the substrate should be hence protected by the coating by a barrier mechanism. However, even without initial defects in Al film, in atmospheric condition, aluminum is sensitive to pitting corrosion which can result in pits coming till the steel [28].

3.3 Passive film breakdown

Corrosion of Al based materials often begins at local defects in the oxide layer [7,28-31]. These defects can be a micro-fracture in the oxide film because of its extremely high hardness or oxide layer in homogeneities due to the presence of intermetallic particles (for instance Fe_2Al_3) for alloys and coatings. The film can also break if the corrosive environment changes locally (pH modification, accumulation of aggressive species like halides …). Fig. 6 illustrates the commonly accepted steps of Al corrosion:

Initiation step:

1: Adsorption of chloride in the defects of oxides.

2: Oxygen reduction (creating the anodic / cathodic sites)

3: Dielectric breakdown in the oxide layer

4: Aluminum oxidation at “weak” points.

Propagation step:

5: Propagation of few pits

6: Formation of soluble $AlCl_4^-$ complex and $Al(OH)_3$ precipitation at pit border resulting in solution acidification in the pit

7: Formation of an $Al(OH)_3$ “hats” on pits

8: Auto-corrosion of aluminum in the pit and H_2 production

9: When corrosion current does not allow the $AlCl_4^-$ formation … re-passivation of the pit.

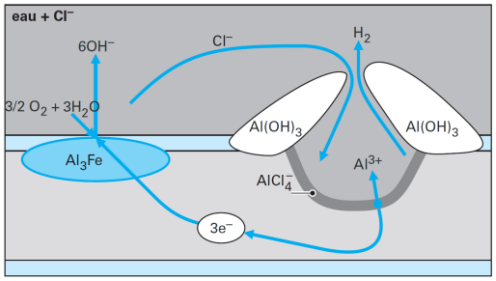


Figure 6 : Illustration of commonly accepted corrosion mechanisms for Al alloys (from [28])

3.4 Effect of alloying elements on the electrochemistry of Al-X solid solutions.

3.4.1 Binary Al-X systems

Depending on the fraction of alloying elements, the solid solution or multiphase microstructure can be formed. For solid solutions, corrosion potential changes depending on the alloying element and its fraction. As shown in Figure 7, alloying with Mn, Cu and Si increases the potential to more noble values whereas Mg and Zn will lower it. Al(Zn) solid solution has the lowest potential in ASTM G69 solution between the presented alloying elements [29].

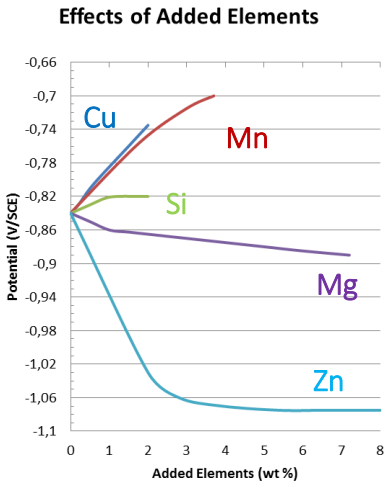


Figure 7 : Alloying elements influence on the dissolution potential of aluminum alloys in ASTM G69. (from [29])

This is largely used in AlZn anode materials. The maximum efficiency of Al anodes is reached at exactly 4.5 wt. % Zn (Figure 8) where α-(Al) phase is saturated but no β-(Zn) phase appears [16]. Corrosion of AlZn anodes highly depends on the distribution of the β-(Zn) at the grain boundaries. The presence of β-(Zn) in these sites can lead to intergranular corrosion and lower the effectiveness of the anode.

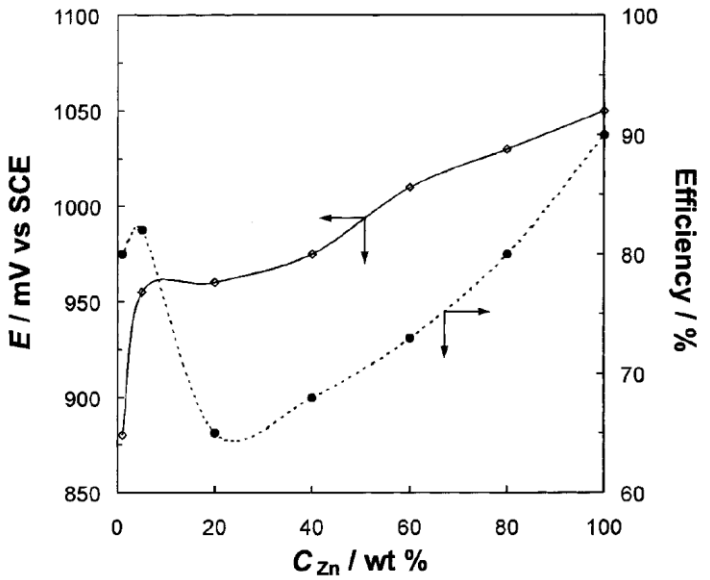


Figure 8 : Anode efficiency and operating potentials of the Al-Zn alloys with different Zn content. (from [16])
Legend: ♦ potential and ● efficiency

Between 4.5 wt. % and 40 wt. % of Zn, potential is driven by α-(Al) phases but the galvanic coupling with β-(Zn) causes undesired corrosion which decreases efficiency. Above 40 wt. % of Zn galvanic corrosion is controlled by β-(Zn) phase and potential increases slightly to reach -1050 mV vs. SCE potential typical for Zn matrix.

For sacrificial AlZn coatings it was observed [24] that AlZn19 PVD coated steel had shown later red rust appearance than AlZn17, AlZn6 or pure Zn PVD coated steels.

Considering sacrificial capacity of AlZn coating with minimum internal galvanic corrosion due to Al and Zn rich phases coupling, Zn optimal content in Al-based coatings is expected between 2 and 4 wt. %. Nevertheless, this should be only true in concentrated chloride environment, in low chloride environments more Zn can be necessary to activate it.

Concerning Al-Mg solid solution phase, at 450 °C Mg solubility in Al is 15 wt. %, but it is only about 1 wt. % at room temperature. Hence, **at concentrations more than 1 wt. %,**

Mg precipitates at the grain boundaries and can enhance intergranular corrosion by the galvanic coupling. The temperature and the time of thermal treatment must be controlled to limit the formation of Mg precipitates however **at Mg concentrations above 5.5 wt. % all AlMg alloys are sensitive to inter-granular corrosion**.

3.4.2 Aluminum anodes activators

Al anodes can be interesting systems when considering the improvement of sacrificial capacity of Al based coatings. AlZn anodes are often used with anode activators. An activator is an element added to the material in less than 0.5 wt. % which modifies anode properties and makes it more active [18]. Many activating agents have been investigated for Al anodes in last decades and the data from the literature are summarized in Table 6.

Table 6 : Typical composition of activators for Al anodes (data from [16,18,32-36])

Alloying element	Concentration range, wt. %	Observations (wt. %)	Source
In	0.01-0.03	Galvanic efficiency improved by 85 % but self-corrosion appears above 0.03 wt. %	[32-34]
Hg	>0.03	Under 0.03 wt. % passivation remains	[35]
Sn	0.12-0.25	Above 0.1 wt. % self-corrosion increases	[16]
Cd	<0.02	Above 0.2 wt. % decrease of current capacity	[18]
Fe	<0.12	Above 0.12 wt. % there is a shift of potential to anodic value	[16]
Cu	<0.01	Above 0.01 wt.% pitting, decrease of current capacity and anodic shift	[16]
Si	0.033-0.11	Can imitate the bad impact of Fe but if Si in excess it increases the self-corrosion rate	[16]
Bi	0.1	Properties can be improved by adding Mg Bismuth helps in expanding the aluminum matrix	[16]
Se	0.1		[36]
Ga	0.01-0.4		[18]
Ti	0.03		[18]
Zr	0.05		[18]
RuO	?		[18]

The effect of an activator is usually measured by the induced modification of the potential of the anode material. Sn, In and Ga are the most investigated activators for Al. In the work of S.M.A. Shibli [36] the best activator combination seems to be 0.5 wt. % Se + 0.1 wt. % Sn + 0.1 wt. % Bi. The mechanisms by which Al reactivity can be enhanced by an activating agent depending on its nature. For Hg, J.B. Bessone [35] proposed the formation of liquid Hg in places were the oxide is weakened which prevent the formation of the passive film by the Hg-Al amalgam impermeable to oxygen but allowing Al^{3+} dissolution. A similar mechanism was described for Ga by the same authors in another publication [37].

Sakano et al. [38] formulated indium-activated aluminum anode with a composition of (Al + 5 wt. % Zn + 0.03 wt. % In). The efficiency of such an anode was measured as close to 80 wt. %. The proposed mechanism of activation by indium was different from the mechanisms proposed for Hg. The presence of chloride ions was mandatory in case of activator. Authors proposed that a true electrical contact between In, Al and Zn promoted the adsorption of chloride ions. Zn facilitated an enrichment of the surface by In and the accumulation of adsorbed Cl^- maintaining Al matrix in an active state.

Activators can be used to increase sacrificial capacity of aluminum anodes to protect steel structures in corrosive media. These activators are added in very small quantities (<0.1 %) and their concentration of the activators need to be precisely controlled to obtain desired effect. The obtained dissolution rates are very high.

Considering the use of activators, however, **one should remember that sacrificial anodes and protective coatings have the same function to protect a metallic structure but the application is very different. An anode can be replaced, whereas a coating cannot. As a result, the anode's efficiency is differently appreciated than the coating's efficiency and needs to be analyzed carefully considering the "on the use" differences.**

***

From the data presented in section 3, one can conclude that significant decrease of corrosion potential can be achieved in Al alloys by addition of Mg and Zn. However, the solubility of these elements in Al matrix is limited and new phases can be formed in presence of excess of Zn or Mg as well due to the presence of Si and Fe (section 2).

4 Effect of precipitates and intermetallic phases on Al reactivity

The values of corrosion potentials of the most known intermetallics typical for Al alloys are presented in Table 7. For comparison the corrosion potential of carbon steel, of pure Al and commercially pure Al (alloy 1050A) are also given.

Table 7 : Corrosion potential of selected intermetallics in ASTM G69 solution. (from [29.p97]).

Intermetallic phase / Second Phase	Corrosion Potential (mV/ECS)
Si	-170
Al_3Ni	-430
Al_2Cu	-440
Al_3Fe	-470
Carbon steel	-660
1050A Al alloy	-750
Al_6Mn	-760
Al	-840
Al_2CuMg	-910
Zn_2Mg	-960
Al_3Mg_2	-1150
Mg_2Si	-1190
Al_8Mg_5	-1240

Table 8 summarises the intermetallic phases which will be considered in this chapter and their relative position versus steel in ASTM G69 electrolyte. As in Tab. 7, steel and Al corosion potentials are given for comparison.

Table 8 : Phases expected in AlSiZnMg coatings and their corrosion potential in ASTM G69 electrolyte (data from [13,29,48])

Intermetallic phase / Second Phase	Corrosion Potential (mV/SCE)	Sources
Si	-170	[29]
AlSiFe Intermetallic	~ -300	[48]
Al_3Fe	-470	[13]
Steel	-660	[12]
Al	-840	[12]
Zn_2Mg	-960	[13]
Mg_2Si	-1190	[13]

In the literature (see for instance [39]), intermetallic particles in aluminum alloys play a major role in passivity breakdown and pit morphology in chloride media and seawater. The understanding of the electrochemical response of the new formed phases and their combinations is hence essential to understand the relation they can make in more complex systems [40,41].

Below, some details of the reactivity of these phases in Al matrix is presented.

4.1 AlFe phase

AlFe phases like Al_3Fe are inevitable in hot dip process due to Fe diffusion. These phases are generally cathodic (Table 8) relative to steel and generate red rust when corroding. In the case of Al-Fe alloys AlFe particles increased both cathodic and anodic activity of the material and were preferential points of corrosion attack [42].

4.2 Zn_2Mg phase

Additional Zn and Mg alloying of AlSi coating can not only modify Al matrix forming solid solutions but also produce new intermetallic phases. One can expect for Zn-rich AlSiZnMg coatings formation of numerous phases: Al rich phase, eutectic Al-Zn and $MgZn_2$. All exhibit a different potential. At neutral pH Zn_2Mg can be selectively dissolved because of its highly anodic potential [43] (Figure 9). Zn_2Mg dissolves at lower rates than independent Zn and Mg which was attributed to a dealloying process forming partially protective ZnO and $Zn(OH)_2$ [44].

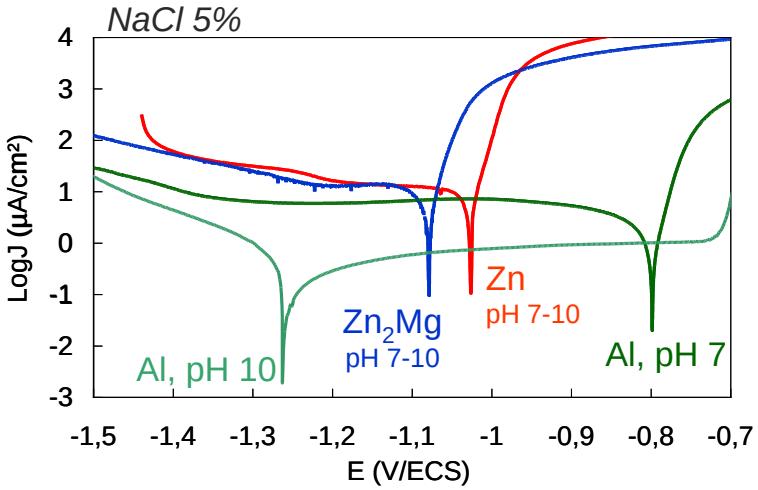


Figure 9: Polarization curves of Zn, Al and Zn_2Mg at pH ranging from 7 to 10 in NaCl 5wt. % (from [43]).

At neutral pH, typical for major part of the electrolytes in accelerated corrosion test, Zn_2Mg appears to be the least noble phase while aluminum rich-phase is the noblest one [45]. Aluminum potential modification with pH (Figure 9) makes it difficult to evaluate its cathodic/anodic behavior with time especially with Zn addition which lower its corrosion potential.

4.3 Si –rich phases in Aluminum

4.3.1 Metallic silicon and silicon inclusions

Pure Si phases are cathodic in Al-solid solution matrix [46]. The pure metallic Si has a potential of -170 mV/SCE [13] and so its segregation on grain boundaries can enhance inter-granular corrosion (Figure 10) of Al matrix.

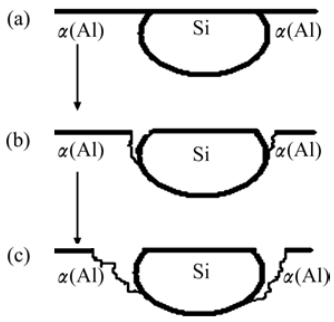


Figure 10 : Schematic mechanism of local corrosion around a Si particle (from [46]).

This phenomenon was also observed on AluSi coatings in chloride solutions [47]. Si did not oxidize and the Al matrix was consumed. Finally, in the absence of a passive oxide layer, the micro-galvanic coupling with Si phase enhances the selective dissolution of Al matrix.

4.3.2 AlSiFe phase

As described in Chapter I, the press hardening process results in the presence of an intermetallic AlFeSi layer that forms between the AlSi deposit and the substrate. This intermetallic can be an important part of the coating, particularly for hot stamped steel. Only few publications study these phases. In a work of H. Danesh Manesh and A. Karimi Taheri [48], relative potential and selective dissolution of AlFeSi in an Al matrix are described. Volta

potential of AlSiFe phases was higher than that of Al matrix and even higher than that of pure Si. This induced selective dissolution of the Al matrix around the cathodic phases.

With Mg addition, AlFeSiMg quaternary phase can be generated. This phase has a potential between Si and aluminum which can be close to the potential of the steel but no results are available on this subject and in AlSiZnMg coatings, magnesium preferentially forms Mg_2Si.

4.4 Mg_2Si phase

Reactivity of Mg_2Si intermetallic at near neutral pH is described as a selective Mg dissolution with remaining insoluble SiO_2 [49]. With pH increase, dissolution decreases which was attributed to the formation of protective oxides such as $Mg(OH)_2$ or $Mg_3Si_2O_5(OH)_4$. The Mg_2Si phase with OC potential around -1538 mV vs. SCE in 0.1 mol.L^{-1} NaCl [13] is anodic in Al-based matrix [48]. A selective dissolution of Mg from Mg_2Si conducts to silicon enrichment modifying the phase potential to more noble values and resulting in the change of the phase behavior from anodic to cathodic vs the surrounding matrix.

The alternating anodic then cathodic state results in the initial selective dissolution of Mg from Mg_2Si first and then in dissolution around the Si enriched particles. In [50], the evolution of Mg_2Si particles in an aluminum rich matrix was studied in detail (Figure 11). The mechanism presented in the figure is coherent with the fact that large Mg_2Si dendrites promoted pitting corrosion around them whereas small particles provided anodic protection during the time of their consumption. Therefore, spatial distribution of phases can play a critical role for corrosion resistance.

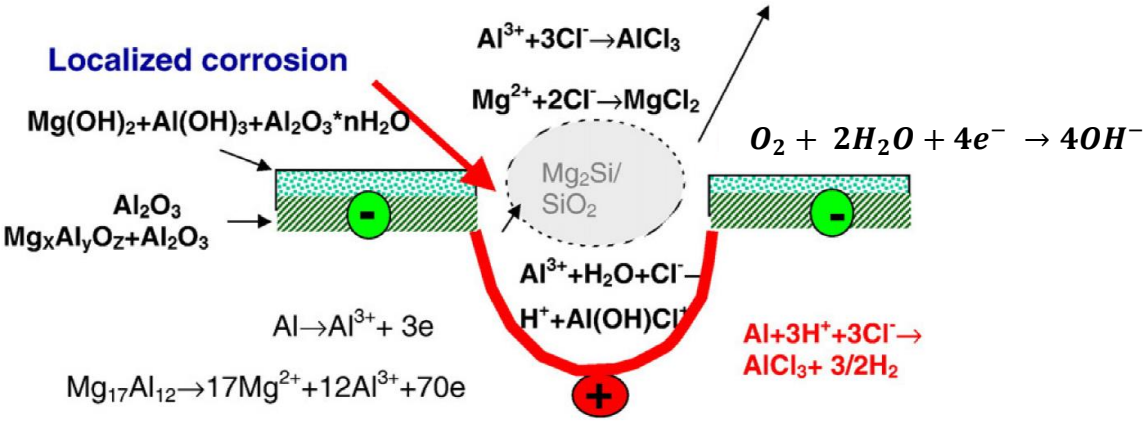


Figure 11 : Localized corrosion mechanisms of Mg_2Si in Al and AlMg matrix (from [50]).

4.5 Intermetallic layers in cold stamped Al(Si) coatings

The electrochemical behavior of different phases directly inside the Al-9 wt. % Si coatings on high strength steel was studied by Ine Schoukens and al [51]. The potential between the different coating layers revealed that the aluminum matrix is anodic to the steel but that the formed intermetallics phases are cathodic (Figure 12).

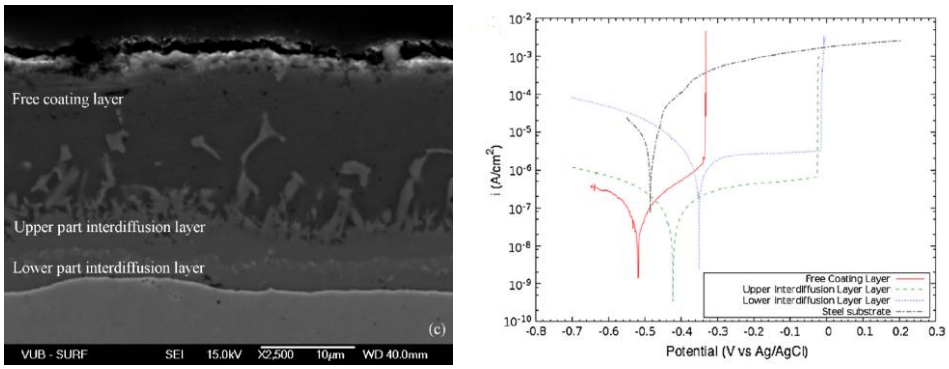


Figure 12 : SEM observation and potentiodynamic polarization curves in 0.1 M NaCl solution of Aluminum-Silicon coating different layers obtained by the electrochemical micro-cell positioned in the GDOES sputter craters (from [51]).

4.6 Summary of the effects of alloying on the reactivity in Al materials

To modify corrosion resistance of Al coatings and their sacrificial capacity, different alloying elements can be added. Zn is largely used to lower the aluminum potential. For binary systems, the maximum efficiency of Zn is obtained when it is fully dissolved in the aluminum matrix. More Zn addition generates a formation of eutectic Zn-rich phase promoting micro-galvanic coupling and preferential sites for corrosion attack and weakness for corrosion properties.

Mg alloying also decreases Al potential but the effect is less significant than for Zn. Mg can also create intermetallic phases as Mg_2Si or Zn_2Mg. Zn_2Mg is strongly anodic in Al matrix and its potential is more stable than that of Al in a large range of pH. This phase stays sacrificial at different pH.

Some other activators can also be used as Ga, Hg or Sn but their concentration is critical to obtain good performances. Indeed, for sacrificial anode the aim is to protect the main structure, in this system the anode could be replaced if it corrodes too rapidly. The latest is not recommended for a sacrificial coating. A brief literature review demonstrated that the electrochemistry of selected intermetallic phases was previously studied however there is very

limited knowledge about the interaction of these phases in multiphase materials. **Better understanding of the individual electrochemical behavior of pure phases possible in AlSiZnMg coatings on steel (Mg_2Si, Zn_2Mg or the intermetallic AlFeSi) and their coupling in Al(Zn) and Al matrix and/or with the substrate steel could be important to better understand general corrosion mechanisms of new AlSi based coatings.**

This chapter reviewed mainly electrochemical potentials of selected phases typical for studied coatings. However, atmospheric corrosion is a complex process and it is important to consider the whole corrosion process in atmospheric conditions. These mechanisms will strongly depend on corrosive media and on the possible corrosion products formed under atmospheric conditions because the formation of new barrier or pH buffering products on the surface can drastically change corrosion behavior.

5 Atmospheric corrosion of Al and Zn based coatings for steel and role of corrosion products

5.1 Corrosion of Usibor AluSi®

In terms of free corrosion potential, standard AluSi® without heat treatment is around -0.76V vs. SCE, only 100 mV below the corrosion potential of the steel 22MnB5 (-0.67 V vs. SCE) [12] which is insufficient for sacrificial protection. After hot stamping heat treatment free corrosion potential evolve to -0.70 vs. SCE coming even closer to steel [12]. After accelerated corrosion test, the coating observation showed pitting corrosion in which however, AlSiFe phase corrosion results in formation of corrosion products limiting the corrosion of the substrate (Figure 13). Despite the decrease of the corrosion rate of the substrate, the corrosion of Fe_2Al_3 intermetallic was responsible for the red rust formation.

Corrosion products on AlSi coating are mainly aluminum oxides or a combination of Al and Fe oxides if pitting is important.

***

The barrier effect of corrosion products on Usibor AluSi coatings was previously noted, however these corrosion products seem to be formed only in places of the corroded coating and cannot be formed on the naked areas (cut edge, artificial defect). Their barrier effect cannot hence be considered for an active anticorrosion protection.

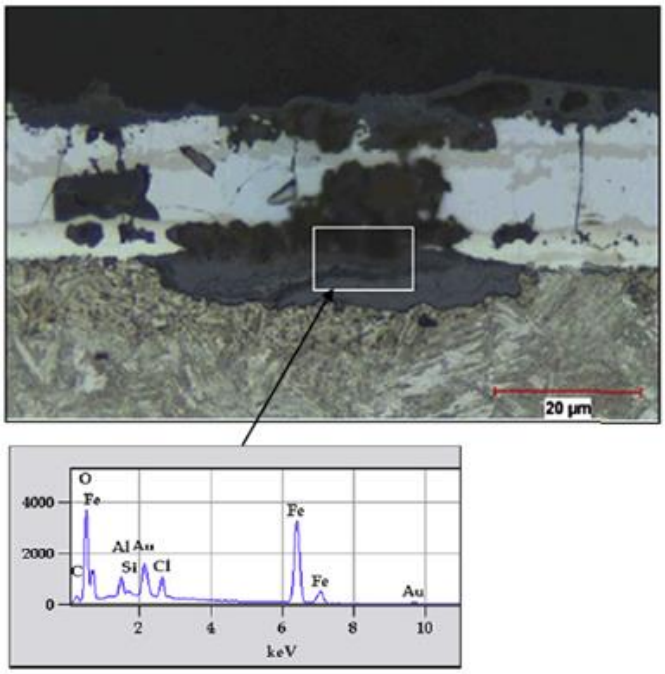


Figure 13 : SEM image and EDS spectra in the corroded zone at the interface between the coating and the substrate (the area of analysis is indicated). The sample was corroded in accelerated tests. Gold (Au) a 20 nm gold layer was sputtered on the surface before SEM observation in order to avoid the charging of the non-conductive corrosion product surface (from [12]).

Additional Zn and Mg alloying can result in formation of new corrosion products which potentially could offer not only barrier but also self-healing effect on naked areas. The next section will review the formation and properties of some of possible corrosion products.

5.2 Corrosion of Zn - 55wt. % Al coatings

Galvalume® coatings contain Al and Zn as major elements and up to 2.5 wt. % of Si and possible addition of Mg. Galvalume® is composed of an Al matrix dendrite and Zn-rich phase segregated between the dendrites [52]. In atmospheric conditions, corrosion begins at Zn-rich zones which are preferentially attacked because of their lower potential. Aluminum-rich matrix corrodes when Zn dendrites are consumed.

Al_2O_3 is the only crystalline corrosion product at the coating surface detected before atmospheric exposure. Xian Zhang et al. [53] observed that Zn is preferentially dissolved during the first year of natural exposure. The effect of Mg alloying on the nature and morphology of corrosion products formed on Galvalume® coating (Zn-55Al-1.6Si) were investigated by Shiwei Li et al. [19]. This work demonstrated that the presence of more than 1.5 wt. % of Mg

refined the corrosion products morphology and this modification correlated with the formation of simonkolleite (Figure 14).

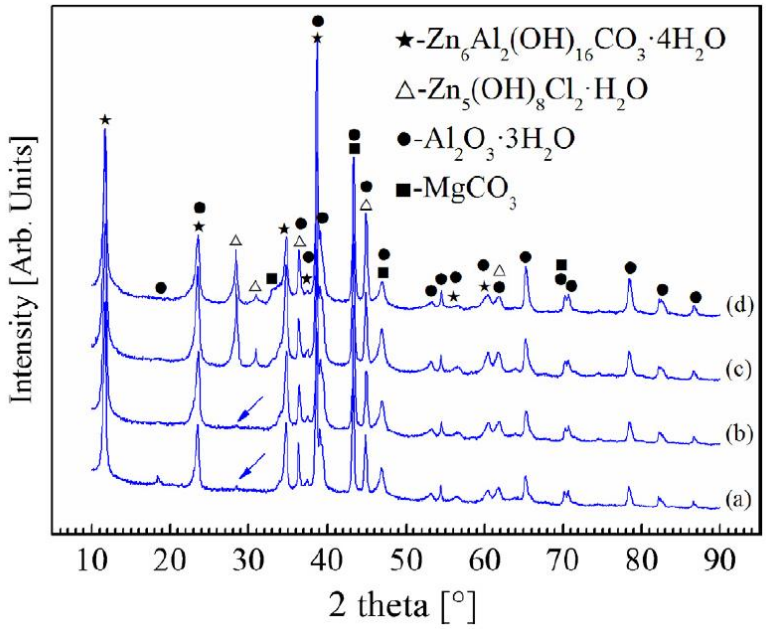


Figure 14 : XRD spectra of different corrosion products collected from the surface of the corroded coatings after 168 h exposure to NSS test according toEN ISO 9227: (a) Galvalume® coating, (b) G–0.5Mg coating, (c) G–1.5Mg coating, (d) G–2.5Mg coating (from [19]).

The authors also concluded that corrosion products on Zn-Al based coatings seem to be Al oxides, Mg carbonates and complex layered double hydroxides and that gradual covering of Al_2O_3 by Zn scales identified by X-ray diffraction as layered double hydroxides improves barrier protection.

This work also demonstrated that despite its lower corrosion potential, the selective dissolution of Zn_2Mg phase is less pronounced than the selective dissolution of Al(Zn) dendrites in Galvalume® and the authors explained it by the morphology and the nature of the formed corrosion products (Figure 15).

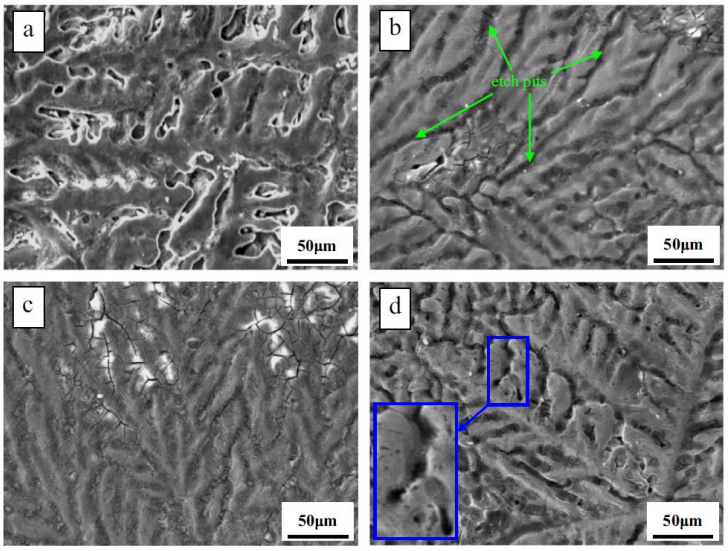


Figure 15 : Morphologies of different corroded coating surfaces after dissolving corrosion products with 10wt. % ammonium persulphate solution: (a) Galvalume coating, (b) G– 0.5Mg coating, (c) G–1.5Mg coating and (d) G–2.5Mg coating (from [19]). etc.

After the removal of corrosion products, all Zn rich interdendrites appeared attacked and selectively dissolved (Figure 15a), and Zn_2Mg interdendrites were less attacked while the matrix was also attacked. Finally, the authors concluded that the corrosion type of Galvalume® coating can be considered as localized corrosion, while that of Galvalume®–1.5Mg coating can be considered as uniform corrosion [19]. The corrosion potential of AlSiMg coating was however close to the corrosion potential of bare steel. It is hence expected to offer significantly less galvanic protection than zinc based coating.

5.3 Corrosion products on Zn-rich coatings

Sections 5.1 and 5.2 introduced the importance of corrosion products for barrier protection. Deeper understanding of the effect of corrosion products which could be formed in presence of Zn and Mg is hence of interest. Steelmakers are now investigating Al based coating with alloying elements as Zn or Mg. Corrosion products on zinc-based coatings are well documented [54,55]. These platelet can form and then be transformed during ageing in humid or dry conditions, as in the example of $Zn_5(OH)_8Cl_2$ (simonkolleite) initially formed in the presence of Cl-anions (reaction (4), but transformed in zinc carbonates, hydroxycarbonates and oxides (reactions (5) et (6)) for longer corrosion times [54].

$$5Zn^{2+} + 8OH^- + 2Cl^- = Zn_5[(OH)_8Cl_2] \quad OH:Zn = 8:5 = 1.6 \tag{4}$$

$$Zn_5(OH)_8Cl_2 + 5HCO_3^- = 5ZnCO_3 + 5H_2O + 3OH^- + 2Cl^- \quad \text{(acid pH)}$$

$$Zn_5(OH)_8Cl_2 + 2HCO_3^- = Zn_5(CO_3)_2(OH)_6 + 2H_2O + 2Cl^- \quad \text{(neutral and basic pH)} \tag{5}$$

$$Zn_5(CO_3)_2(OH)_6 = 5ZnO + 2CO_2 + 3H_2O \tag{6}$$

Environmental conditions, as pH or presence of specific pollutants, influence the morphology and the composition of corrosion products (see an example in (Figure 16 from. [54]).

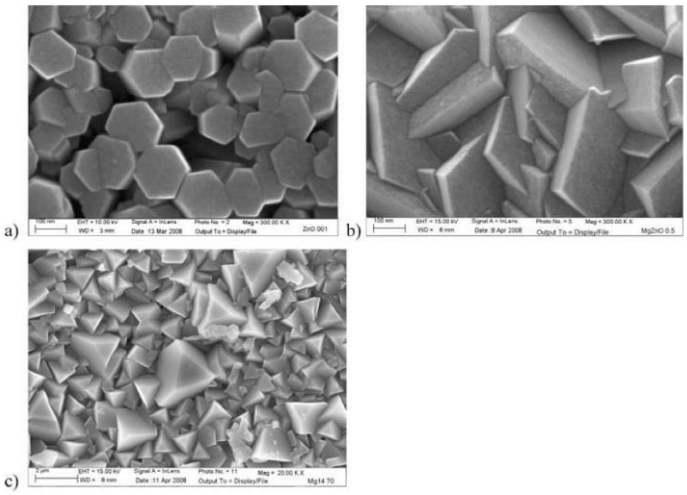


Figure 16 : Typical morphology (SEM–FEG) of ZnO electrodeposited from the solution in absence (a) and in presence (b) Mg^{2+} in comparison with the morphology of ZnO formed by the corrosion of Zn–Mg coating after 70 cycles of ECC1 test (c) (from [54)].

A series of works of J. D. Yoo et al. [56-58] demonstrated the effect of zinc basic salts (zinc hydroxyl chloride, zinc hydroxycarbonate, zinc hydroxyl sulphate…) on the cathodic and anodic reactivity of underlying Zn and carbon steel and the role of the environment evolution during corrosion for the stability of the barrier effect.

***

An ideal metallic coating should not only offer a sacrificial protection to the substrate, but also have reduced corrosion consumption rate still maintaining the minimum reactivity. This could be achieved if not completely passivating but protective and stable corrosion products are formed on the surface.

In AlZnMg containing systems, two types of corrosion products are often considered: basic zinc salts and layered double hydroxides (LDH). The next section will detail some properties of LDH relevant to anticorrosion protection.

6 Layered double hydroxides

6.1 Definition and structure

LDH are materials with a general formula $[M(II)_{1-x} M(III)_x (OH)_2]^{x+}(Y^{n-})_{x/n} \cdot yH_2O$ where M(II) and M(III) represent respectively divalent and trivalent metals (which in case of corrosion products come from the coating or from the corrosive environment) and Y^{n-} is an anion between the layers coming from the corrosive environment [59]. Their structure is composed of positively charged metal hydroxide layers and interlayer anions (Figure 17).

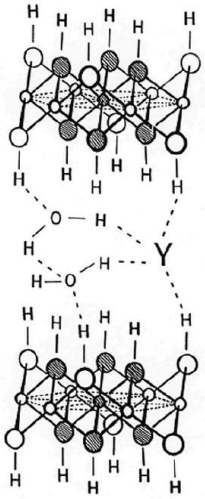


Figure 17: Theory scheme of LDH structure (from [59])

In LDH materials, divalent metals can be Mg^{2+}, Ca^{2+}, Zn^{2+}, Co^{2+}, Cu^{2+}, etc.; trivalent metals can be Al^{3+}, Cr^{3+}, Co^{3+}, Fe^{3+}, Mn^{3+}. Many anions can be used, including Cl^-, NO_3^-, CO_3^-. So, these corrosion products can be formed in conventional salt spray industrial tests.

LDH can form platelet shaped particles in an adherent product covering the surface

6.2 Air permeability through precipitated Al- Zn –Mg LDHs

To study barrier effect for air permeability, synthetic corrosion products can be obtained by precipitation. This approach was used in series of works of Ishikawa and co-workers [60]. The authors mixed $ZnCl_2$, $AlCl_3$ and $MgCl_2$ in different ratios and precipitated different LDH

by pH increase. The morphology of the formed products varied in function of the cation composition and mixed metal hydroxide chlorides were formed in the presence of Al and Zn. The addition of Mg improved their compactness and decreased the air permeability through them (Figure 17). The authors concluded that AlZnMg LDH are the most stable and protective corrosion products formed around pH 9. They proposed that the platelets morphology typical for LDH is in the origin of their better barrier effect than the effect to agglomerates (ZnO) or spherical fine particles ($Al(OH)_3$, AlOOH and $Mg(OH)_2$).

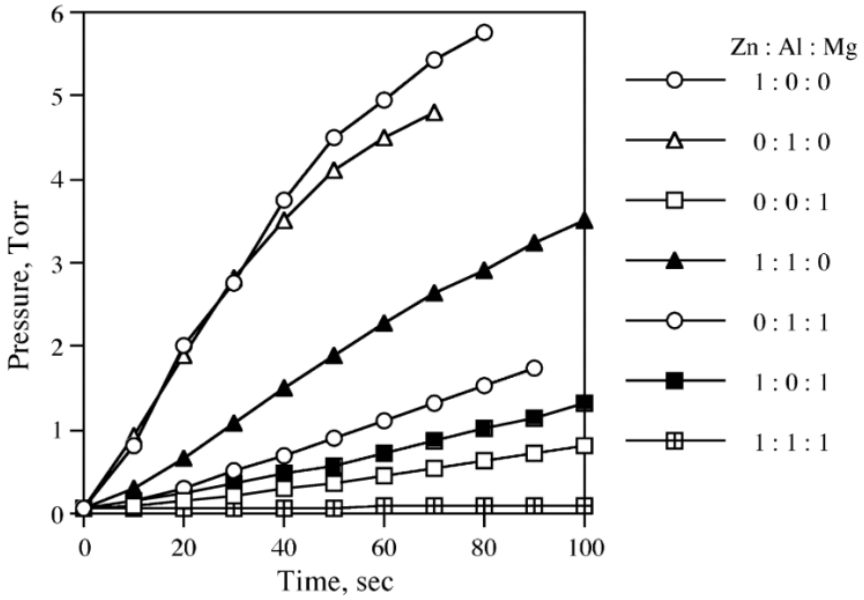


Figure 17 : Graph of permeability test on different corrosion products. (from [60])

Several mechanisms explaining anticorrosion action of LDH were found in the literature:

Tatsuo Ishikawa and al. [60] argued in terms of barrier effect: finer the LDH particles are lower air diffusion to the substrate. If the oxygen from the air cannot access the metal surface, oxygen reduction cannot occur and the corrosion reaction stops.

Fen Zhang et al. [46] explained the protective effect of LDH on MgAl alloys by the preferential Cl^- absorption in the LDH via exchange with carbonate ions and precipitation of stable carbonate containing corrosion products blocking the pits. This mechanism however should be criticized because it is known that carbonate containing LDH are the most stable and it is known that many anions are exchanged with carbonates in order to form carbonate containing LDHs and releasing other anions [61]. The idea of the ion exchange is however important and the Cl- ions could be exchanged with OH- anions.

***

To conclude, depending on the exposure conditions, different corrosion products can be formed on Al-based coatings. It was shown that LDH and basic zinc salts can reduce corrosion rates by blocking oxygen diffusion to the metallic surface. In case of Zn/Mg-Al LDH, addition of Mg seems to refine the LDH crystal size which is interpreted as improvement of the barrier effect.

7 Conclusions of Chapter 1

Al-based coatings for steel are important materials but passivation of Al makes sacrificial protection of the underlying steel substrate insufficient. At the same time, passive film promotes pitting corrosion of the coating. Literature shows that aluminum corrosion is governed by three main factors:

- Defects (cracks, intermetallic phases etc.) are preferential sites for pit initiation.
- Solution composition, namely local pH and presence of halide ions in the electrolyte, which promote pitting corrosion locally destabilizing the passive layer.
- Composition and properties of corrosion products.

The use of some low alloying elements as activators (In, Ga, Hg or Sn) can be interesting for activation of Al anodes. The control of the concentration of the activator is critical to obtain good performances. It is not easy to control in industrial process where four elements are already present. Moreover, these elements have significantly lower melting temperature than Al and there is a risk of their uncontrolled diffusion and redistribution during hot stamping process. Also, corrosion rates in the presence of activators is often very high because in this system the anode could be replaced. In automotive coatings the replacement is impossible and reasonable limitation of corrosion rate is very important.

To activate aluminum, several alloying elements can be used. Zn and Mg alloying makes Al far more active than pure aluminum. Magnesium can also form intermetallic phases such as Mg_2Si or Zn_2Mg, which are strongly anodic vs Al. The corrosion potential of Zn_2Mg is less sensitive to pH variation in chloride media than the Al potential and stays sacrificial in most of corrosive environments. Addition of Mg in a system which already contains Si can potentially reduce the cathodic effect of Si by creating anodic Mg_2Si. It seems also that the presence of Mg ions can significantly modify the nature and the morphology of corrosion products on Al and Zn alloys.

Some mechanisms were proposed to explain the positive effect of Mg on the corrosion resistance of AlSiZnMg coatings with high Zn content, but lower Zn and Mg fractions can modify the nature and distribution of the phases in the microstructure and corrosion resistance of the coatings. They essentially considered the effect of corrosion products like LDH but did not detail the conditions of their formation, their stability and their effect on the substrate reactivity. The effect of the alloy composition on the LDH morphology and their effectiveness was also unexplored.

To conclude, for AlSi(Zn,Mg) coatings for steel the literature let suppose the formation of several new phases: Al matrix can be modified by formation of AlZn and/or AlMg solid solution, some intermetallic phases (Zn_2Mg, Mg_2Si, AlFeSi) could appear. The literature cannot however predict their real appearance, morphology and spatial distribution, as well as the resulting anticorrosion behavior of new coatings. In the experimental work of the PhD thesis we would like to response on these questions which stays open after the literature review:

- How Zn and Mg alloying modifies AlSi coatings microstructure? What phases are really formed?
- How these new coatings microstructure behave in accelerated corrosion test? Which phases preferentially corrode? What corrosion products are formed?
- How the electrochemical properties of the pure phases present in AlSiZnMg coatings can explain corrosion mechanisms? What are the possible beneficial or detrimental coupling between the phases?
- How corrosion products impact coatings reactivity and corrosion mechanisms with advancement of corrosion?

References

[1] Nicolas Rouet, Galvanized steel sheet in an automotive sector as a barometer of Zinc market growth, Presentation, Metal Bulletin - 18th Zinc & its Markets Seminar, Lisbon, October 23, 2014.

[2] Marcele Salgueiro Azevedo, Mécanismes de corrosion de l'acier revêtu d'alliage à base de ZnMgAl en tests accélérés et en environnement naturel, PhD, Chimie inorganique. Université Pierre et Marie Curie - Paris VI, 2014. Français.

[3] User manual, Metallic coated steel, ArcelorMittal Flat Carbon Europe 19, avenue de la Liberté L-2930 Luxembourg.

[4] S.Caporali, A.Fossati, A.Lavacchi, I.Perissi, A.Tolstogouzov, U.Bardi, Aluminium Electroplated from Ionic Liquids as Protective Coating against Steel Corrosion, Corrosion Science 50.2 (2008), pp. 534–539.

[5] O.A.Fasuba, A.Yerokhin, A.Matthews, A.Leyland, Corrosion Behaviour and Galvanic Coupling with Steel of Al-Based Coating Alternatives to Electroplated Cadmium, Materials Chemistry and Physics 141.1 (2013), pp. 128–137.

[6] S.Han, H.LI, S.Wang, L.Jiang, X.Liu, Influence of Silicon on Hot-Dip Aluminizing Process and Subsequent Oxidation for Preparing Hydrogen/tritium Permeation Barrier, International Journal of Hydrogen Energy 35.7 (2010), pp. 2689–2693.

[7] Q.X.Liu, S.Z.ElAbedin, F.Endres, Electroplating of Mild Steel by Aluminium in a First Generation Ionic Liquid: A Green Alternative to Commercial Al-Plating in Organic Solvents, Surface and Coatings Technology 201.3–4 (2006), pp. 1352–1356.

[8] Y.Du, J.Schuster, Z.Liu, R.Hu, P.Nash, W.Sun, W.Zhang, J.Wang, C.Tang, Z.Zhu, S.Liu, Y.Ouyang, W.Zhang, N.Krendelsberger, A Thermodynamic Description of the Al–Fe–Si System over the Whole Composition and Temperature Ranges via a Hybrid Approach of CALPHAD and Key Experiments, Intermetallics 16.4 (2008), pp. 554–570.

[9] N.Takata, M.Nishimoto, S.Kobayashi, M.Takeyama , Morphology and Formation of Fe–Al Intermetallic Layers on Iron Hot-Dipped in Al–Mg–Si Alloy Melt, Intermetallics 54 (2014), pp. 136–142.

[10] S.Milenkovic, V.Dalbert, R.Marinkovic, A.W.Hassel, Selective matrix dissolution in an Al–Si eutectic, Volume 51, Issue 7 (2009), pp. 1490–1495.

[11] H.Karbasian, A.ETekkaya, A Review on Hot Stamping, Journal of Materials Processing Technology 210.15 (2010), pp. 2103–2118.

[12] C.Allely, L.Dosdat, O.Clauzeau, K.Ogle, P.Volovitch, Anticorrosion Mechanisms of Aluminized Steel for Hot Stamping, Surface and Coatings Technology 238 (2014), pp.188–196.

[13] N.Birbilis, RG.Buchheit, Electrochemical Characteristics of Intermetallic Phases in Aluminum Alloys, Journal of The Electrochemical Society 152.4 (2005), pp. 140–B151.

[14] F.Andreatta, Local Electrochemical Behaviour of 7xxx Aluminium Alloys, PhD, Applied Sciences, 2004.

[15] X. Li, X. Nie, L. Wang, D.O. Northwood, Corrosion protection properties of anodic oxide coatings on an Al–Si alloy, Surface & Coatings Technology 200 (2005) pp. 1994 – 2000

[16] WH.Hartt, EJ.Lemieux, KE.Lucas, A Critical Review of Aluminum Anode Activation, Dissolution Mechanisms, and Performance, NACE International, CORROSION (2001).

[17] DR.Salinas, SG.Garcia, JB.Bessone, Influence of Alloying Elements and Microstructure on Aluminium Sacrificial Anode Performance: Case of Al–Zn, Journal of Applied Electrochemistry 29.9 (1999), pp. 1063–1071.

[18] N.Idusuyi, OO.Oluwole, Aluminum Anode Activation Reasearch – A review, International Journal of Science and Technology, Volume2 N°8 (2012), pp. 561-566.

[19] S.Li, B.Gao, G.Tu, L.Hu, S.Sun, G.Zhu, S.Yin, Effects of Magnesium on the Microstructure and Corrosion Resistance of Zn–55Al–1.6Si Coating, Construction and Building Materials 71 (2014), pp. 124–131.

[20] W.Liu, M.Li, Q.Luo, H.Fan, J.Zhang, H.Lu, K.Chou, X.Wang, Q.Li, Influence of alloyed magnesium on the microstructure and long-term corrosion behavior of hot-dip Al–Zn–Si coating in NaCl solution, Corrosion Science Volume 104 (2016), pp. 217–226.

[21] Q.Li, YZ.Zhao, Q.Luo, SL.Chen, JY.Zhang, KC.Chou, Experimental study and phase diagram calculation in Al–Zn–Mg–Si quaternary system, Journal of Alloys and Compounds 501, (2010), pp. 282–290.

[22] D.Pradhan, M.Manna, M.Dutta, Al–Mg–Mn Alloy Coating on Steel with Superior Corrosion Behavior, Surface and Coatings Technology 258 (2014), pp. 405–414.

[23] Y.Kyo, AP.Yadav, A.Nishikata, T.Tsuru, Hydrogen entry behaviour of newly developed Al–Mg–Si coating produced by physical vapour deposition, Corrosion Science 53, (2011), pp. 3043–3047.

[24] A.Perez, A.Billard, C.Rébéré, C.Berziou, S.Touzain, J.Creus, Influence of metallurgical states on the corrosion behaviour of Al–Zn PVD coatings in saline solution, Corrosion Science 74, (2013), pp. 240–249.

[25] Y.Prieto, Etude Comparative Du Comportement électrochimique Des Alliages D'aluminium 2024 T351 et 7075 T7351 En Milieu Neutre de Sulfate de Sodium, PhD Thesis, 2012.

[26] D.Landolt, Corrosion et chimie de surfaces des métaux, PPUR presses polytechniques, Vol. 1 (1997), Traités des matériaux 12.

[27] AJ.Bard, R.Parsons, J.Jordan, Standard Potentials in Aqueous Solution. Edited by autor, CRC Press, 1985.

[28] M. Reboul, Corrosion Des Alliages D'aluminium, Techniques de l'Ingénieur, COR325 (2005).

[29] C.Vargel, Corrosion of Aluminium, Elsevier (2004) pp. 81–109.

[30] M.Reboul, La Corrosion de L 'Aluminium et de Ses Alliages, Lecture, (2014).

[31] Z.Szklarska-Smialowska, Pitting Corrosion of Aluminum, Corrosion Science 41.9 (1999), pp. 1743–1767.

[32] A,Zazou, N. Azzouz, An Investigation on the Use of Indium to Increase Dissolution of AlZn Anodes in Sea Water, Materials & Design 29.4 (2008) pp. 806–810.

[33] I.Gurrappa, Cathodic Protection of Cooling Water Systems and Selection of Appropriate Materials, Journal of Materials Processing Technology 166.2 (2005), pp. 256–267.

[34] AG.Muñoz, SB.Saidman, JB.Bessone, Corrosion of an Al–Zn–In Alloy in Chloride Media, Corrosion Science 44.10 (2002), pp. 2171–2182.

[35] JB.Bessone, The Activation of Aluminium by Mercury Ions in Non-Aggressive Media, Corrosion Science 48.12 (2006), pp. 4243–4256.

[36] SMA.Shibli, VS. Gireesh, Activation of Aluminium Alloy Sacrificial Anodes by Selenium, Corrosion Science 47.8 (2005), pp. 2091–2097.

[37] DO.Flamini, SB.Saidman, JB.Bessone, Aluminium Activation Produced by Gallium, Corrosion Science 48.6 (2006), pp. 1413–1425.

[38] NL.Sukiman, AE.Hughes, GE.Thompson, JMC.Mol, Durability and Corrosion of Aluminium and Its Alloys: Overview, Property Space, Techniques and Developments. InTech (2012).

[39] H.Ezuber, A.El-Houd, F.El-Shawesh, A Study on the Corrosion Behavior of Aluminum Alloys in Seawater, Materials & Design 29.4 (2008), pp. 801–805.

[40] N Birbilis, RG Buchheit, Electrochemical characteristics of intermetallic phases in aluminum alloys an experimental survey and discussion, Journal of The Electrochemical Society, 152 (4), pp. 140-B151

[41] N Birbilis, RG Buchheit, Investigation and discussion of characteristics for intermetallic phases common to aluminum alloys as a function of solution pH, Journal of The Electrochemical Society 155 (3), pp. 117-126.

[42] R.Ambat, AJ.Davenport, GM.Scamans, A.Afseth, Effect of Iron-Containing Intermetallic Particles on the Corrosion Behaviour of Aluminium, Corrosion Science 48.11 (2006), pp. 3455–3471.

[43] C.Allely, T. Machado, C.Klam, Séminaire Optigal, Maizières Les Metz, (2015).

[44] J. Han, K. Ogle, Dealloying of MgZn2 Intermetallic in Slightly Alkaline Chloride Electrolyte and Its Significance in Corrosion Resistance, Journal of The Electrochemical Society 164 (14) (2017), C952-C961

[45] Hausbrand R. Hausbrand, M. Rohwerder, M. Stratmann, C. Schwerdt, B. Schuhmacher, and G. Grundmeier, Model Study on the Corrosion of Magnesium-Containing Zinc Coatings on Steel Sheets, in Galvatech, International Conference on zinc and zinc ally coated steel sheet, 2001, no. 5, pp. 161–167.

[46] F.ZENG, Z.WEI, C.LI, X.TAN, Z.ZHANG, Corrosion Mechanism Associated with Mg2Si and Si Particles in Al–Mg–Si Alloys, Transactions of Nonferrous Metals Society of China 21.12 (2011), pp. 2559–2567.

[47] AQ.Vu, B.Vuillemin, R.Oltra, C Allély, In Situ Investigation of Sacrificial Behaviour of Hot Dipped AlSi Coating in Sulphate and Chloride Solutions, Corrosion Science 70 (2013), pp. 112–118.

[48] HD.Manesh, AK.Taheri, Bond Strength and Formability of an Aluminum-Clad Steel Sheet, Journal of Alloys and Compounds 361.1–2 (2003), pp. 138–143.

[49] O. Gharbi, N. Birbilis, Clarifying the Dissolution Mechanisms and Electrochemistry of Mg2Si as a Function of Solution pH, Journal of The Electrochemical Society 165 (9) (2018), C497-C501.

[50] P.Volovitch, L.Barrallier, W.Saikaly, Microstructure and Corrosion Resistance of Magnesium Alloy ZE41 with Laser Surface Cladding by Al–Si Powder, Surface and Coatings Technology 202.20 (2008), pp. 4901–4914.

[51] I.4eGraeve, I.Schoukens, A.Lanzutti, F.Andreatta, A.Alvarez-Pampliega, J.DeStrycker, L.Fedrizzi, H.Terryn, Mechanism of Corrosion Protection of Hot-Dip Aluminium–silicon Coatings on Steel Studied by Electrochemical Depth Profiling, Corrosion Science 76 (2013), pp. 325–336.

[52] JC.Zoccola, HE.Townsend, AR.Borzillo, JB.Horton, Atmospheric Corrosion Behavior of Aluminum-Zinc Alloy-Coated Steel (1978).

[53] X.Zhang, T.Vu, P.Volovitch, C.Leygraf, K.Ogle, I.OdnevallWallinder,The Initial Release of Zinc and Aluminum from Non-Treated Galvalume and the Formation of Corrosion Products in Chloride Containing Media, Applied Surface Science 258.10 (2012), pp. 4351–4359.

[54] P.Volovitch, C.Allely, K.Ogle, Understanding Corrosion via Corrosion Product Characterization: I. Case Study of the Role of Mg Alloying in Zn–Mg Coating on Steel, Corrosion Science 51.6 (2009), pp. 1251–1262.

[55] C.Leygraf, I.O. Wallinder, J.Tidblad, T.Gredel, Atmospheric Corrosion, Book, John Wiley & Sons, 2016.

[56] J.D. Yoo, P. Volovitch, A.A. Aal, C. Allely, K. Ogle "The effect of an artificially synthesized simonkolleite layer on the corrosion of electrogalvanized steel" Corrosion Science 70 (2013), pp. 1-10

[57] J.D. Yoo, K. Ogle, P. Volovitch "The effect of synthetic zinc corrosion products on corrosion of electrogalvanized steel: I. Cathodic reactivity under zinc corrosion products" Corrosion Science 81 (2014), pp. 11-20.

[58] J.D. Yoo, K. Ogle, P. Volovitch "The effect of synthetic zinc corrosion products on corrosion of electrogalvanized steel. II. Zinc reactivity and galvanic coupling zinc/steel in presence of zinc corrosion products" Corrosion Science 83 (2014), pp. 32-37

[59] PS Braterman, Layered Double Hydroxides: Synthesis, Characterization and Interaction of Mg-Al Systems with Intercalated Tetracyanonickelate (II), Master of Science. University of North Texas, (2004).

[60] T.Ishikawa, M.Ueda, K.Kandori, T.Nakayama, Air Permeability of the Artificially Synthesized Zn–Al–Mg Alloy Rusts, Corrosion Science 49.6 (2007), pp. 2547–2556.

[61] X.Duan, Xue, and G.D Evans. Layered Double Hydroxides, book, Springer Science & Business Media, 2006.

Chapter II

Experimental

Chapter II – Experimental

Based on the literature review presented in Chapter I – State of the art, different techniques were identified for investigation of corrosion mechanism of aluminum-based protective coatings for steel. Accelerated corrosion tests following industrial automotive standards were performed in order to evaluate the effect of alloying on the corrosion resistance and corrosion mechanisms. Lixiviated electrolytes and insoluble corrosion products were collected, solubilized and analyzed by Inductive Coupled Plasma Optical Emission Spectrometry (ICP-OES) to realize material balance. This technique was used to check the coating's elemental compositions and to investigate selective dissolution of the phases composing them. Scanning Electronic Microscopy (SEM) and Energy Dispersive Spectroscopy (EDS) were applied to observe the morphology and the distribution of metallic phases and corrosion products on initial and corroded surfaces. Electrochemical experiments were performed for model coatings with and without corrosion products but also for pure phases and possible galvanic coupling. Corrosion products were identified by XRD, Raman and ATR spectroscopy. Scanning Vibrating Electrode Technique (SVET) and local and global electrochemical impedance techniques were used to estimate effect of corrosion products on coating reactivity.

The objective of this chapter is to give an overview of materials and techniques used in this work. The reason of their use and the limitations of such techniques will be explained. Details and specific parameters of measurements are given in the experimental section of the respective result chapters.

1 Materials

Model coatings used in this work were produced by ArcelorMittal on pilot line. AlSi(ZnMg) coated steel were studied in a range of 0-9 % of Si, 0 to 30 wt. % of Zn, 0 to 10 wt. % of Mg and aluminum to reach balance. Samples were prepared by industrial hot dip process (Appendix 1) based on AluSi© coating described in the US 6296805 B1 patent [1]. The AluSi© coatings with 9 wt. % of Si on 22MnB5 steel were used as a reference material.

Phases identified in model coatings microstructure are listed in the Tab. 1. Pure metals were supplied by Goodfellow and the other phases were synthesized in partnership with the University of Chemistry and Technology of Prague in Czech Republic (UTC). Details on the fabrication process are given in Chapter IV.

Table 1 : Phases weight composition and suppliers.

Phases	Composition / wt. %	Supplier
Al	~ 100(Al)	GoodFellow
Al(Zn)	-	UCT Prague
Fe	~ 100(Fe)	GoodFellow
Si	~ 100(Si)	Goodfellow
Al3FeSi2	73(Al) 9(Fe) 18(Si)	UCT Prague
Zn2Mg	84(Zn) 16(Mg)	UCT Prague
Mg2Si	68(Mg) 32(Si)	UCT Prague
SiO2	NA	Goodfellow + post treatment

2 Accelerated corrosion tests

Different kinds of tests are used in automotive industry to evaluate coatings corrosion resistance [2-7]. Those tests are divided in two main families: natural exposures and accelerated corrosion tests. In field exposure, samples are set on outdoors racks. Environments are classified following their type (Industrial, Marine, Rural, Urban) [6-7] and corrosivity (From C1 to CX) [8]. These tests require however long time to be completed. In order to faster obtain results and for a quality control, laboratory accelerated tests have been designed.

In accelerated tests samples are placed in climatic chambers (Appendix 2). Temperature, humidity and atmosphere are regulated and solution spray or fog (continuous or intermittent) are often used. The most common spray/fog used in those tests is 1-5 wt. % NaCl aqueous solution which corresponds to severe corrosive conditions encountered on roads with de-icing salt during winter. Others electrolytes can be used to test other corrosive media or simulate other conditions [3-5]. Parameters variations are generally set up in cycles varying from several days to several weeks and cycles can be repeated as much as desired (often stopped when red rust reaches a given surface ratio). The simplest corrosion test is the Salt Spray Test (SST), it consists in exposure with a continuous 5 wt. % NaCl aqueous solution fog at 35°C and neutral pH.

In this work, the accelerated corrosion test follows the VDA 233-102 [7] standard (also called NewVDA or N-VDA in the literature). N-VDA cycle lasts one week and its conditions are detailed in Fig 1.

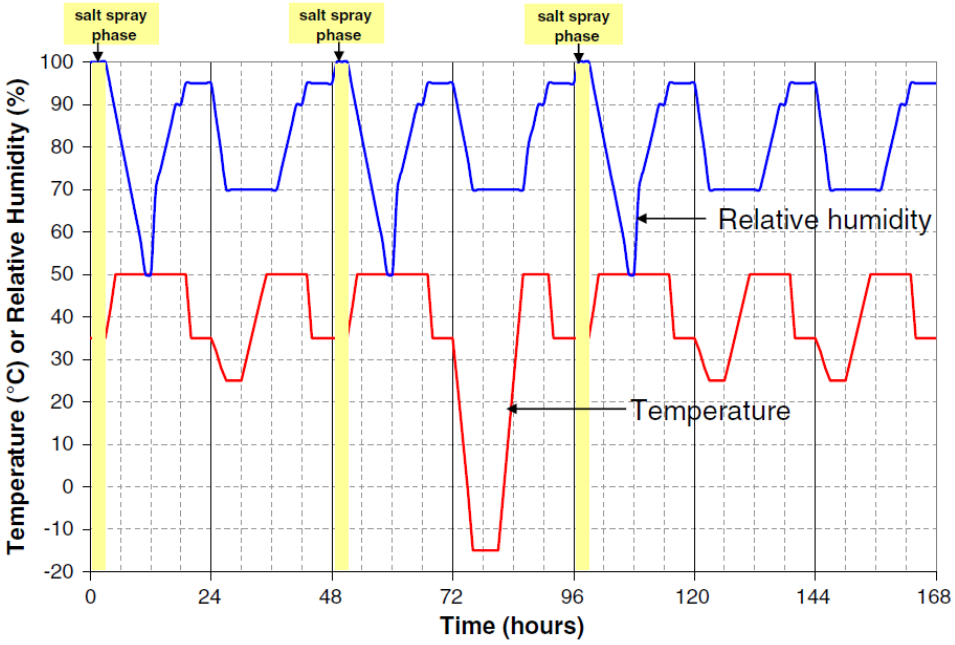


Figure 1 : Temperature and humidity variation during a one-week single cycle of the VDA 233-102 test. (from [7])

General corrosion resistance is tested using a full panel, to evaluate corrosion rate and barrier properties of the coatings samples are kept in corrosive environment and their mass is regularly measure. The evolution of the mass during corrosion test gives information on the dissolution or the precipitation of corrosion products on the samples. After the test corrosion products can be removed by dissolution and the final mass loss of the coating can be calculated. Sacrificial power is tested with scratched samples, in which coating is voluntary damaged by a clean scratch going down to steel or by shot peening. Samples are used to test adherence or delamination encountered with some coatings.

3 Corrosion product removal and dissolution rates determination

To calculate global mass loss and analyze corrosion products composition corrosion products are removed at the end of corrosion tests. After corrosion products dissolution, average dissolution rates are determined using the following equation [9]:

$$v_{corr} = \frac{\Delta m}{A \, .t} \qquad \textbf{(1)}$$

Here v_{corr} is the corrosion rate (µg.cm^{-2}.day^{-1}), Δm is the mass loss of the corresponding element (µg) during the corrosion test, A is the exposed surface (cm^{-2}) and t is the exposure time (fixed time unit). This calculation can be made on the global mass loss, on soluble and insoluble corrosion products depending on Δm determination and the analysis level. This value however is representative only in case of homogeneous corrosion. For local corrosion the pit depth can be more critical than the mass loss.

In order to obtain elemental dissolution rates, leachates collected during corrosion tests are analyzed by ICP OES. Remaining corrosion products are dissolved following a modified ISO 8407 [10] norm then also analyzed by ICP OES. ISO 8407 is set for zinc and zinc alloys corrosion products dissolution and not for aluminum based coatings. To adapt the procedure for Al corrosion products, the 250 g/L glycine aqueous solution used in ISO 8407 was replaced by 65 % nitric acid aqueous solution which is accurate to dissolve Al-based corrosion products. Corroded samples where immerged in nitric acid for 2-10 minutes depending on corrosion damage, in an ultrasonic bath at room temperature (20-25°C).

4 Phases identification

Different characterization techniques were used to obtain complementary information. Scanning Electronic Microscopy (SEM) coupled with EDS, Energy Dispersive Spectroscopy [11,12] was used to verify the presence or absence of corrosion products and check the surface state as well as to obtain a first idea of the elemental composition of the observed phase or product. For semi quantitative elemental analysis, 15 keV acceleration tension was used. In order to reduce electronic interaction volume EDS measurement were also made at 5keV. Depth penetration of electrons (R) can be calculated with Kanaya-Okayama formula [13] (obtained from Bethe formula [14]):

$$R = \frac{0.0276 \, A \, E_0^n}{(Z^{0.89} \, \rho)} \qquad \textbf{(2)}$$

where R is the penetration depth, A is the atomic weight (g/mole), n is a constant (=1.68), E_0 is the electron beam energy (keV), Z is the atomic number and ρ is the density $(g/cm)^2$. This equation applied to pure aluminum gives R ~ 2.4 µm at 15 keV and R ~ 400 nm at 5keV. Attain a 400 nm depth penetration is adequate when oxides formed at the coatings surface are often under 1 µm scale.

XRD was used to identity metallic phases and crystalline corrosion products at the coatings surface. In this study XRD was directly made on uncorroded and corroded coatings. In the case of corroded coatings, the XRD spectra analysis requires to differentiate the signal of corrosion products from the substrate peaks which can be difficult for multiphasic metallic coatings [15,16].

Raman and Infra-Red spectroscopy were used as complementary techniques to XRD to verify XRD interpretation, identify amorphous species and give information about their spatial distribution.

5 Inductive Coupled Plasma Optical Emission Spectrometry (ICP-OES) and Atomic Emission SpectroElectroChemistry (AESEC).

ICP-OES is used in this work to identify elemental composition of leaking electrolytes and dissolved corrosion products, during and after accelerated corrosion tests. Some experiments were made using a coupling of ICP-OES an electrochemical flow cell so called AESEC [17-20] in which the electrolyte volume is limited and pumped continuously in an ICP-OES. Appendix 3 gives the general scheme of AESEC. The polychromator of AESEC will give intensity of characteristic emission peaks of the element in the solution injected in the plasma. With standard solution the experiment can be calibrated to give real-time concentration (C_M) of the flowing electrolyte. Knowing the flow rate (f) and the exposed surface (A), elemental flux (v_M) can be calulated as following:

$$v_M = C_M f / A \quad \textbf{(3)}$$

Considering the dissolution equation of the metallic elements ($Me \rightarrow Me^{n+} + ne^-$) we can calculate elemental current (j_M) as following:

$$j_M = n F v_M \quad \textbf{(4)}$$

where (F) is Faraday constant.

The aim of the AESEC is to continuously analyze elemental dissolution occurring in the electrochemical flow cell. In this way we can investigate selective dissolution from the coating or pure phases in varying electrochemical (imposed current or potential) or chemical (change of pH or anionic content) conditions.

6 Electrochemical experiments

6.1 Potentiodynamic polarization

Electrochemical experiments as Open Circuit Potential (OCP) and polarization measurements were done in a classic thermostatic (25°C) three electrode cell (Appendix 4). Samples were used as working electrodes, the reference was a Saturated Calomel Electrode, and the counter electrode was a platinum wire. In case of coupling experiments, working and counter electrodes were two different pure phases.
Precise description of the used electrochemical sequence is given in the experimental section of each part chapter of this manuscript.

6.2 Local electrochemical technics: Scanning Vibrating Electrode Technics (SVET) and Local Electrochemical Impedance Mapping (LEIM)

SVET (Figure 2) and LEIM (Figure 3) are local electrochemical techniques used in this work to appreciate local surface reactivity's evolution impacted by corrosion and corrosion products formation. Local Electrochemical Impedance Spectroscopy (LEIS) and Local Electrochemical Impedance Mapping (LEIM) [21,22] normal set up is composed of a potentiostate coupled with a lock-in amplifier. A three-electrode configuration is used with a metallic sample as working electrode, a Ag/AgCl electrode as reference and a platinum wire as counter electrode. Impedance measurement are done with a homemade local probe composed of two Ag wires of 250 µm diameter. The probe is positioned at 150±25 µm above the working electrode (WE) and scan the surface.

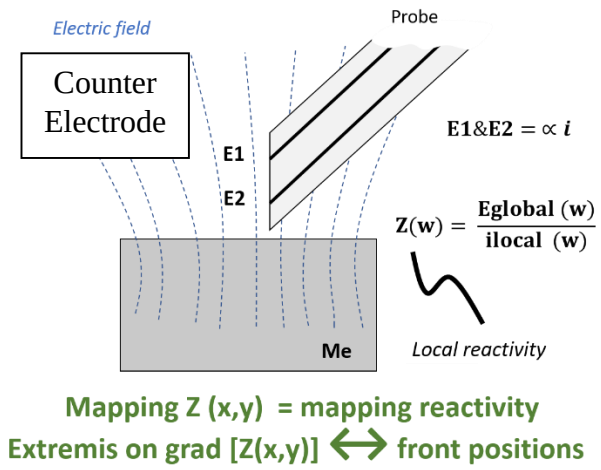


Figure 2 : Local Electrochemical Impedance Spectroscopy (LEIS) explanatory diagram.

This technique gives the same results as Electrochemical Impedance Spectroscopy (EIS) but the scanned area is of 300x300 µm². Local current density component normal to the WE surface ($\boldsymbol{i_{loc}(r)}$) is calculated from the potential difference sensed between the two Ag wires composing the probe:

$$\boldsymbol{i_{loc}(r)} = \frac{\boldsymbol{(E1-E2)\sigma_s}}{\boldsymbol{d}} \quad (5)$$

where $\left(\varphi_1(r) - \varphi_2(r)\right)$ is the potential difference between the two microelectrodes and *d* is the distance between two Ag wires center. The local impedance was defined as:

$$\boldsymbol{z(r)} = \frac{\boldsymbol{V-\Phi_{ref}}}{\boldsymbol{i_{loc}(r)}} \quad (6)$$

where $V - \Phi_{ref}$ represents the potential difference between the working electrode (WE) and the reference electrode (RE) in the solution.

Scanning Vibrating Electrode Technique (SVET) [23] consists of a metallic sample immerged in an electrolyte with a scanning vibratring electrode which measure potential difference induced by current lines (electric field) in the electrolyte.

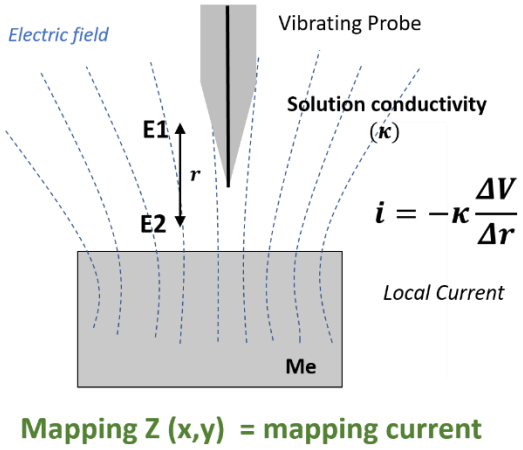


Figure 3 : Scanning Vibrating Electrode Technique (SVET) explanatory diagram.

The SVET probe is typically positioned at 150±25 µm above the sample and vibrates at 50-80 Hz with 30-50µm amplitude. This technique is complementary with the LEIM: indeed, it gives information on cathodic and anodic activity intensity on the surface. This measurement system gives a potential value corresponding to the probe potential difference, between its lower and higher position during its oscillation. Current $\boldsymbol{i}$ is recalculated according to equation (3):

$$\boldsymbol{i = -\kappa \frac{\Delta V}{\Delta r}} \quad \textbf{(7)}$$

where $\boldsymbol{\Delta V}$ is the potential difference measured by the electrode during its oscillation of $\boldsymbol{\Delta r}$ amplitude and $\boldsymbol{\kappa}$ the solution conductivity. Positive current values are associated to anodic activity (metal $\boldsymbol{Me}$ dissolution):

$$\boldsymbol{Me \rightarrow Me^{n+} + ne^{-}} \quad \textbf{(8)}$$

and negative values are associated with cathodic current (typically oxygen reduction at the surface):

$$\boldsymbol{\frac{1}{2}O_2 + 2e^{-} + H_2O \rightarrow 2OH^{-}} \quad \textbf{(9)}$$

Current mappings are given assuming that solution conductivity does not evolve during the experiment which could cause metallic ions dissolution but the volume at the end of the

experiment is too small to measure proper conductivity. Nevertheless, it is worth to mention that is should evolve because of the metal ions dissolution. According to that limitation, the current maps will be interpreted qualitatively.

[1] J.P. Laurent, J.P. Hennechart, D. Spehner, J. Devroc, “Coated hot- and cold-rolled steel sheet comprising a very high resistance after thermal treatment", U.S. Patent 6296805B1, issued October 2, (2001).

[2] ASTM International B 117 – 09 “Standard practices for operating salt spray (fog) apparatus” (2009).

[3] ISO 9227:2006 “Corrosion tests in artificial atmospheres – Salt spray tests” July 2006

[4] ISO 14993-2001 “Corrosion of metals and alloys – Accelerated testing involving cyclic exposure to salt mist, ‘dry’ and ‘wet’ conditions”, September 2011

[5] ISO 16701 “Corrosion of metals and alloys – Corrosion in artificial atmosphere – Accelerated corrosion test involving exposure under controlled conditions of humidity cycling and intermittent spraying of a salt solution”, December 2003

[6] Test Method D17 2018, “Corrosion test by automatic change of phases of salt spray, dryig and humidity (ECC1)” Standardization of Renault Automobiles – DMI / Service 65810, revision of October 2007

[7] VDA 233-102 “Cyclic corrosion testing of materials and components in automotive construction” June 2013

[8] European standard – French standard, NF EN ISO 9223 “Corrosion of metals and alloys – Corrosivity of atmospheres – Classification, determination and estimation” March 2012

[9] European standard – French standard, NF EN ISO 9226 “Corrosion of metals and alloys – Corrosivity of atmospheres – Determination of corrosion rate of standard specimens for the evaluation of corrosivity” March 2012

[10] ISO 8407:2009 “Corrosion of metals and alloys – Removal of corrosion products from corrosion test specimens” November 2009.

[11] A. E. Vladar, M. T. Postek “The Scanning Electron Microscope” in Handbook of Charged Particle Optics, Second Edition, CRC Press, 2008

[12] P. Echlin, J. Goldstein, L. Sawyer, D. E. Newbury, C. E. Lyman, D. C. Joy E. Lifshin, J. R. Michael “Scanning Electron Microscopy and X-ray Microanalysis” Third Edition, Springer, 2003

[13] K. Kanaya, S. Okayama, J. Phys. D., J. Appl. Phys. 1972, 5, 43.

[14] H. Bethe, Handbook of Physics, Springer, Berlin Heidelberg New York, 1933.

[15] D. M. Moore, R. C. Reynolds Jr. “X-ray diffraction and the identification and analysis of clay minerals” Second Edition, Oxford University Press, 1997

[16] H. P. Klug, L. E. Alexander “X-ray diffraction procedures: for polycrystalline and amorphous materials” Second Edition, ISBN 0-471-49369-4, Wiley-VCH, 1974

[17] K. Ogle, J. Baeyens, J. Swiatowska, P. Volovitch “Atomic emission spectroelectrochemistry applied to dealloying phenomena: I. The formation and dissolution of residual copper films on stainless steel” Electrochim. Acta 54 (2009) pp. 5163-5170

[18] M. Mokaddem, P. Volovitch, F. Rechou, R. Oltra, K. Ogle “The anodic and cathodic dissolution of Al and Al-Cu-Mg alloy”, Electrochim. Acta 55 (2010) pp. 3779-3786

[19] J. Swiatowska, P. Volovitch, K. Ogle “The anodic dissolution of Mg in NaCl and Na2SO4 electrolytes by atomic emission spectroelectrochemistry” Corros. Sci. 52 (2010) 2372-2378

[20] K. Ogle, M. Mokaddem, P. Volovitch, "Atomic emission spectroelectrochemistry applied to dealloying phenomena II. Selective dissolution of iron and chromium during active - passive cycles of an austenitic stainless steel" Electrochimica Acta 55 (2010) pp. 913- 921

[21] V. Shkirskiy, A. Maltseva, K. Ogle, P. Volovitch, Environmental effects on selective dissolution from ZnAlMg alloy under low frequency alternating current perturbations, Electrochimica Acta, (2017) 238 pp. 397-409

[22] V. Shkirskiy, P. Volovitch, V. Vivier , Development of quantitative Local Electrochemical Impedance Mapping: an efficient tool for the evaluation of delamination kinetics , Electrochimica Acta, (2017) 235 pp. 442-452.

[23] A. C. Bastos, O. V. Karavai, M. L. Zheludkevich, K. A. Yasakau, M. G. S. Ferreira, Localised Measurements of pH and Dissolved Oxygen as Complements to SVET in the Investigation of Corrosion at Defects in Coated Aluminum Alloy, Electroanalysis (2010).

Chapter III

Effect of Zn and Mg alloying on microstructure and anticorrosion mechanisms of AlSi based coatings for high strength steel

C. Nicard, C. Allély, P. Volovitch
Corrosion Science 146 (2019) 192–201 (Accepted 28 October 2018)

Investigated topics:

- What is the influence of Zn and Mg alloying on AlSi coatings microstructure?
- How these new coatings behave in accelerated corrosion test?
- What corrosion products are formed on these coating in accelerated corrosion test?

Highlights:

- AlSiZn(Mg) coatings sacrificially protect high strength steel in cyclic corrosion test
- Sacrificial effect is attributed to new Al(Zn) and Mg_2Si phases
- AlSiZn patinas formed in scratch dissolve with cycling loosing barrier effect
- AlSiZnMg patinas formed in scratch doesn’t dissolve with corrosion advancement
- Long lasting barrier effect is attributed to higher pH stability of Mg-rich patinas

Chapter III - Effect of Zn and Mg alloying on microstructure and anticorrosion mechanisms of AlSi based coatings for high strength steel

Abstract

The effect of Zn and Mg alloying on the microstructure and anticorrosion mechanisms of AlSi coatings for steel was studied combining electrochemical tests, material balance after accelerated corrosion tests, visual observation, phase identification on corroded and uncorroded surfaces by X-ray diffraction, Raman spectroscopy and electron microscopy. Zn alloying promoted an AlZn solid solution therefore improving sacrificial protection of steel at first cycles of the test. With cycling, the AlSiZn coatings were rapidly consumed by selective dissolution of AlZn coupled with cathodic Si. Additional Mg alloying increased the coating life, binding Si in more anodic Mg_2Si and stabilizing corrosion products.

Keywords

Metal Coatings (A); Al (A); Zn (A); Mg (A); X-ray diffraction (B); Raman spectroscopy (B); Atmospheric corrosion (C);

1 Introduction

Considering anticorrosion actions of metallic coatings to protect steel, an ideal coating should be sacrificial, but should corrode with a reasonable rate and form suitable corrosion products able to reduce coating consumption and to heal steel if it is accidently exposed because of damages in the coating [1-4]. Regarding high strength steel there are two main groups of coatings on the market – ZnAl based and AlSi based which can be used with and without heat treatment [5,6]. In case of AlSi coatings, Si is added to increase the thickness of the intermetallic layer formed at the coating-steel interface [5,7,8]. . AlSi-based protective coatings for steel demonstrate good anticorrosion performances [9] but Al spontaneous passivation makes Al inefficient to protect steel in low chloride environments [7,10,11]. Al coatings are known to passivate by formation of a dense and partially hydrated layer of oxides, providing a very good barrier protection for the coating, but at the same time resulting in loss of sacrificial protection [9,12]. At the same time, at high chlorides concentrations, Al suffers from localized corrosion [13] reducing coating efficiency. Alloying of Al coatings [14,15] can be chosen as a strategy to improve sacrificial protection when Al-based coating is present by lowering its corrosion potential. The alloyed coatings can also form new corrosion products, which potentially could offer a supplementary self-healing effect [2,3].

For sacrificial Al anodes, Zn alloying lowers the coating potential [16,17] and makes them more efficient to protect steel structures. Magnesium is also know to reduce Al corrosion potential [11, 18, 19]. At the same time, alloying can result in formation of new solid solutions (AlZn, AlMg…) and intermetallic precipitates [20,21] like $MgZn_2$, or Mg_2Zn_{11}, $Mg_{17}Al_{12}$. In the presence of Si, Mg_2Si is expected and the excess of Si can stay as metallic inclusions [22-24]. For AlSiMg(Zn) quaternary system [25,26] Mg_2Si, Zn_2Mg and Mg_2Zn_{11} were shown to be the most stable phases. Due to the contact with steel during the coating process, Al_3Fe and AlFeSi can also be formed [8,9]. These new phases can modify the coating potential but also its capacity to micro galvanic coupling; this could result in enhanced corrosion of both coating and steel, especially at the interfaces [4,22,27]. Therefore, it is important to determine the phase composition and their distribution in new alloyed materials.

Regarding corrosion products, the presence of Zn^{2+} and Mg^{2+} ions during corrosion can modify the nature of the formed patinas. In particular, the formation of Zn and Mg hydroxides, basic zinc salts and layered double hydroxides (MgAl-LDH) with general formula $M_xAl_y(A)_m(OH)_n.zH2O$ (where A is an anion, like CO_3^{2-} for hydrotalcite and M is a di-valent

cation) can be expected [2,6,28-33]. The presence of Zn^{2+} and Mg^{2+} ions can also influence the local pH by the precipitation of corrosion products.

Recently, the effect of Mg alloying on AlSi-Zn coating was studied for high (>40 wt. % of Zn) composition alloys [14,15]. In this work we communicate the effect of lower Zn and Mg contents (< 30 wt. %) on the phase composition and microstructure of AlSi coating and the consequences of this new microstructure for anticorrosion resistance in accelerated cyclic corrosion test VDA 233-102 [34].

2 Experimental

2.1 Materials

The coated steel samples were supplied by ArcelorMittal. Samples were prepared by industrial hot dip process based on AluSi© coating described in the US 6296805 B1 patent [35] but modified with Zn and Mg alloying in the range of 2–30 wt. % of Zn and 1–10 wt. % of Mg. The AluSi© coatings with 2–9 wt. % of Si on Mn22 steel were used as a reference material. AlSi, AlSiZn and AlSiZnMg were studied, the number of variations for each combination of alloying elements is presented in Table 1.

Table 1 : Summary information about studied AlSi(Zn,Mg) coatings on high strength steel. Types of material, number of tested compositions, composition range, number of cycles in accelerated corrosion test VDA 233-102 at which the red rust appears for the first time and measured corrosion potential in 0.1 M NaCl aqueous solution with initial pH 7 are presented.

Material type	Number of Compositions	Compositions range / wt. %	Number of VDA 233-102 cycles before red rust		Corrosion Potential / mV vs SCE	
			unscratched coatings	scratched coatings	After 0-5s	After 1h
AlSi	2	1 < Si <10	>12	1	-750±25	-700±25
AlSiZn	6	1 < Si <10 2 < Zn <30	10±1	5±1	-920±25	-920±25
AlSiZnMg	9	1 < Si <10 2 < Zn <30 1 < Mg <10	>12	>6	-1400±150	-920±25

The samples were degreased in an ether solution at room temperature for 15 minutes prior to electrochemical and corrosion tests.

2.2 Microstructural analysis

Phases identification was performed by X-Ray Diffraction (XRD) using a PANalytical X'Pert diffractometer with the Cu(Ka1) radiation, directly on the sample surface (analysed area approximately 63 mm^2). The XRD were collected with angular resolution of 0.02° over the angular range 5–80° (2θ) with 0.3 s acquisition time per point. The spectra were treated using the HighScore Plus software package, including the JCPDS (ICDD) database files (version 2013) and completed with the files from RRUFF™ database [36] for corrosion products identification.

Distribution and morphology of metallic phases and corrosion products before and after accelerated corrosion tests were observed by a JEOL 7800 F Field Emission Gun Scanning Electron Microscope (FEGSEM) coupled with Brucker Xflash 6160 Energy Dispersive Spectroscopy (EDS) with a Si(Li) detector and equipped with QUANTAX 1.9 software (Bruker AXS). An accelerating voltage of 5 kV was used for electron imaging and of 15 kV for EDS. The cross-section observations were performed on samples mounted in resin, cut and mechanically polished. Before observation, a layer of 10–20 nm of Au was sputtered on the cross section. Raman spectrometry was performed directly on the corroded samples using a InVia Renishaw Confocal Raman Spectrometer with green laser (laser wavelength 532 nm) at power 100 mW. The results were compared with the reference spectra taken from the literature and mineralogical database RRUFF™ [36].

2.3. Electrochemical characterizations

Open circuit potential (OCP) evolution survey and potentiodynamic polarization experiments were performed in 0.172 M (1 wt. %) NaCl aqueous solution at initial pH 7 (adjusted by 0.5 M NaOH solution) using a BioLogic VMP3 potentiostate. A three-electrode cell thermostated at 25 ± 2 °C was used with a saturated calomel electrode (SCE) as the reference electrode, a platinum plate (total area of 1 cm^2) as the counter electrode and the coated steel as the working electrode (the stested area of 0.6 cm^2).

For polarization curves, the sequence was set to perform an OCP measurement followed by anodic or cathodic polarization with a sweep rate of 1 $mV.s^{-1}$. Separate experiments were made for cathodic and anodic polarization with potential domains from OCP to -1.6 V vs. SCE for cathodic polarization and from OCP to -0.5 V vs. SCE for anodic polarization. Cathodic and anodic polarizations were performed separately on different samples with fresh electrolyte.

2.4. Accelerated corrosion tests

Accelerated cyclic corrosion tests according to procedure VDA 233-102 (often called "new-VDA" or "N-VDA") [34] were performed with samples oriented at 20° to the vertical. One-week cycle of VDA 233-102 consists in alternating 1 wt. % NaCl salt spray, humid periode, freezing and ambient (or drying) periods, in which the salt solution pH stayed between 6.5 and 7.2. The VDA 233-102 test in this work was performed in a 15 m^3 chamber supplied by Airtemp©.

Two types of samples were tested. Unscratched samples were used to measure the time for the red rust to appear and the mass loss, as well as to establish the mass balance and the composition of the formed corrosion products. Scratched samples were used to test the sacrificial protection offered by the coatings to steel and to observe corrosion products formed in the scratch and the effect of these products on the steel reactivity. Cut edges were protected with a Nichiban© adhesive tape and the exposed surfaces were about 50 mm x 150 mm. Photos of the scratched samples surface were taken every week to follow the evolution of the corrosion. Prior to the corrosion tests the unscratched samples where weighted to allow further mass balance analysis.

During the corrosion tests, the presence of metallic samples in the fog resulted in condensation of the electrolyte at the surface. The condensate flowed down because of 45° orientation of the samples in the chamber and was collected separately under each of the unscratched samples. Every week the collected solutions were removed and analysed by induced coupled plasma optical emission spectroscopy (ICP-OES). At the end of the test, remaining corrosion products were dissolved in 150 ml of 65 wt. % HNO_3 aqueous solution for 3.5 min under ultrasonic agitation. For the dissolution, the protective adhesive tape on the cut edges was removed and a RESIN (Slotowax Finish Coat by Schlötter) inactive in HNO_3 was used to protect the cut edges and prevent steel dissolution. After the dissolution of corrosion products, 1 ml of 36 wt. % HCl solution was added to HNO_3 and the acidic solution was diluted twice with water and analysed by ICP-OES to quantify the elements present in the corrosion products insoluble in water (I). The remaining samples, after the corrosion product dissolution, where weighted once more for mass loss determination. The total mass loss (T) was considered as the difference between the obtained weight value and the sample weight before the accelerated test. To approximate a possible dissolution of the substrate during corrosion product

removal, an uncorroded AlSiZnMg sample was analysed by the same procedure. The dissolution of the uncorroded coating reached 1.51 g.m^{-2}.

3 Results

3.1 Coatings microstructure

Typical phase compositions of the AlSi, AlSiZn and AlSiZnMg coatings revealed by XRD are presented in Fig. 1.

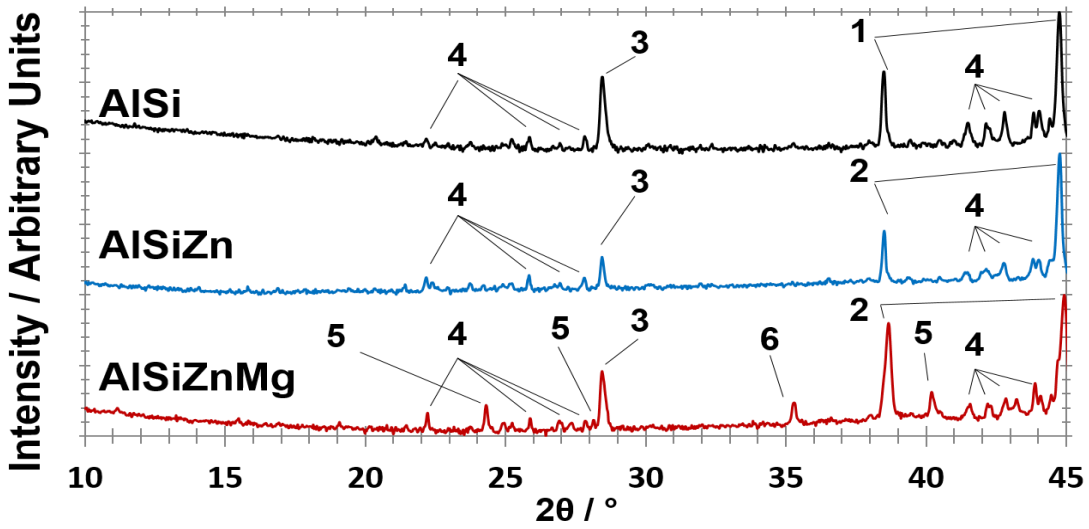


Figure 1 : Typical X-ray diffraction spectra of AlSi, AlSiZn and AlSiZnMg coated steels. The identified phases and related labels are listed in Tab. 2.

The labels used to name the identified phases are listed in Table 2. Corrosion potentials found in the literature for these phases [23,37] are also presented in the table. Typical coating microstructures are shown in Figure 2 for the cross sections and for the surfaces.

Table 2 : Main phases detected in AlSi(Zn,Mg) coatings: labels used for Figs. 1–3, chemical compositions and expected corrosion potentials, E, in unbuffered 0.1 M NaCl aqueous solution.

Phase label	Composition	E / mV vs SCE (from [23])
1	Al	-823
2	Al(Zn)	-920
3	Si	-441
4	Al_xFe_ySi (τ5)	-470
5	Mg_2Si	-1538
6	$MgZn_2$	-1029

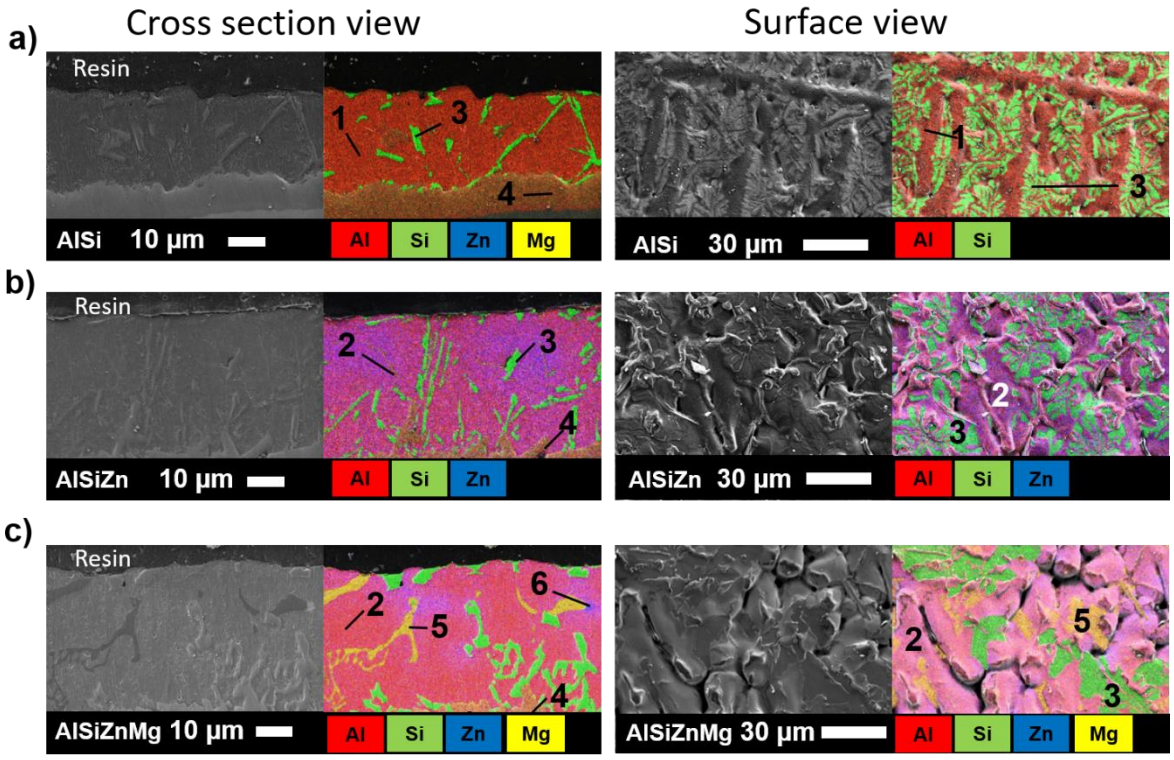


Figure 2 : Typical secondary electron images and corresponding EDS elemental maps of cross sections and surfaces of the (a) AlSi, (b) AlSiZn, (c) AlSiZnMg coated steels with high Si content. The proposed phase attribution is shown using the phase labels listed in Table 2.

These microstructures are representative for different fractions of alloying elements, however the quantity of the phases and their distribution can be affected by the amount of alloying elements. As expected from the literature [38], AlSi coatings (Figure 2a) consist of an Al matrix with Si needles at inter-dendrites and an AlFeSi intermetallic at coating/steel interface with the quantity of Si needles and the AlFeSi layer thickness dependent on Si content. The composition of the intermetallic layer is close to τ5 or τ6 phases described in the ternary diagram Al-Fe-Si [38]. Some Si needles can cross the coating thickness and the metallic Si fraction at the surface can be important. For AlSiZn coatings (Figure 2b), the Al matrix is transformed in Al(Zn) solid solution. Despite limited Zn solubility in Al matrix (4.5 wt. %) the matrix doesn't show the expected binary structure [17] even at Zn contents > 15 wt. %. However, Zn seems to be more concentrated around the intermetallic layer and Si precipitates. Si needles are thinner and the dendrites are visible at the surface. With Zn + Mg alloying (Figure 2c) Mg_2Si and Zn_2Mg intermetallics are formed, which is coherent with the results communicated in the literature for AlZn coatings with high Zn content and for Al alloys of 6000 and 7000 series [14,15,23-26]. . Compared to Al alloyed with Zn and Mg (7000 series), the Mg_2Zn_{11} intermetallic formed in Al alloys is not observed. Depending on Mg content, the new phases can appear in the matrix along Si needles or be present at the surface of the coating. This is

illustrated in Figure 3 where two AlSiZnMg coatings with different Mg fraction are compared: in the coating with twice lower Mg content (Figure 3a), Mg_2Si is located only at the surface, whereas for higher Mg content (Figure 3b) it is present at both, the surface and the coating-intermetallic layer interface.

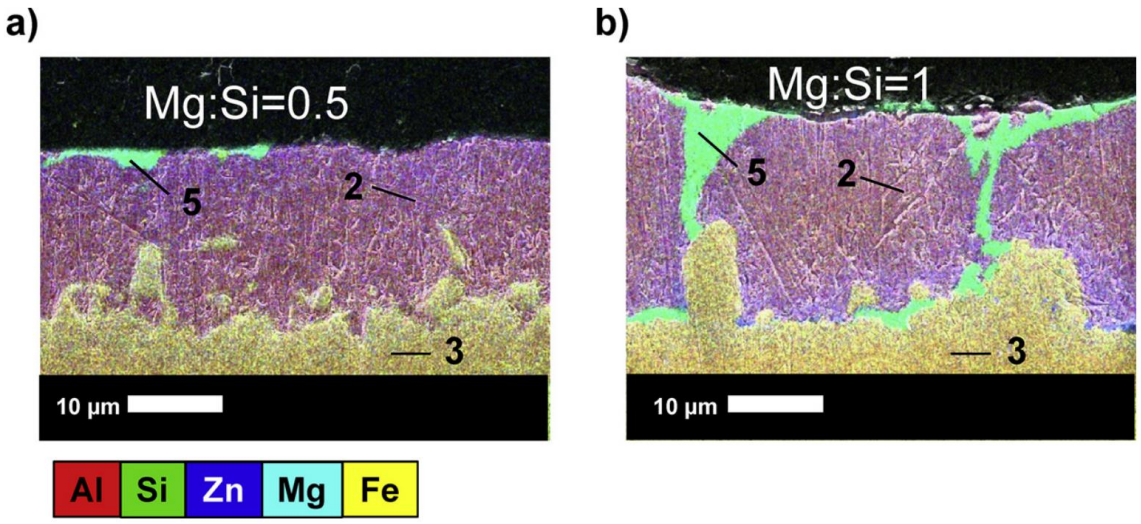


Figure 3 : Phases distribution in AlSiZnMg coated steel with low Si content and Mg to Si weight ratio (a) Mg:Si = 0.5, and (b) Mg:Si = 1. The phase attribution is shown using the labels listed in Tab. 2.

3.2 Electrochemical characteristics

*Figure 4*a presents the typical evolution of the OCP during immersion of AlSi, AlSiZn and AlSiZnMg coatings in 0.172 M NaCl solution. For AlSi the coating potential after 1 h of immersion (−698 mV vs. SCE) is very close to the steel potential (−660 mV vs. SCE). Zn alloying lowers and stabilizes the free potential of the coating at around -920 mV vs. SCE. Mg addition in AlSiZn results in a lowered potential at the beginning of the sequence (1380 mV vs. SCE) however after 1 h of immersion the OCP reaches 920 mV vs. SCE, the value similar to the OCP of the AlSiZn coating.

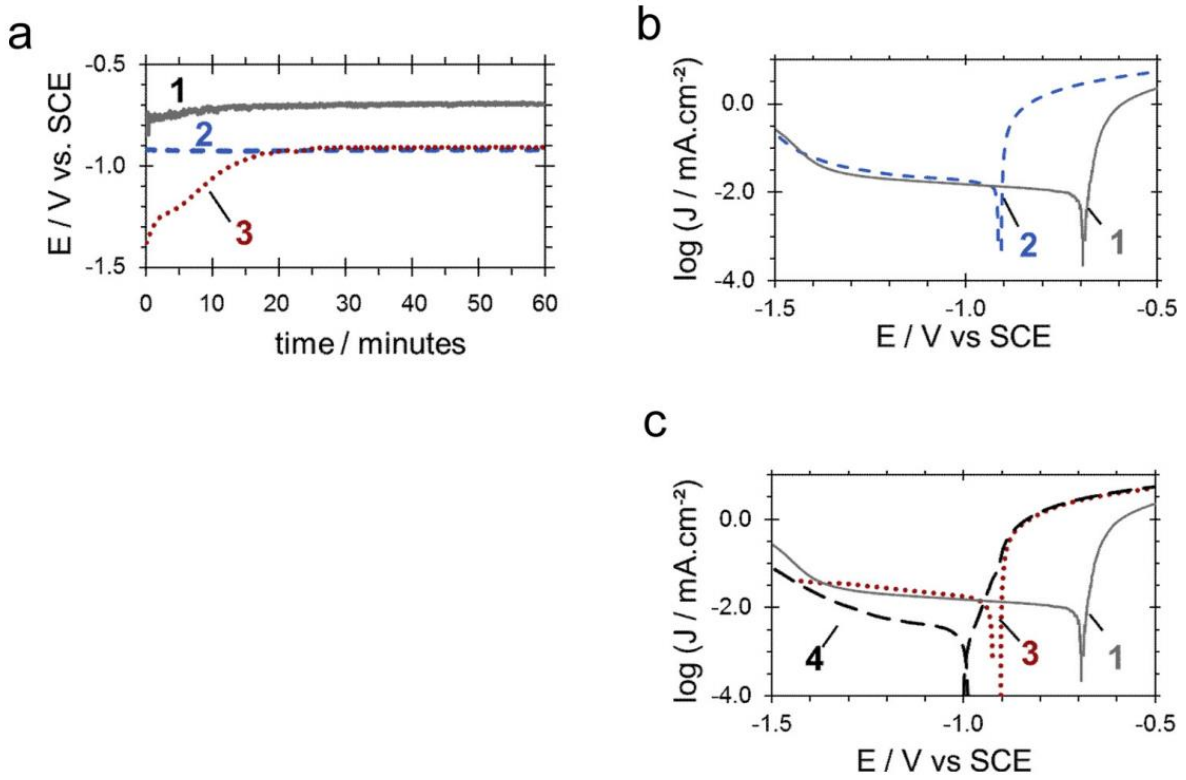


Figure 4 : Electrochemical behaviour of studied coatings in unbuffered 1 wt. % NaCl solution with initial pH 7. a) Open circuit potential (E) evolution vs time for AlSi, AlSiZn and AlSiZnMg coated steels as indicated. b)–c) Cathodic and anodic polarization curves (log current (J) vs potential E) for AlSi (curve 1), AlSiZn (curve 2) and AlSiZnMg (curves 3,4) coated steels. The polarization curves 1–3 were recorded after the open circuit potential stabilization for all phases (1 h of immersion). For comparison the polarization curve 4 shows the initial behaviour of AlSiZnMg coating before the potential stabilization (after 10 min of immersion). Polarization directions are indicated by arrows.

*Figure 4*b–c) present the typical polarization curves recorded for the coatings after the potential stabilization (1 h of immersion, curves 1–3). An additional polarization curve is presented for AlSiZnMg coating (curve 4), which was recorded after only 10 min of immersion, in order to detect the electrochemical behaviour in the transition period when the potential is not yet stable. The corrosion potentials measured from polarization curves for the AlSi, AlSiZn and AlSiZnMg coated steels (respectively 693, 910, −909 mV vs. SCE) are coherent with the free potential measured in *Figure 4*a after 1 h of immersion. Regarding the current density evolution, Zn alloying does not modify cathodic currents but increases anodic currents relative to the AlSi coatings. After 1 h of OCP, the polarization curves of the AlSiZn and AlSiZnMg coated steels look similar. The curve 4, obtained after 10 min of OCP, is different, especially the values of cathodic currents are lower. One should note that the behaviour shown in *Figure 4* is representative for all the compositions.

3.3 Accelerated corrosion tests results

3.3.1 Visual evolution

Figure 5 shows the samples evolution during the cyclic accelerated corrosion tests. The average number of the cycles before red rust appearance is presented in Table 1. In the table, for each elemental composition (AlSi, AlSiZn and AlSiZnMg) the number of cycles when the red rust was observed for the first time is averaged for the whole data set for the composition and the mean value and the standard deviation are presented. It is clear from the table and the figure that the difference in the behaviour of the 3 types of coatings is fundamental and the tendency doesn't depend on the exact content of Zn or Mg in the coating.

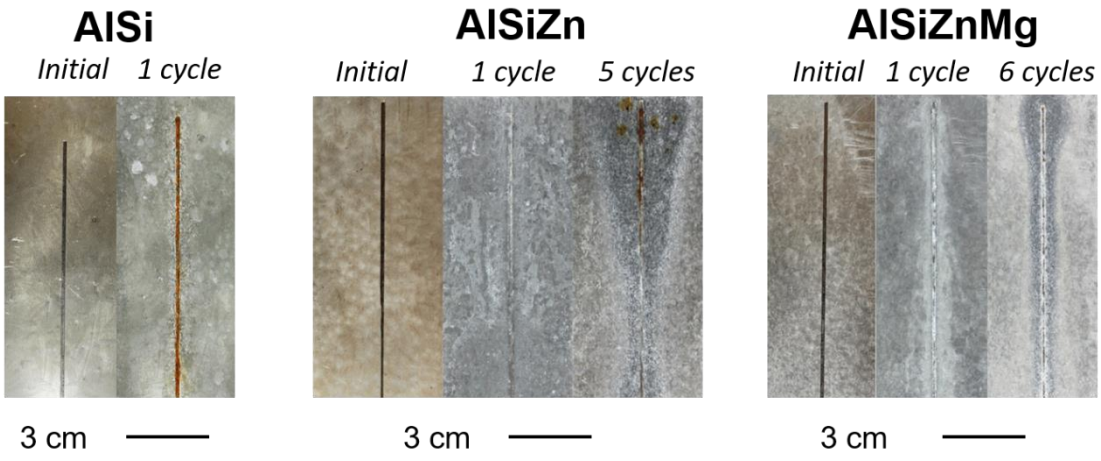


Figure 5 : Typical surface appearance of AlSi, AlSiZn and AlSiZnMg coated steels before (initial) and after several cycles of accelerated corrosion test VDA 233-102 (as indicated).

The AlSi coating seems to be inefficient for sacrificial protection as the red rust in the scratch is observed after 1 cycle of the test. Zn alloying delays the red rust formation, but the coating looks consumed after 5–6 test cycles. Zn + Mg alloying prevents the red rust formation longer than only alloying with Zn and the coating looks less attacked after 6 cycles. The activation of the coating by Zn is coherent with more anodic coating potential relative to steel (section 3.3.1) expected for Al(Zn) matrix (Table 2). The strong effect of the Mg on long term corrosion behaviour can't be explained by the electrochemical results.

3.3.2 Mass balance

The mass balance for different coatings after 6 cycles of the accelerated test is presented in Table 3. The total mass loss (T) was calculated as the difference between the sample weight before corrosion tests and the weight after 6 cycles of the accelerated corrosion test and corrosion products removal.

Table 3 : Mass balance for different coatings: total (T), soluble (S) and insoluble (I) weight loss after 6 cycles of the accelerated test. T values were obtained from weight measurements before the test and after the test and corrosion products removal. The error in T values because of the dissolution of uncorroded coating in nitric acid can reach 1.51 g.m^{-2}. S and I were calculated from the ICP-OES analysis of the lixiviate collected under each sample during corrosion test and the ICP-OES analysis of the solution obtained by the removal of insoluble corrosion products in nitric acid (see text for details).

	I g m^{-2}	S g m^{-2}	S / I	I +S g m^{-2}	Mass loss (T) g m^{-2}	Standard deviation ΔT / g m^{-2}
AlSi	0.81	0.25	0.31	1.1	1.6	± 0.32
AlSiZn	8.8	1.3	0.14	10	8.8	±1.2
AlSiZnMg	5.6	0.47	0.08	6.0	6.2	± 1.0

The soluble (S) and insoluble (I) contributions to the mass loss were calculated from the ICP-OES analysis of the lixiviate collected under each sample during corrosion test and the ICP-OES analysis of the solution obtained during corrosion product removal as explained in section 2.4. It can be seen from the table that for AlSi coating the total coating consumption (T) is the smallest but the ratio between the dissolved mass in soluble (S) and insoluble (I) parts, S/I, is the highest. With Zn or Zn + Mg alloying, the total coating consumption (T and S + I) increases while the fraction of the soluble products (S/I) decreases. The coating intake and the fraction of soluble lixiviated species are however lower in the presence of Mg, indicating that the presence of insoluble corrosion products is accompanied by reduced coating consumption.

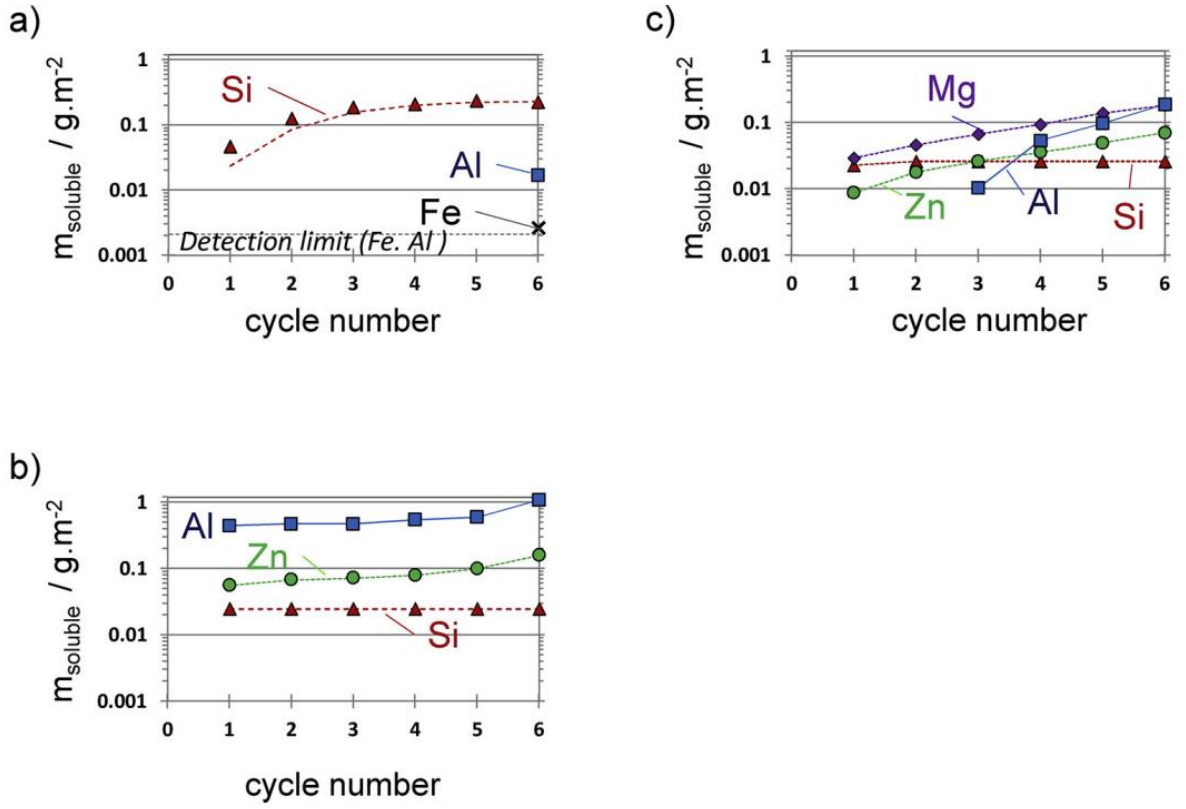


Figure 6 : Evolution of the quantity of soluble Al, Si, Zn and Mg in the solution collected with cycling in accelerated corrosion test VDA 233-102 for (a) AlSi, (b) AlSiZn and (c) AlSiZnMg coatings. For each chemical element the total dissolved mass is normalized by the sample surface area, msol / g.m^{-2}.

The evolution of the lixiviate composition with the increasing number of cycles of the accelerated test is shown in Figure 6. In the case of the AlSi coating (Figure 6a), the Al dissolution is detected only after 6 cycles of the test. In AlSiZn (Figure 6b), Al dissolution is detected from the 3rd cycle. After 6 cycles the quantity of the dissolved Al is about 100 times higher for the AlSiZn coated than for the AlSi coated steel. The concentrations of Zn and Al in the lixiviate seems to increase in a similar way and the weight ratio of Zn to Al in the lixiviate is systematically higher than in the bulk alloy, indicating the selective dissolution of Zn. Additional Mg alloying (Figure 6c) results in reduced dissolution of both, Al and Zn and the effect is much stronger for Al.

The soluble Fe was detected only for AlSi coatings. The traces of Fe in the lixiviate of the AlSi coatings combined with the smallest mass loss for this type of material between all studied coatings are coherent with a localized corrosion mode and a possible local penetration of the electrolyte until the intermetallic layer. The high concentration of Si in lixiviate of AlSi coating can be due to the detachment of Si particles less than 10 µm [39].

The elemental analysis of the insoluble (I) and soluble (S) products after 6 cycles of the test are presented in Table 4.

Table 4 : Enrichment or depletion of soluble and insoluble corrosion products by Al, Si, Zn and Mg after 12 cycles of VDA 233-102 test of unscratched AlSi(Zn,Mg) coatings. The coefficients of selectivity, K_{sel} (X), were calculated as a fraction of the element X (X = Al, Mg, Si or Zn) present in the lsolution (water or nitric acid for soluble and insoluble components respectively), normalized by the content of X in the coating. The values of $K_{sel}(X) > 1$ are in bold, these values indicate that the corresponding product (soluble or insoluble) is enriched by the element X, while the values of $K_{sel}(X) < 1$ correspond to the depletion of X. $K_{sel}(X) = 1$ for a congruent oxidation or dissolution of X.

Coating / number of compositions	Type of corrosion product	Ksel(Al)	Ksel(Si)	Ksel(Zn)	Ksel(Mg)
AlSi / 1	insoluble	1.1	0.33	-	-
	soluble	0.80	**10**	-	-
AlSiZn / 3	insoluble	**1.1**	0.11	0.88	-
	soluble	1.0	0.21	**1.9**	-
AlSiZnMg / 5	insoluble	0.53	0.11	**1.9**	**15**
	soluble	0.47	0.11	**2.0**	**19**

The table presents the dimensionless coefficients of the selectivity $K_{sel}(X)$ for each element (X = Al, Zn). The $K_{sel}(X)$ values are calculated for a representative composition as a fraction of the element X detected in the solution, $C_{lix}(X)$, normalized by its fraction expected from the congruent dissolution of the coating (bulk fraction), $C_{bulk}(X)$

$$K_{sel}(X) = C_{lix}(X)/C_{bulk}(X) \quad (1)$$

The value of $K_{sel}(X) > 1$ indicates that the product (soluble or insoluble) is enriched by the element X, while the values of $K_{sel}(X) < 1$ describe the depletion of X. $K_{sel}(X) = 1$ means a congruent oxidation or dissolution. It can be seen from the table, that for the AlSi and AlSiZn coated steels, the insoluble corrosion products are rich in Al. For AlSiZnMg both, aqueous lixiviate collected during the test and insoluble corrosion product, are depleted in Al. Si is selectively dissolved from the AlSi coating while Zn alloying enhances the selective dissolution of Al and inhibits it for Si. Mg is selectively dissolved and is also accumulated in the insoluble corrosion products.

3.3.3 Corrosion products identification

Typical XRD patterns and typical Raman spectra obtained on 3 types of coatings after 6 cycles of accelerated test are presented in Fig. 7. The numbers used for the peak labels correspond to the phases presented in Table 5.

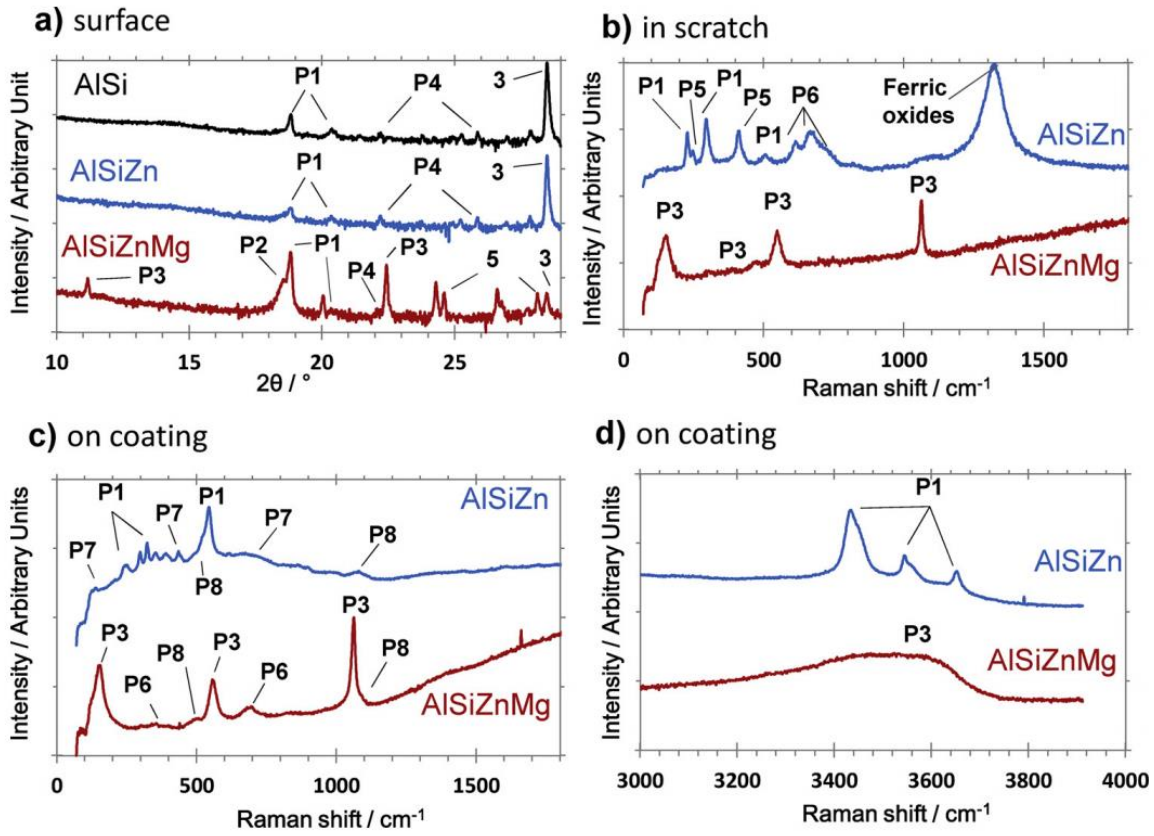


Figure 7 : (a) X-ray diffraction spectra and (b–c) Raman spectra of AlSiZn and AlSiZnMg coatings after 12 cycles of accelerated corrosion test VDA 233-102. Raman spectra recorded in the scratch (b) and on the coating (c–d) are shown. The identified phases and related labels are listed in Tables 2 and 5.

The main difference between the coatings alloyed with Mg and not alloyed with Mg is the form in which Al is present in corrosion product: nordstrandite (P1, $Al(OH)_3$) for AlSi and AlSiZn coated steel and layered double hydroxide (P3) for AlSiZnMg coated steel. Simonkolleite (P5) and hydrozincite (P7) were detected far from the scratch on AlSiZn.

Table 5 : Corrosion products identified on AlSi(Zn,Mg) coated steel by XRD and Raman spectroscopy.

Labels	Mineral name	Abbreviation	Composition	Reference	Raman shifts (cm-1)
P1	Nordstrandite	-	$Al(OH)_3$	[21] ID:R050592	249-303-536-3491-3566-3670
P2	Brucite	-	$Mg(OH)_2$	[21] ID:R040077	273-440-1080
P3	Hydrotalcite	LDH	$Mg_6Al_2CO_3(OH)_{16}.4H_2O$	[21] ID:R050457	152-554-1056-3344
P4	Cristobalite	-	SiO_2	JCPDS (ICDD) 01-089-8944	115-224-417
P5	Simonkolleite	-	$Zn_5(OH)_8Cl{\cdot}H_2O$	[21] ID:R130616	108-254-393
P6	Corundum	-	Al_2O_3	[21] ID:R110117	416-700-747
P7	Hydrozincite	-	$Zn_5(CO_3)_2(OH)_6$	[21] ID:050635	150-225-384-701-729-1058
P8	Analcime	-	$Na(AlSi_2O_6){\cdot}H_2O$	[21] ID:040128	490-1102

3.3.4 Corrosion morphology and corrosion products distribution

Phase consumption and corrosion products distribution on the cross section (corrosion profiles) of unscratched coatings observed by SEM are presented in Figure 8. The expected phases are labeled according to notations in Table 2 andTable 5. It can be seen from the figure and the table that in all cases corrosion is initiated around Si particles. However, AlSiZn matrix is much more consumed than AlSiZnMg. Mg is still present in intermetallic form inside the coating. Figure 9 illustrates a typical phase distribution after 6 cycles of the accelerated test for AlSiZn and AlSiZnMg coated steels near the scratch. The amount of corrosion product in scratch is much higher on AlSiZnMg coated steel than on AlSiZn coated steel. At higher resolution (Figure 9c–f), one can see that not only the quantity but also the morphology of the corrosion product are different. The EDS analysis of the platelet-like products shown in Figure 9f revealed an atomic ratio of Mg:Al = 3:1 (Table 6). The ratio Mg:Al = 3:1 is coherent with a layered double hydroxide $Mg_6Al_2CO_3(OH)_{16}{\cdot}4H_2O$.

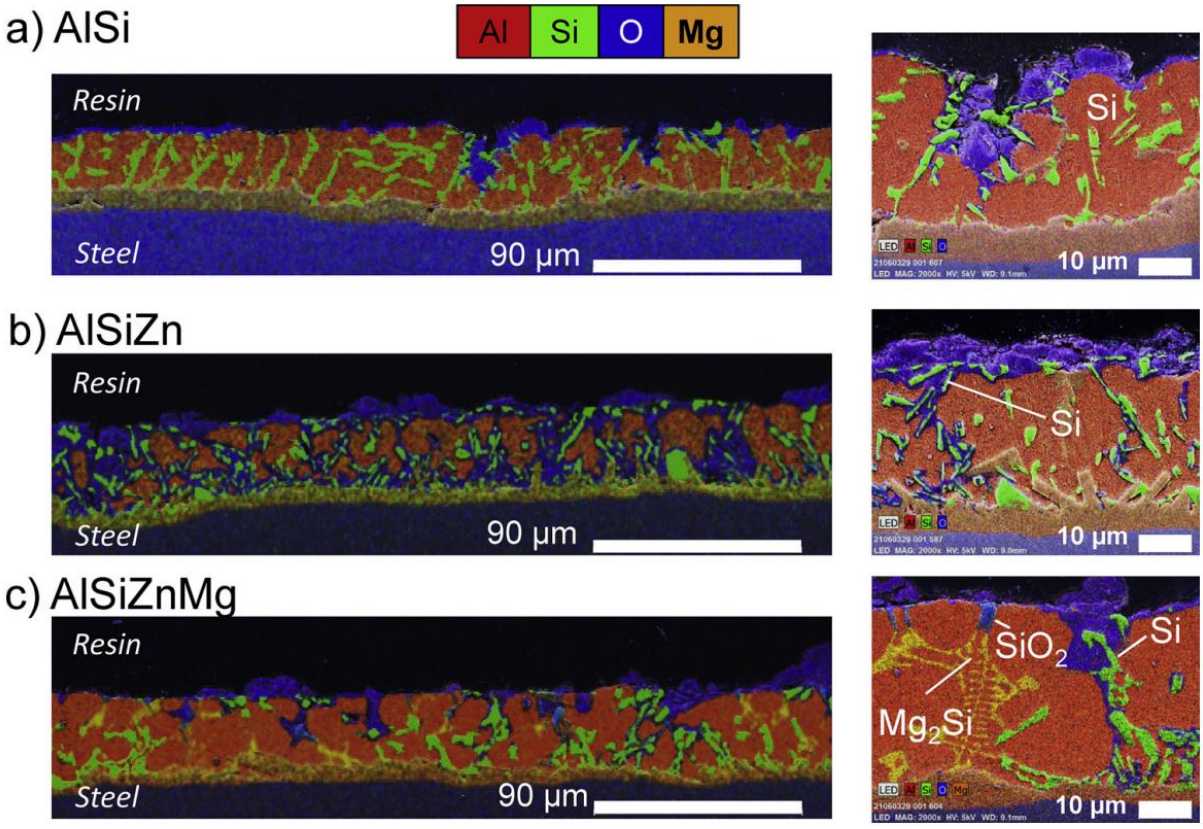


Figure 8 : EDS maps showing corrosion products distribution after 12 cycles of the VDA 233-102 test in the cross sections of unscratched (a) AlSi, (b) AlSiZn and (c) AlSiZnMg coated steels with high Si content. O distribution permits to distinguish corrosion products from non-corroded areas while Al, Si and Mg distributions help to identify the phases. General view and more resolved images are shown.

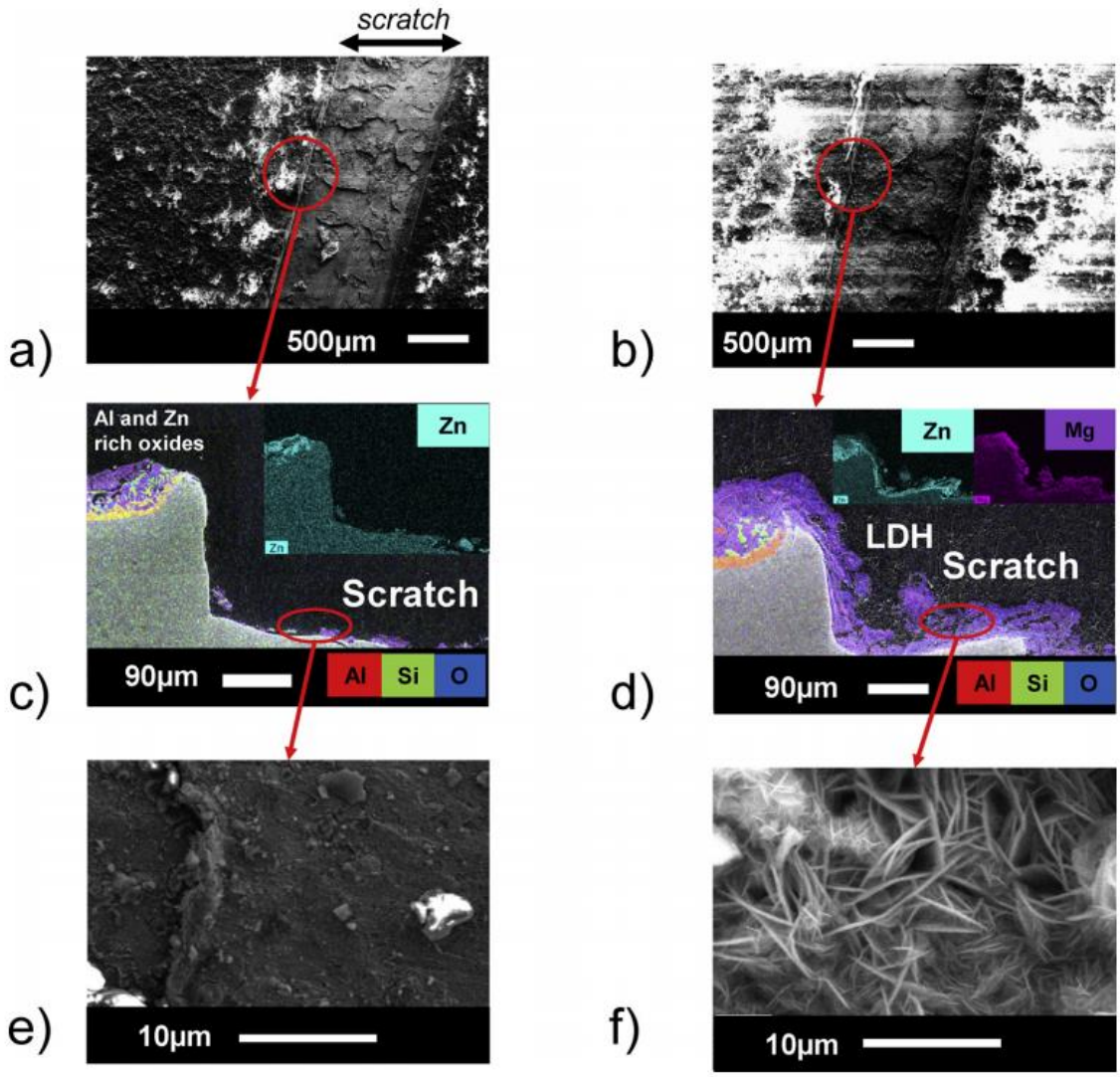


Figure 9 : Distribution of corrosion products near the scratch of (a, c, e) AlSiZn and (b, d, f) AlSiZnMg coated steels after 6 cycles of VDA 233-102 test. General top view of the scratch (a, b) and the morphology of corrosion products inside the scratch (c, d) are shown from the top by secondary electron images, the element distribution in the cross section is shown using EDS mapping (c, d).

Table 6 : Chemical composition determined from EDS analysis of platelets shown in Fig. 9f.

Element	Wt. %	At. %	At. ratio X/Al
Al	8	7	1
Mg	22	20	3.0
O	46	64	9.6
Fe	20	8	1.2
Zn	3.5	<2	-
Si	0.3	<1	-

4 Discussion

4.1 Role of new phases for intrinsic coating stability

Si-containing phases in Al alloys are expected to promote selective dissolution of the Al-based matrix due to galvanic coupling [22, 4, 12, 27, 40]. The modification of the coating microstructure by Zn and Mg alloying is expected hence to alter the galvanic coupling between the Si containing phases and the Al rich matrix, becoming one of the important factors explaining the modification of anticorrosion performance and corrosion mechanisms.

As expected from the literature [17], Zn alloying promoted the formation of Al(Zn) solid solution and resulted in more anodic OCP of the coating (*Figure 4*a) and higher current under polarization. This correlated well with the improved sacrificial protection of steel observed in the accelerated tests (delay of the red rust appearance in comparison with AlSi reference illustrated in Figure 5 and Table 1) even at relatively low fractions of Zn. In contrast, this improved sacrificial capacity was accompanied by a quicker coating consumption in both, electrochemical tests and accelerated cyclic corrosion test and the formed corrosion product did not offer a barrier protection for steel. Mass balance (Table 4 andTable 6) demonstrates that Zn was selectively dissolved (Zn fraction in lixiviate is higher than in the bulk material). Zn selective dissolution was supplemented by more than a 10 times increase of Al dissolution rate and a 10 times decrease of Si dissolution rate compared to AlSi. One can expect in this case that a galvanic coupling between the Si dendrites and the Al(Zn) matrix is stronger than between the Si dendrites and the Al matrix because of a higher potential difference and a less stable a oxide layer on Al(Zn). This is consistent with the fastest coating consumption. The hypothesis which needs to be verified to explain this premature consumption could be a spontaneous local cathodic activity on the AlSiZn coatings surfaces.

Additional alloying with Mg modified the nature and the distribution of Si-containing phases. First of all, as predicted from the phase diagram [25] the Si phase was partially transformed into the Mg2Si intermetallics (Figure 2), significantly more anodic than Si [23] and even AlZn [17] matrix (see Table 2). The fact that after 1 h of immersion in the electrolyte the electrochemical behavior of AlSiZn and AlSiZnMg looked similar (*Figure 4*) can be explained by the rapid selective dissolution of Mg from active Mg_2Si and $MgZn_2$ intermetallic phases coupled with the surrounding AlZn matrix [27]. The selective dissolution of Mg was evidenced by the mass balance (Figure 5 and Table 4). However, in the accelerated tests

additional Mg alloying of the AlSiZn coatings clearly decreased the rate of the coating consumption. This can be due to different factors illustrated in *Figure 10*b. Firstly, the AlZn matrix is expected to be cathodically protected during selective dissolution of Mg [27].

$$Mg_2Si + 2H_2O \rightarrow 2Mg^{2+} + SiO_2 + 4H^+ + 8e^- \quad (2)$$

Secondly, even when the selective Mg dissolution from Mg_2Si is stopped, the galvanic coupling Al(Zn) / SiO_2 is expected to be weaker than Al(Zn) / Si because SiO_2 is less conductive and less cathodically active than metallic Si. Thirdly, the abundant corrosion product can be in the origin of the barrier effect [30]. Finally, the precipitation of Mg containing corrosion products will tend to buffer the pH at the interface limiting it to neutral values (in case of the direct precipitation of the Mg-Al layered double hydroxides) [28]. The reactivity of both, Zn and Al, are minimal at neutral or slightly alkaline pH [41].

4.2 Effect of alloying on steel protection

Sacrificial protection of steel by AlSi based coating was improved by Zn alloying at contents less than 30 wt. %. The effect was achieved due to the transformation of Al matrix into an AlZn phase. However, the high coating consumption rate and the absence of a stable corrosion product resulted in the loss of steel protection with cycling. Experimental results suggest that Mg addition to AlSiZn coating did not modify significantly the sacrificial protection but increased the coating lifetime and favored the formation of stable corrosion products covering steel in the defects. These products are expected to offer barrier protection to the underlying steel in case if the metallic coating is completely consumed [1,42]. Indeed, the nature, the quantity and the distribution of corrosion products on the surface of the AlSiZnMg coated steel was very different from that of AlSiZn coated steel (Section 3.4). The absence of corrosion products in the scratches of AlSiZn can be related to the significant pH increase by cathodic reaction (eq. 3) and corresponding dissolution of Zn and Al containing products (eq. 4–5).

$$O_2 + 2H_2O + 4e^- \rightarrow 4OH^- \quad (3)$$

$$ZnO + H_2O + OH^- \rightarrow Zn(OH)_4^{2-} \quad (4)$$

$$Al(OH)_3 + OH^- \rightarrow Al(OH)_4^- \quad (5)$$

Etc.

For the AlSiZnMg coated steel, the improved steel protection was achieved due to the synergic effect of Zn and Mg. Zn activated Al matrix dissolution contributes to the sacrificial capacity and liberated Al ions contributed to the formation of layered double hydroxides. Mg did not bring long term sacrificial effect to the matrix by itself because it was distributed only in isolated intermetallics. However, Mg alloying reduced the quantity of the metallic Si inclusions by the formation of more active Mg_2Si. The microgalvanic coupling of Al-rich matrix with Mg_2Si is less critical for the coating than the coupling with Si particles: the Si phase is cathodic for AlZn matrix and enhances its consumption while Mg_2Si is anodic versus AlZn matrix and contributes to its cathodic protection. Leached Mg^{2+} also favored formation and stabilization of corrosion products in the defect which contributed to the prolongated coating life. The protection of the scratch could be also enhanced due to synergic inhibiting effect of Mg^{2+} and Zn^{2+} cations on the cathodic reactivity of steel demonstrated in the literature [43].

Higher stability of corrosion products in the scratch of AlSiZnMg can be explained by the low solubility of Mg^{2+} at alkaline pH which can limit the pH increase related to cathodic oxygen reduction by the precipitation of $Mg(OH)_2$

$$Mg^{2+} + 2OH^- \rightarrow Mg(OH)_2 \quad pKs=10.5 \qquad (6)$$

The formation of a thin Mg(OH)2 layer can also be responsible for a “skin effect” explaining a high pH stability of Mg-containing layered double hydroxides which are far more protective [6,28,29]. Zn^{2+} cations can also interact with iron oxides at the surface and make them more protective and Mg^{2+} could enhance this phenomenon [44,45].

The proposed corrosion mechanisms and the mechanisms of steel protection by AlSiZn and AlSiZnMg coatings are schematically summarized in *Figure 10* in which three main steps are considered:

1 Sacrificial effect due to the coating dissolution with a “sacrificial” current between the matrix and the steel in the scratch and a current “lost” in the micro galvanic coupling with Si containing phases.

2 Precipitation of corrosion products in the scratch due to cathodic pH increase.

3 Dissolution of Zn and Al corrosion products because of strong pH increase (pH > 12). The 3rd step is absent when corrosion products contain Mg because at pH > 10 in place of dissolution Mg-containing corrosion products can form $Mg(OH)_2$ films offering a “skin effect”.

The verification of the mechanistic hypotheses formulated below will be presented in our forthcoming publications.

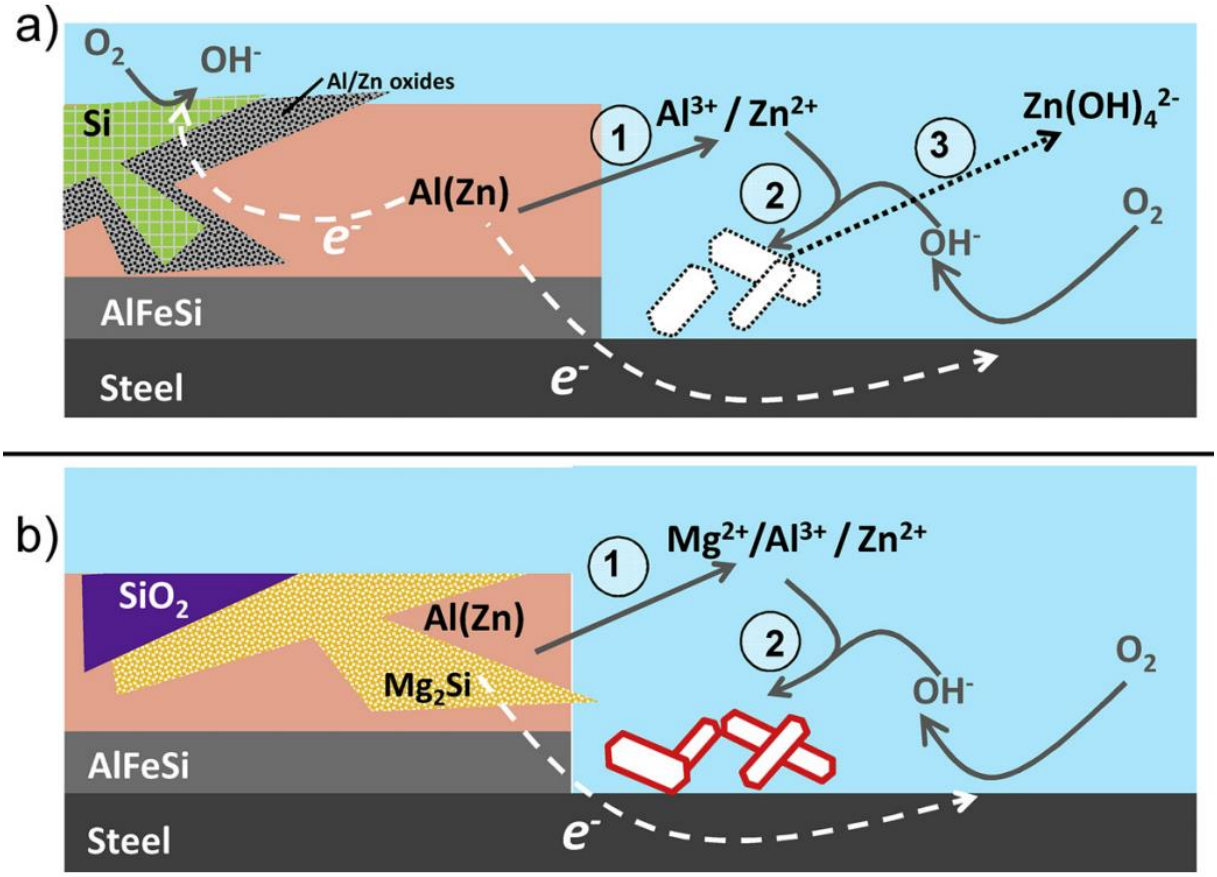


Figure 10 : *Schematic representation of proposed corrosion and protection mechanisms in (a) AlSiZn and (b) AlSiZnMg coated steel in the presence of the defect going up to the steel. Step 1. Coating dissolution and sacrificial effect. For AlSiZn two types of mirogalvanic coupling are proposed - "sacrificial" coupling protecting steel and "lost" current used in micro galvanic coupling with Si because Si potential (60.5 V vs. SCE) is close to potential of steel and cathodic versus AlZn. Step 2. Precipitation (and partial modification) of corrosion products due to pH increase and drying. Step 3. Dissolution of Zn and Al containing corrosion products from AlSiZn at advanced stages of corrosion because of continuous pH increase. This step is absent when corrosion products contain Mg^{2+} because of their high pH stability (for instance $Mg(OH)_2$ formation in place of dissolution of LDH resulting in a skin effect). As a result, Mg is expected to extend both, the coating life (and hence a sacrificial protection) and the barrier effect of corrosion products in the scratch*.

5 Conclusions

The effect of Zn and Mg alloying on the microstructure and anticorrosion mechanisms of AlSi coatings for high strength steel was studied by a combination of electrochemical tests, mass balance in accelerated cyclic corrosion tests, visual observation, phase identification on corroded and uncorroded surfaces by X-ray diffraction, Raman spectroscopy and electron microscopy. Alloying resulted in the modification of the phase composition and the complex microstructure which significantly influenced the corrosion resistance and corrosion mechanisms. Zn alloying resulted in the anodic activation of the coating which was attributed

to the transformation of the Al matrix into AlZn solid solution. AlSiZn coating offered sacrificial protection for the steel substrate in accelerated cyclic corrosion tests but the gain in sacrificial power was tarnished by a premature coating consumption. The last was attributed to the enhanced micro-galvanic coupling between Si inclusions and the de-passivated matrix and to the fact that the AlSiZn coating corrosion did not result in the formation of a suitable corrosion product which could protect steel by a barrier effect at long times. Compared to the AlSiZn, the AlSiZnMg coating demonstrated identical electrochemical behavior after 1 h of the OCP stabilization. However, in the accelerated tests the AlSiZnMg was less consumed and the AlZn matrix was less attacked in the AlSiZnMg than in the AlSiZn coating. As a result, the coating life time was increased and a significantly longer sacrificial protection was achieved. Several hypotheses about corrosion mechanisms were formulated. The decrease of AlSiZnMg coating corrosion rate compared to AlSiZn was attributed to:

1) lowering galvanic coupling between the Al rich matrix and Si containing phases because of the partial transformation of Si particles into more anodic Mg_2Si,

2) initial cathodic protection of AlZn matrix due to selective Mg dissolution evidenced by mass balance,

3) reduced microgalvanic currents even after selective Mg dissolution from Mg_2Si phase because of the formation of SiO_2 in place of metallic Si inclusions and

4) formation of significant quantities of Mg-ions contributing in both, formation of Mg-rich corrosion products, which could limit the reactivity of the coating by different mechanisms, and synergic effect of soluble Mg^{2+} and Zn^{2+} ions on steel cathodic reactivity.

The proposed hypotheses need mechanistic verification on model systems. Finally, it seems that two main factors are critical for corrosion mechanisms of the AlSi(Zn,Mg) alloyed coatings on high strength steel: micro-galvanic coupling between Al-rich matrix and Si-containing precipitates and the nature and stability of corrosion products containing Mg.

Acknowledgements

Authors are grateful for French National Agency of Research and Technology (ANRT) for partial financial support of C. Nicard PhD program (convention CIFRE 2015/0472).

References

[1] W.B. Nowak, Thin metallic films for corrosion control, Metallurgical Coatings and Thin Films (1991), pp. 71–77.

[2] K. Ogle, S. Morel, D. Jacquet, Observation of self-healing functions on the cut edge of galvanized steel using SVET and pH microscopy, Journal of The Electrochemical Society, 153 (2006), B1-B5.

[3] F. Thebault, B. Vuillemina, R. Oltra, K. Ogle, C. Allely, Investigation of self-healing mechanism on galvanized steels cut edges by coupling SVET and numerical modeling, Electrochimica Acta 53 (2008), pp. 5226–5234.

[4] F. Zeng, Z. Wei, C. Li, X. Tan, Z. Zhang, Corrosion mechanism associated with Mg2Si and Si particles in Al–Mg–Si alloys, Transactions of Nonferrous Metals Society of China 21.12 (2011), pp. 2559–2567.

[5] S. Han, H. Li, S. Wang, L. Jiang, X. Liu, Influence of silicon on hot-dip aluminizing process and subsequent oxidation for preparing hydrogen/tritium permeation barrier, International Journal of Hydrogen Energy 35.7 (2010), pp. 2689–2693.

[6] M. Salgueiro Azevedo, C. Allely, K. Ogle, P. Volovitch, Corrosion mechanisms of Zn(Mg, Al) coated steel in accelerated tests and natural exposure: 1. The role of electrolyte composition in the nature of corrosion products and relative corrosion rate, Corrosion Science 90 (2015), pp. 472–481.

[7] A. Bahadur, Aluminum coatings for steel, Materials and Manufacturing Processes (1996), pp. 225-232.

[8] N. Takata, M. Nishimoto, S. Kobayashi, M. Takeyama , Morphology and formation of Fe–Al intermetallic layers on iron hot-dipped in Al–Mg–Si alloy melt, Intermetallics 54 (2014), pp. 136–142.

[9] C. Allely, L. Dosdat, O. Clauzeau, K. Ogle, P. Volovitch, Anticorrosion mechanisms of aluminized steel for hot stamping, Surface and Coatings Technology 238 (2014), pp. 188–196.

[10] Z. Szklarska-Smialowska, Pitting corrosion of Al, Corrosion Science 41.9 (1999), pp. 1743–1767.

[11] C. Vargel, Corrosion of Aluminium, Elsevier, (2004), pp. 81–109.

[12] I. DeGraeve, I. Schoukens, A. Lanzutti, F. Andreatta, A. Alvarez-Pampliega, J. DeStrycker, L. Fedrizzi, H. Terryn, Mechanism of corrosion protection of hot-dip aluminium–silicon coatings on steel studied by electrochemical depth profiling, Corrosion Science 76 (2013), pp. 325–336.

[13] A. Alvarez-Pampliega, S.V. Lamaka, M.G. Taryba, M. Madani, J. De Strycker, E. Tourwé, M.G.S. Ferreira, H. Terryn, Cut-edge corrosion study on painted aluminum rich metallic coated steel by scanning vibrating electrode and micro-potentiometric techniques, Electrochimica Acta 61 (2012), pp. 107–117.

[14] S. Li, B. Gao, G. Tu, L. Hu, S. Sun, G. Zhu, S. Yin, Effects of Mg on the Microstructure and Corrosion Resistance of Zn–55Al–1.6Si Coating, Construction and Building Materials 71 (2014), pp. 124–131.

[15] W. Liu, M. Li, Q. Luo, H. Fan, J. Zhang, H. Lu, K. Chou, X. Wang, Q. Li, Influence of alloyed Mg on the microstructure and long-term corrosion behavior of hot-dip Al–Zn–Si coating in NaCl solution, Corrosion Science Volume 104 (2016), pp. 217–226.

[16] W.H. Hartt, E.J. Lemieux, K.E. Lucas, A critical review of Al anode activation, dissolution mechanisms, and performance, NACE International, CORROSION (2001).

[17] D.R. Salinas, S.G. Garcia, J.B. Bessone, Influence of alloying elements and microstructure on aluminium sacrificial anode performance: case of Al–Zn, Journal of Applied Electrochemistry 29.9 (1999), pp. 1063–1071.

[18] J. Macanás, L. Soler, A. María Candela, M. Muñoz, J. Casado, Hydrogen generation by aluminum corrosion in aqueous alkaline solutions of inorganic promoters: The AlHidrox process, Energy 36 (2011), pp. 2493-2501.

[19] M. Reboul, Corrosion des alliages d'aluminium, Techniques de l'Ingénieur, COR325 (2005).

[20] N.A. Belov, D.G. Eskin, A.A. Aksenov, Multicomponent phase diagrams: applications for commercial Al alloys, Elsevier Science (2005) pp. 193-222.

[21] J. Soto, G. Aramburo, C. Gonzalez, J. Genesca, R. Herrera, J.A. Juarez-Islas, Distribution and prediction of solute in Al–Zn–Mg alloys, Materials Science and Engineering (2005).

[22] A.Q. Vu, B. Vuillemin, R. Oltra, C. Allély, In situ investigation of sacrificial behaviour of hot dipped AlSi coating in sulphate and chloride solutions, Corrosion Science 70 (2013) pp. 112–118.

[23] N. Birbilis, RG. Buchheit, Electrochemical characteristics of intermetallic phases in aluminum alloys, Journal of The Electrochemical Society 152.4 (2005), pp. 140–151

[24] F. Andreatta, Local electrochemical behaviour of 7xxx aluminium alloys, PhD, Applied Sciences, 2004.

[25] Q. Li, Y.Z. Zhao, Q. Luo, S.L. Chen, J.Y. Zhang, K.C. Chou, Experimental study and phase diagram calculation in Al–Zn–Mg–Si quaternary system, Journal of Alloys and Compounds 501 (2010) pp. 282–290.

[26] R. Valdes, A. Freulon, J.-B. Deschamps, Ma Qian, Jacques Lacaze, Phase equilibria and solidification of Mg-rich Al-Mg-Si alloys, Materials Science Forum, Volume 508, (2006), pp. 621-628.

[27] P. Volovitch, L. Barrallier, W. Saikaly, Microstructure and corrosion resistance of Mg alloy ZE41 with laser surface cladding by Al–Si powder, Surface and Coatings Technology 202.20 (2008), pp. 4901–4914.

[28] M. Salgueiro Azevedo, C. Allely, K. Ogle, P. Volovitch, Corrosion mechanisms of Zn(Mg,Al) coated steel: 2. The effect of Mg and Al alloying on the formation and properties of corrosion products in different electrolytes, Corrosion Science 90 (2015) pp. 482–490.

[29] M. Salgueiro Azevedo, C. Allely, K. Ogle, P. Volovitch, Corrosion mechanisms of Zn(Mg,Al) coated steel: The effect of HCO3_ and NH4+ ions on the intrinsic reactivity of the coating, Electrochimica Acta 153 (2015) pp. 159–169.

[30] T. Ishikawa, M. Ueda, K. Kandori, T. Nakayama, Air permeability of the artificially synthesized Zn–Al–Mg alloy rusts, Corrosion Science 49.6 (2007), pp. 2547–2556.

[31] P.S. Braterman, Layered Double Hydroxides: synthesis, characterization and interaction of Mg-Al systems with intercalated tetracyanonickelate (II), Master of Science. University of North Texas, (2004).

[32] X. Duan, G.D Evans. Layered Double Hydroxides, book, Springer Science & Business Media, (2006).

[33] P. Visser, Y. Gonzalez-Garcia, J.M.C. Mol, H. Terryn, Mechanism of passive layer formation on AA2024-T3 from alkaline lithium carbonate solutions in the presence of sodium chloride, Journal of The Electrochemical Society, 165 (2) (2018), C60-C70.

[34] F. Beier, K-H. Dtellnberger, S. Geisler, A new accelerated cyclic corrosion test for automotive substrates, in: Proceeding of the Eurocorr, Nice, France, (2009).

[35] J.P. Laurent, J.P. Hennechart, D. Spehner, J. Devroc, “Coated hot- and cold-rolled steel sheet comprising a very high resistance after thermal treatment", U.S. Patent 6296805B1, issued October 2, (2001).

[36] RUFF database website : http://rruff.info/general=hydrotalcite/display=default/R050457 (accessed on 12-18-2017).

[37] D. Landolt, Corrosion et chimie de surfaces des métaux, PPUR presses polytechniques, Vol. 1 (1997), Traités des matériaux 12.

[38] Y.Du, J. Schuster, Z. Liu, R. Hu, P. Nash, W. Sun, W. Zhang, J. Wang, C. Tang, Z. Zhu, S. Liu, Y. Ouyang, W. Zhang, N. Krendelsberger, A Thermodynamic Description of the Al–Fe–Si System over the Whole Composition and Temperature Ranges via a Hybrid Approach of CALPHAD and Key Experiments, Intermetallics 16.4 (2008), pp. 554–570.

[39] M. Serdechnova, P. Volovitch, K. Ogle, Atomic emission spectroelectrochemistry study of the degradation mechanism of model high temperature paint containing sacrificial aluminum particles, Surf. Coat. Technol. 206 (2012), pp. 2133-2139

[40] L. Wei, L. Qian, L. Mou-Cheng, Corrosion behaviour of hot-dip Al–Zn–Si and Al–Zn–Si–3Mg coatings in NaCl solution, Corrosion Science, Volume 121, (2017), pp. 72–83.

[41] X. Zhang, T. Vu, P. Volovitch, C. Leygraf, K. Ogle, I. OdnevallWallinder,The initial release of Zn and Al from non-treated Galvalume and the formation of corrosion products in chloride containing media, Applied Surface Science 258.10 (2012), pp. 4351–4359.

[42] X.G. Zhang, Corrosion and Electrochemistry of Zinc, Springer Science & Business Media, (1996), pp. 157-178.

[43] N. LeBozec, D. Thierry, M. Rohwerder, D. Persson, G. Luckeneder, L. Luxem, Effect of carbon dioxide on the atmospheric corrosion of Zn–Mg–Al coated steel, Corros. Sci. 74 (2013) 379–386

[44] R. Krieg, M. Rohwerder, S. Evers, B. Schuhmacher, J. Schauer-Pass, Cathodic selfhealing at cut-edges: the effect of Zn2+ and Mg2+ ions, Corros. Sci. 65 (2012) 119–12.

[45] R. Krieg, A. Vimalanandan, M. Rohwerder, Corrosion of zinc and Zn-Mg, J. Electrochem. Soc. 161 (3) (2014) C156–C161.

Chapter IV

Electrochemical reactivity of Al(Zn), Al_3FeSi_2 and Mg_2Si phases and its consequence for corrosion mechanisms of AlSiZnMg coated steel

C. Nicard, C. Allély, J. Stoulil, V. Self, P. Volovitch
Paper in preparation for submission to the Journal of Electrochemical Society

Investigated topics:

- How the electrochemical properties of the pure phases present in AlSiZnMg coatings can explain corrosion mechanisms?
- What are the possible beneficial or detrimental coupling between the phases?

Highlights:

- Zn alloying of Al enhances its galvanic coupling with all intermetallics.
- Si and AlFeSi intermetallics enhance selective dissolution of Al and Al(Zn).
- Mg_2Si, firstly anodic versus Al(Zn) solid solution, became cathodic transforming in SiO_2.
- Galvanic current for Al(Zn)/SiO_2 is significantly lower than for Al(Zn)/Si explaining less matrix consumption.

Chapter IV – Electrochemical reactivity of Al(Zn), Al_3FeSi_2 and Mg_2Si phases and its consequence for corrosion mechanisms of AlSi(Zn,Mg) coated steel

Abstract

Selective dissolution from pure phases composing AlSi(ZnMg) steel coating and galvanic coupling between them and Mn22B5 steel were analyzed combining electrochemical tests and downstream solution analysis by AESEC. Surface analysis were completed by Scanning Electronic Microscopy (SEM), X-Ray Diffraction (XRD) and Energy Dispersive Spectroscopy (EDS). Replacement of Al matrix by Al(Zn) resulted in increased galvanic currents between the different phases and the matrix. Surface of Mg_2Si phase rapidly transformed into SiO_2 in aqueous solutions. Mg silicates and SiO_2 being less electrochemically active than metallic Si, galvanic current Mg_2Si/Al and Mg_2Si/Al(Zn) was reduced compared to Si/Al and Si/Al(Zn) even at long exposures. The consequences of phase composition on the coating corrosion mechanisms are discussed.

Keywords

Metal Coatings (A); Al (A); Zn (A); Mg (A); Electrochemistry (B); AESEC (B); Galvanic Coupling (C);

1 Introduction

New AlSiZnMg anticorrosion coatings are developed to protect high strength steel in automotive application [1-6]. The results of corrosion tests demonstrated that these coatings offer an interesting compromise between sacrificial power and barrier protection.

Zinc and magnesium alloying in AlSi based coatings modifies the phase composition and microstructure of the coating [7,8]. An AlSiZnMg coating is basically composed of an Al(Zn) solid solution matrix, with Si and/or Mg_2Si precipitates and an $Al_xFe_ySi_z$ intermetallic layer [9] at the interface between the coating and steel. Mg_2Si quantity depends on Mg/Si ratio and $MgZn_2$ can sometime be found near Mg_2Si if Mg/Si and Zn/Si ratios are high [5]. All these phases have very different corrosion potentials [10 - 13] and electrochemical behavior. Compared to steel which corrosion potential is around -0.66 V vs. SCE in chloride media (0.1 M) at neutral pH, Mg_2Si, $MgZn_2$ and Al(Zn) solid solution [7] have more negative corrosion potential than Al matrix therefore being anodic, while Si, SiO_2, $Al_xFe_ySi_z$ [14] have more positive corrosion potential than Al matrix therefore being cathodic. Because of the differences in electrochemical behaviour of Al(Zn) solid solution compared to pure Al and the high number of phases with very different corrosion potentials, AlSiZnMg coatings are expected to undergo strong micro–galvanic coupling effects. This phenomenon can cause premature consumption of the coatings compared to unalloyed AlSi coatings.

In corrosion processes, one should consider not only the effect of the initially present pure phases but also the newly formed phases. This can result from the fact that during corrosion some phases can evolve by oxidation or selective dissolution, modifying the microstructure and the electrochemical response of the system. For example, Mg_2Si intermetallic in Al matrix was reported to dissolve forming SiO_2 [15] in Cl-containing solutions. The transformation is caused by selective dissolution of Mg and reaction of remaining Si with water [16]. The corrosion potentials of some of the expected phases in AlSiZnMg coated steel were previously reported in the electrolytes with high Cl content. While it is well known that Al-based materials are highly sensitive to Cl^-content in the electrolyte [17], we have not found a publication reporting the electrochemistry of the selected pure phases and their coupling in more diluted solutions, common for modern accelerated corrosion tests in automotive industry VDA 233-102 [18]. The role of individual phases in corrosion mechanisms of the coating in low Cl environment needs hence to be better understood.

Based on the literature review, several hypotheses on the effect of phase composition on the reactivity can be made. Indeed, Al(Zn) solid solutions are widely used to make effective

protective anodes [19,20] and studies reveal that Zn can cause selective cathodic dissolution of Al. The Al(Zn) coatings matrix is expected to cathodically protect the substrate steel stronger than Al matrix due to lower corrosion potential [21]. This sacrificial capacity however should result in a higher coating consumption [22].Added magnesium bonds with Si, forming Mg_2Si intermetallic which becomes anodic versus Al(Zn) matrix in neutral solutions [23] which could potentially slow corrosion reactions. Finally, Al(Zn), Al_3FeSi_2 and Mg_2Si phases can be formed in AlSiZnMg coated steel in place of Al, Si and AlSiFe in case of unalloyed coating. Their electrochemical properties and their consequences for the corrosion mechanisms of AlSiZnMg coated steel need to be understood.

In the present work, the synthesis and the characterization of the reactivity of the selected phases individually and in different combinations between them and with the steel substrate are presented. Particular attention is given to the effect of the phase composition on the sacrificial capacity for steel and to the intrinsic galvanic coupling which can result in enhanced coating consumption.

2 Experimental

2.1 Materials synthesis

Pure Al, Zn, Si, Fe were ordered from GoodFellow at respectively 99.999 %, 99.95 %, 99.999 %, 99.5 % purity. Mg_2Si, $MgZn_2$, Al(Zn) solid solution were synthesized from pure metals: Al 99.998 wt.% (Laurand Associates), Zn 99.99 wt. %, Mg 99.99 wt. % and Si 99.95 wt. % (all Metal Trade Comax). Zn-Al based samples were melted in muffle furnace and cast into cylindrical brass mold with diameter 50 mm. Ingots were cut to 5 mm thick discs and then annealed at 500 °C for 24 h. All samples were then water quenched in order to obtain homogenized structure of α-Al solid solution. $MgZn_2$ and Mg_2Si samples were melted in argon induction furnace (Leybold-Heraeus) and cast into the same mold. Castings contained high amounts of non-reacted elements and oxide inclusions. Ingots were mechanically crushed, particles were homogenized by high energy ball milling in VM4 device (OPS Prerov) at 400 revs.min^{-1} for 3 minutes. Powder fraction 25-45 μm was then used for spark plasma sintering (SPS) in HP D device (FCT Systeme). Both powders were pressed into 20 mm mold by 15 kN using 5.250SP1-VM device (LabTest). $MgZn_2$ was sintered at 500 °C for 10 minutes with 100 °C.min^{-1} step. Mg_2Si was sintered at 900°C for 10 minutes with step 200 °C.min^{-1}. The final dimensions of the Mg_2Zn and Mg_2Si samples were 20 mm diameter and 5 mm height.

Table 1 : Phases weight and molar compositions and suppliers.

Phases	Composition / wt. %	Composition / mol. %	Supplier
Al	~ 100 (Al)	~ 100(Al)	GoodFellow
Al(Zn32)	64 (Al) 36 (Zn)	81(Al) 19(Zn)	UCT Prague
Al(Zn20)	78 (Al) 22 (Zn)	90(Al) 10(Zn)	UCT Prague
Al(Zn10)	89 (Al) 11 (Zn)	95 (Al) 5 (Zn)	UCT Prague
Fe	~ 100 (Fe)	~ 100 (Fe)	GoodFellow
Si	~ 100 (Si)	~ 100 (Si)	Goodfellow
Al_3FeSi_2	62 (Al) 30 (Fe) 8 (Si)	73 (Al) 9 (Fe) 18 (Si)	UCT Prague
Zn_2Mg	84 (Zn) 16 (Mg)	66 (Zn) 34 (Mg)	UCT Prague
Mg_2Si	55 (Mg) 44 (Si)	68 (Mg) 32 (Si)	UCT Prague
SiO_2	NA	NA	hot treatment of good fellow samples

Phase Al_3FeSi_2 (Al - Si35 wt. % - Fe 15 wt. %) [6] was prepared by reactive sintering method from powders: Fe 99.9 wt. % and Al 99.7 wt. % (both Strem Chemicals), Si 99.5 wt. % (Alfa Aesar). Powders were homogenized by mixing, compacted with 65 kN and then heat-sealed in ampoule, which was heated up to 800° C to start the reaction which ran for 30 minutes. Reacted powder was homogenized by the same milling procedure as previous samples, compacted by 15 kN and then sintered by SPS at 700° C for 10 minutes with 200 $°C.min^{-1}$ step. SiO_2 phase was prepared from GoodFellow 99.999 % purity silicon pulverization target thermally treated at 900 °C during 2 h 30 with a +20 °C dew point in an atmosphere controlled oven.

Mg_2Si, Al_3FeSi_2, and $MgZn_2$ are brittle phases, in order to make them easier to manipulate (polishing, experiments and observation), they were mounted in resin. The samples were ground from both sides in order to access the metal on the two sides and permit electrical contact.

2.2 Surface characterization

Formed phases where characterized by X-Ray Diffraction (XRD) (Appendix 6). The morphology was observed by a JEOL 7800F Field Emission Gun Scanning Electron

Microscope (FEG-SEM) coupled with Brucker Xflash 6160 Energy Dispersive Spectroscopy (EDS) with a Si(Li) detector and equipped with QUANTAX 1.9 software (Bruker AXS) at accelerating voltage of 5 kV for electron imaging and 15 kV for quantitative EDS. For SEM and EDS, the pure phases were polished with 2400 grade silicon carbide paper.

SiO_2 was also analyzed by photoelectrons spectroscopy (XPS) using monochromatic aluminum source, at 50W and 15kV. Analyzed area was 200 μm^2, and the analyzed depth about 10 nm. XRD spectra of pure phases in their initial state and XPS spectra of SiO_2 are presented in Appendix 6.

2.3 Open Circuit Potential and Potentiodynamic polarization

Potentiodynamic polarization curves of the synthesized pure phases were performed in 0.172 M (1 wt. %) NaCl aqueous solution at initial pH 7 and 11 (adjusted by 0.5 M NaOH solution) using a BioLogic VMP3 potentiostat. Corrosion potentials of the some phases were also measured in 0.086 M (2.4 wt. %) Na_2SO_4 to evaluate electrochemical behavior in non-chloride environment. A standard three-electrode cell held at 25 ± 2 °C was used with a saturated calomel electrode (SCE) as a reference electrode, a platinum plate as a counter electrode (total area of 1 cm^2) and the chosen phase as a working electrode (0.6 cm^2 of exposed surface).

Cathodic and anodic polarizations were performed separately on different samples with a renewed electrolyte. For polarization curves, the sequence was set to perform a 15 minutes of open circuit potential (OCP) measurement followed by anodic or cathodic polarization from the OCP value with 1 $mV.s^{-1}$ sweep rate. The potential ranges were from OCP to -1.6 V vs. SCE for cathodic polarization and from OCP to -0.5 V vs. SCE for anodic polarization.

Aluminum sensitivity to zinc ions was also tested by immersion of pure aluminum in 0.172 M NaCl and 0.086 M $ZnCl_2$ aqueous solution at different pH adjusted (from 7 to 11) with 0.5 M NaOH or 0.5 M HCl. The predominance area for Al or Zn based species in an aqueous system containing 0.172 M NaCl, 0.086 M Zn^{2+} and 0.001 M Al^{3+} was calculated using Hydra Medusa software [24] taking into account all complexes presented in the database (12-2015).

2.4 Galvanic coupling experiments

Galvanic coupling experiments were made in the same electrolyte as polarization curves. A conventional three electrodes cell was used in the same configuration as in section 2.3 except that the second pure phase was used as a counter electrode in place of the platinum plate. Before all the experiments, pure phases were mechanically polished with 1200 grade silicon carbide paper in ethanol in order to remove surface oxides. For each experiment the electrochemical sequence consisted of alternating periods of 30 minutes of uncoupled immersion to measure the evolution of the OCP potential, and 5 h 30 min of coupled measurement recording galvanic current between the phases.

2.5 Dissolution experiments

Dissolution experiments were performed using Atomic Emission Spectro Electro-Chemistry (AESEC) [25,26,27] which consists in an electrochemical cell coupled with an induced coupled plasma optical emission spectroscopy (ICP-OES). The electrochemical cell contains two compartments separated with a porous membrane. On one side, a calomel saturated electrode and the platinum plate counter electrode and on the other side the metallic samples with a surface area of 0.5 cm^{-2} are placed. The electrolyte was continuously pumped in the electrochemical cell with the flow rate of 3 $ml.min^{-1}$ and continuously analyzed by ICP OES after the contact with the sample. The intensity of characteristic emission of each element was measured by ICP OES in the solution injected in the plasma. With standard solution (with fixed element concentration) the experiment can be calibrated to give real-time concentration (C_M) in the flowing electrolyte. Knowing the flow rate (f) and the exposed surface (A), elemental flux (v_M) can be calulated as following:

$$v_M = C_M f / A \qquad (1)$$

Considering the dissolution equation of the metallic elements ($Me \rightarrow Me^{n+} + ne^-$) we can calculate elemental current (j_M) as following:

$$j_M = n F v_M \qquad (2)$$

Where (F) is Faraday constant and n is the oxidation state of the element M. In this work we considered n=2 for Zn, Mg, Fe, n=3 for Al and n=4 for Si.

Two series of experiments were made. In the first one, pure phases were anodically polarized at constant applied current density = 100 µA.cm^{-1}, 200 µA.cm^{-1}, 500 µA.cm^{-1} and 1000 µA.cm^{-1}. The elemental dissolutions were measured at each imposed current. In the second series the anodic current was set to 500 µA.cm^{-1} and the pH of the solution was modified (adjusted by 0.5 M NaOH aqueous solution) to 7, 9, 11 and 13. The elemental dissolution currents were measured at each pH value.

3 Results

3.1 Pure phases composition

Table 1 sums up the elemental compositions (wt. and at. %) of the phases used in this work. XRD and XPS analysis of these phases are presented in Appendix 6. Obtained Al(Zn) solid solutions were homogeneous except for Al(Zn32), in which some quantity of η-phase was detected. Al(Zn) was the only material with a bi-phase microstructure composed by the α and η phases usually found in Al solid solution with more than 20 wt % of Zn [21]. Mg_2Si and Al_3FeSi_2 phases were homogenous, however they were slightly porous due to the fabrication process. $MgZn_2$ and Mg_2Si were the most difficult to make because magnesium easily combines with oxygen to form oxides and the atmosphere during the synthesis must be controlled. The SiO_2 phase synthesis from metallic Si was simple to make but the formed oxide was very thin (<500nm) and it was impossible to easily confirm its formation with XRD. SiO_2 formation at Si surface during the thermal treatment was confirmed by EDS and XPS spectra (Appendix 7). The stability of pure Si to thermal treatment and its difficulty to transform into oxide even at such a temperature is coherent with the presence of numerous needles of metallic Si in AlSi(Zn) coatings.

3.2 Open circuit potential and polarization curves in different electrolytes

Fig. 1 and Tab. 2 present the measured corrosion free potentials of studied phases in various electrolytes, and polarization curves of all phases in 0.172 M NaCl aqueous solution. The phase ranking according to their corrosion potential from the most cathodic to the most anodic, is the following: Al_3FeSi_2, Si > Steel, Fe > Al > Al(Zn32-20-10) > $MgZn_2$ > Mg_2Si. SiO_2 free corrosion potential seems to be around -0.68 V vs. SCE but the measured currents are so low that it was hard to accurately determine it. In Tab. 2 a color code is associated to each phases depending of their potential in 0.172 M NaCl aqueous solution. Compared to iron (steel)

potential (shown in yellow), cathodic phases are shown in green and anodic in orange, red and purple. This color code will be used for schematic representation of the coating microstructure.

Table 2 : Corrosion potential of the studied phases (Ecorr / V vs. SCE) measured in different electrolytes as indicated and color code associated with each phase for schematic presentation of the phases.

Phase	**0.5 wt. % NaCl initial pH6**	**1 wt. % NaCl initial pH7**	**1 wt. % NaCl initial pH11**	**2.4 wt. % Na2SO4 initial pH7**	**Color used in schematic presentation**
Al_3FeSi_2	X	-0.40	-0.4	X	
Si	-0.45	-0.50	-0.33	-0.35	
Fe	-0.66	-0.59	-0.62	-0.64	
Al	-0.82	-0.74	-1.6	-0.72	
Al(Zn10)	X	-0.94	X	X	
Al(Zn20)	X	-0,95	X	X	
Al(Zn32)	X	-0,96	X	X	
Zn_2Mg	-1.0	-1,1	-1.3	-0.82	
Mg_2Si	-1.5	-1.4	-1.3	-1.4	
SiO_2	X	-0,68	X	X	

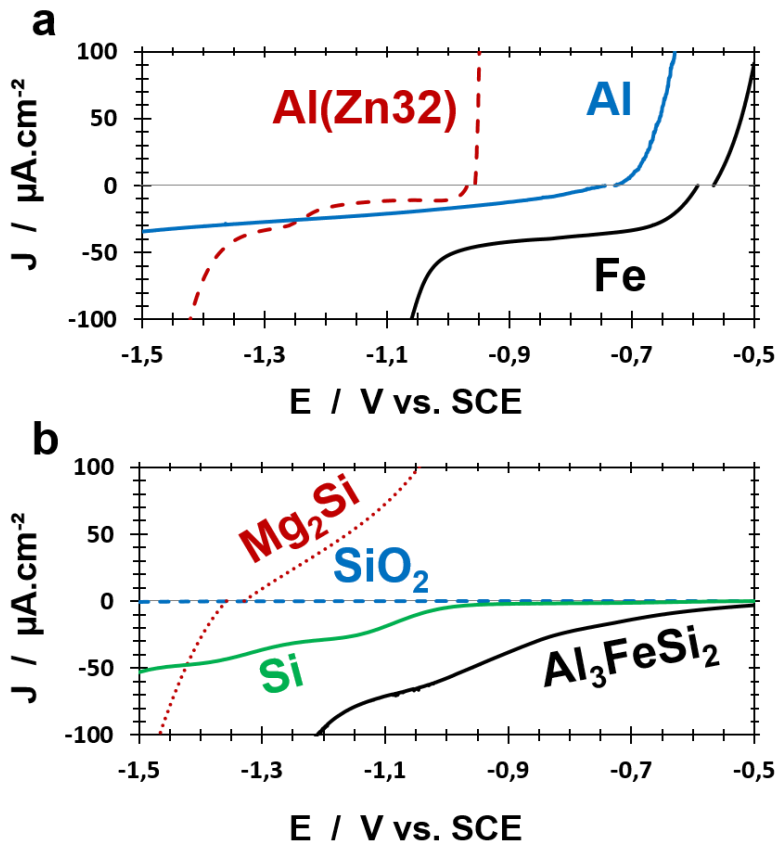


Figure 1 : Typical polarization curves of (a) Al, Fe, Al(Zn) solid solution, and (b) Mg_2Si, SiO_2, Si, Al_3FeSi_2 in NaCl 0,172 M (1 wt. %) aqueous solution at pH 7.

Fig. 2 regroups the evolution of Al free corrosion potential in NaCl solutions containing Zn^{2+} ions electrolyte with initial pH 5, 6 and 7. The OCP of Al in NaCl without Zn^{2+} ions is stable and stays around -0.7 V vs. SCE for both pH. In the presence of $ZnCl_2$ the OCP is rapidly stabilized to -0.7 V vs. SCE at pH 5 but is significantly more anodic at higher pH (goes up to -0.9 V vs. SCE at pH 7). The behavior seems to change when the transition between the predominance of soluble Zn^{2+} species (pH 5) is changed to the predominance of insoluble $Zn_5(OH)_8Cl_2 \cdot H_2O$ simonkolleite (from pH 6).

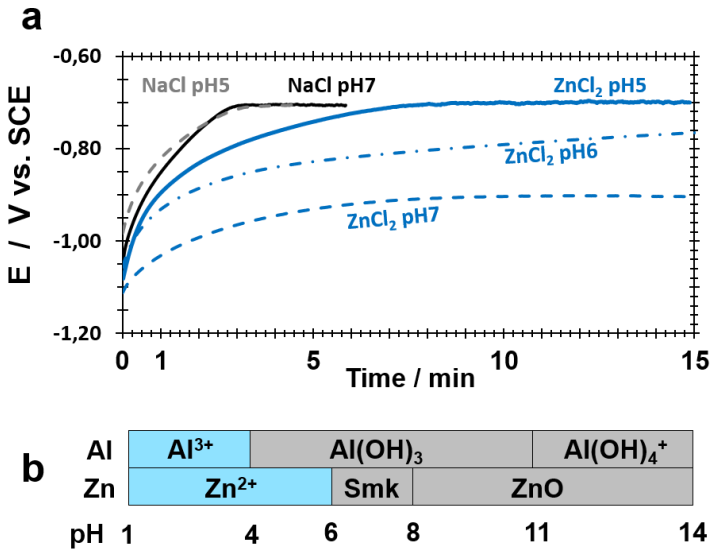


Figure 2 : (a) Open circuit potential of pure aluminum in NaCl 0.172 M or $ZnCl_2$ 0.086 M aqueous solution at pH 5 to 7 (adjusted with NaOH 1 M aqueous solution). (b) Simulated predominant Al/Zn containing species formed in an aqueous solution with 0.172 M NaCl , 0.086 M $ZnCl_2$, 0.001 M $AlCl_3$ (Hydra Medusa). Smk = simonkolleite.

3.2 Galvanic coupling of initial phases

The evolution of the OCP of uncoupled phases and the evolution of galvanic coupling potentials in coupling experiments are presented in Figs. 3-4-6 while Tab. 3 presents the highest values of the galvanic current values measured in the last (fourth) cycle of the coupling experiments.

Table 3 : Galvanic current ($\mu A.cm^{-2}$) measured on Al and Al(Zn) phases when coupled with different Si, Fe or Mg containg phases in 0.172 M NaCl aqueous solution (initial pH 7).

Phase	Al	Al(Zn32)	Al(Zn20)
Fe	59	78	X
Al_3FeSi_2	42	58	X
Si	34	38	37
Zn_2Mg	X	X	X
Mg_2Si	0,2	27	X
SiO_2	1.1	0.08	0.08

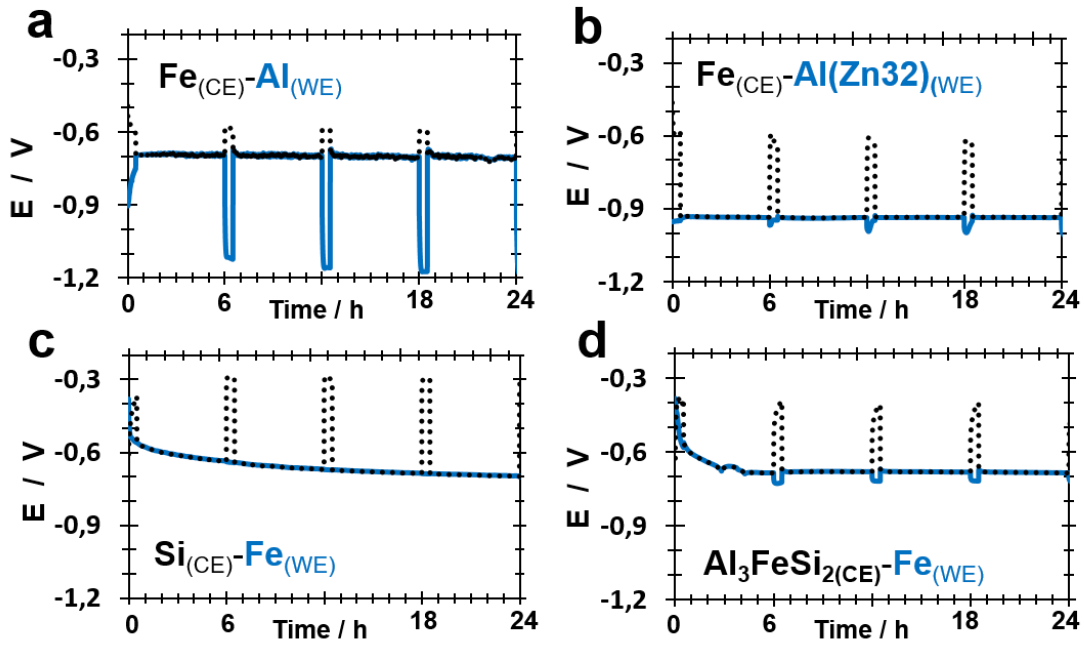


Figure 3 : Evolution of the potentials measured in coupling experiments between the substrate steel and the phases relevant for the AlSi(Zn,Mg) coating. Coupled phases: (a) Fe-Al, (b) Fe-Al(Zn32), (c) Si-Fe and (d) Al_3FeSi_2-Fe in 0.172 M NaCl aqueous solution. Coupling tests consisted of 6 h cycles, each cycle consisted of 30 minutes of the OCP measurement on two uncoupled phases followed by 5 hours and 30 minutes of galvanic coupling).

Fig. 3 shows the results for the coupling between the main phases composing a standard AlSiZn coatings and iron (steel). For Al or Al(Zn32) coupling with Fe (Fig. 3.a-b) the coupling potential remains stable during the 24 h experiment while for Si and Al_3FeSi_2 (Fig. 3.c-d) the coupling potential evolves to more anodic value. For Si and Al_3FeSi_2 coupling with iron, the iron potential also evolves from -0.6 V vs. SCE to -0.7 V vs. SCE. Silicon and Al_3FeSi_2 intermetallic phases coupling with Fe result in lower potential. The coupling potential of Al and Al(Zn) with Fe is always closer to the Al phase, regardless whether it is pure Al ($E_{Al/Fe}$ = -0.6 V vs. SCE) or Al(Zn) ($E_{Al(Zn)/Fe}$ = -0.6V vs. SCE). Potential of Al(Zn) does not vary while Al free potential decreases to -1.2 V vs. SCE at 24 h of experiments. Measured galvanic coupling current is presented in Table 3, Al_3FeSi_2-Al and Al_3FeSi_2-Al(Zn) systems have a maximum coupling current after 24 h experiment of 44 µA/cm² which is higher the coupling current of Si-Al and Si-Al(Zn). Concerning Al-rich phases coupling with iron, coupling current density of Al(Zn32) is 30 % higher than Al.

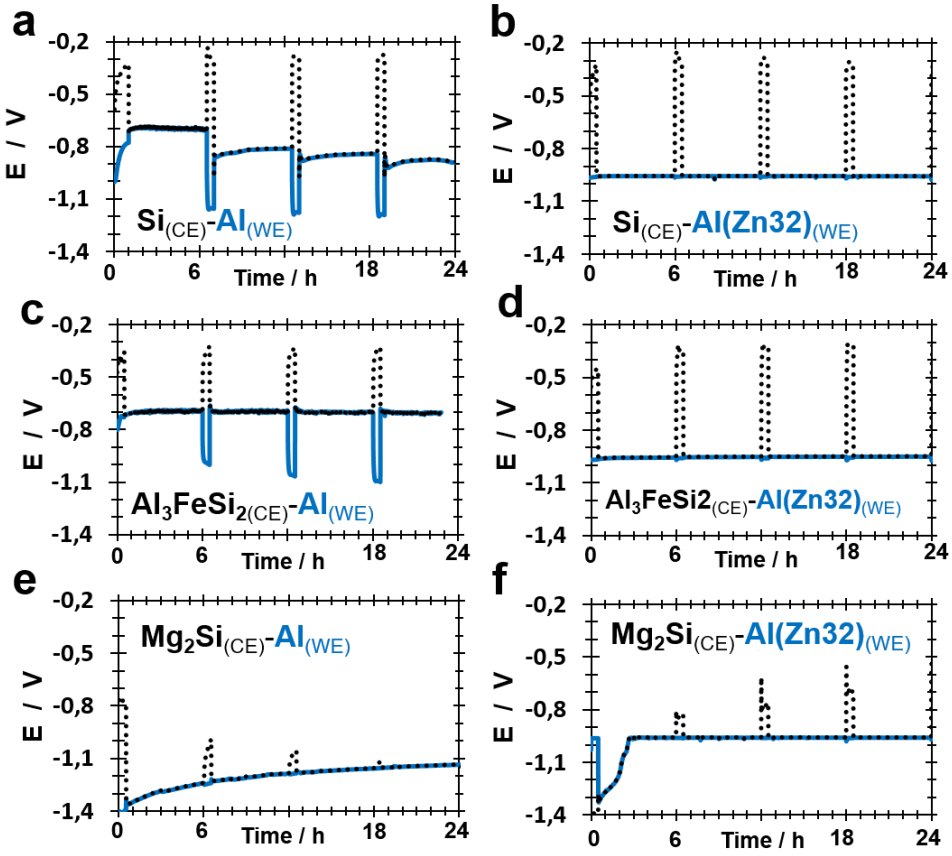


Figure 4 : Evolution of the potentials measured on phases relevant for intrinsic microgalvanic coupling in AlSi(Zn,Mg) coating during coupling tests. Coupled phases: (a) Si-Al, (b) Si-Al(Zn32), (c) Al_3FeSi_2-Al, (d) Al_3FeSi_2-Al(Zn32), (e) Mg_2Si-Al and (f) Mg_2Si Al(Zn32) in 0.172 M NaCl aqueous solution. Coupling tests consisted of 6 h cycles, each cycle consisted of 30 minutes of the OCP measurement on two uncoupled phases followed by 5 hours and 30 minuts of galvanic coupling).

.

Fig. 4 presents the potential evolution for coupling between Al or Al(Zn32) and Si, Al_3FeSi_2 or Mg_2Si. Coupled with aluminum-rich phases both Al_3FeSi_2 and Si stabilize at a potential around -0.4 V vs. SCE. Free corrosion potential and coupling potential of Al(Zn32) are in all three cases close and stable at around -0.95 V vs. SCE. The potential of pure Al decreases from -0.7 V vs. SCE to -1.2 V vs. SCE. Coupling potential is stable for Al-Al_3FeSi_2 experiment while it becomes more negative over time for Al-Si coupling. The measured galvanic currents are close for Al and Al(Zn) coupled with the same second phase, however, they are systematically a little bit higher for couples containing Al(Zn32) than for couples containing Al. Interesting situation is observed when Al or Al(Zn32) are coupled with Mg_2Si. Mg_2Si potential is initially anodic (-1.4 V vs. SCE) relative to Al-rich phase but it increases rapidly up to -0.7 V vs. SCE for Al(Zn32) and more slowly up to -1.14 V vs. SCE for pure Al. For pure Al the evolution of the coupling potential follows the evolution of the Mg_2Si OCP

while Al OCP decreases until both phases have the same potential. For Al(Zn32)-Mg_2Si, the coupling potential stabilizes at -0.96 V vs. SCE which is Al(Zn32) potential. At the beginning of all experiments, Mg_2Si is the anodic phase, but with time Al-Mg_2Si coupling current decreases until +0.2 µA/cm² while for Al(Zn32)-Mg_2Si coupling Mg_2Si becomes cathodic and the coupling current reaches -27 µA.cm^{-2}.

3.3 Effect of Mg_2Si transformation on galvanic coupling

The change from cathodic to anodic behavior supposes a major change in the surface properties. Infra-Red spectroscopy (ATR) has shown formation of amorphous silicates on Mg_2Si phase after Mg_2Si-Al(Zn32) coupling experiment (Fig. 5).

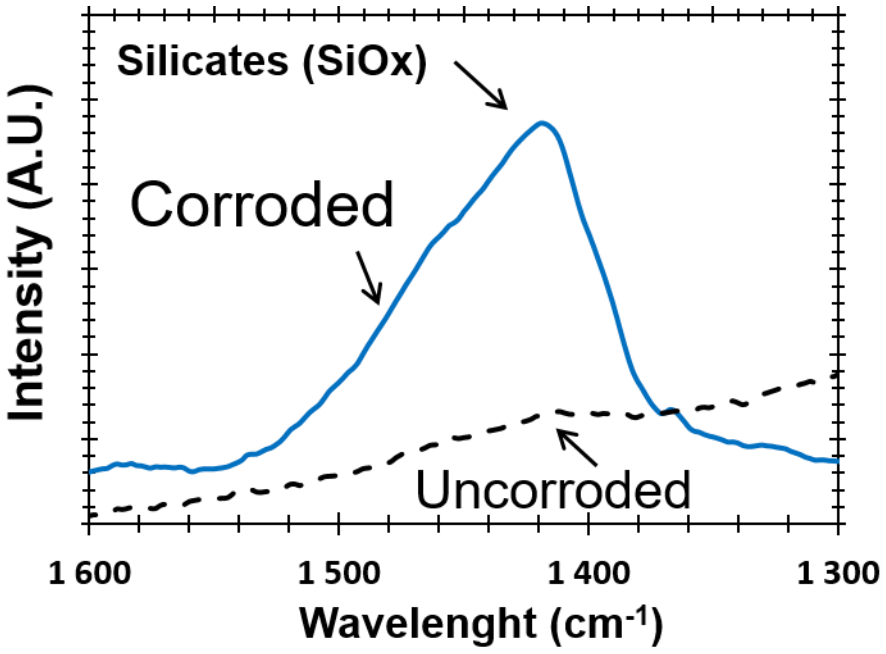


Figure 5 : ATR spectra of uncorroded and corroded Mg_2Si.

This phase modification can be detrimental for galvanic consumption of several phases, which were cathodic versus Mg_2Si but could become anodic and corrode preferentially when coupled with SiO_2. The accelerated corrosion tests [18] however did not show the preferential consumption of Al rich matrix around Mg_2Si. In order to compare the effect of Si and SiO_2 on the matrix consumption, the coupling experiments with SiO_2 were also performed. Fig. 6 shows the coupling potentials of Al or Al(Zn32) coupled with SiO_2 and the coupling current between Al or Al(Zn32) and Si, Mg_2Si or SiO_2. For both Al-rich phases, SiO_2 free corrosion potential stabilizes between -0.3 and -0.2 V vs. SCE and the coupling potential stays close to the Al-rich

phase OCP, -0.8 V vs. SCE for Al and -1.05 V vs. SCE for Al(Zn32). Fig. 6c demonstrates the evolution of galvanic currents with time. It shows that replacing Si with SiO_2 strongly limits the galvanic current, while if Si is replaced by Mg_2Si, the current is initially strong but reduces with time. In Si coupled with Al or Al(Zn32) the galvanic current increases with time and Si-Al coupling is less important than Si-Al(Zn32) coupling in the first hours.

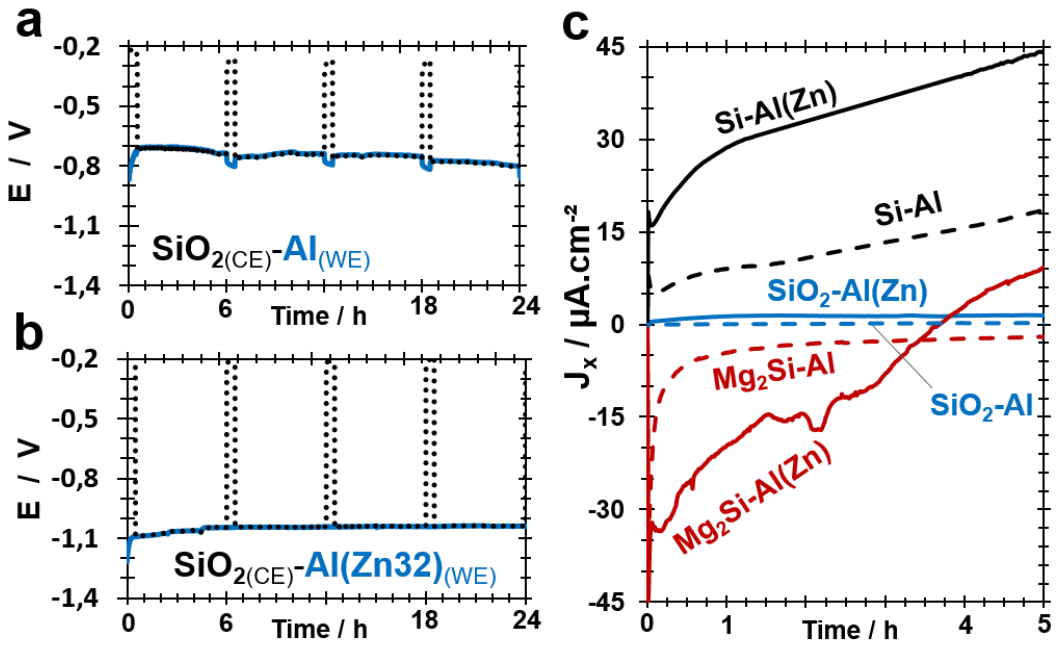


Figure 6 : Evolution of potential measured on 2 phases during coupling tests for (a) SiO2-Al and (b) SiO2-Al(Zn32) in NaCl 0.172 M aqueous solution. (c) Galvanic current of Si containing phases and Al or Al(Zn32) in NaCl 0.172 M aqueous solution.

3.4 Selective dissolution from pure phases under galvanostatic condition

The elemental dissolution currents measured by AESEC for uncoupled Al(Zn32), Mg_2Si and $MgZn_2$ under different applied anodic currents are presented in Fig. 7 (solution pH was initially adjusted to 7 in all experiments). For each applied current, the elemental contribution of each dissolved ion is calculated using eqs. 1-2. Each elemental current j_M is represented by a specific associated symbols and black cross represents the sum of the measured elemental currents. The diagonal dash line represents the situation when the total external current is equal to the sum of the elemental currents:

$$j_{external} = \sum j_M \qquad (3)$$

It can be seen from Figure 7, that $MgZn_2$ behaves like an ideal phase, dissolving at near stoichiometric ratios as well at low as at high current. Al(Zn32) phases shows a small selective zinc dissolution at low applied currents which becomes less important at higher currents. In Mg_2Si the dissolution of Mg represents 100 % of the total current flowing throughthe system while Si slight dissolution makes the total dissolution higher than the expected. This can be interpreted as a possible local galvanic coupling resulting in supplementary cathodic (j_n^{GC}) and anodic (j_n^{GC}) currents not measured by the potentiostat in the external circuit:

$$j_{total} = j_{app} + j_{an}{}^{GC} + j_{cath}{}^{GC} \qquad (4)$$

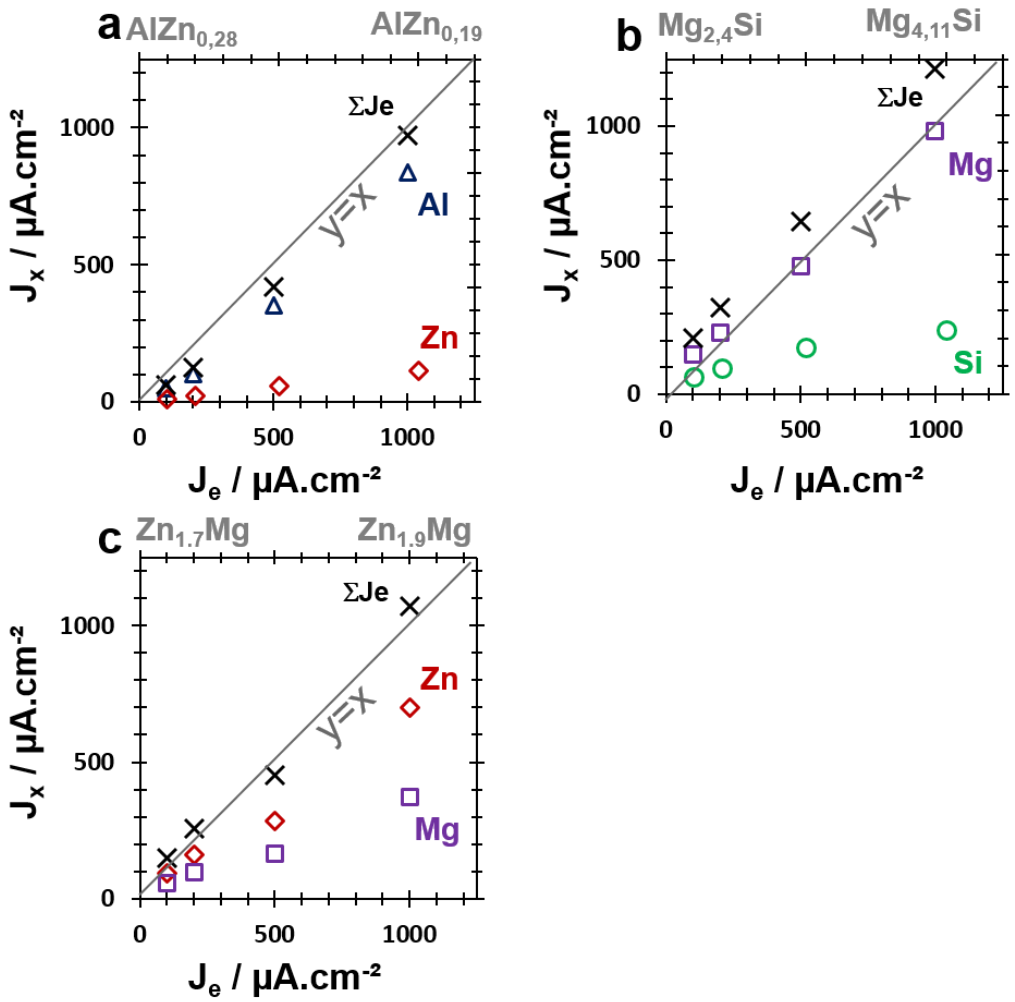


Figure 7 : Calculated from AESEC data elemental dissolution currents J_x (X=Al, Si, Mg and Zn as indicated) for dissolution of (a) Al(Zn32), (b) Mg_2Si, (c) Zn_2Mg in 0.172 M NaCl aqueous solution as a function of the imposed current J_e=100, 200, 500 and 1000 µA.cm⁻².

3.5 Effect of solution pH on selective dissolution from pure phases under applied current

The effect of the pH on the elemental currents dissolution under applied anodic current fixed at 500 µA.cm^{-2} is presented in Fig. 8. For each fixed pH value, the elemental contribution of each element is represented with associated symbols and black cross represents the sum of all elemental currents. The horizontal dash line delimits the value of applied current (500 µA.cm^{-2}):

$$\sum j_{elemental} = j_{applied}$$

As in previous experiments, $MgZn_2$ dissolution is stoichiometric for pH range from pH 7 to 11. At pH 13 the dissolution of both elements is not detectable.

In Mg_2Si the selective dissolution of Mg occurs at pH from 7 to 9. At pH 11 Si dissolution stops and at pH 13 no Mg is detected.

Al is selectively dissolved from Al(Zn32) phase in all range of pH, however at pH 13 Al dissolution is even 8 times higher than the imposed current. This is coherent with chemical dissolution of Al [25] as self-corrosion of Al becomes more important at higher pH and the sacrificial efficiency dramatically decreases.

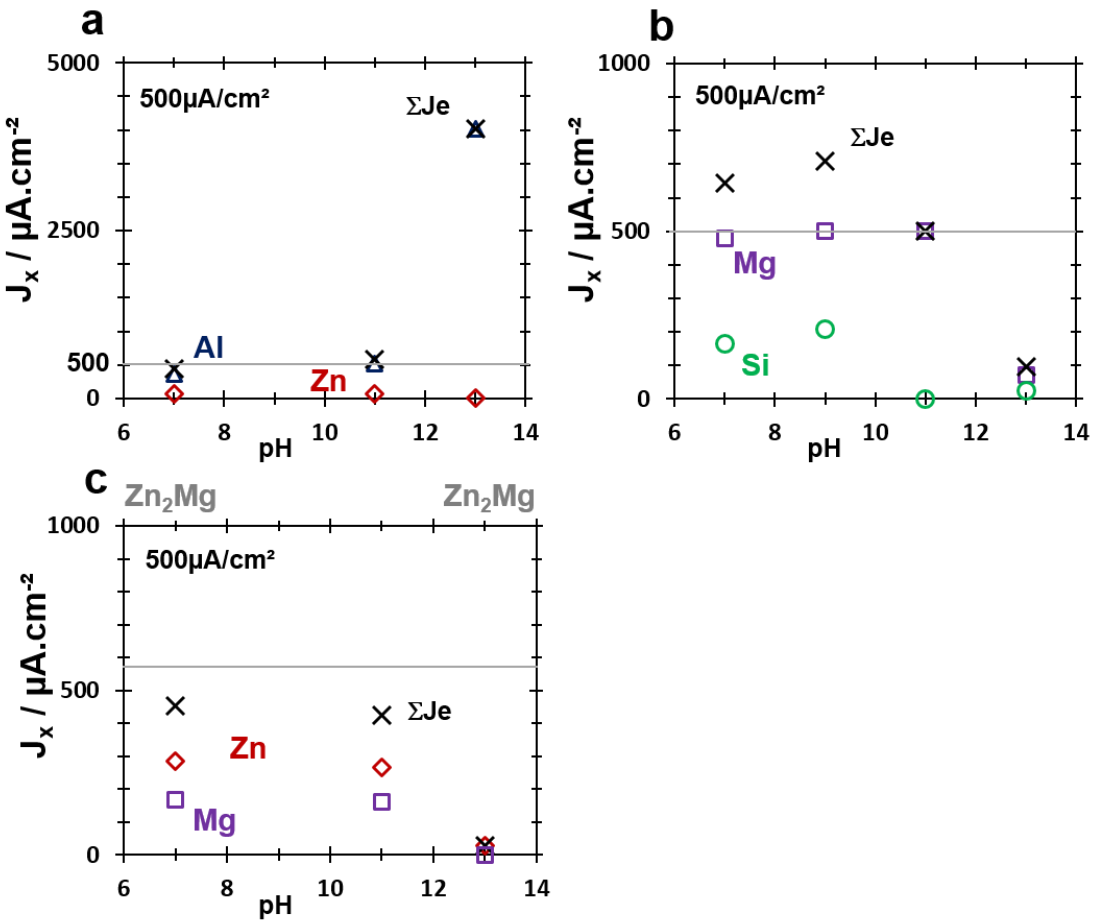


Figure 8 : Effect of pH on the elemental dissolution currents Jx (x=Al, Zn, Mg, and Si) for (a) Al(Zn32), (b) Mg_2Si, (c) Zn_2Mg dissolving inn 0.172 M NaCl aqueous solution with different pH under imposed anodic current of 500 µA.cm^{-2}.

4 Discussion

4.1 Impact of Zn ions on Al activation

The results confirm the non-sacrificial behavior of AlSi coating for steel observed in accelerated tests. Even if Al is active metal [7,8], its OCP very quickly approaches the OCP of the substrate steel and this is even more true in chloride free environment where aluminum OCP is higher than steel OCP (Tab. 2) [28]. Al(Zn) is expected to be more efficient in protecting steel galvanically which is illustrated by the fact that Al(Zn)-Fe coupling current is about 20 % higher and galvanic potential is about 200 mV more negative than for Al-Fe. Some mechanisms of Al activation by Zn alloying in solid solution are proposed in literature [29] but it does not explain pure Al activation by Zn ions observed in our experiments. The evolution of OCP of Al in the presence of Zn^{2+} ions and the effect of pH on this evolution let us suppose that it's the

presence of Zn^{2+} that changes aluminum behavior and prevent the passivation [8]. A possible explanation could hence be in the modification of the surface chemistry of Al with formation of defective spinel-like Zn-Al oxides or Al-Zn layered double hydroxides [30,31]. Alternative explanations could be proposed, for instance spontaneous deposition of metallic Zn could contribute to the oxidation of Al but it could not explain the pH effect on the potential evolution. Deeper study of the Zn^{2+} effect on Al reactivity is necessary.

4.2 Impact of pure phases modification on intrinsic galvanic coupling in AlSiZnMg coating

The activation of Al by Zn makes it more protective for steel but it also increases the galvanic coupling with all the other phases composing the coatings. If we combine the information about the coating microstructure from *Chapter III* and the phases corrosion potential ranking in 0.172 M NaCl aqueous solution, the microgalvanic coupling inside the coating can be schematically presented (Fig. 9) and the reactivity can be better understood.

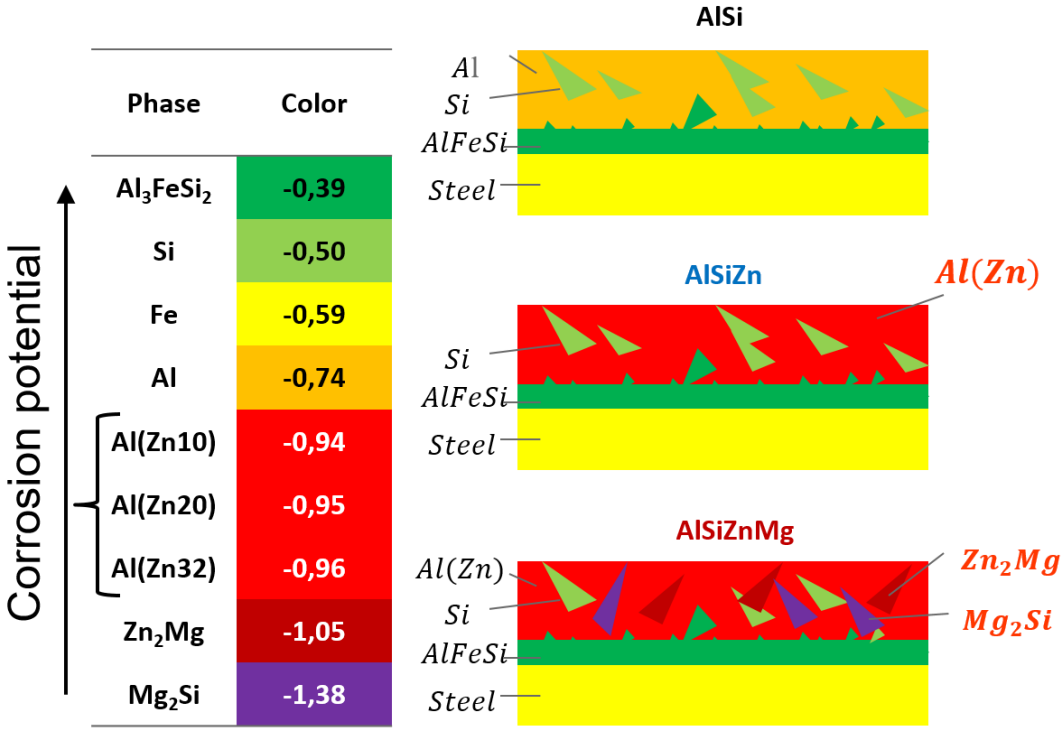


Figure 9 : Microstructural scheme of (a) AlSi, (b) AlSiZn and (c) AlSiZnMg with color scale depending on phase potential in NaCl 0.172 M aqueous solution. Color scale is described in Tab. 2.

Si and Al_3FeSi_2 are the most critical in this aspect because their corrosion potential is around -0.4 V vs. SCE. Coupling experiments reveal that the galvanic current is indeed in order of magnitude higher when Si or AlFeSi are coupled with Al(Zn) instead of Al. This could explain quicker coating consumption in case of Zn-alloyed coating compared to unalloyed AlSi

coating in accelerated corrosion tests [20]. This can't however explain the low consumption of AlSiZnMg coatings which also contain Al(Zn) matrix. Moreover, Mg_2Si and $MgZn_2$ initially have a more negative corrosion potential than Al and Al(Zn) and are supposed to be anodic and hence sacrificial for steel but also contribute to the localized corrosion of the coating. Mg_2Si when coupled with Al or Al(Zn) gradually changes the behavior from anodic to cathodic due to selective dissolution of Mg (Fig. 8). The formed surface is however not composed of metallic Si but by Si oxides and the galvanic coupling experiments SiO_2 and Al or Al(Zn) demonstrated that galvanic currents in coupling with SiO_2 are systematically lower than in coupling with Si or Mg_2Si. SiO_2 coupling with Al(Zn) matrix is hence less critical than Si coupling and the presence of Si-rich phases is expected to be less detrimental for self-corrosion of AlSiZnMg coatings than for AlSi or AlSiZn coatings.

4.3 pH effect on the phases stability

The complex microstructure of AlSiZnMg coatings can be regarded as a guarantee of reactivity in any pH domain. Indeed, Al(Zn) phase is active in neutral and alkaline solutions and Al becomes even more reactive at high pH. Aluminum sensitivity to pH variation can be also seen as a weakness of Al based coating because of too rapid coating consumption. In this case the presence of Mg can limit the increase of alkalinity by $Mg(OH)_2$ precipitation and prolongate the coating life. More detailed analysis of the effect of leached species on the reactivity via modification of the surface chemistry will be a subject of the next chapter.

5 Conclusions

The phase composing AlSiZnMg coatings were synthesized independently and characterized by X-ray Diffraction, Scanning Electronic Microscopy, Energy Dispersive Spectroscopy and X-ray Photoelectronic Spectroscopy. The electrochemical properties of these phases in corrosive media currently used in automotive corrosion test and the possible galvanic interaction between these phases were studied. Aluminum activation by zinc alloying leads to an increased sacrificial capacity of the coating for steel protection but also to enhancement in the galvanic coupling with all the phases composing the coating and possible premature coating consumption.

Aluminum matrix activation by Zn is confirmed and the high current in Al(Zn) coupling experiments with all the phases explains well why AlSiZn coatings exhibit strong premature and selective dissolution around Si-rich phases like Al_3FeSi_2 intermetallic and Si precipitates

[20]. Iron tendency to lower its potential when coupled with a phase with higher corrosion potential makes activation of aluminum by zinc even more useful. The OCP of Al is clearly affected by zinc ions, however, the precise mechanisms of aluminum activation are not yet determined.

AlSi coatings in accelerated corrosion test do not exhibit premature galvanic corrosion [19] because Al-Si coupling current at the in the first hour is 3 times less intense relative to Al(Zn)-Si coupling.

While Al_3FeSi_2 and Si are clearly detrimental phases in terms of possible galvanic coupling, the alloying with Mg reduce the harmful effect of Si containing phases. At initial stages of reactivity Mg_2Si is more anodic than both, aluminum and iron, protecting both of them. Due to selective dissolution of Mg, Mg_2Si transforms into silicon oxide which does not exhibit the same galvanic problem as pure Si in AlSiZn [20]. The latest was confirmed by the fact that the galvanic coupling currents for SiO_2-Al and SiO_2-Al(Zn) are in orders of magnitude smaller than the galvanic currents for Si-Al or Si-Al(Zn).

Finally, it seems that the AlSiZn coating corrosion mechanisms can be well explained by taking into account all the individual contribution of the phases. The huge increases in terms of anticorrosion properties of AlSiZnMg coating can partially be explained by the replacement of pure Si by beneficial Mg_2Si but the effect of magnesium on the corrosion mechanisms seems not to be limited by this effect. The electrochemical properties and the contribution of corrosion products on AlSiZnMg coatings corrosion mechanism need to be further investigated.

Acknowledgements

Authors are grateful for French National Agency of Research and Technology (ANRT) for partial financial support of C. Nicard PhD program (convention CIFRE 2015/0472).

Graphical Abstract

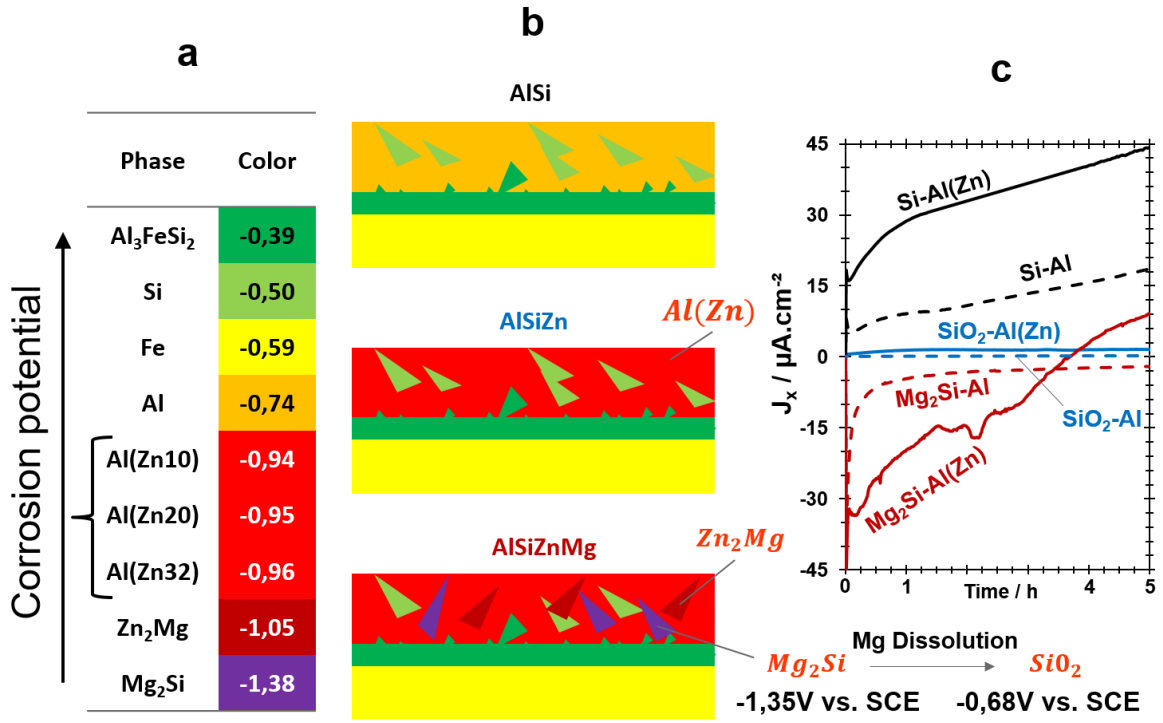


Figure 10 : (a) Phases sorted by corrosion potential in NaCl 1 wt. 1 % aqueous solution from Si (-0,170 V vs. SCE) to Mg_2Si (-1,35 V vs. SCE). (b) Microstructural scheme of AlSi, AlSiZn and AlSiZnMg with color scale. (c) Galvanic coupling potential evolution of Al-Si, Al(Zn32)-Si, Al-Mg_2Si, Al(Zn)-Mg_2Si, SiO_2-Al and SiO_2-Al(Zn) in NaCl 1 wt. 1 % aqueous solution.

References

[1] J.P. Laurent, J.P. Hennechart, D. Spehner, J. Devroc, Coated hot- and cold-rolled steel sheet comprising a very high resistance after thermal treatment, US 6296805 B1 patent.

[2] A. Bahadur, Aluminum coatings for steel, Materials and Manufacturing Processes (1996), pp. 225-232.

[3] I. DeGraeve, I. Schoukens, A. Lanzutti, F. Andreatta, A. Alvarez-Pampliega, J. DeStrycker, L. Fedrizzi, H. Terryn, Mechanism of corrosion protection of hot-dip aluminium–silicon coatings on steel studied by electrochemical depth profiling, Corrosion Science 76 (2013), pp. 325–336.

[4] Stoulil, J., et al., Corrosion properties of model aluminium alloys for coating steel substrate. Materials and Corrosion 2017, 68 (1), pp. 77-81

[5] Kruehong, C., et al., Influence of second phases on the electrochemical behavior of hot dipped Al–Mg–Si coated steel. Corrosion Science 2010, 52 (7), pp. 2379-2386

[6] Kyo, Y., et al., Hydrogen entry behaviour of newly developed Al–Mg–Si coating produced by physical vapour deposition. Corrosion Science 2011, 53 (9), pp. 3043-3047

[7] S. Han, H.LI, S. Wang, L. Jiang, X. Liu, Influence of Silicon on Hot-Dip Aluminizing Process and Subsequent Oxidation for Preparing Hydrogen/tritium Permeation Barrier, International Journal of Hydrogen Energy 35.7 (2010), pp. 2689–2693.

[8] S. Li, B. Gao, G. Tu, L. Hu, S. Sun, G. Zhu, S. Yin, Effects of Magnesium on the Microstructure and Corrosion Resistance of Zn–55Al–1.6Si Coating, Construction and Building Materials 71 (2014), pp. 124–131.

[9] Y. Du, J. Schuster, Z. Liu, R. Hu, P. Nash, W. Sun, W. Zhang, J. Wang, C. Tang, Z. Zhu, S. Liu, Y. Ouyang, W. Zhang, N. Krendelsberger, A Thermodynamic Description of the Al–Fe–Si System over the Whole Composition and Temperature Ranges via a Hybrid Approach of CALPHAD and Key Experiments, Intermetallics 16.4 (2008), pp. 554–570.

[10] N. Birbilis, RG. Buchheit, Electrochemical Characteristics of Intermetallic Phases in Aluminum Alloys, Journal of The Electrochemical Society 152.4 (2005), pp. 140–B151.

[11] C. Vargel, Corrosion of Aluminium, Elsevier (2004) pp. 81–109.

[12] D. Landolt, Corrosion et chimie de surfaces des métaux, PPUR presses polytechniques, Vol. 1 (1997), Traités des matériaux 12.

[13] F. Andreatta, Local Electrochemical Behaviour of 7xxx Aluminium Alloys, PhD, Applied Sciences, 2004.

[14] HD. Manesh, AK. Taheri, Bond Strength and Formability of an Aluminum-Clad Steel Sheet, Journal of Alloys and Compounds 361.1–2 (2003), pp. 138–143.

[15] P. Volovitch, L. Barrallier, W. Saikaly, Microstructure and Corrosion Resistance of Magnesium Alloy ZE41 with Laser Surface Cladding by Al–Si Powder, Surface and Coatings Technology 202.20 (2008), pp. 4901–4914.

[16] O. Gharbi, N. Birbilis, Clarifying the Dissolution Mechanisms and Electrochemistry of Mg2Si as a Function of Solution pH, Journal of The Electrochemical Society, 165 (9) C497-C501 (2018)

[17] M. Salgueiro Azevedo, C. Allely, K. Ogle, P. Volovitch, Corrosion mechanisms of Zn(Mg, Al) coated steel in accelerated tests and natural exposure: 1. The role of electrolyte composition in the nature of corrosion products and relative corrosion rate, Corrosion Science 90 (2015), pp. 472–481.

[18] F. Beier, K-H. Dtellnberger, S. Geisler, A new accelerated cyclic corrosion test for automotive substrates, in: Proceeding of the Eurocorr, Nice, France, (2009).

[19] M. Salgueiro Azevedo, C. Allely, K. Ogle, P. Volovitch, Corrosion mechanisms of Zn(Mg,Al) coated steel: 2. The effect of Mg and Al alloying on the formation and properties of corrosion products in different electrolytes, Corrosion Science 90 (2015) pp. 482–490.

[20] J. Han, K. Ogle, Cathodic Dealloying of α-Phase Al-Zn in Slightly Alkaline

Chloride Electrolyte and Its Consequence for Corrosion Resistance, Journal of The Electrochemical Society, 165 (7) C334-C342 (2018)

[21] D.R. Salinas, S.G. Garcia, J.B. Bessone, Influence of alloying elements and microstructure on aluminium sacrificial anode performance: case of Al–Zn, Journal of Applied Electrochemistry 29.9 (1999), pp. 1063–1071.

[22] C. Allely, L. Dosdat, O. Clauzeau, K. Ogle, P. Volovitch, Anticorrosion mechanisms of aluminized steel for hot stamping, Surface and Coatings Technology 238 (2014), pp. 188–196.

[23] C. Nicard, C. Allély, P. Volovitch, Effect of Zn and Mg alloying on microstructure and anticorrosion mechanisms of AlSi based coatings for high strength steel, Corrosion Science (2018).

[24] I. Puigdomenech, Hydra/Medusa Chemical Equilibrium Database and Plotting Software KTH Royal Institute of Technology, 2004

[25] K. Ogle, J. Baeyens, J. Swiatowska, P. Volovitch, Atomic emission spectroelectrochemistry applied to dealloying phenomena: I. The formation and dissolution of residual copper films on stainless steel, Electrochim. Acta 54 (2009), pp. 5163–5170.

[26] K. Ogle, M. Mokaddem, P. Volovitch, Atomic emission spectroelectrochemistry applied to dealloying phenomena II. Selective dissolution of iron and chromium during active - passive cycles of an austenitic stainless steel, Electrochim. Acta 55 (2010), pp. 913–921.

[27] M. Mokaddem, P. Volovitch, K. Ogle, The anodic dissolution of zinc and zinc alloys in alkaline solution. I. Oxide formation on electrogalvanized steel, Electrochim. Acta 55 (2010) pp. 7867–7875.

[28] M. Reboul, Corrosion Des Alliages D'aluminium, Techniques de l'Ingénieur, COR325 (2005).

[29] Andreev, Y. Goncharov, A. V., Thermodynamic calculation and experimental investigation of the surface enrichment of electrochemically activated Al–Me (Sn, In, Zn) alloys. Electrochimica Acta 2005, 50 (13), 2629-2637

[30] T. Ishikawa, M. Ueda, K. Kandori, T. Nakayama, Air Permeability of the Artificially Synthesized Zn–Al–Mg Alloy Rusts, Corrosion Science 49.6 (2007), pp. 2547–2556.

[31] PS. Braterman, Layered Double Hydroxides: Synthesis, Characterization and Interaction of Mg-Al Systems with Intercalated Tetracyanonickelate (II), Master of Science. University of North Texas, (2004).

Chapter V

Role of corrosion products in corrosion mechanisms of AlSi(Zn,Mg) coated high strength steel

C. Nicard, C. Allély, P. Volovitch,
Paper in preparation for submission to Journal of the Electrochemical Society

Investigated topics:

- How corrosion products impact coatings reactivity and corrosion mechanisms with advancement of corrosion?

Highlights:

- AlSiZn coating are faster consumed than AlSiZnMg.
- LDH are formed on both AlSiZn and AlSiZnMg.
- AlSiZn patinas formed in scratch does not form systematically, loosing barrier effect.
- AlSiZnMg corrosion products reduces and make surface reactivity more homogeneous.

Chapter V – Role of corrosion products in corrosion mechanisms of AlSi(ZnMg) coated high strength steel

Abstract

AlSi(ZnMg) coated steel with naked areas (cut edges, samples with artificial scratches) were observed during immersion in NaCl electrolytes and under cathodic polarization at different times of immersion. The nature of corrosion products and their spatial distribution were characterized by Scanning Electron Microscopy with X-ray Energy Dispersive Spectroscopy (SEM-EDS) and X-ray diffraction. The effect of corrosion products on the local and global reactivity was appreciated combining electrochemical tests (potentiostatic polarization after different immersion times, electrochemical impedance spectroscopy, Local Electrochemical Impedance Mapping (LEIM) and Scanning Vibrating Electrode Techniques (SVET)). Zinc alloying of AlSi coatings strongly improved sacrificial protection of steel in NaCl environments but the initially formed corrosion products disappeared with corrosion advancement, in particular on naked areas, and the coating was prematurely consumed. Mg alloying of AlSiZn coatings modified corrosion products composition and morphology. The scales on AlSiZnMg coated steel were formed and remained stable on both coated areas and naked steel and reduced reactivity of both types of area at advanced stage of corrosion. These scales were identified as layered double hydroxides (LDH). The effect of LDH and pH buffering by leached from them Mg^{2+} ions can be considered as a reason of a significantly longer coating life and better self-healing effect of AlSiZnMg coating compared to AlSiZn.

Keywords

Metal Coatings (A); Al (A); Zn (A); Mg (A); LEIS (B); SVET (B); Galvanic Coupling (C); Corrosion products (A)

1 Introduction

Aluminum coatings for steel are known to form spontaneously a thin and dense layer of surface oxides [1,2] which is an excellent barrier protection in most natural corrosive environment but decreases the sacrificial protection of the substrate in case of scratch to the steel [3]. During hot dip process a relatively thick layer of a fragile intermetallic at the interface steel-coating for commercially pure Al and Si alloying reduces its thickness and improves the mechanical properties [4]. Recently, it was shown that Zn and Al alloying of AlSi based anticorrosion coatings for high strength steel can significantly improve the service time of the coated steel acting on both, sacrificial capacity of the coating to protect steel and the coating life. From electrochemical data and accelerated corrosion tests it was concluded that Zn prevents aluminum passivation [5-7] activating the matrix and improving sacrificial capacities of the coating. Mg alloying also result in formation of new anodic phases [5,8,9] but for AlSiZnMg accelerated tests has demonstrated significantly lower matrix consumption than for AlSiZnMg *"Chapter III"*. In presence of Mg the amount of corrosion products but also their composition, morphology and effect on the electrochemical reactivity can be modified [3].

Various corrosion products can be formed on coated steels [3-12] depending on coatings composition and corrosive environment. For coatings containing Al, Si, Zn and Mg, layered double hydroxides (LDH) and basic zinc salts [13] are often found at the samples surface after the corrosion experiments [3]. These LDH have a general formula $[M(II)_{1-x}\ M(III)_x\ (OH)_2]^{x+}\ (Y^{n-})_{x/n} \cdot yH2O$ where A is an anion, like Cl^-, NO_3^-, CO_3^- , M(II) are bi-valent cations (Mg^{2+}, Zn^{2+}, …) and M(III) are tri-valent cations (Al^{3+}, Fe^{3+}, etc.) [14]. In function of exposure conditions, the most common corrosion products found in ZnAlMg systems are hydrotalcite like compounds (MgAl and ZnAl LDH), hydrozincite ($Zn_5(OH)_6(CO_3)_2$), simonkolleite ($Zn_5(OH)_8Cl_2$) and Al and Zn oxides. The exact identification of LDH formed during corrosion can be complex because their chemical composition is flexible and their crystallographic structure can vary with modifying stoichiometry between M(II) and M(III) cations and between Y and OH-anions.

The improved corrosion resistance of ZnAlMg was often attributed to the formation of LDH. The LDH compounds were also used directly as barrier coatings for light alloys [15] and as nanocontainers to improve corrosion resistance [16]. The properties of LDH were reviewed [12] in order to verify their effectiveness. The formation of LDH products during corrosion of AlSiZnMg coating and their possible self-healing effect for uncoated steel surfaces (cut edges, scratches) need to be verified. To distinguish the local reactivity at different areas and correlate

it with the nature of corrosion products local electrochemical technics such as local electrochemical impedance mapping (LEIM) [17 , 18] and scanning vibrating electrode techniques (SVET) [19,20] can be used. The objective of the present work was to identify corrosion products formed in immersion and under polarization of AlSi(Zn,Mg) coated steels with naked steel areas and to verify their stability and their effect on the local electrochemical reactivity.

2 Experimental

2.1 Materials

Coated steel plates were supplied by ArcelorMittal. Samples were prepared by industrial hot dip process based on AluSi© coating as described in the US 6296805 B1 patent [21] but with a bath composition modified by Zn and Mg addition in the range of 2 to 30 wt. % of Zn and 1 to 10 wt. % of Mg. The substrate was Mn22 boron steel. The samples were degreased in an ether solution at room temperature for 15 minutes and cleaned with ethanol prior to experiments. In order to test sacrificial protection of the substrate steel and self-healing effects the experiments were designed on cut edges or scratched samples. Scratches were 1 mm wide and approximately 40 µm deep.

2.2 Materials Characterization

Cut edges and surfaces with scratches were observed before and after corrosion experiments using a JEOL 7800F Field Emission Gun Scanning Electron Microscope (FEG-SEM) coupled with Brucker Xflash 6160 Energy Dispersive Spectroscopy (EDS) with a Si(Li) detector and equipped with QUANTAX 1.9 software (Bruker AXS) at accelerating voltage of 5 kV for electron SEM imaging and EDS.

In order to complete corrosion products identification, supplementary X-ray diffraction characterizations (XRD) were made. Because of insufficient spatial resolution of XRD and specific scratch geometry the detected phases spatial distribution cannot be localized and the main contribution to the signal comes from the coated areas and not from the naked steel in the scratches. The identification was performed by X-Ray Diffraction (XRD) using a PANalytical X'Pert diffractometer with the Cu(Ka1) radiation, directly on the sample surface. The analyzed area was approximately 63 mm^2. The XRD were collected with angular resolution of 0.02° over the angular range 5–80° (2θ) with 0.3 s acquisition time per point. The spectra were treated

using the HighScore Plus software package, including the JCPDS (ICDD) database files (version 2013) and was completed with data from the RRUFF™ database [22,23] for corrosion products analysis.

2.3 Corrosion and electrochemical tests on undamaged AlSi(ZnMg) coated steel.

AlSi(ZnMg) coatings were let in immersion during 48h in a 0.172 M (1 wt. %) NaCl aqueous solution with initial pH 9 (adjusted by 0.5 M NaOH solution).

A specific experiment was designed to form corrosion products on coated steel and test their electrochemical stability. Electrochemical testing was performed in a homemade three-electrode cell thermostated at 25 ± 2 °C was: a saturated calomel electrode (SCE) as the reference electrode, a platinum plate as the counter electrode (total area of 1 cm^2) and the coated steel as the working electrode (0.6 cm^2 exposed surfaces). Electrochemical sequence was designed to alternate open circuit potential (OCP) measurement and cathodic polarization. At, OCP coating corroded spontaneously, forming corrosion products. Cathodic polarization was performed under applied potential of – 1.15 V vs SCE which is typical for oxygen reduction. The effect of the formed corrosion products on the oxygen reduction current was measured and the stability of the formed corrosion products versus continued pH increase due to cathodic oxygen reduction was studied by surface characterization after the test. The precise electrochemical sequence was as follows: 1 h at OCP, then 6 h under cathodic polarization at -1.15 v vs. SCE, then 12 h at OCP, then 48 h under cathodic polarization at -1.15 v vs. SCE, and finally 1 h at OCP.

2.4 Test of AlSi(ZnMg) coated steels with naked steel areas.

In order to test sacrificial power and the self-healing effect of corrosion products on coatings reactivity when the coating is damaged the experiments were made on the cut edges and on the scratched samples. For cut edge corrosion studies, coated steel panels were cut and mounted in resin in a way that only the cut edges could contact the electrolyte. The samples were polished with SiC paper from grade 80 to 2400 with ethanol prior to exposure. The cut edges were immersed during 48 h in 0.172 M (1 wt. %) NaCl aqueous solution at initial pH7 (adjusted by 0.5 M NaOH solution). Optical images were regularly taken during the experiment

and the SEM images and EDS spectra were made at different locations of the cut edges after the immersion.

2.4.1 Local electrochemical impedance spectroscopy and mapping

Electrochemical impedance spectroscopy (EIS) and local electrochemical impedance mapping (LEIM) were carried out in 25 ml of a 0.172 M (1 wt. %) NaCl aqueous solution at initial pH 7 (adjusted by 0.5 M NaOH solution). Coated steel plates of 32 mm diameter, scratched down to the steel (scratch dimension: 1 cm x 1 mm x 40 µm) were mounted as working electrodes (WE) at the bottom of a 3D printed electrochemical cell. The counter-electrode was a platinum wire and the reference was an Ag/AgCl electrode. A homemade set-up using a Solartron potentiostate was used. Measurements were done with a homemade local probe composed of two Ag wires of 200 µm diameter in a glass capillary (sealed in two joined capillaries with the distance between the two Ag wires centers d = 500 µm). The probe was positioned at 150±25 µm above the WE and moved with a 3-axis positioning system (UTM25, Newport) driven by a motion encoder (MM4005, Newport). The data treatment was made with a homemade software. All impedance maps were measured on 6x6 cm² areas with steps of 200 µm along x-axis and 250 µm along y-axis which required about 20 minutes for each map. The surface was scanned following horizontal lines, from the left to the right and from top to bottom. Each step included a LEIS measurement for frequencies from 1 MHz to 1 Hz and a LEIM mapping at constant frequency at 100 Hz. The typical output used so far in the literature to report on LEIM experiments is mapping of the local impedance, $z(r)$, or the local admittance, $z^{-1}(r)$, at a fixed frequency [17]. In the present work, the local admittance is used to present the results.

2.4.2 Scanning Vibrating Electrode Technique

Scanning Vibrating Electrode Technique (SVET) measurements were performed with an Ameteck VersaSCAN equipment equipped with a SVET probe provided by MicroProbes©. The SVET probe was positioned at 150±25 µm above the sample and vibrated at 80Hz with 30 µm amplitude during the measurement. The scanned area was 6x6 cm² with a step of 100 µm on both, x-axis and y-axis. Two hours required for each map mapping. The surface was scanned following horizontal lines, from the left to the right, from top to bottom.

Coated steel plates cut into 32 mm diameter pastille and scratched to the steel (scratch dimension: 1 cm x 1 mm x 40 µm) were mounted as working electrodes (WE) at the bottom of a 3D printed electrochemical cell containing 25 ml of 0.1 $g.L^{-1}$ (0.00172 M) NaCl aqueous solution at initial measured pH 5.2 and conductivity 234 $\mu S.cm^{-1}$.

3 Results

3.1 Cut edge's corrosion

Typical surface appearances during the second day of immersion of AlSi, AlSiZn and AlSiZnMg cut edges in 1 wt. % NaCl are presented in Fig. 1. AlSi cut edge shows a lot of red rust, for AlSiZn and AlSiZnMg coated steels no red rust is visible and a lot of bubbles forms on the samples.

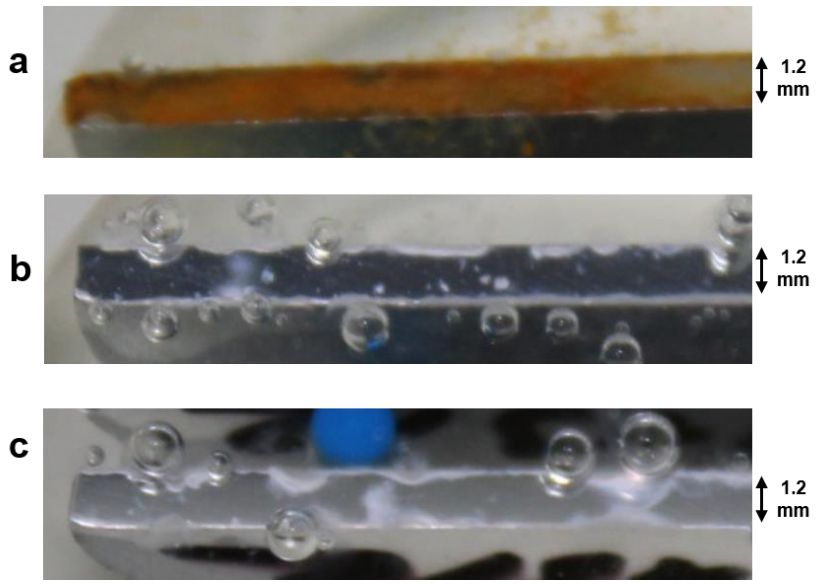


Figure 1 : Typical example of in-situ optical images of immersed cut edges of (a) AlSi, (b) AlSiZn, (c) AlSiZnMg after 48h immersion in 1 wt. % NaCl aqueous solution at initial pH 7.

Fig. 2 presents SEM images of the cut edges of AlSiZn and AlSiZnMg coated steel. AlSiZn(Mg) coatings are composed of an Al(Zn) matrix and Si precipitates. AlFeSi intermetallic is visible at the steel-coating interface. The layers are schematically delimitated in the figure. After corrosion, the matrix of AlSiZn coating near the cut edge is consumed while AlSiZnMg coating is less dissolved and the dissolution is located preferentially at the coating/intermetallic interface. Corrosion products are visible on both, intermetallic and steel, exposed areas. The products look finer on AlSiZnMg coated steel cut edge. In the center of the

cut edge, which represents the steel substrate, the corrosion products are visible for both AlSiZn and AlSiZnMg coatings.

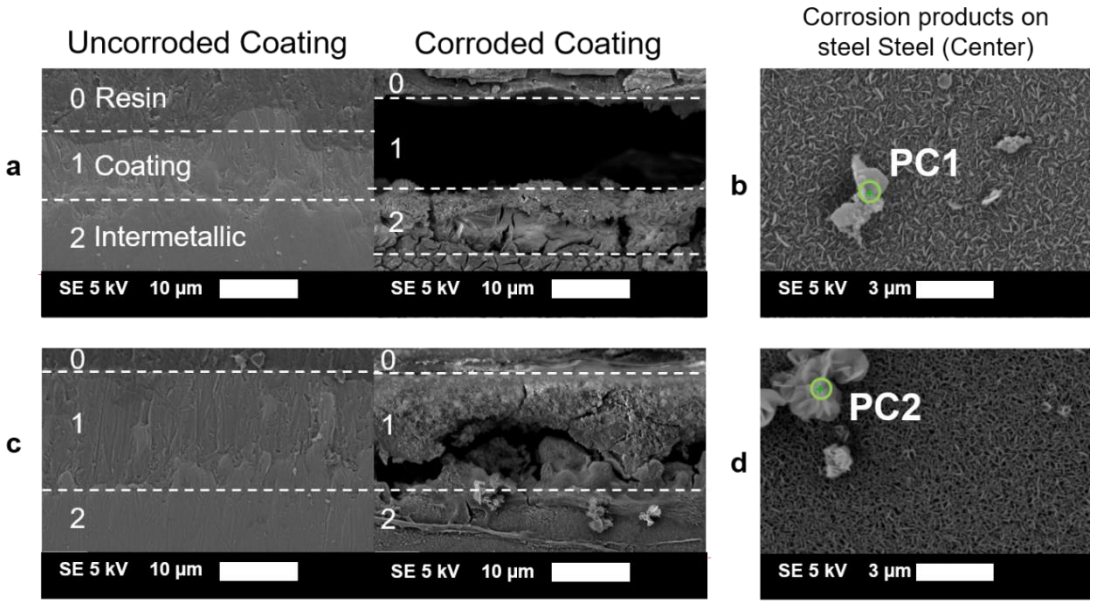


Figure 2 : Secondary Electron Images of (a,b) AlSiZn and (c,d) AlSiZnMg coatings cut edges after 48h immersion in 1 wt. % NaCl aqueous solution at initial pH 7. Images (a,c) show general appearance of the cut edges before and after corrosion while (b,d) illustrate the morphology of corrosion products formed on the steel (in the center of the cut edge). Zones corresponding to the resin (zone 0), coating (zone 1) and the intermetallic layer (zone 2) are schematically limited by dash lines.

The EDS spectra measured at different areas containing corrosion products are presented in Fig. 3. Spectra labeled as PC1 and PC2 correspond to the surfaces labeled in Fig. 2 c and d. The spectra PC3-PC5 are collected on scratched surfaces and will be discussed in the corresponding section. All spectra are scaled in order to normalize the intensity by the O peak. For AlSiZn corrosion products the cut edge were composed by O, Zn and Al whereas for AlSiZnMg they mainly contain O, Mg and Al. The probable compositions of the corrosion products are suggested in the figure.

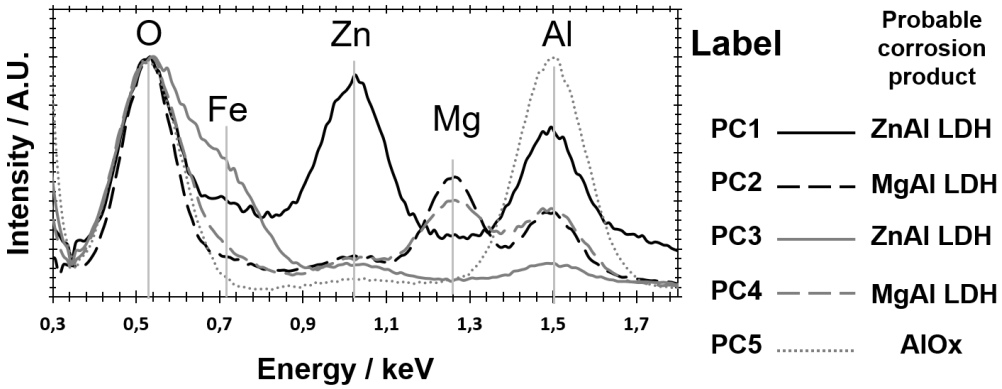


Figure 3 : EDS Spectra (normalized on oxygen peak) of corrosion products detected on cut edges, the collation of PC1-2 is shown in Fig. 2 and the location of PC 3-5 is shown in Fig,10. Considering elemental composition, some corrosion products are proposed.

3.2 Electrochemical tests of unscratched coatings

Fig. 4 presents the potential (a) and current (b) evolution of AlSiZnMg coatings during the proposed electrochemical sequence. The values of the potential and currents measured at different experiment times are also summarized in Tab. 1. It can be seen from the table that at the end of the polarization (72h), the oxygen reduction current is about 4 times smaller for AlSiZnMg than for AlSiZn and the final OCP of AlSiZnMg stays at -0.90 V vs. SCE while the OCP of AlSiZn rises up to at -0.82 V vs. SCE.

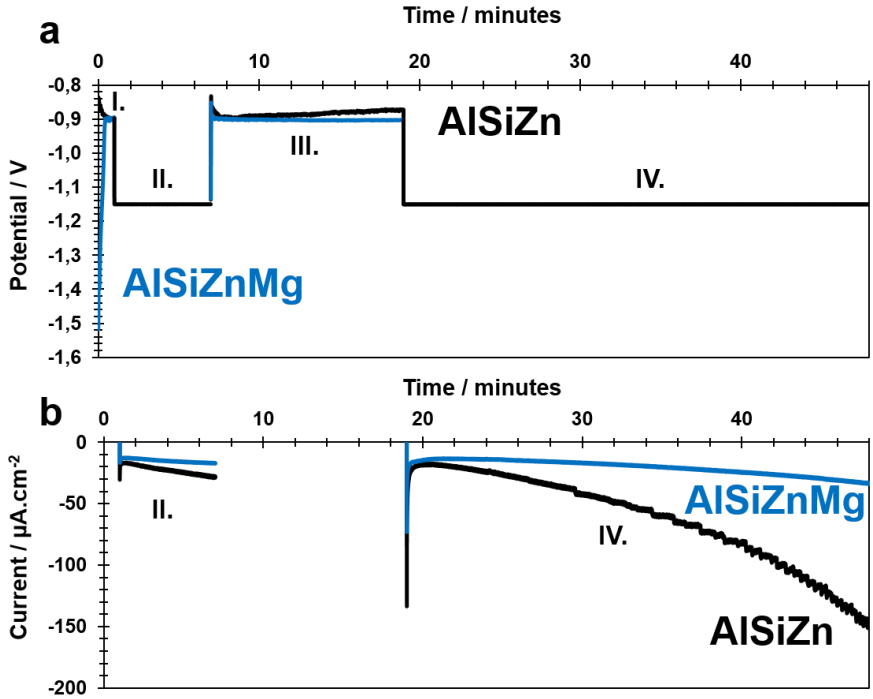


Figure 4 : (a) Potential and (b) current evolution at OCP and under cathodic polarization in 1 wt. % NaCl aqueous solution at initial pH7.

Table 1 : Potential and current evolution on AlSiZn and AlSiZnMg coated steels during electrochemical tests described in Fig. 4.

Step	Time	AlSiZn E / V vs. SCE	AlSiZnMg E / V vs. SCE	AlSiZn I / µA.cm^2	AlSiZnMg I / µA.cm^2
I	**T = 0 (OCP)**	**-0.84**	**-1.52**	**0**	**0**
II	**T = 1 h**	**-1.15 (applied)**	**-1.15 (applied)**	**-15**	**-12**
III	**T = 7 h**	**-1.15 (applied)**	**-1.15 (applied)**	**-28**	**-17**
IV	**T = 19 h (OCP)**	**-0.87**	**-0.90**	**0**	**0**
V	**T= 72h**	**-1.15 (applied)**	**-1.15 (applied)**	**-459**	**-116**
6	**T= 72.5 h (OCP)**	**-0.82**	**-0.90**		

3.3 Surface characterization after the electrochemical tests of unscratched coatings

SEM images of the coatings at different stage of the electrochemical sequence are presented in Fig. 5. Fig. 5 a and 5d describe the surface before the experiment, Fig. 5 b, e the surface after the first cathodic polarization (end of step I) and Fig. 5 c and 5 f correspond to the surface after the second OCP period (end of step III). At the end of the first cathodic polarization, both coatings surface is covered by platelet like corrosion products but the products seem to be finer and more covering for AlSiZnMg. After the second OCP, corrosion products on AlSiZn are no more present whereas AlSiZnMg corrosion products remain.

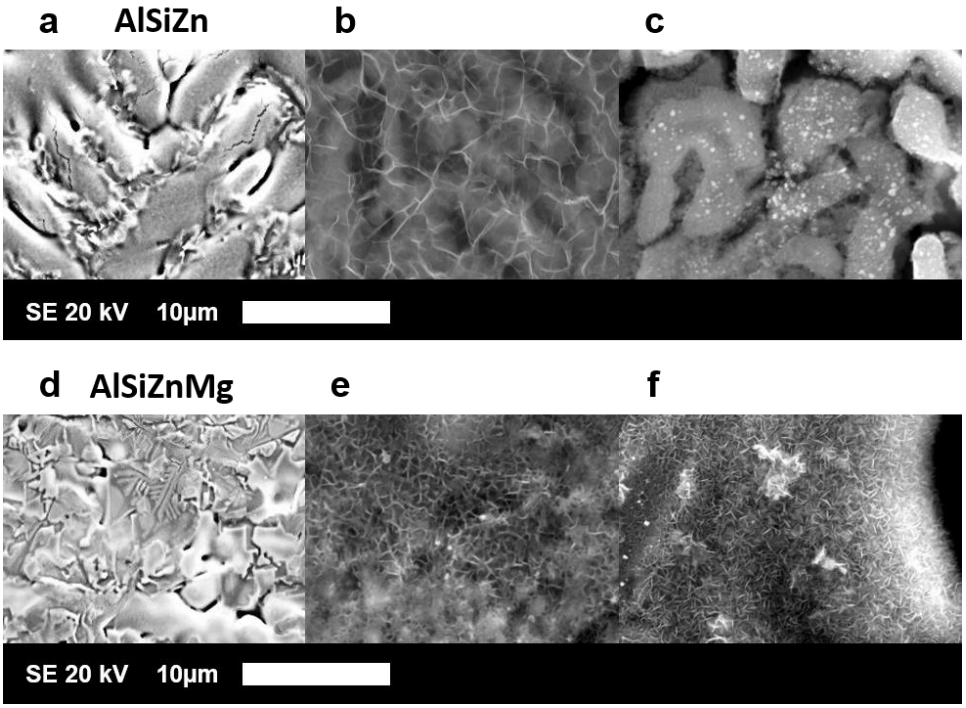


Figure 5 : Secondary Electron mages of (a,b,c) AlSiZn and (d,e,f) AlSiZnMg during electrochemical sequence described in figure 4. (a, d) are before the test, (b, e) at the end of stage II (7 h) and (c, f) at the end of stage III (19 h).

The XRD spectra obtained after the corrosion products identified by XRD are illustrated in Fig. 6.

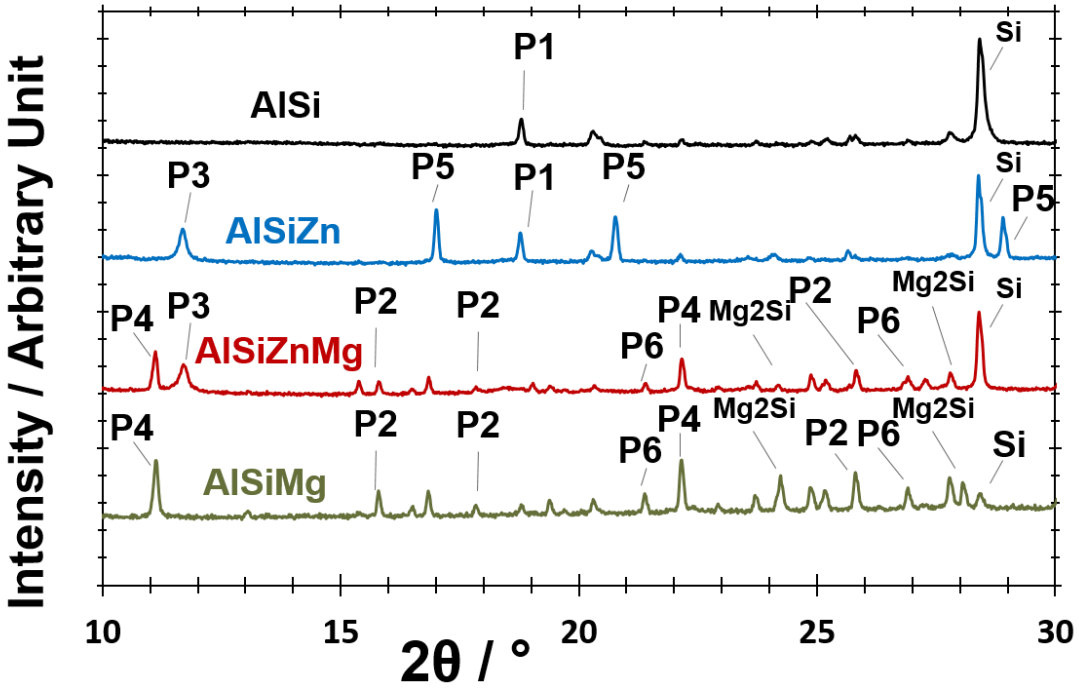


Figure 6 : XRD spectra for AlSi, AlSiZn, AlSiZnMg and AlSiMg coated steel after the complete electrochemical sequence (Cu) Ka. The peak identification is shown using the labels listed in Tab. 2.

Table 2 : . Corrosion products identified by XRD.

Labels	Mineral name	Abbreviation	Composition	Reference
P1	**Nordstrandite**	**-**	**$Al(OH)_3$**	**[18] ID:R050592**
P2	**Analcime**	**-**	**$Na(AlSi_2O_6)\cdot H_2O$**	**[18] ID:040128**
P3	**Zn Al LDH**	**ZnAlLDH**	**$Zn_6Al_2CO_3(OH)_{16}.4H_2O$**	**[19]**
P4	**Hydrotalcite**	**AlMgLDH**	**$Mg_6Al_2CO_3(OH)_{16}.4H_2O$**	**[18] ID:R050457**
P5	**Goethite**	**-**	**FeO(OH)**	**[18] ID:R050142**
P6	**Cristobalite**	**-**	**SiO_2**	**JCPDS (ICDD) 01-089-8944**

3.3 Surface reactivity of scratched samples by EIS and LEIM

Fig. 7 and Fig. 8 present EIS and LEIM results obtained on scratched AlSiZn(Mg) coatings. The chosen electrochemical sequence is detailed in Fig. 7 a and the evolution of the (global) impedance modulus of the system measured during the OCP periods of this sequence are plotted in Fig. 7 b for AlSiZn and in Fig. 7 c for AlSiZnMg for impedance spectra taken in frequency range from 0.1 MHz to 0.1 Hz. The choice of the electrochemical sequence (anodic and cathodic polarizations) was made to accelerate the coating reactivity and separate the effect of cathodic and anodic polarization on the local reactivity. For AlSiZn, the EIS taken at OCP shows a peak of impedance at 1 Hz which is absent for AlSiZnMg. Under anodic polarization both impedance spectra look similar (not shown). After the first anodic polarization impedance modulus is slightly higher at lower frequencies for AlSiZnMg (198 Ω) than for AlSiZn (126 Ω). Corrosion corresponds to ionic exchange, generally associated with the low frequency. First AlSiZn base global impedance (Fig 7.b step I) exhibits a drop at low frequency which indicates high rate of corrosion reaction. For AlSiZnMg (Fig7.c step I) there is no such drop in the impedance modulus. After the first anodic polarization (Fig 7.b&c - step III) the impedance at low frequencies decreases for both coatings and the maximum impedance of AlSiZn remains constant whereas for AlSiZnMg it increases (732 Ω) indicating formation of a passivating layer. After cathodic polarization, the impedance modulus increases for both coatings which is consistent with the corrosion products precipitation due to pH increase. In all cases the absolute

values of the AlSiZnMg impedance modulus (1600 Ω) stay higher than the impedance modulus of AlSiZn (710 Ω).

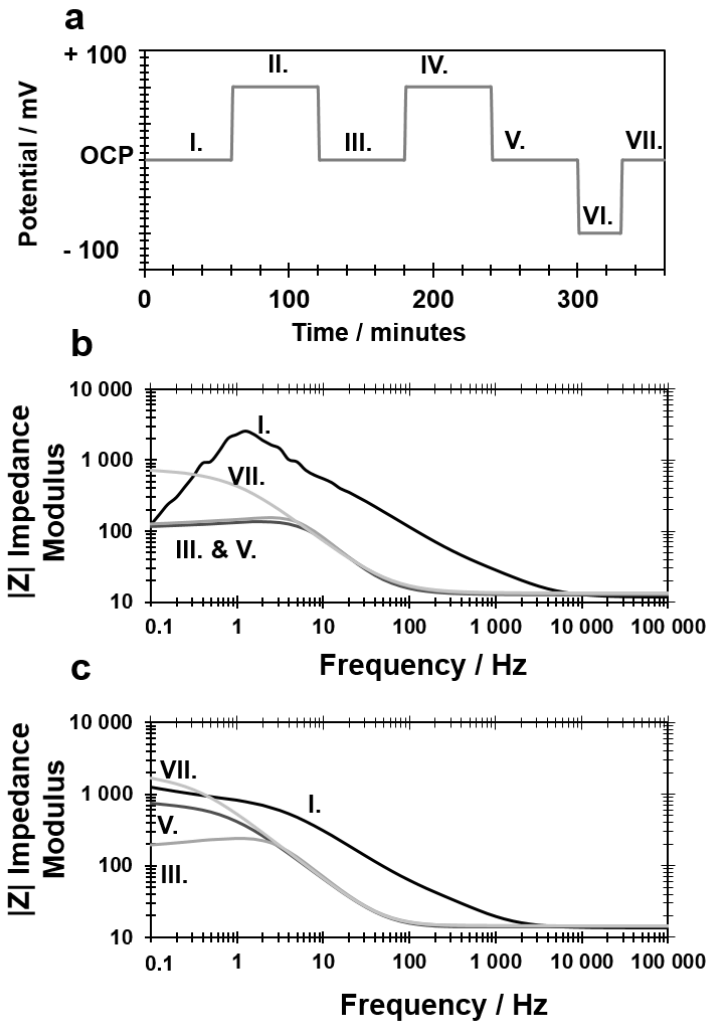


Figure 7 : Impedance modulus as a function of applied frequency for (b) AlSiZn (c) AlSiZnMg at different stage of the electrochemical sequence described in fig. 4.

Fig. 8 shows the admittance maps performed at 100 Hz at different stages of the electrochemical sequence described in Fig.7 a (the step numbers are indicated by roman numerous). In the cartographies a-b made during the first OCP period (step I) the scratch reactivity is clearly marked by its high admittance (high reactivity). After the first anodic polarization (step III), the admittance profile is inverted for AlSiZn because admittance values are lower in the scratch than outside which indicates the activation of the coating and partial protection of the scratch. The new admittance distribution is not as symmetrical as it was before the anodic polarization. For AlSiZnMg, the admittance distribution is more homogeneous and the difference between the inside and the outside of the scratch is less visible. After cathodic polarization (step VII), these difference between the reactivity inside and the outside of the

scratch looks reduced and not affected by the local position for AlSiZnMg coated steel indicating gradual passivation of the whole surface probably by the formed corrosion products. The coating looks much more reactive than the scratch on AlSiZn coated steel indicating that even if the coating keeps its sacrificial capacity at these times its reactivity is very high and the expected consumption rate is very high.

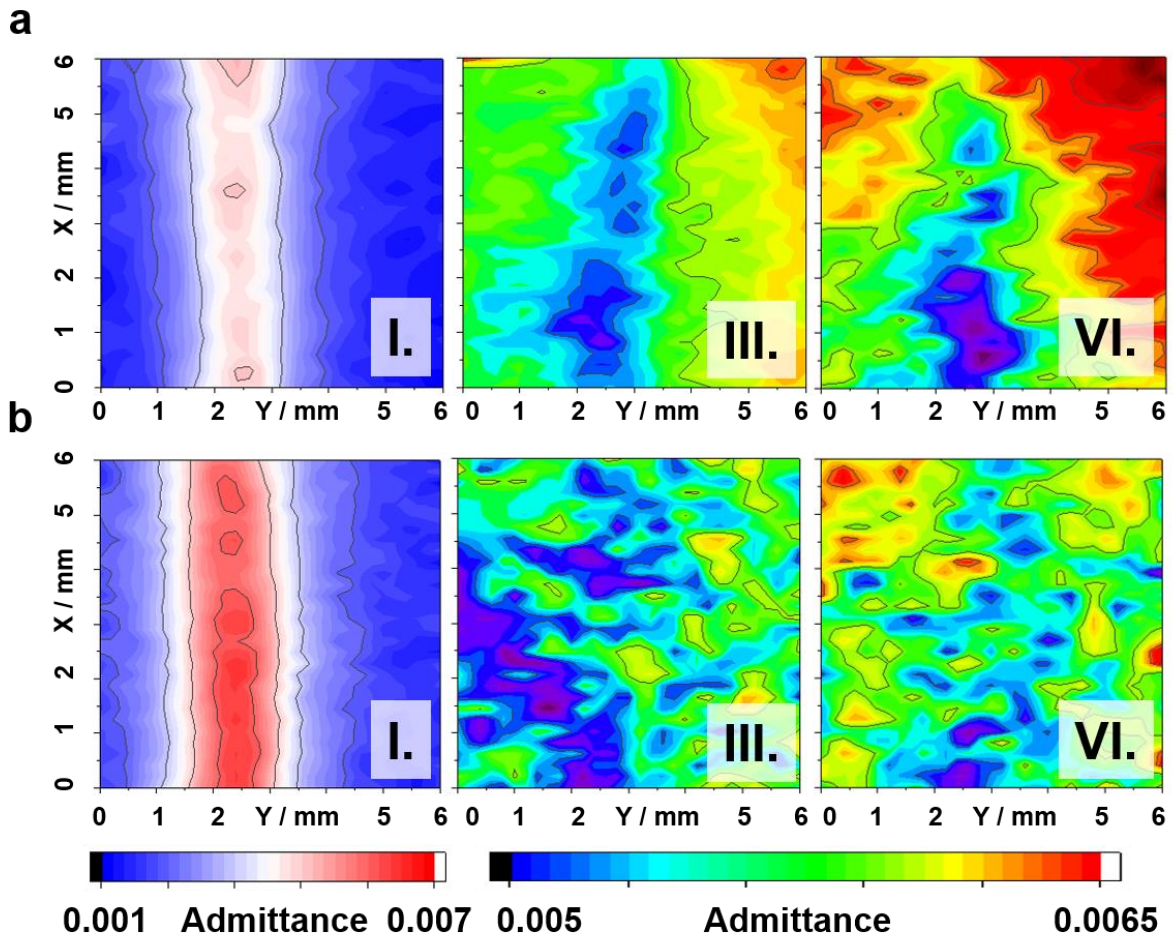


Figure 8 : Admittance cartography of (a) AlSiZn (b) AlSiZnMg during electrochemical sequences presented in Fig. 7. (a,b) are taken at stage I, III and VI.

3.4 Scanning Vibrating Electrode Technique

Fig. 9 shows the results obtained with the Scanning Vibrating Electrode Technique (SVET) on scratched AlSi, AlSiZn and AlSiZnMg coatings. For AlSi coating, at the beginning of the experiment, high cathodic reactivity is localized in the scratch. The scratch becomes anodic after 60 h of immersion indicating passivation of the coating. For AlSiZn, at the beginning of the experiment (2 h), scratch is slightly cathodic, and anodic currents are localized at scratches edges but also at some points which are possible defects or weakness sites (for instance Si needles). In AlSiZnMg coated steel the scratch edges are less active and even if the

cathodic activity inside the scratch is initially higher it decreases rapidly. For AlSiZn coated steel, the cathodic reactivity in the scratch increases with time while the anodic activity is localized for the coating up to long distances from the scratch. This can be interpreted as non-useful coating consumption. The cathodic reactivity in AlSiZnMg coating scratch decreases to finally be non-significantly different from the rest of the surface. Anodic activity of AlSiZnMg also stays limited.

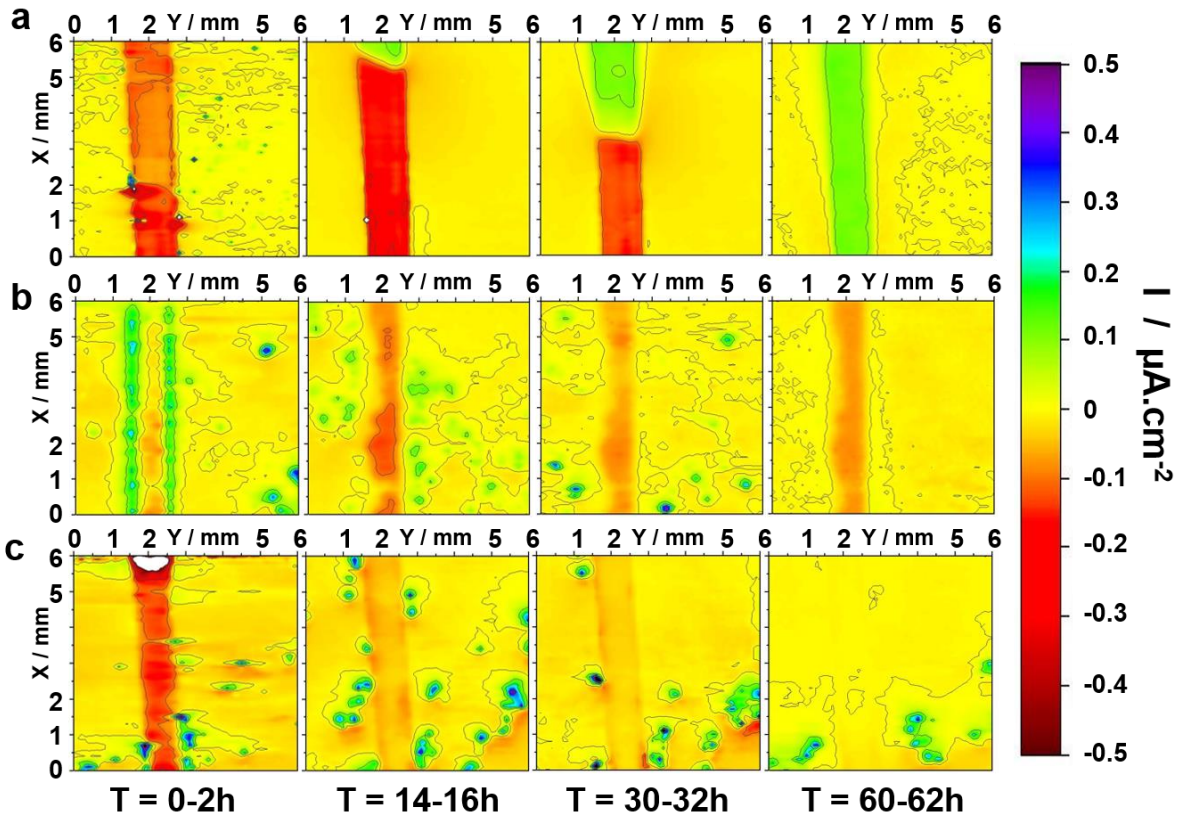


Figure 9 : SVET cartography of (a) AlSi, (b)AlSiZn and (c) AlSiZnMg scratched coating at different times in NaCl 100 mg.L^{-1}.

3.5 Surface observation of scratched samples after SVET experiments

SEM observation and EDS elemental maps after SVET experiments are presented in Fig. 10 . On AlSiZn a block of corrosion products is developed at coating scratch interface. The images b) and d) give more resolved morphology of corrosion products formed inside the scratch. The EDS spectra of corrosion products PC 3 and PC4 visible in the center of the scratch were presented in Fig.3. PC3 formed on AlSiZn coated steel is Zn-rich while PC4 formed in the scratch of AlSiZnMg coated steel is rich in Mg and Al. The PC4 looks much finer then PC3 in Fig. 10 confirming the reported in the literature effect of Mg on the refinement of LDH particles [11].

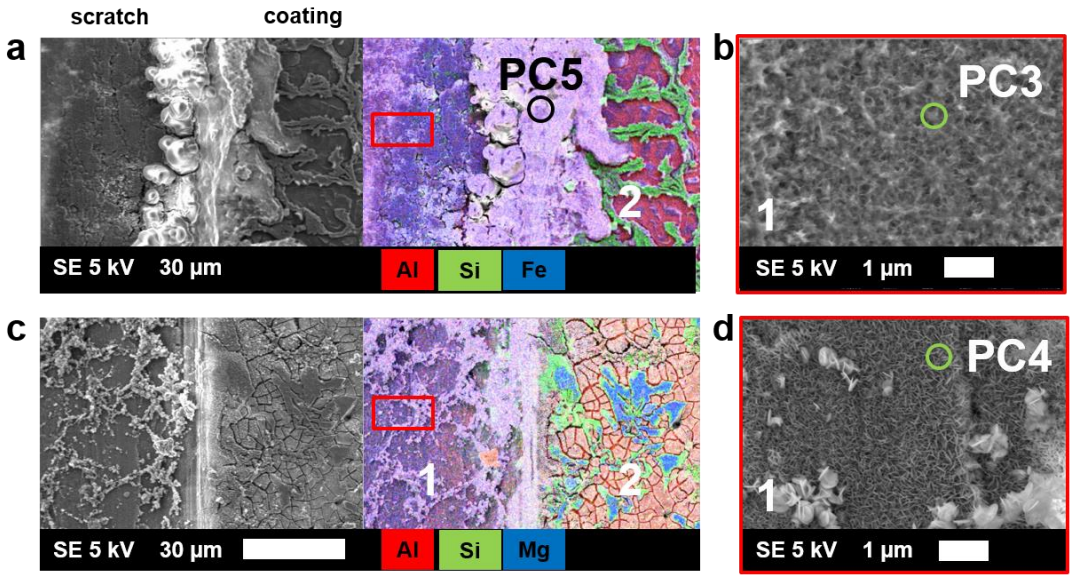


Figure 10 : Secondary electron images and corresponding EDS elemental of (a,b) AlSiZn, (c,d) AlSiZnMg scratched coated steels surface. (a,b) are located at scratch right edges while (b,d) are focused in the scratch (on substrate steel).

4 Discussion

4.1 Effect of alloying on the reactivity in scratches and at cut edges

Cut edges corrosion experiment and local electrochemistry in scratch confirmed the absence of sacrificial protection of steel by AlSi coating and high initial sacrificial effect of AlSiZn coatings [3] accompanied by intensive self-corrosion of the coating. Cut edge observations also confirmed that AlFeSi intermetallic is not consumed even after the complete dissolution of the coating which indicate the absence of sacrificial effect of this layer. Additional Mg alloying reduced coating consumption while maintaining the reactivity at sufficient level to protect the naked steel areas. Furthermore, corrosion products formed at steel surface are finer and seems more covering. The effect of Mg can be attributed to the overall surface reactivity decrease due to formation of continuous corrosion product platelets. ……..

The difference in the reactivity between AlSiZn and AlSiZnMg coated steels correlates with the difference in corrosion products composition. AlSiZn corrosion products are rich in Zn while for AlSiZnMg corrosion products look like Al-Mg LDH. In long immersions in 0.01 wt. % NaCl, hydrotalcite is always present at AlSiZnMg scratch surface whereas iron oxide is covering AlSiZn scratch. Moreover, a huge quantity of aluminum oxides looking as alumina [24] is formed at the border of the scratch. This alumina is generally formed around pits corresponding to a pH transition zone. These observations allow to consider that the formation

of corrosion products is favored by the local pH increase by cathodic reaction which is consistent with the observations that corrosion products are formed preferentially on cathodic areas in accelerated corrosion tests [3]. We suppose hence that the difference in the behavior of the AlSiZn and AlSiZnMg coated steels is mainly influenced by the different nature of corrosion products.

4.2 Effect of corrosion products on the reactivity

Local electrochemistry confirmed that AlSiZn and AlSiZnMg coatings reactivity evolves with time in a different way. For AlSiZn coating, at initial corrosion stage, surface and scratch are slightly cathodic (Fig. 9), anodic activity is held at the scratch borders after few hours of corrosion, then the overall surface became more and more active with the increasing anodic reactivity in the coating and the increasing cathodic reactivity in the scratch. The initially lower reactivity can be due to spontaneous passivation of the samples during storage in air, which requires some time to reactivate the coating in solution by the presence of Zn ions [5]. Once the coating is activated, it offers galvanic protection for the scratch however because of the unlimited pH increase by cathodic reaction, the corrosion products formed in the scratch cannot stay in it and once the coating near the scratch is completely consumed the scratch will corrode. In case of AlSiZnMg the overall coating reactivity decreases with time and the difference between the scratch and the coating becomes less pronounced. Different mechanisms can be discussed to explain these difference in local electrochemistry.

First, the difference in the barrier properties of the formed platelets can be considered. However, in the literature the less permeable LDH for air diffusion was proposed to be composed by three cations: Al, Zn and Mg [11] while in the present study, even if the exact identification of the LDH is complex for corrosion products because of the variety of their stoichiometry [17,18], it seems that the scale formed on AlSiZnMg scratches is Al-Mg LDH (hydrotalcite) and not a tri-cation product. This corrosion product presents a fine platelet-like structure (Fig. 6) and its effect on the oxygen reduction current is clear from the electrochemical experiment discussed in section 3.2 - at the end of the second cathodic polarization oxygen current for AlSiZnMg coating is about four times less intense than for AlSiZn coating. This effect can be interpreted either as a better barrier effect of the formed product than the barrier effect of the scales formed on AlSiZn coated steels or in terms of the high stability of these scales and/or the stabilizing effect of these scale on the Zn scales in changing corrosion environment when corrosion advances. The fact that corrosion products initially formed on

AlSiZn are not detected after the complete electrochemical sequence are in favor of the second mechanism.

The following explanation can be proposed: for AlSiZnMg the formed scales contain Mg^{2+} which is not soluble at high alkaline pH. As a result, when the cathodic reactivity result in intensive OH- production, these OH- are consumed to transform the LDH scales into insoluble $Mg(OH)_2$ and the pH increase is limited. Because the whole surface is covered by a similar precipitated scale, the differences in the local reactivity decrease with time and almost disappear in long experiments.

5 Conclusions

Formation of corrosion products on AlSi(ZnMg) coatings, their effect on electrochemical properties and corrosion mechanisms was studied by a combination of electrochemical test, Scanning Electronic Microscopy (SEM), Energy Dispersive Spectroscopy (EDS), X-Ray Diffraction (XRD), Impedance techniques (LEIM;LEIS) and Scanning Vibrating Electrodes Technique (SVET). Small addition of magnesium in AlSiZn coatings modifies corrosion products stability, their composition and morphology. The local reactivity in AlSi(Zn,Mg) coated steels and their corrosion mechanisms strongly depend on the formation of these scales.

The increase of sacrificial protection of naked steel at the cut edges and in scratches by Zn alloying of AlSi is confirmed as well as the benefit effect of additional Mg alloying on the reduced rate of the coating consumption and self-healing effect of Mg-containing corrosion products in initially naked steel regions.

Corrosion products formed on AlSi, AlSiZn and AlSiZnMg are different. At the cut edges immersed in 1 wt. % NaCl aqueous solution, only $Al(OH)_3$ oxides are formed on AlSi coated steel, while AlZn-LDH are formed on AlSiZn and MgAl-LDH are formed on AlSiZnMg. AlSiZn corrosion products are however less stable at more advanced stages of corrosion and under alternating anodic and cathodic polarization. In low chloride environment only MgAl-LDH hydrotalcite scales were formed on AlSiZnMg coatings.

Corrosion products formed on AlSiZn coatings being less stable, they cannot be considered as self-healing while the higher stability of the scales formed in the presence of Mg let us define a self-healing effect of AlSiZnMg coating’s corrosion products. This effect can be attributed to the pH stabilization and probable skin effect of Mg containing corrosion products which stay insoluble even at extremely high pH.

Acknowledgements

Special thanks to Thomas Sanchez and Viacheslav Skirshkiy for their help during LEIM and LEIS experiments and fruitful discussions.

Graphical Abstract

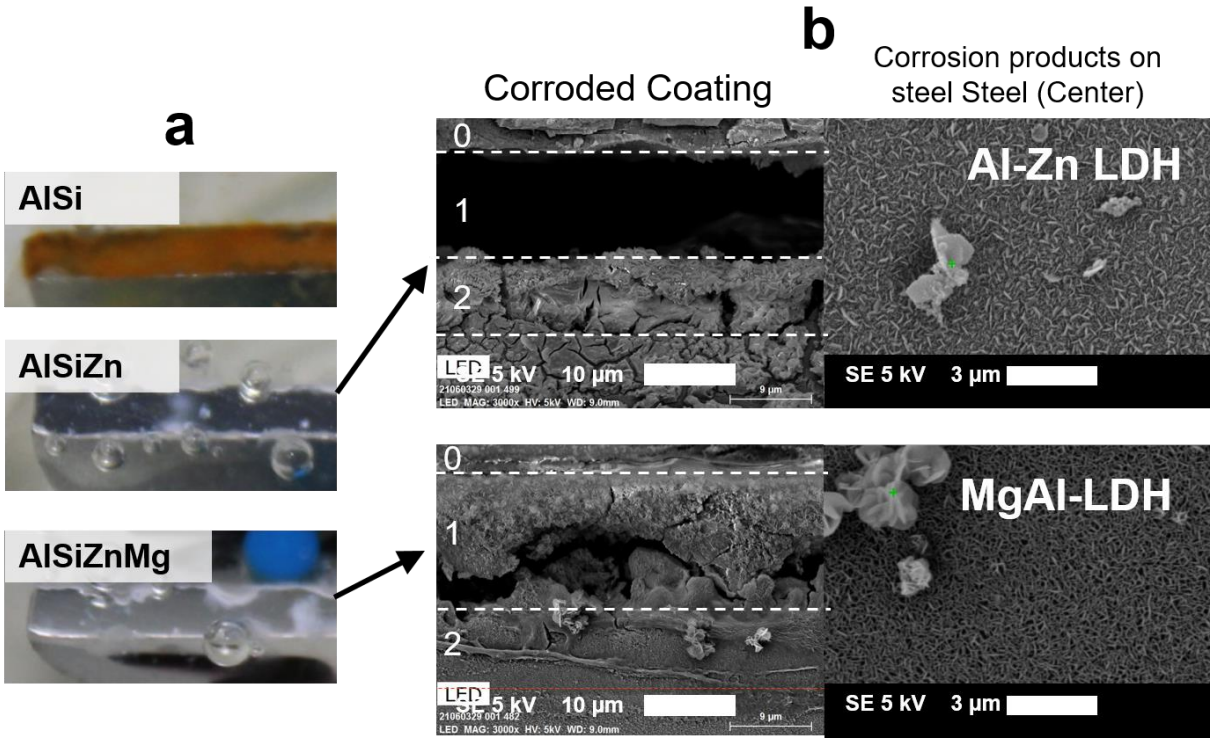


Figure 11 : (a) Typical cut edges appearance of AlSi, AlSiZn, AlSiZnMg coatings after 48h immersion in 1 wt. % NaCl aqueous solution at initial pH7. (b) Secondary Electron Images of AlSiZn and AlSiZnMg coatings cut edges after 48h immersion in 1 wt. % NaCl aqueous solution at initial pH7. 0: Resin; 1: Coating; 2: Intermetallic.

References

[1] M. Reboul, Corrosion Des Alliages D'aluminium, Techniques de l'Ingénieur, COR325 (2005).

[2] C. Vargel, Corrosion of Aluminium, Elsevier (2004) pp. 81–109.

[3] C. Nicard, C. Allély, P. Volovitch, Effect of Zn and Mg alloying on microstructure and anticorrosion mechanisms of AlSi based coatings for high strength steel, Corrosion science (2018).

[4] S.Han, H.LI, S.Wang, L.Jiang, X.Liu, Influence of Silicon on Hot-Dip Aluminizing Process and Subsequent Oxidation for Preparing Hydrogen/tritium Permeation Barrier, International Journal of Hydrogen Energy 35.7 (2010), p.2689–2693.

[5] C. Nicard, C. Allély, P. Volovitch, Galvanic coupling and selective dissolution of pure phases in AlSi(ZnMg) anticorrosion coatings for high strength steel, Journal (2018).

[6] DR. Salinas, SG. Garcia, JB. Bessone, Influence of Alloying Elements and Microstructure on Aluminium Sacrificial Anode Performance: Case of Al–Zn, Journal of Applied Electrochemistry 29.9 (1999), pp. 1063–1071.

[7] WH. Hartt, EJ. Lemieux, KE. Lucas, A Critical Review of Aluminum Anode Activation, Dissolution Mechanisms, and Performance, NACE International, CORROSION (2001).

[8] R. Hausbrand, M. Rohwerder, M. Stratmann, C. Schwerdt, B. Schuhmacher, and G. Grundmeier, Model Study on the Corrosion of Magnesium-Containing Zinc Coatings on Steel Sheets, in Galvatech, International Conference on zinc and zinc ally coated steel sheet, 2001, no. 5, pp.161–167

[9] F. Zeng, Z.Wei, C.Li, X.Tan, Z.Zhang, Corrosion Mechanism Associated with Mg2Si and Si Particles in Al–Mg–Si Alloys, Transactions of Nonferrous Metals Society of China 21.12 (2011), pp. 2559–2567.

[10] X. Zhang, T. Vu, P. Volovitch, C. Leygraf, K. Ogle, I. OdnevallWallinder, The Initial Release of Zinc and Aluminum from Non-Treated Galvalume and the Formation of Corrosion Products in Chloride Containing Media, Applied Surface Science 258.10 (2012), pp. 4351–4359.

[11] T. Ishikawa, M. Ueda, K. Kandori, T. Nakayama, Air Permeability of the Artificially Synthesized Zn–Al–Mg Alloy Rusts, Corrosion Science 49.6 (2007), pp. 2547–2556.

[12] PS. Braterman, Layered Double Hydroxides: Synthesis, Characterization and Interaction of Mg-Al Systems with Intercalated Tetracyanonickelate (II), Master of Science. University of North Texas, (2004).

[13] P. Nalawade, B. Aware, V.J. Kadam, R.S. Hirlekar, Layered Double Hydroxide: A review, CSIR (2009), Book, pp. 267-272.

[14] X. Duan and G.D Evans. Layered Double Hydroxides, book, Springer Science & Business Media, 2006.

[15] Fazhi Zhang, Lili Zhao, Hongyun Chen, Sailong Xu, David G. Evans, and Xue Duan, Corrosion Resistance of Superhydrophobic Layered Double Hydroxide Films on Aluminum, Angew. Chem. Int. Ed. 2008, 47, pp. 2466-2469.

[16] M.L. Zheludkevich, S.K. Poznyak, L.M. Rodrigues, D. Raps, T. Hack, L.F. Dick, T. Nunes, M.G.S. Ferreira, Active protection coatings with layered double hydroxide nanocontainers of corrosion inhibitor, Corrosion Science 52 (2010), pp. 602–611

[17] V. Shkirskiy, A. Maltseva, K. Ogle, P. Volovitch, Environmental effects on selective dissolution from ZnAlMg alloy under low frequency alternating current perturbations, Electrochimica Acta, (2017) 238 pp. 397-409

[18] V. Shkirskiy, P. Volovitch, V. Vivier , Development of quantitative Local Electrochemical Impedance Mapping: an efficient tool for the evaluation of delamination kinetics , Electrochimica Acta, (2017) 235 pp. 442-452.

[19] F. Thebault, B. Vuillemina, R. Oltraa, K. Ogle, C. Allely, Investigation of self-healing mechanism on galvanized steels cut edges by coupling SVET and numerical modeling Electrochimica Acta 53 (2008) pp. 5226–5234.

[20] K. Ogle, S. Morel, D. Jacquet, Observation of Self-Healing Functions on the Cut Edge of Galvanized Steel Using SVET and pH Microscopy, Journal of The Electrochemical Society, 153 (1B1-B5) 2006.

[21] J.P. Laurent, J.P. Hennechart, D. Spehner, J. Devroc, “Coated hot- and cold-rolled steel sheet comprising a very high resistance after thermal treatment", U.S. Patent 6296805B1, issued October 2, (2001).

[22] RUFF database website : http://rruff.info/general=hydrotalcite/display=default/R050457 (accessed on 12-18-2017).

[23] Yanzhen Liu, Zhanhong Yang, Intercalation of Sulfate Anion into a Zn-Al Layered Double Hydroxide: Synthesis and Application in Zn-Ni Secondary Battery, RSC Advances (2016), Issue 73.

[24] JB. Bessone, The Activation of Aluminum by Mercury Ions in Non-Aggressive Media, Corrosion Science 48.12 (2006), pp. 4243–4256.

Chapter VI

Conclusion and perspectives

Chapter VI – Conclusion and Perspectives

The effects of Zn and Mg alloying on the internal reactivity of AlSi coatings for high strength steel were studied. The work has demonstrated that the alloying can improve not only the internal corrosion resistance of the coating and hence the barrier protection of the substrate but also the protection of the naked substrate at cut edges or in the coating defects (scratches, perforations) as well as the formation and stability of self-healing corrosion products on the naked substrate (in the coating defects or at cut edges). Corrosion mechanisms of unalloyed AlSi, Zn alloyed AlSi and Zn and Mg alloyed AlSi coatings were understood and synergic effect of Zn and Mg was explained.

Combining accelerated corrosion tests, electrochemical tests of coated steels, galvanic coupling experiments on model pure phases detected in the coating between them and with the substrate steel, and the ex-situ surface characterization, the corrosion mechanisms of AlSi(ZnMg) coatings were understood. Two main factors contributing to the benefic effect of Zn and Mg alloying were selected. First of all, the alloying results in the modification of phase composition and phase distribution inside the coatings and in the corresponding modification of corrosion potentials and micro galvanic coupling inside the coating and between the coating and the substrate. Secondly, the presence of new leached cations (Zn^{2+} and Mg^{2+}) is responsible for the formation and stabilization of new corrosion products on the coating and naked substrate. These corrosion products are suggested to offer self-healing effect and longer service time of the coated steels. Finally, it was possible to correlate the coatings composition and the microstructure to their final anticorrosion properties. The following corrosion and protection mechanisms were proposed for the three coatings.

1) Unalloyed AlSi coatings exhibit the behavior typical for Al alloys with initial formation of a thin layer of aluminum oxides on the coating surface which promotes localized corrosion down to the intermetallic layer (Fig. 1 a). Spontaneous passivation of Al matrix makes it inefficient for sacrificial protection of the underneath substrate and the only protection mechanisms is a barrier effect of the coating. In the case of cut edge or damage of AlSi coating, the naked substrate became anodic as the aluminum matrix passivated and iron potential went down because of the galvanic coupling.

2) Two effects could be expected from Zn alloying – improvement of sacrificial capacity of the coating and the self-healing due to formation of protective Zn corrosion products. The first effect was confirmed while the second effect was present only at initial stages of corrosion. The mechanisms of these effect can be explained as follows. The observation of corrosion profiles

and measure of coating electrochemical behavior, confirms that Zn alloying in AlSiZn coatings results in activation of the coating which become sacrificial for steel and efficiently protect it at initial stages of atmospheric corrosion. However, strong galvanic coupling between Al(Zn) matrix and Si inclusions results in the selective dissolution around Si needles and premature coating consumption (Fig. 1. b).

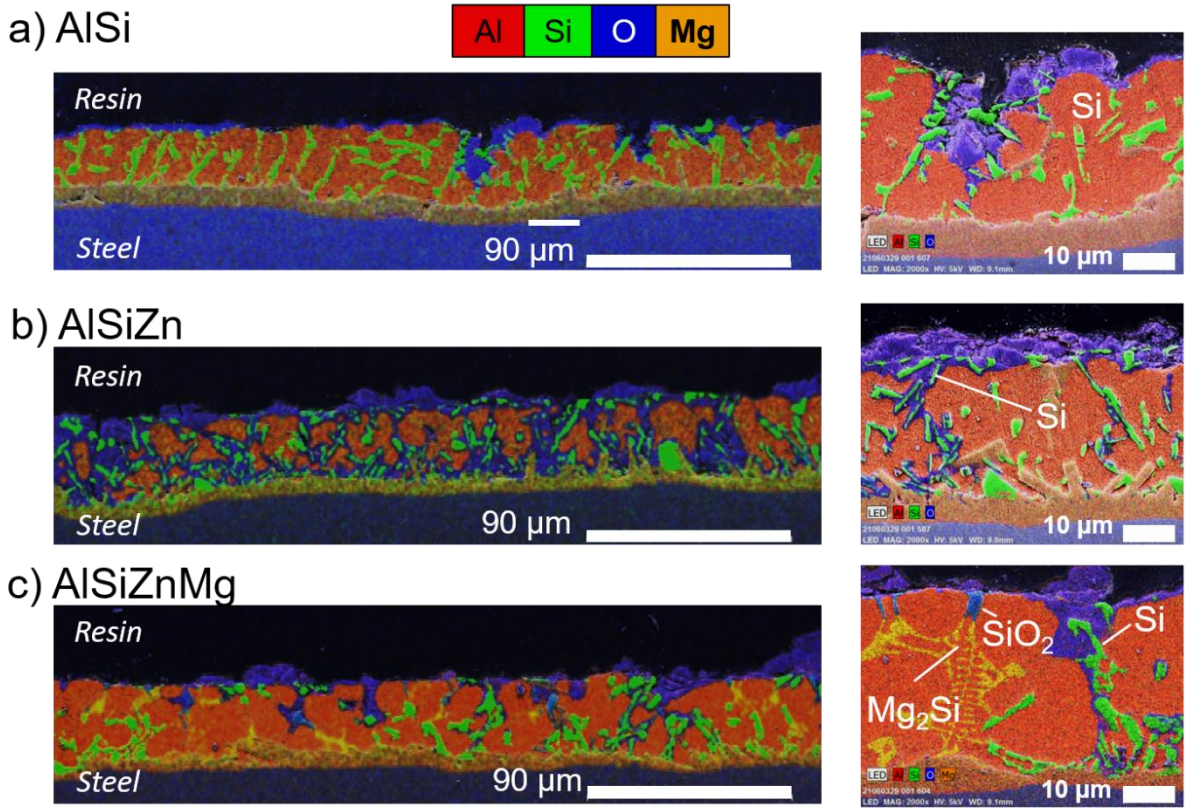


Figure 1 : Elemental distribution obtained from EDS maps showing corrosion product distribution after 12 cycles of VDA 233-102 test in the cross sections of unscratched (a) AlSi, (b) AlSiZn and (c) AlSiZnMg coated steels with high Si content. O distribution permits to distinguish corrosion products from non-corroded areas while Al, Si and Mg distributions help to identify the phases. General view and more resolved images are shown.

Such a behavior of Al(Zn) coating in accelerated corrosion tests is coherent with the properties of the phases composing the coating and the microstructure schematically summarized in Fig. 2. Indeed, the corrosion potential of Al(Zn) solid solution in 1 wt.% NaCl electrolytes is about 200 mV more negative than the potential of pure Al and the potential of the steel substrate which allows cathodic protection of the steel by galvanic coupling. At the same time, the galvanic coupling with the Si containing phases (Si inclusions with OCP= -0.503 mV vs SCE) and intermetallic AlFeSi phases (OCP= -0.394 mV vs SCE) present in all AlSi-based coatings becomes stronger and causes the selective corrosion of the matrix around them and premature consumption of the coating.

The effect of the strong galvanic coupling is not limited to premature coating consumption but affects also Zn corrosion products. Simonkolleite is initially formed on undamaged coatings, Al-Zn LDH at cut edges. These products, initially formed on the coating and on the uncoated steel (in the coating defects or at the cut edges) could dissolve at advanced corrosion stages because of strong pH increase at cathodic areas:

Simonkolleite:

$$5Zn^{2+} + 8OH^{-} + 2Cl^{-} \rightarrow Zn_5(OH)_8Cl_2 \qquad (1)$$

Al-Zn LDH:

$$2Al(OH)_4^{-} + 6Zn^{2+} + OH^{-} + CO_{2}^{2-} \rightarrow Zn_6Al_2(OH)_{16}CO_3 \qquad (2)$$

$$2Al(OH)_4^{-} + 6Zn^{2+} + 8OH^{-} + 2Cl^{-} \rightarrow Zn_6Al_2(OH)_{16}Cl_2 \qquad (3)$$

These reactions can explain why the corrosion products detected after short immersion or electrochemical tests were not detected on the naked substrate after longer corrosion tests and the absence of the self-healing expected from Zn corrosion products (Fig. 4). The presence of ZnO in the defects can be a result of re-precipitation from soluble zincates during drying:

$$Zn(OH)_4^{2-} \rightarrow ZnO + H_2O + 2\,OH^{-} \qquad (4)$$

3) In AlSiZnMg coatings, the presence of new Mg containing phases (Mg_2Si and Zn_2Mg) with even more anodic potential than the potential of Al(Zn), could be expected in even stronger galvanic with Si and AlFeSi intermetallic.

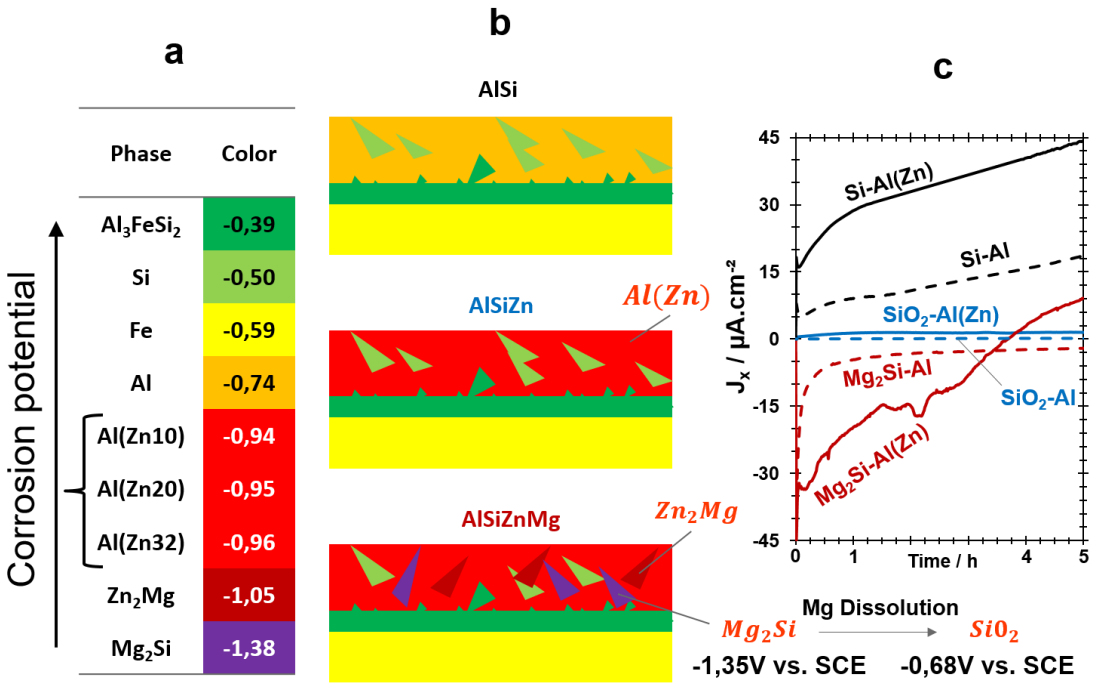


Figure 2 : (a) Phases ranked by corrosion potential in 1 wt. % NaCl aqueous solution from Si (-0,170 V vs. SCE) to Mg_2Si (-1,35 V vs. SCE). (b) Schematic phase distribution in the coating microstructure for AlSi, AlSiZn and AlSiZnMg with the color scale indicating relative corrosion potential – more red color indicates more anodic behavior. (c) Evolution of galvanic coupling potentials for Si containing phases coupled with Al or Al(Zn32) in 1 wt. % NaCl aqueous solution which explains the benefits of Mg alloying.

However, AlSiZnMg coatings consumption in accelerated tests and electrochemical tests is far slower than the consumption of AlSiZn coatings. This effect was explained by multiple facets of Mg alloying. From the surface examination and solution analysis it was shown that at initial stages of corrosion, Mg is selectively dissolved from Mg_2Si present in AlSiZnMg microstructure and due to this selective dissolution the Mg_2Si surface transforms into SiO_2. This new surface becomes cathodic versus Al and steel but does not causes so strong micro galvanic corrosion around it as Si needles (Figure 2.c). Magnesium ions leached in the solution also modifies the solution chemistry near the surface which results in formation of new corrosion products (layered double hydroxides) and in stabilization of corrosion products of Zn and Al. The latest can be due to a pH buffering effect at cathodic areas by precipitation of $Mg(OH)_2$ and probably by a "skin effect" of the formed $Mg(OH)_2$ on the corrosion products which otherwise could be soluble at high pH due to amphoteric character of Zn and Al (Equation 1-4) and:

Brucite :

$$Mg^{2+} + 2OH^- \rightarrow Mg(OH)_2 \qquad (5)$$

Hydrotalcite (MgAl LDH) :

$$2Al(OH)_4^- + 6Mg^{2+} + 8OH^- + CO_3^{2-} \rightarrow Mg_6Al_2(OH)_{16}CO_3 \quad (6)$$

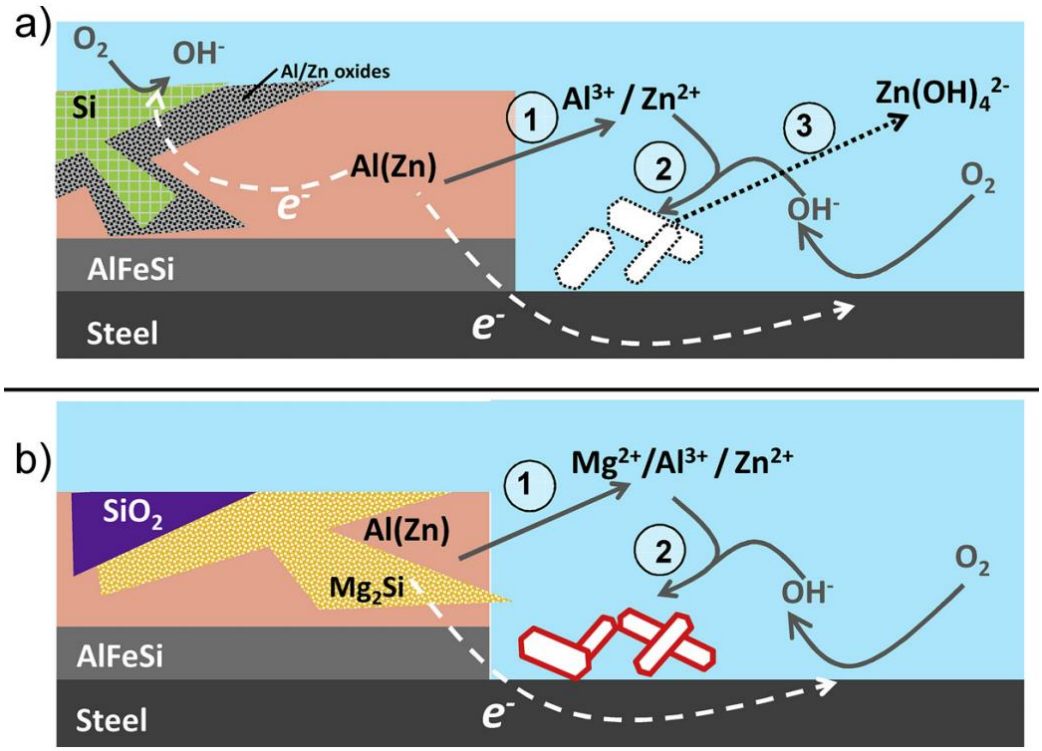


Figure 3 : Schematic representation of proposed corrosion and protection mechanisms in (a) AlSiZn and (b) AlSiZnMg coated steel in the presence of the defect going up to the steel. Step 1. Coating dissolution and sacrificial effect. For AlSiZn two types of mirogalvanic coupling are proposed - "sacrificial" coupling protecting steel and "lost" current used in micro galvanic coupling with Si because Si potential (60.5 V vs. SCE) is close to potential of steel and cathodic versus AlZn. Step 2. Precipitation (and partial modification) of corrosion products due to pH increase and drying. Step 3. Dissolution of Zn and Al containing corrosion products from AlSiZn at advanced stages of corrosion because of continuous pH increase. This step is absent when corrosion products contain Mg2+ because of their high pH stability (for instance Mg(OH)2 formation in place of dissolution of LDH resulting in a skin effect). As a result, Mg is expected to extend both, the coating life (and hence a sacrificial protection) and the barrier effect of corrosion products in the scratch.

The proposed mechanisms could explain the observed absence of sacrificial and self-healing effect of AlSi coating, the sacrificial and initial but not long lasting self-healing effect of AlSiZn coatings and long term sacrificial and self-healing effect of AlSiZnMg coatings for steel protection. These effects were also illustrated with local electrochemistry (Fig. 4) for different coatings with an artificial scratch. For AlSi, the scratch is initially cathodic but with time it becomes more and more anodic because of the passivation of Al coating. For AlZn coating, the coating acts as a sacrificial anode however the cathodic reactivity in the scratch becomes stronger with time because no protective corrosion products are formed. At long times, once the coating is consumed, steel is expected to stay unprotected. In case of AlSiZnMg, formed in the scratch corrosion products reduce oxygen diffusion and hence slow down

corrosion reactions in cathodic areas. The very active Mg_2Si and Zn_2Mg makes the AlSiZn coatings more active than AlSiZn at initial corrosion stages but corrosion products reduce rapidly the general activity to an acceptable level and the coating consumption is expected to be reduced with time whereas for AlSiZn the activity stays too high and coating will be premature consumed.

From the methodological point of view, the work has illustrated the possibilities which a fundamental study of pure phases and their combinations in galvanic coupling can offer to understand corrosion mechanisms of the coatings with a complex multiphase microstructure. At the same time, it demonstrated that the electrochemistry is not able to explain all the observed features and that chemical reactions with leached ions leading to formation of specific corrosion products and modification of the solution chemistry are as important as the electrochemical reactions. This confirms that the understanding of the corroding systems requires hence a complete study and cannot be limited to only one aspect of the reactivity.

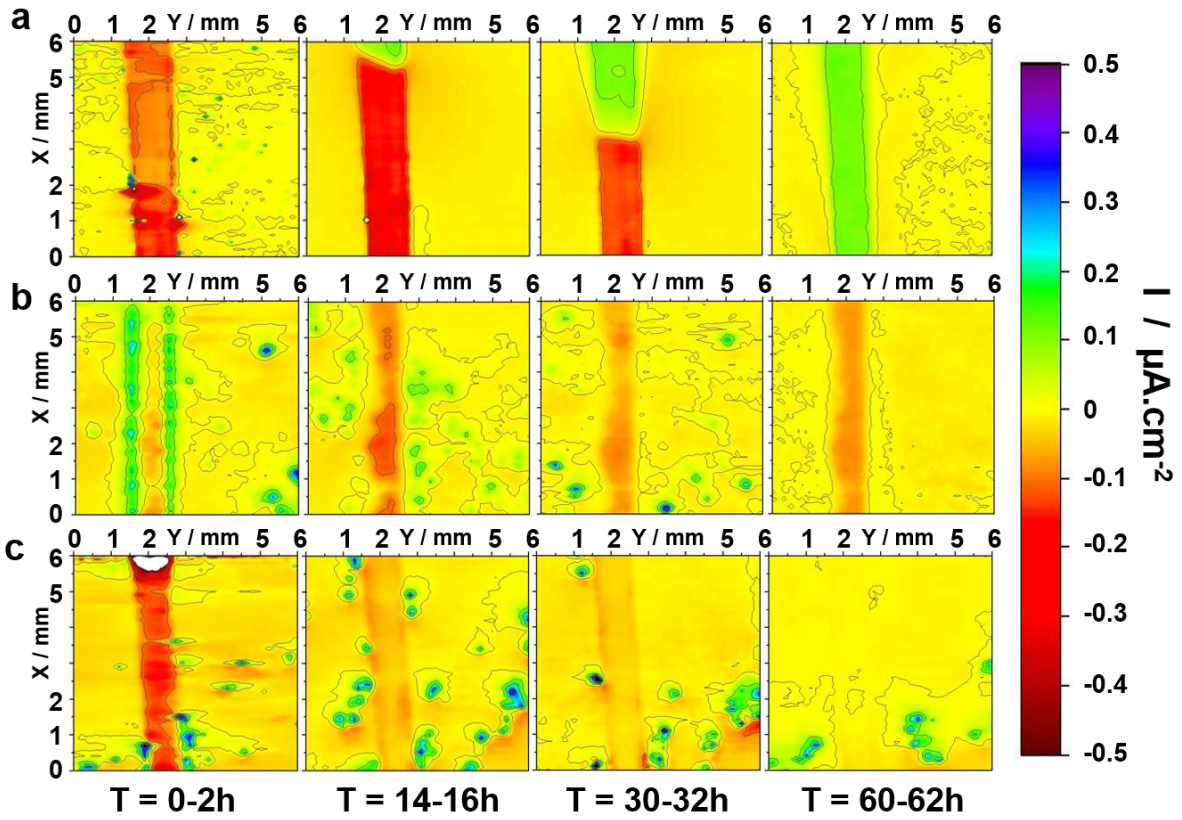


Figure 4 : SVET cartography of (a) AlSi, (b) AlSiZn and (c) AlSiZnMg scratched coating at different times of immersion in 100 mg.L^{-1} NaCl solution.

Perspectives

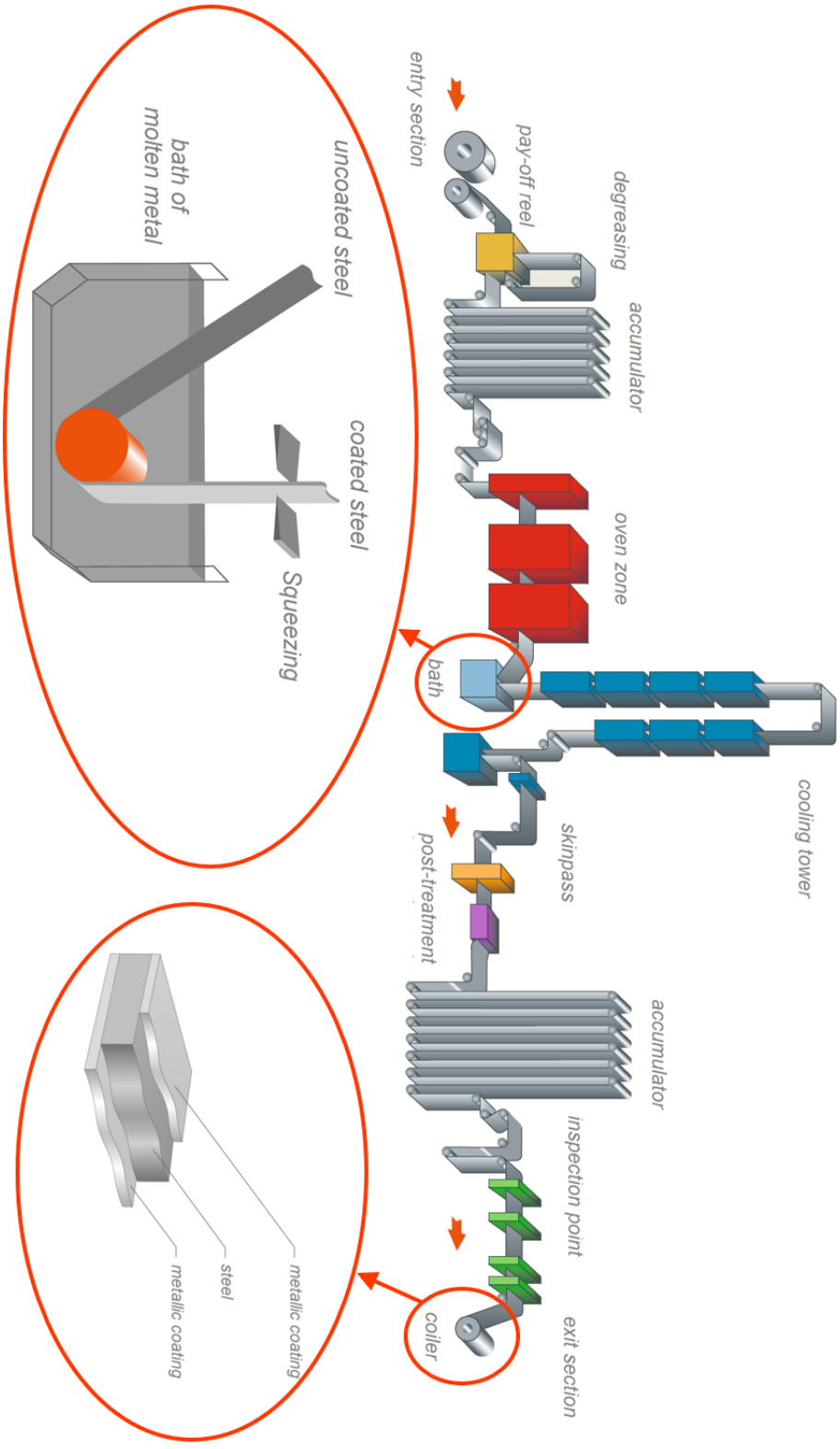
Although this work evidences the interest of Zn and Mg alloying and give an insight into corrosion mechanisms of AlSi(ZnMg) coatings and the mechanisms of the steel protection by these coatings, these mechanisms are limited to NaCl solutions relevant for accelerated tests in automotive industry.

However, the corrosion mechanisms strongly depend on the corrosive environment. The behavior in Cl-free or low Cl environments as well as the effects of CO_2 or O_2 free atmosphere which can appear in confined zone (under paint corrosion, crevice corrosion, assemblies, etc.…) need further investigation. The self-healing effect of corrosion products observed in accelerated corrosion tests and by local electrochemistry during immersion of AlSiZnMg coatings can be also modified by the limitation of ion formation and mobility in painted systems. The effect of solution composition and the effect of drying and of the temperature should hence be deeper studied. Another aspect of this work is that the studied mechanisms are relevant for accelerated corrosion tests used in automotive industry and it needs to be confirmed in long term natural exposures that the acting mechanisms are still the same.

Appendix

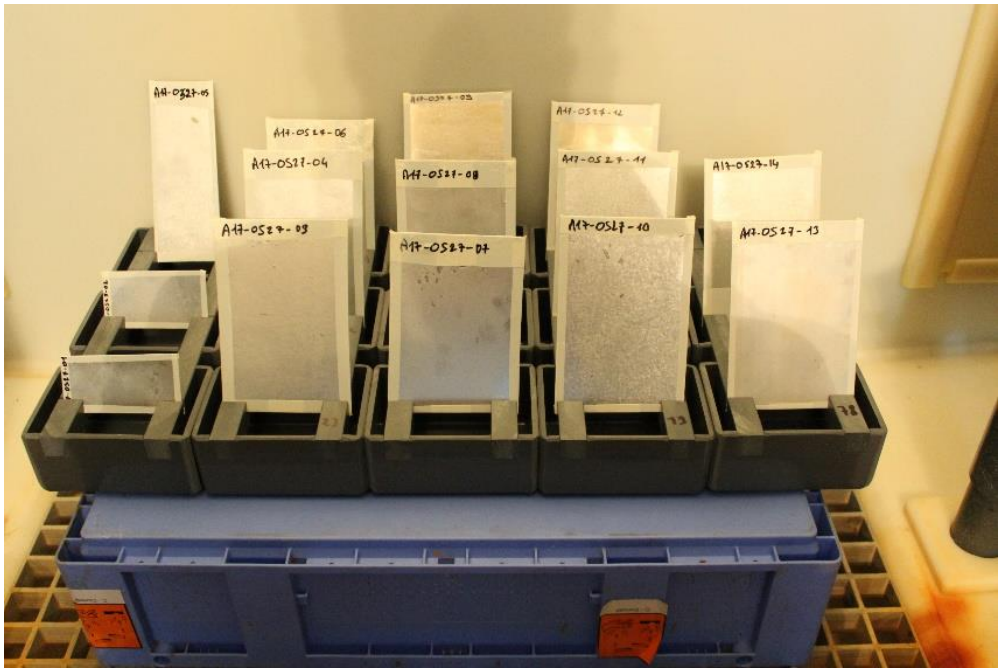
Appendix

1 Schematic representation of hot dip process for high strength steel

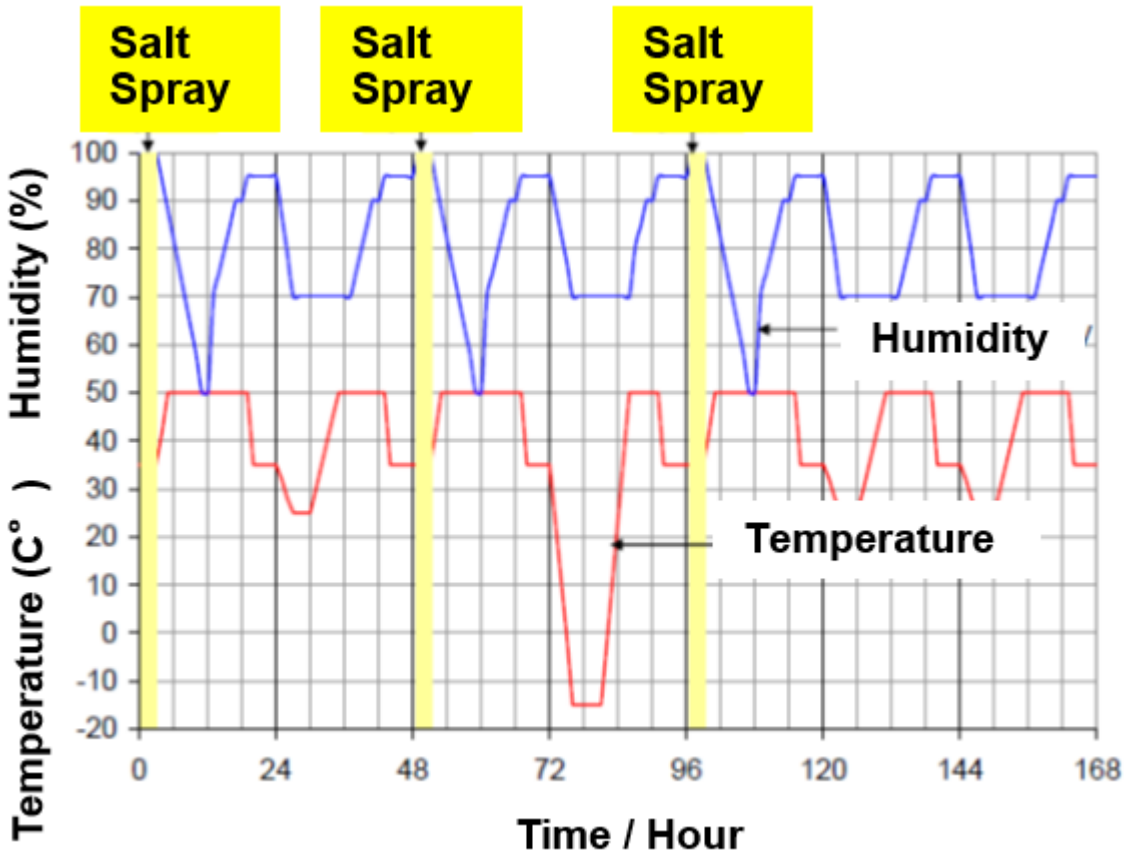


2 Samples positions (a) and recommended evolution of temperature, humidity and salt spray periods (b) during accelerated corrosion test VDA 233-102.

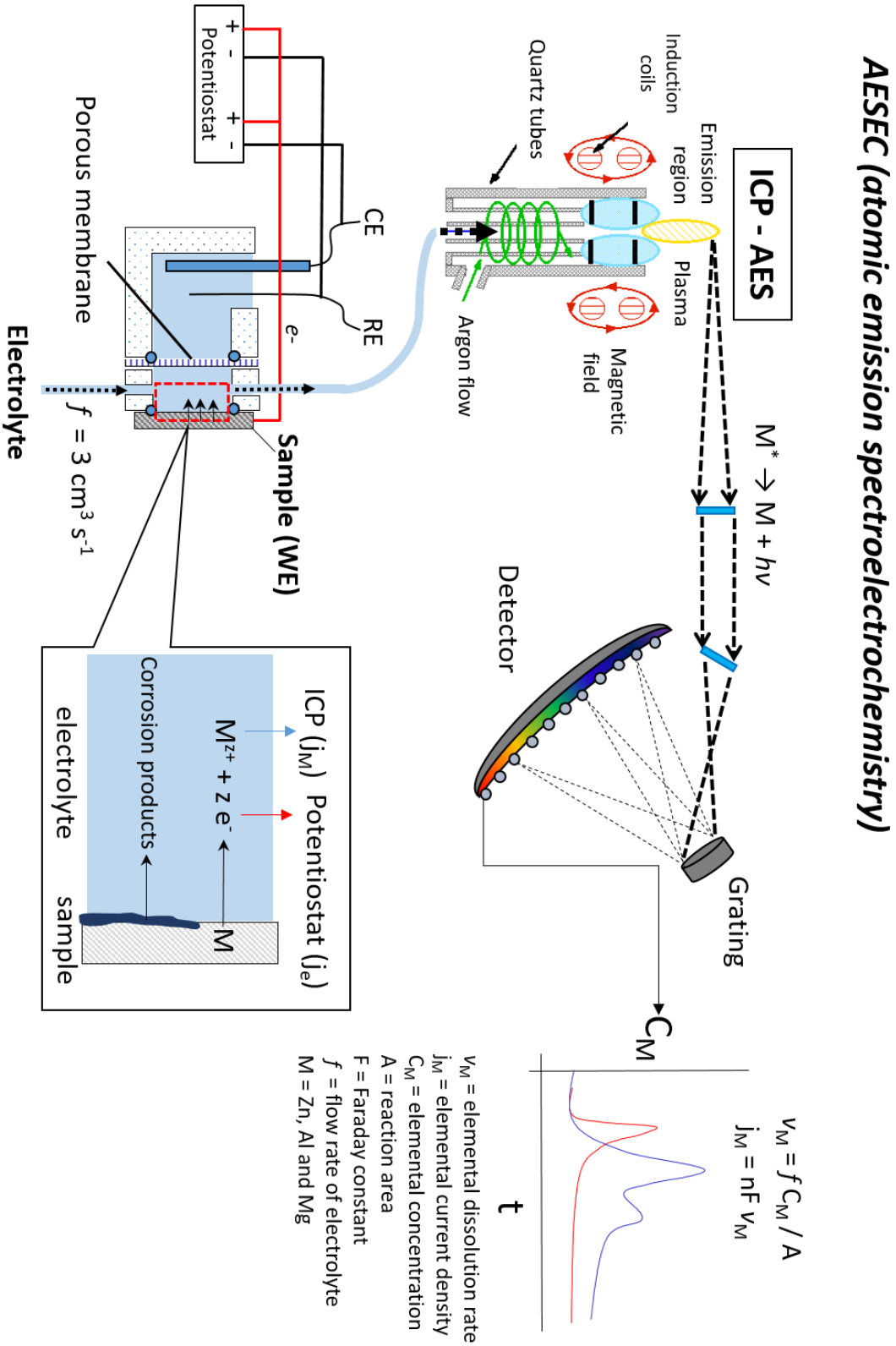
a)



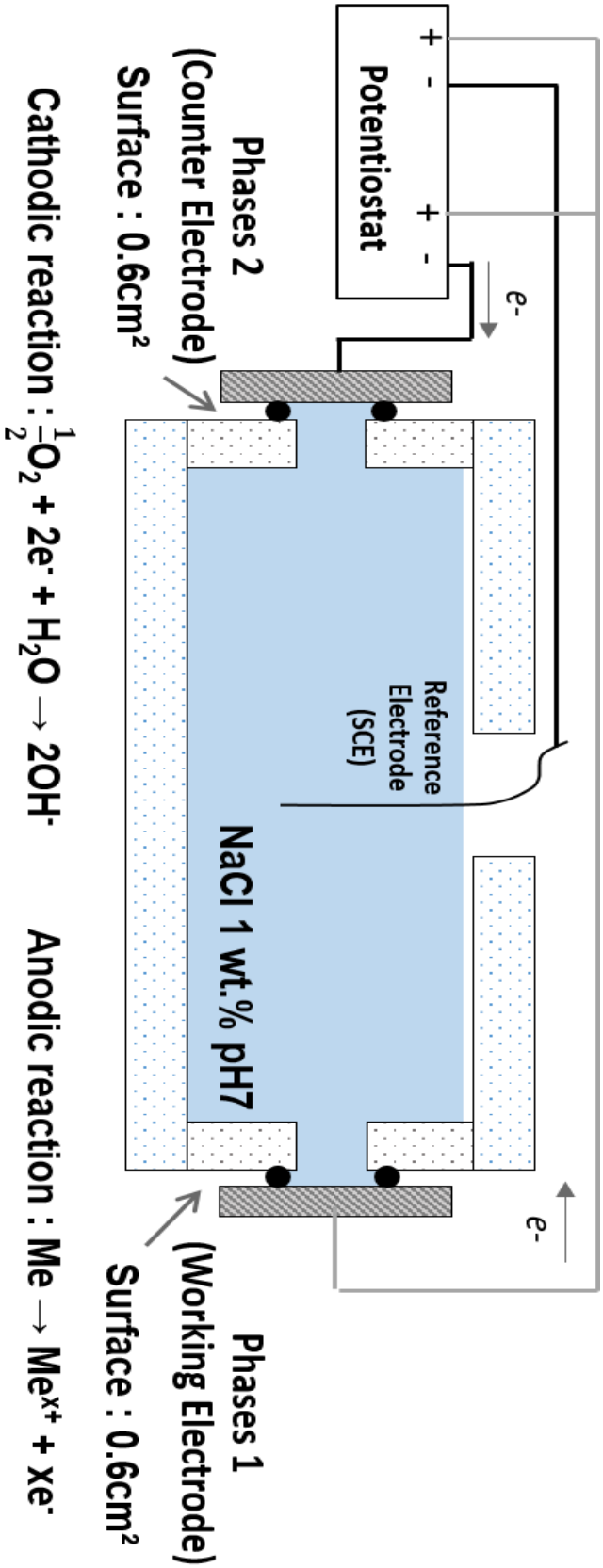
b)



3 Principles of AESEC

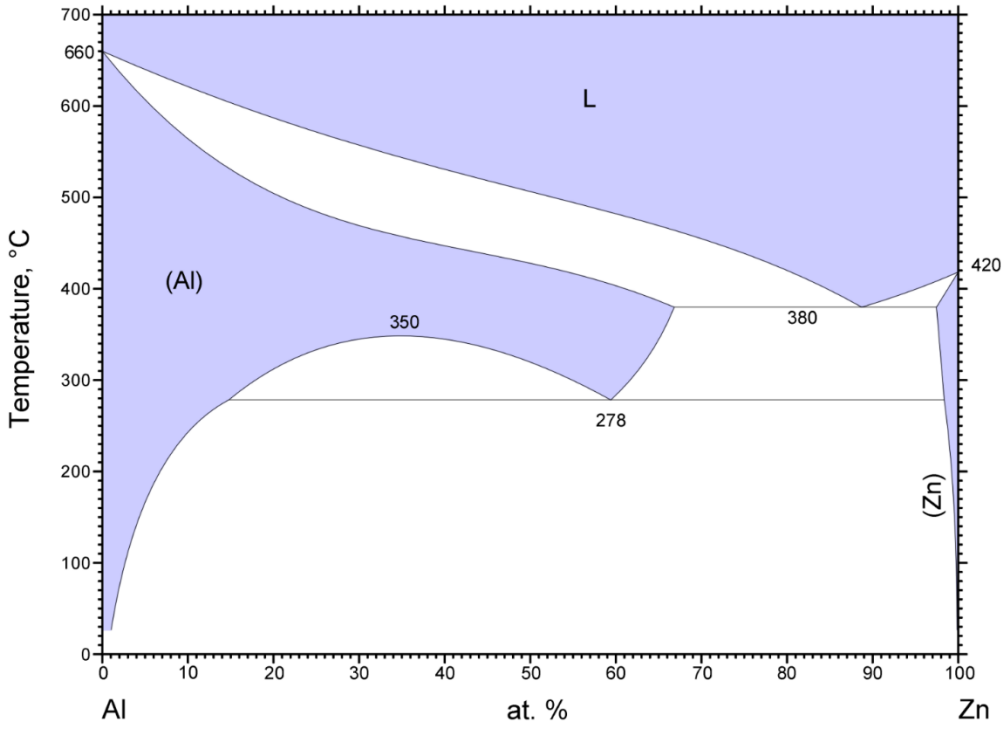


4 Homemade electrochemical cell used in galvanic coupling experiments for pure phases

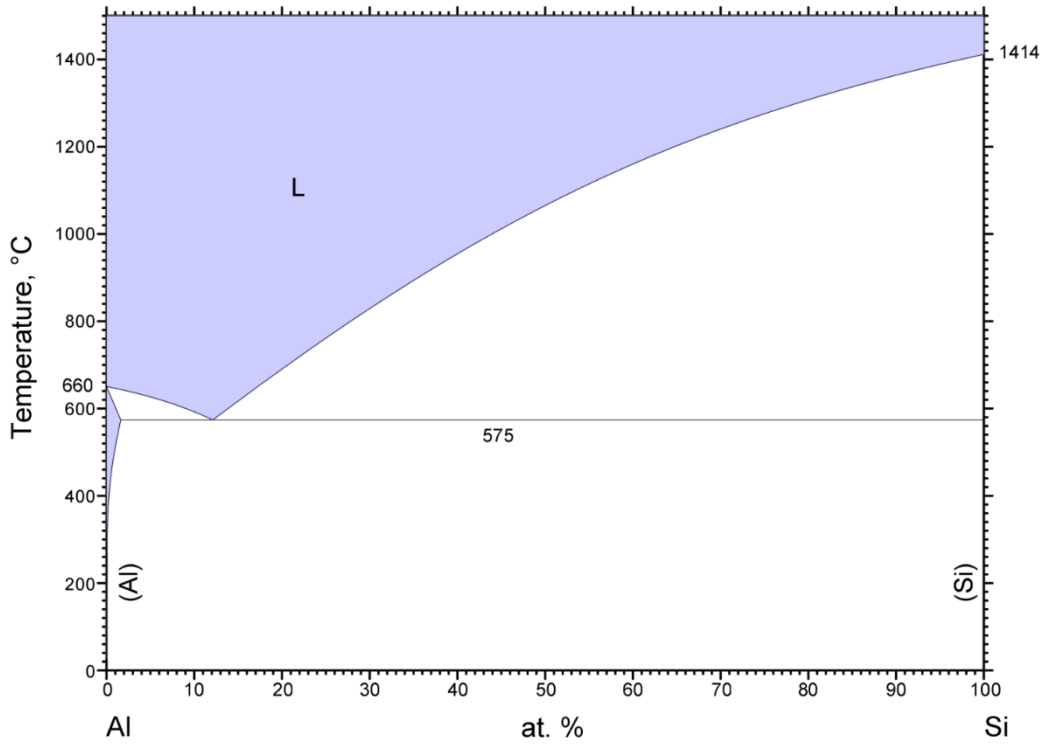


5 Binary phases diagrams Al-Zn, Al-Si, and sections of ternary phase diagrams Al-Si-Mg and Al-Si-Zn

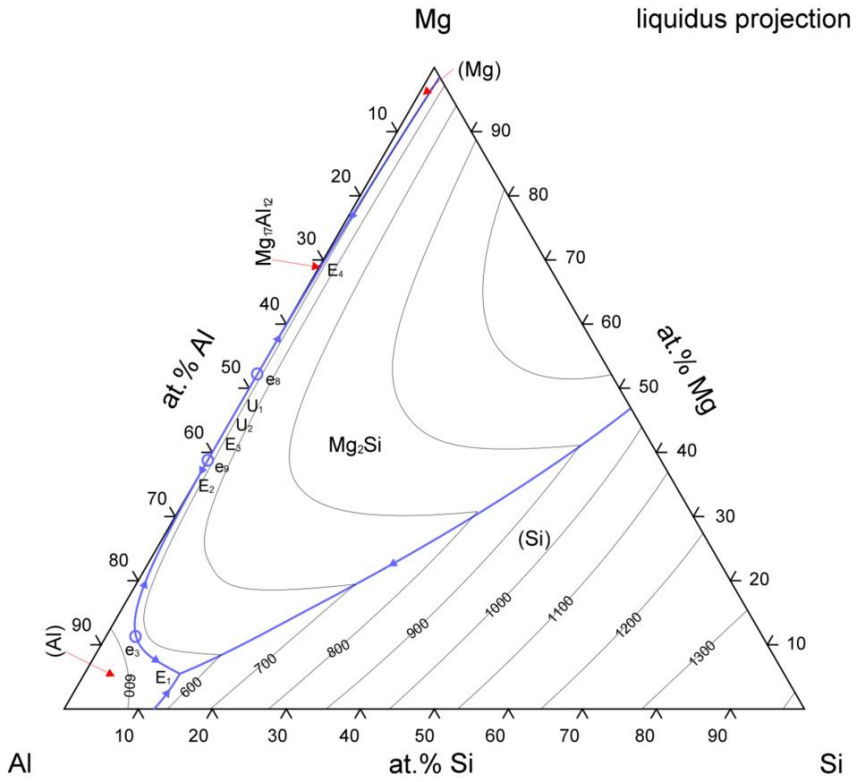
Al-Zn



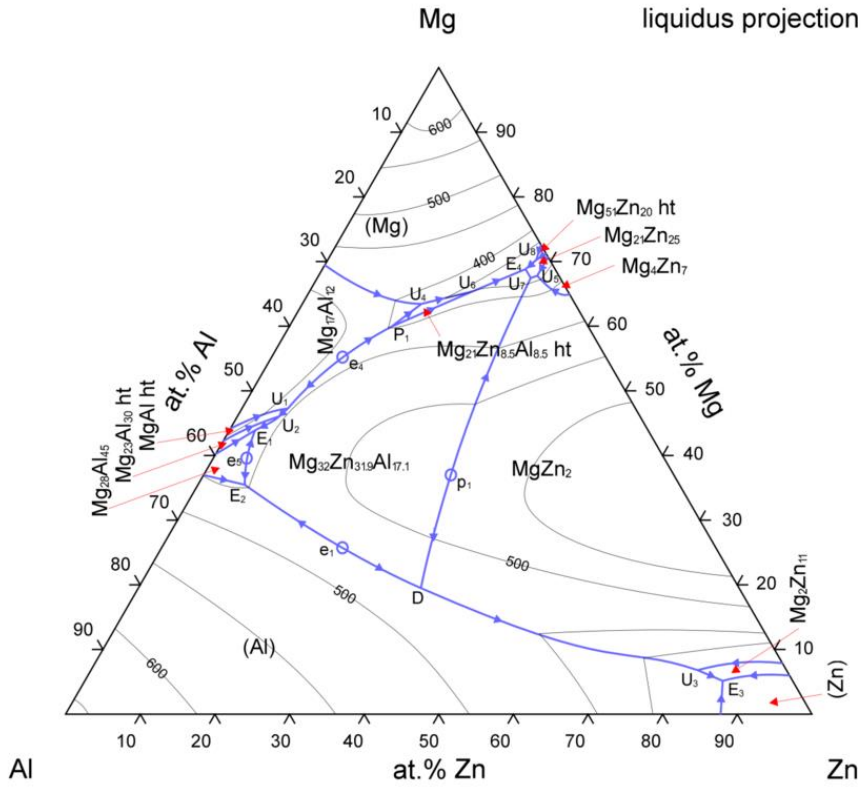
Al-Si



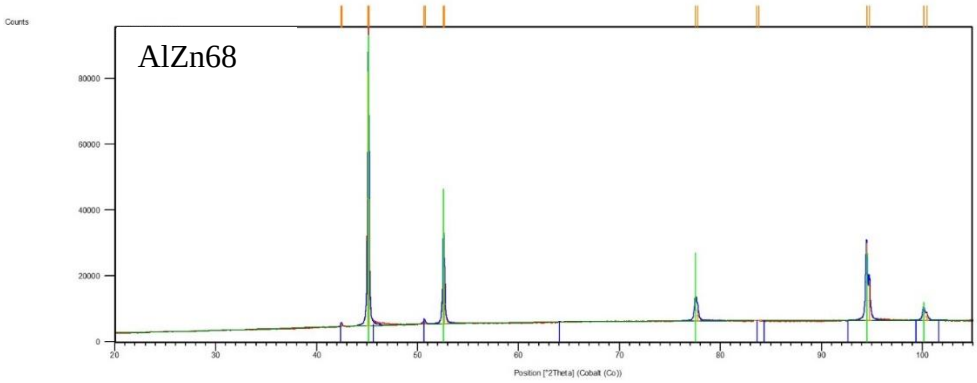
Al-Si-Mg

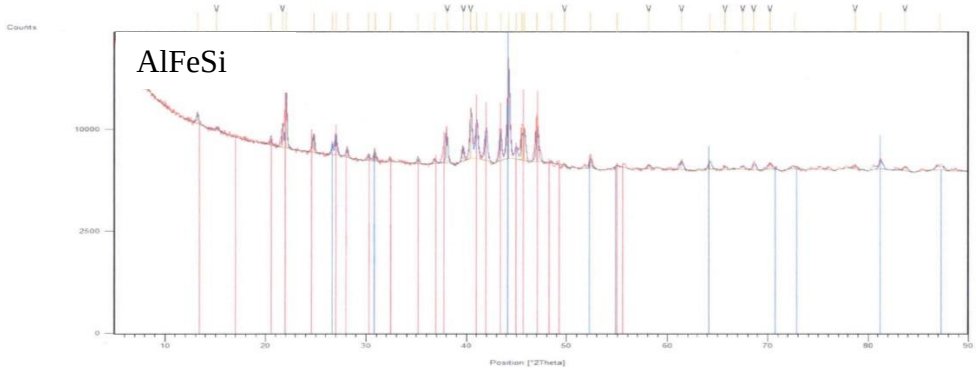


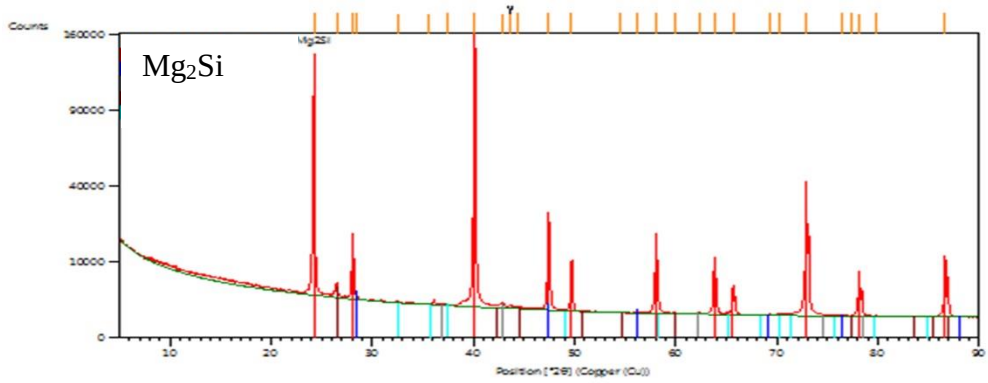
Al-Si-Zn

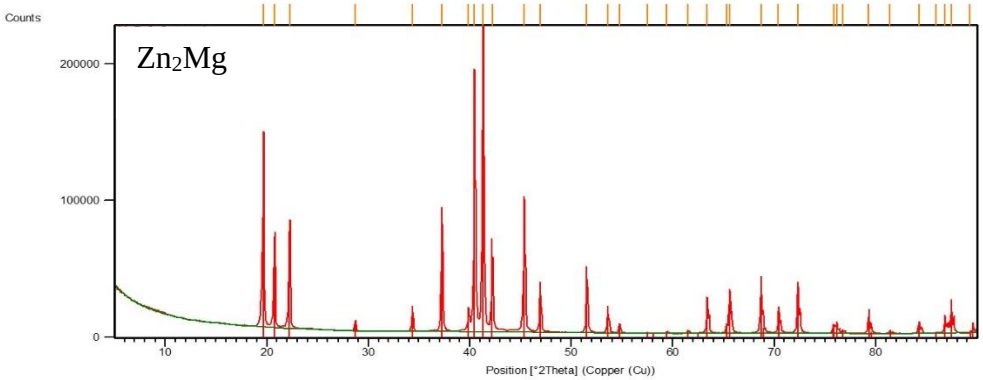


6 X-ray diffraction spectra of the synthetic pure phases

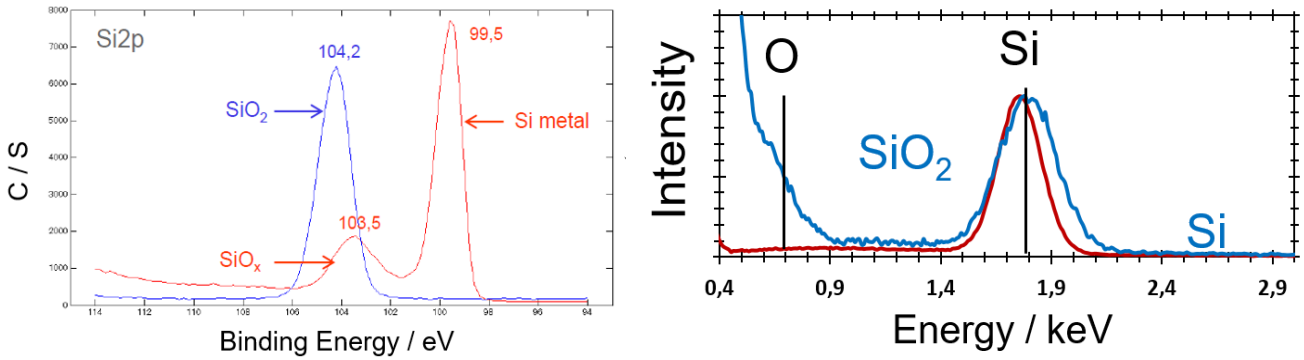




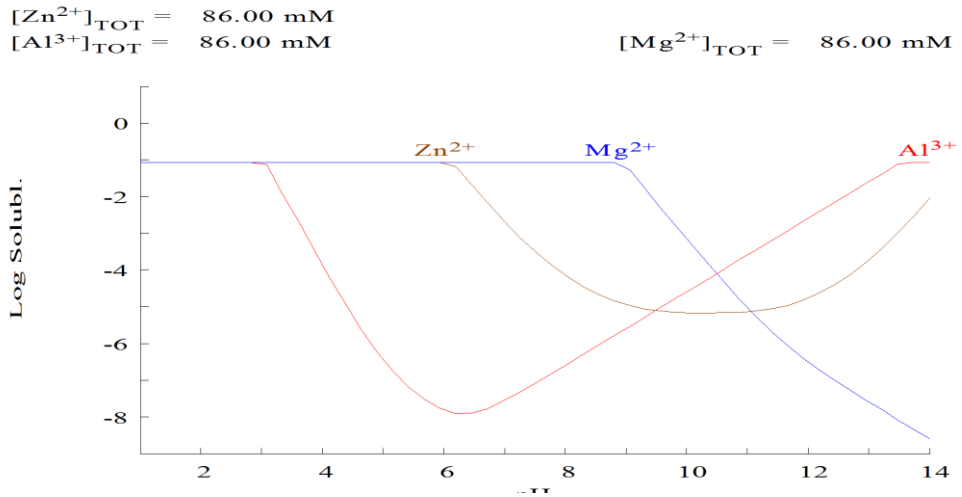




7 XPS spectra of the reference metallic Si phase and formed by heat treatment SiO_2



8 Solubility diagram of AlZnMg



Résumé

« Mécanismes de corrosion d'aciers revêtus par AlSi(ZnMg) »

Par Cyril NICARD

Thèse de doctorat en Chimie Physique et Chimie Analytique

RESUME

Introduction

Contexte

Depuis une dizaine d'années, la priorité des constructeurs automobiles est de rendre les véhicules plus légers afin de réduire les émissions de carbone tout en maintenant un haut niveau de sécurité pour les passagers. Pour répondre à cette demande et réduire l'épaisseur de tôle utilisée, de nouvelles nuances d'acier à haute résistance mécanique ont été développées. Comme pour les aciers standards, ces nouvelles nuances sont commercialisées avec un revêtement métallique pour les protéger contre la corrosion. Les alliages de zinc sont utilisés historiquement dans l'industrie automobile comme revêtement anticorrosion pour l'acier. Cependant, pour les aciers à haute résistance, l'emploi du zinc est de plus en plus dénigré en raison de sa sensibilité à la fragilisation par pénétration de métal liquide ("Liquid Metal Embrittlement" (LME) en anglais) au profit d'autres matériaux comme l'aluminium.

L'aluminium est utilisé comme matériau alternatif pour les revêtements anticorrosion des aciers à haute résistance. Aujourd'hui, le revêtement AluSi® (AlSi9) est la solution la plus largement utilisée pour l'emboutissage à chaud car son point de fusion est plus élevé que celui du zinc (200 ° C de différence) ce qui évite les problèmes de fissuration. De plus, il protège également la surface de l'acier de la corrosion et de l'oxydation lors du traitement thermique d'austénitisation. Cependant, comparé aux revêtements à base de zinc, il présente plusieurs inconvénients : peu ou pas de protection sacrificielle et un comportement de corrosion localisée (piqûres). Le concept de base des revêtements aluminium-silicium doit être amélioré pour atteindre des performances anticorrosion acceptables. L'ajout de Zn et de Mg dans les revêtements à base AlSi a été proposé pour améliorer les performances anticorrosion. Pour optimiser ces nouveaux revêtements AlSi (ZnMg), la compréhension de leur réactivité lors de la corrosion et en particulier le rôle joué par chaque élément d'alliage est primordial.

Objectifs

Dans le contexte décrit précédemment, la présente thèse vise à identifier et étudier les mécanismes de corrosion des revêtements à base d'aluminium et en particulier :

- Déterminer les effets des éléments d'alliage sur la composition de phase et la microstructure des revêtements à base d'aluminium fabriqués par immersion à chaud.
- Corréler la composition de phase et la microstructure avec la réponse électrochimique du revêtement.
- Identifier les produits de corrosion formés lors des essais de corrosion accélérée en fonction de la composition et de la microstructure des revêtements.
- Corréler la formation et la stabilité des produits de corrosion spécifiques à la microstructure du revêtement, en tenant compte de la dissolution sélective des phases et de la nature de l'environnement corrosif.
- Corréler les modifications de la nature des produits de corrosion sur la réactivité intrinsèque du revêtement.

Méthodologie

Pour atteindre ces objectifs, des essais de corrosion accélérée dans des chambres conditionnées et des tests électrochimiques sur des revêtements modèles et des phases pures ont été réalisés. La Microscopie Electronique à Balayage et l'analyse dispersive en énergie ont été utilisées pour observer et analyser les profils de microstructure et de corrosion des revêtements avant et après les tests de corrosion accélérée. Les phases composant les revêtements ainsi leur dissolution sélective et les produits de corrosion formés ont été identifiés par spectroscopie Raman et Diffraction des Rayons X. Les phases pures identifiées dans la microstructure des revêtements ont été synthétisées en partenariat avec L'Université technologique de Prague afin de les tester et de comprendre leur contribution individuelle aux mécanismes généraux de corrosion. Des expériences de couplage galvanique entre phases pures ont été menées pour explorer les couplages micro-galvaniques possibles dans les revêtements et évaluer leur criticité dans les mécanismes de corrosion. Parmi les techniques électrochimiques locales : La spectroscopie d'impédance électrochimique locale et la cartographie d'impédance électrochimique locale ont été utilisées pour vérifier la puissance

sacrificielle du revêtement métallique et les propriétés d'auto-cicatrisations des produits de corrosion formés dans le cas de revêtements endommagés.

Structure de la thèse

Cette thèse est divisée en trois parties regroupant six chapitres. La première partie est composée du chapitre d'introduction, de « l'état de l'art » (chapitre I) et de la méthodologie expérimentale (chapitre II) décrivant succinctement les techniques utilisées. La deuxième partie comprend trois chapitres de résultats sous formes de publications et découpent la problématique générale en 3 sous-thématiques de la façon suivante :

- Chapitre III « L'effet de l'ajout de Zn et de Mg sur la microstructure et les mécanismes de corrosion des aciers haute résistance revêtus par AlSi. » qui traite de la microstructure des revêtements AlSi(ZnMg) et de l'impact des tests accélérés de corrosion sur la microstructure.

- Chapitre IV « Couplage galvanique et dissolutions sélectives des phases pures dans les revêtements anticorrosion AlSi(ZnMg) pour les aciers haute résistance. » qui étudie les propriétés électrochimiques des phases pures identifiées dans le chapitre précédent de façon indépendante ou lors de test de couplage galvanique.

- Chapitre V « Effet protecteur des produits de corrosion des revêtements anticorrosion AlSi(ZnMg) pour les aciers haute résistance. » qui analyse l'effet des produits de corrosion formés sur la réactivité du revêtement AlSi(ZnMg).

La dernière partie est constituée d'un unique chapitre VI « conclusions et perspectives ».

Ce résumé en français reprend la même structure que le manuscrit de thèse (en anglais) en proposant à chaque fois la synthèse des informations et conclusions importantes des différentes parties du manuscrit.

1 Etat de l'art

Les revêtements à base de zinc sont utilisés depuis longtemps dans l'industrie automobile. La figure 1 liste les revêtements à base de Zn et à base d'Al utilisés dans l'industrie automobile. Les revêtements à base d'aluminium sont relativement nouveaux, bien que ce métal fût déjà présent dans des revêtements à base de zinc en tant qu'élément d'alliage.

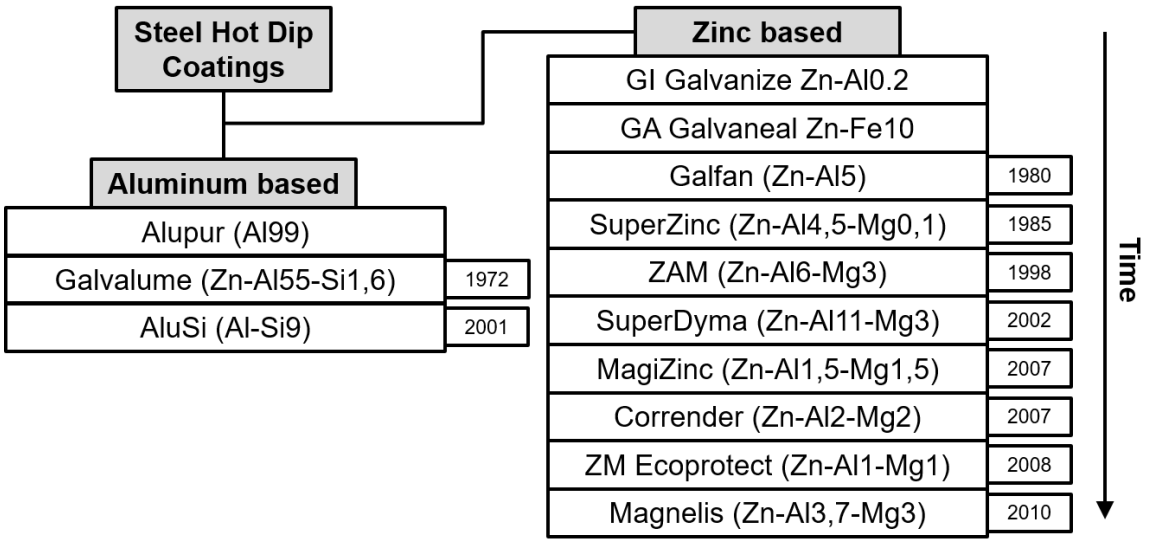


Figure 1 : Revêtements anticorrosion à base d'aluminium (Al-based) ou de zinc (Zn-based) utilisés dans l'industrie (Compositions données en pourcentage massique)

Ces revêtements sont généralement obtenus par un procédé d'immersion à chaud (Hot Dip en anglais). Ce procédé consiste à dérouler une bobine d'acier dans un bain d'alliage à base de zinc ou d'aluminium afin de l'en revêtir. La microstructure d'un revêtement à base AlSi est composée d'une matrice d'aluminium, d'aiguilles de silicium (qui précipitent entre les dendrites de la matrice) et d'un intermétallique se développant à l'interface revêtement/acier par diffusion du fer liée à la température du bain. L'ajout de silicium permet de réduire l'épaisseur de l'intermétallique formé.

L'aluminium est un métal très actif mais sa tendance à créer une couche passive réduit sa capacité à fournir une protection sacrificielle (protection cathodique) à l'acier. Le film passif favorise la corrosion par piqûres du revêtement. La littérature montre que la corrosion généralisée de l'aluminium est régie par deux facteurs principaux:

- Le nombre de défauts à la surface (fissures, phases intermétalliques etc.) qui sont des sites préférentiels pour l'amorçage de la corrosion.
- La présence d'ions halogénures dans l'électrolyte qui favorise la corrosion par piqûration car ils déstabilisent localement la couche passive.

Différents éléments peuvent être ajoutés à l'aluminium afin de modifier ses propriétés. En restant dans le domaine de solution solide de l'aluminium, les éléments d'alliage les plus couramment utilisés peuvent être classés du plus soluble au moins soluble comme suit :

Zn>Mg>Mn>Cu>Si

Le tableau 1 présente les phases préférentiellement formées qui apparaissent dans différents systèmes à base d'aluminum pouvant être utilisés dans l'aéronautique, dans les anodes pour protéger les structures enterrées et/ou en milieu marin. La proportion et la répartition des phases dépendra de la composition et des conditions de fabrication.

Tableau 1 : Phases préférentiellement formées en fonction des éléments en présence (Al > 60 %m.)

Composition	Phases préférentiellement formées
Al	Al
Al+Si	Al , Si
Al+Zn	(Al) , $Al-Zn$ *binaire*
Al+Mg	$AlMg_2$, $AlMg_5$
Al+Fe	Al_3Fe, Al_6Fe
Al+Fe+Si	$Al_xFe_ySi_z$ *Intermétallique*
Al+Si+Zn	(Al) , Si
Al+Si+Mg	$Al + Mg_2Si$

En raison de la diffusion du fer pendant le processus d'immersion à chaud, certaines de ces phases ne peuvent pas se former. Le tableau 2 présente les phases identifiées dans les revêtements à base d'aluminium pour acier.

Tableau 2 : Phases identifiées dans des revêtements à base d'Aluminium (stch = stœchiométrie)

Composition du revêtement %m.	Phases formées préférentiellement
Al	Al, Al_3Fe, Al_6Fe
AlSi	Al , Si, $Al_xFe_ySi_z$ ($\tau 5$ et $\tau 6$)
AlZnMg	Al , Zn_2Mg, Al_3Fe, Al_6Fe
AlSiZn(Zn<10 %)	(Al) , Si, $Al_xFe_ySi_z$ ($\tau 5$ et $\tau 6$)
AlSiZn(Zn>10 %)	(Al) , $Al-Zn$ *binaire*, *Si* $Al_xFe_ySi_z$ ($\tau 5$ et $\tau 6$)
AlSiMg(Mg<Mg2Si stch)	$Al, Si, Mg_2Si, Al_xFe_ySi_z$ ($\tau 5$ et $\tau 6$)
AlSiMg(Mg>Mg2Si stch)	$Al, Si, Mg_2Si, AlMg_2$, $Al_xFe_ySi_z$ ($\tau 5$ et $\tau 6$)

Pour modifier la résistance à la corrosion de l'aluminium et son pouvoir sacrificiel, différents éléments d'alliage peuvent être ajoutés. Pour abaisser le potentiel de l'aluminium, le Zn est largement utilisé. L'efficacité maximale du Zn est obtenue lorsqu'il est complètement dissous dans la matrice d'aluminium mais l'effet du Zn sur les propriétés de passivation de l'aluminium n'est pas encore compris et nécessite d'autres études. Un surplus de Zn génère une

seconde phase eutectique riche en Zn favorisant un couplage galvanique et l'apparition de sites préférentiels pour l'initiation de la corrosion.

L'addition de magnésium en solution solide dans l'aluminium n'a pas un effet aussi fort que le Zn sur son potentiel de corrosion mais en présence de zinc ou de magnésium les phases intermétalliques nouvellement créées telles que Mg_2Si ou Zn_2Mg sont fortement anodiques. Le potentiel de corrosion de Zn_2Mg est peu sensible à la variation du pH dans les milieux chlorures et peut être sacrificiel pour l'acier dans la plupart des environnements corrosifs. L'étude des comportements électrochimiques individuels des phases pures comme Mg_2Si, Zn_2Mg ou l'AlFeSi intermétallique et leur couplage dans la matrice Al est importante pour mieux comprendre les mécanismes globaux de corrosion des nouveaux revêtements à base d'AlSi.

Il semble également que la présence d'ions Mg puisse modifier significativement la nature et la morphologie des produits de corrosion sur les alliages Al et Zn. Certains mécanismes ont été proposés pour expliquer l'effet positif de Mg sur la résistance à la corrosion des revêtements AlSiZnMg. L'effet des produits de corrosion comme les Doubles Hydroxides Laméllaires (LDH) a été étudié mais sans détailler les conditions de leur formation, leur stabilité et leur effet sur la réactivité de surface. L'effet de la composition de l'alliage sur la morphologie LDH et leurs performances restent également inexplorés.

Certains activateurs (In, Ga, Hg ou Sn) sont utilisés pour activer les anodes Al. Cependant, la concentration de ces activateurs est cruciale pour obtenir de bonnes performances et elle n'est pas forcément facile à contrôler dans un processus industriel où quatre éléments sont déjà présents. De plus, la vitesse de corrosion en présence de tels activateurs est souvent très élevée, paramètre indésirable pour un revêtement mais moins néfaste pour des anodes protectrices pouvant être remplacées.

2 Expérimental

Sur la base de la revue de littérature présentée au précédent chapitre, différentes techniques ont été identifiées comme adéquates pour notre étude sur le mécanisme de corrosion des revêtements protecteurs à base d'aluminium pour aciers haute résistance.

Les essais de corrosion accélérée ont été effectués selon les normes utilisées dans l'industrie automobile. Les électrolytes ruisselants sur les échantillons et les produits de corrosion ont été collectés et analysés par ICP-OES (Spectrométrie à plasma à couplage inductif) pour réaliser un bilan matière. Cette technique a été utilisée pour obtenir la

composition élémentaire et pour étudier la dissolution sélective des phases composant les différents revêtements. La Microscopie Electronique à Balayage (MEB) permet d'observer avec précision le profil de corrosion et la Microscopie à Dispersion d'Energie (EDS) est très efficace pour mettre en évidence l'oxydation sélective et obtenir des phases de composition élémentaire. Des expériences électrochimiques ont été réalisées pour donner des informations électrochimiques sur les revêtements, les produits de corrosion, les phases pures et les couplages possibles. Les techniques de Cartographie par Electrode Vibrante (SVET) et de Cartographie d'Impédance Electochimique Locale (LEIM-LEIS) ont été utilisées pour estimer l'effet des produits de corrosion sur la réactivité du revêtement.

La suite de ce chapitre présente brièvement les matériaux et techniques experimentales utilisés pour les travaux de recherche.

2.1 Matériaux

Les échantillons soumis aux essais sont des aciers revêtus d'un alliage AlSi(ZnMg) avec une composition variant entre 0-9 %m. de Si, 0-30 %m. de Zn, de 0-10 %m. de Mg complété avec de l'aluminium. Les échantillons d'aciers revêtus ont été fournis par ArcelorMittal. Les échantillons ont été fabriqués par un procédé d'immersion à chaud industriel basé sur le revêtement AluSi décrit dans le brevet US 6296805 B1. Les revêtements AluSi © avec 9 wt. % de Si sur des aciers de type 22MnB5 ont été utilisés comme matériaux de référence.

2.2 Tests de corrosion accélérée

Dans ce travail de recherche, le test de corrosion accélérée en chambre conditionnée respecte la norme VDA 233-102 (également appelée NewVDA ou N-VDA dans la littérature). Le cycle N-VDA dure une semaine avec des conditions variant entre 50 à 100 % d'humidité et des températures allant de -15 °C à +50 °C avec des phases de pulvériastion d'une solution acqueuse saline à 1 % NaCl (pH neutre).

2.3 Dissolution des produits de corrosion

Afin d'obtenir les cinétiques de dissolution élémentaire, les électrolytes ruisselants et les produits de corrosion restants (après dissolution selon la norme ISO 8407 modifiée) ont été analysés par ICP-OES. La solution aqueuse de 250 $g.L^{-1}$ de glycine préconisée par la norme ISO 8407 (permettant la dissolution des produits de corrosion du zinc) a été remplacée dans notre cas par une solution aqueuse à 65 % d'acide nitrique qui dissout efficacement les produits de corrosion à base d'aluminium.

2.4 Caractérisation des phases et produits de corrosion

La microscopie électronique à balayage a été utilisée pour vérifier la présence ou l'absence de produits de corrosion et évaluer l'état de surface des échantillons. Couplée avec le MEB, la spectroscopie à dispersion d'énergie a été utilisée pour obtenir une analyse élémentaire semi-quantitative des produits de corrosion et des phases. Une tension d'accélération de 15 keV a été choisie car les instruments du site sont généralement étalonnés à cette tension. Afin de réduire le volume d'interaction électronique (poire d'interaction), la mesure EDS a également été effectuée à 5 keV. La profondeur de pénétration électronique dans l'aluminium à 15 keV est légèrement supérieure à 2 µm et moins de 500 nm à 5 keV.

2.5 SpectroElectroChimie par Emission Atomique

La technique de SpectroElectroChimie par Emission Atomique (AESEC) est constituée d'une cellule électrochimique à trois électrodes dans laquelle le volume d'électrolyte est limité et pompé en continu dans un ICP-OES. La figure "Appendix 3" présente le schéma général de cette technique. Le but de l'AESEC est d'analyser en continu la dissolution élémentaire survenant dans la cellule électrochimique. De cette façon, nous pouvons étudier la dissolution sélective du revêtement ou des phases pures dans différentes conditions de courant imposé (anodique ou cathodique) ou de variation du pH.

2.7 Expériences électrochimiques

2.7.1 Electrochimie globale

Les expériences électrochimiques de mesure de potentiel de circuit ouvert (OCP) et de polarisation ont été effectuées dans une cellule à trois électrodes thermostatée (25 ° C). Les

échantillons d'aciers revêtus sont montés comme électrode de travail, une électrode au calomel saturé comme référence et un fil de platine comme contre électrode. Dans le cas d'expériences de couplage, les électrodes de travail et les contre-électrodes étaient deux phases pures différentes.

2.7.2 Electrochimie locale

La Cartographie d'Impédance Electrochimique Locale (LEIM) est une technique électrochimique locale employée pour évaluer l'évolution de la réactivité de surface impactée par la corrosion et la formation de produits de corrosion. Une configuration à trois électrodes est utilisée, un échantillon métallique (acier revêtu) constitue l'électrode de travail, une électrode Ag / AgCl est utilisée comme référence et un fil de platine comme contre-électrode.

La technique de cartographie de courant par électrode vibrante (SVET) consiste en un échantillon métallique immergé dans un électrolyte avec une électrode vibrante qui mesure la différence de potentiel induite par les lignes de courant dans l'électrolyte. Cette technique est complémentaire du LEIM car elle donne des informations sur l'intensité de l'activité cathodique et anodique en surface.

3 L'effet de l'ajout de Zn et de Mg sur la microstructure et les mécanismes de corrosion des aciers haute résistance revêtus par AlSi.

L'ajout de zinc au revêtement AlSi modifie la matrice aluminium des revêtements AlSi en une solution solide de Al(Zn). Suite à cette modification, les résultats observés lors des tests accélérés ont montré une amélioration de la protection superficielle de l'acier (retard de l'apparition de la rouille rouge par rapport à la référence AlSi), pouvant s'expliquer par un potentiel libre du revêtement plus négatif (figure 2a) et un courant sous polarisation anodique plus élevé.

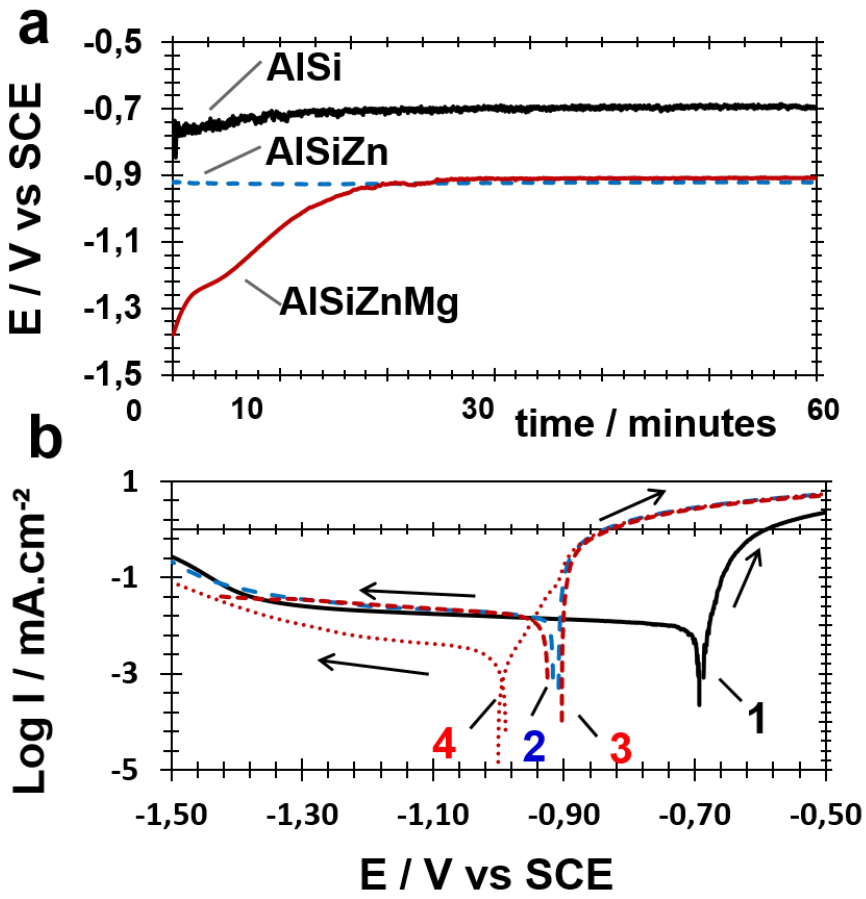


Figure 2 : Electrochimie des revêtements étudiés dans une solution aqueuse de NaCl 1 % massique (pH initial 7). a) Evolution du potentiel en circuit ouvert (E) en fonction du temps pour les aciers revêtus par AlSi, AlSiZn et AlSiZnMg. b) Courbes de polarisation cathodique et anodique (courant logarithmique I en fonction du potentiel E) d'acier revêtus par AlSi (courbe 1), AlSiZn (courbe 2) et AlSiZnMg (courbes 3,4) AlSiZnMg après 1 h d'immersion (courbes 1-3) à 10 min d'immersion (courbe 4). Le sens de la polarisation est indiqué par des flèches.

L'amélioration de ce pouvoir sacrificiel s'accompagne d'une corrosion de revêtement plus rapide tant dans les tests électrochimiques que dans les tests de corrosion accélérée (figure 3). On observe clairement une dissolution sélective de la matrice Al(Zn) autour des aiguilles de silicium. Un couplage galvanique entre les dendrites Si et la matrice Al(Zn) est prévisible au vu de la différence entre les potentiels de ces deux phases mais qu'il soit plus fort nous interroge sur son absence dans les revêtements AlSi.

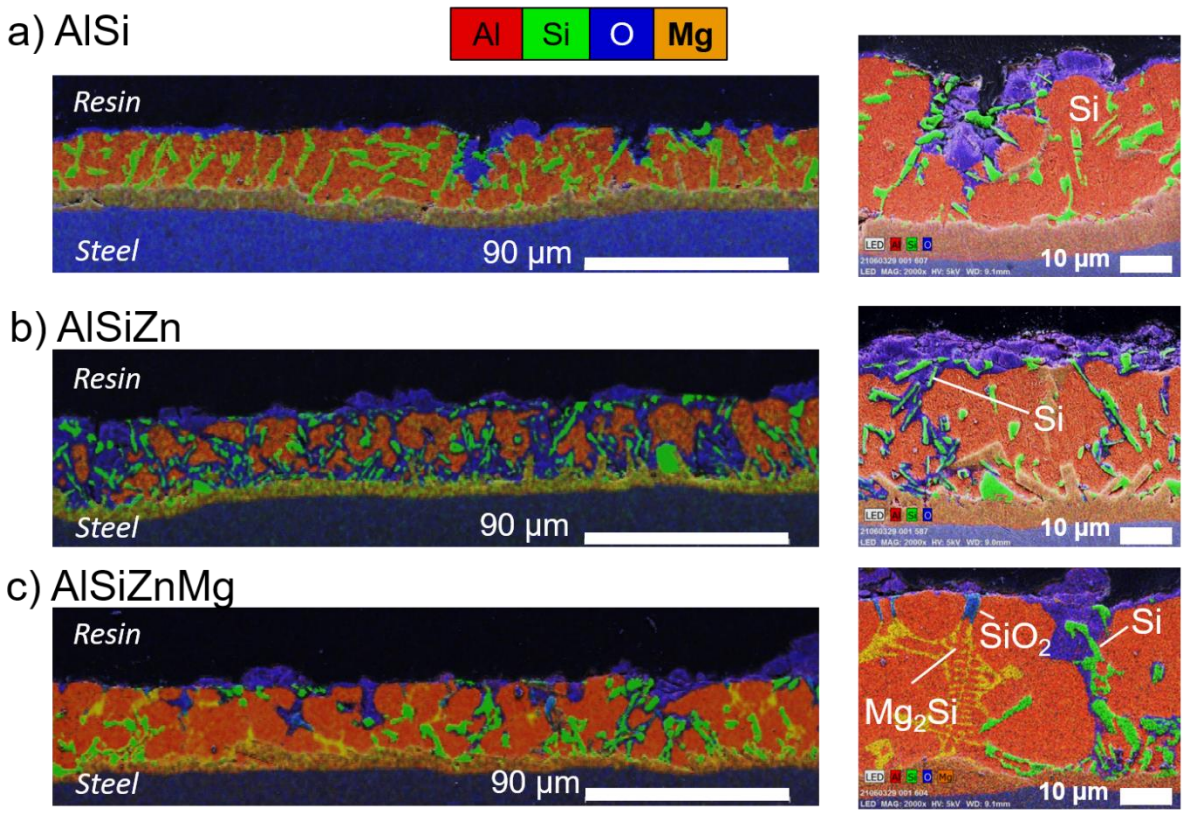


Figure 3 : Cartes EDS montrant la distribution des produits de corrosion après 12 cycles de test VDA 233-102 dans les tranches d'aciers revêtus par (a) AlSi, (b) AlSiZn et (c) AlSiZnMg.

Un ajout de magnésium aux revêtements AlSiZn modifie la microstructure du revêtement en ajoutant deux nouvelles phases. La phase Si est partiellement transformée en intermétallique Mg_2Si significativement plus anodique que Si, Fe ou Al(Zn). La matrice Al(Zn) devrait être protégée cathodiquement lors de la dissolution sélective de Mg.

$$Mg_2Si + 2\ H_2O \rightarrow 2\ Mg^{2+} + SiO_2 + 4\ H^+ + 8\ e^- \qquad (5)$$

Les résultats expérimentaux en tests accélérés suggèrent que l'addition de Mg au revêtement AlSiZn ne modifie pas significativement la protection sacrificielle, mais augmente la durée de vie du revêtement et favorise la formation de produits de corrosion stables recouvrant les défauts de l'acier.

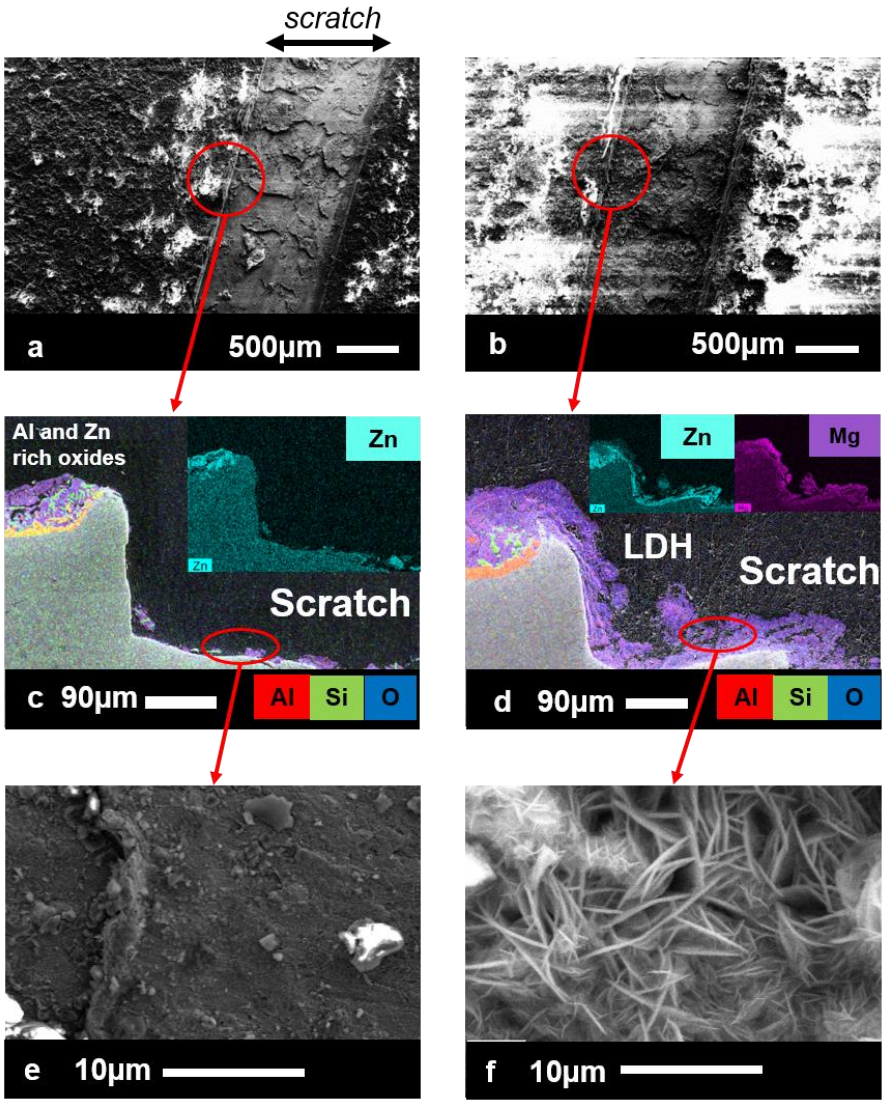


Figure 4 : Distribution des produits de corrosion à proximité de la rayure réalisée sur des aciers revêtus par (a, c, e) AlSiZn et (b, d, f) AlSiZnMg après 6 cycles de test VDA 233-102. La vue générale de dessus de la rayure et la morphologie des produits de corrosion à l'intérieur de la rayure sont montrées par imagerie d'électrons secondaires, la distribution des éléments dans la tranche est montrée en ajoutant la cartographie élémentaire en EDS.

On peut supposer que ces produits offrent une protection de barrière à l'acier qu'ils recouvrent. En effet, la nature, la quantité et la répartition des produits de corrosion à la surface de l'acier revêtu d'AlSiZnMg est très différentes de celles de l'acier revêtu d'AlSiZn. La Fig. 4 présente des observations en MEB faites sur la surface d'échantillons rayés à l'acier puis mis en test de corrosion accélérée. L'absence de produits de corrosion dans la rayure dans le cas d'un revêtement AlSiZn peut être liée à l'augmentation significative du pH par réaction cathodique et à la dissolution correspondante des produits contenant du Zn et de l'Aluminium.

$$O_2 + 2\,H_2O + 4\,e^- \rightarrow 4\,OH^- \qquad (6)$$

$$ZnO + H_2O + OH^- \rightarrow Zn(OH)_4^{2-} \quad (7)$$

$$Al(OH)_3 + OH^- \rightarrow Al(OH)_4^- \quad (8)$$

Une plus grande stabilité des produits de corrosion dans la rayure d'AlSiZnMg peut s'expliquer par la faible solubilité de Mg^{2+} à pH élevé limitant l'augmentation du pH par la précipitation de $Mg(OH)_2$.

$$Mg^{2+} + 2\ OH^- \rightarrow Mg(OH)_2 \quad pKs=10.5 \quad (9)$$

La formation d'une fine couche de $Mg(OH)_2$ peut également être responsable d'un « effet de peau » à l'origine d'une stabilité élevée du pH de doubles hydroxydes lamellaire (LDH) contenant du Mg.

Pour l'acier revêtu d'AlSiZnMg, la protection améliorée de l'acier a été obtenue grâce à l'effet synergique de Zn et du Mg. Le Zn semble activer la dissolution de la matrice Aluminium, contribuant à son pouvoir sacrificiel et libérant des ions aluminium nécessaires à la formation de doubles hydroxydes lamellaires. Le Mg n'apporte pas d'effet sacrificiel à long terme car il n'est distribué que dans des intermétalliques isolés et que sa dissolution en surface est rapide (moins de quelques heures). Cependant, l'addition de Mg réduit la quantité d'inclusions de Si métallique par la formation de Mg_2Si plus actif, ce qui réduit la consommation prématurée du revêtement par couplage micro-galvanique à l'intérieur du revêtement. Le Mg dissous favorise la formation et la stabilisation des produits de corrosion dans les défauts, ce qui contribue à prolonger la durée de vie du revêtement.

4 Couplage galvanique et dissolution sélective des phases pures dans les revêtements anticorrosion AlSi(ZnMg) pour les aciers haute résistance.

Les phases pures identifiées dans l'analyse microstructurale des revêtements AlSiZnMg du chapitre précédent ont été synthétisées en collaboration avec l'université de Prague ou commandées. Le seul matériau biphasique est la solution solide Al(Zn32) qui présente les phases α-Al et la phase β-Al habituellement trouvées dans les alliages d'aluminium avec plus de 20 %m de Zn. Les phases Zn_2Mg et Mg_2Si ont été les plus difficiles à fabriquer car le magnésium se combine facilement avec l'oxygène pour former des oxydes, par conséquent l'atmosphère pendant la synthèse doit être contrôlée. La synthèse de la phase de SiO_2 à partir

de Si a été réalisée mais l'oxyde formé était si mince (<500 nm) qu'il était impossible d'en confirmer la présence avec les techniques classiques de XRD, spectroscopie Raman et infrarouge. La présence de SiO_2 et sa stœchiométrie ont donc été vérifiées par l'intermédiaire d'une analyse l'XPS (Appendix 7). La stabilité du Si au traitement thermique et sa difficulté à se transformer en oxyde même à cette température est cohérente avec la présence de nombreuses aiguilles de Si pur dans les revêtements AlSi.

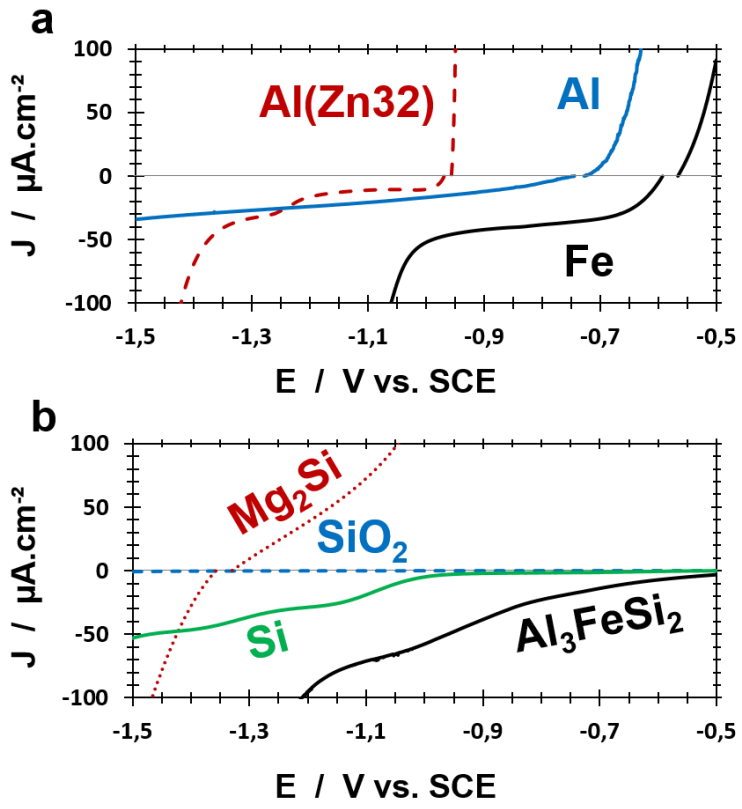


Figure 5 : Courbes de polarisation de (a) solution solide Al (Zn), Al, Fe et (b) Mg2Si, SiO2, Si, Al3FeSi2 dans une solution aqueuse de NaCl 0,172 M (1 % massique).

Bien que l'aluminium soit bien positionné dans la série galvanique pour protéger l'acier, les courbes de polarisation des différentes phases (figure 5) révèlent un potentiel de corrosion et une courbe très similaire à ceux de l'acier impliquant une capacité limitée à le protéger. Le potentiel de corrosion de Al(Zn) est plus négatif et laisse penser que Al(Zn) devrait être plus protecteur que Al. Dans les expériences de couplage, le courant de couplage Fe-Al est moins important que le couplage Al(Zn)-Fe.

L'expérience sur le potentiel libre de l'aluminium en solution aqueuse NaCl 0,172 M ou $ZnCl_2$ 0,086 M laisse penser que c'est la présence de zinc ionique qui change le comportement de l'aluminium et empêche la passivation attendue (Fig.6) . Le changement de comportement

de l'aluminium se produit avec $ZnCl_2$ à pH = 6. Cette valeur de pH correspond à la transition entre un domaine à pH bas où Zn est sous sa forme ionique Zn^{2+} et un autre où il peut former des espèces comme la Simonkolleite (proposée par le logiciel hydra medusa) mais aussi d'autres espèces comme des Al-Zn LDH. La formation de ces espèces pourrait déstabiliser la formation d'oxyde d'aluminium et empêcher sa passivation mais cette hypothèse ne peut pas être confirmée à ce stade.

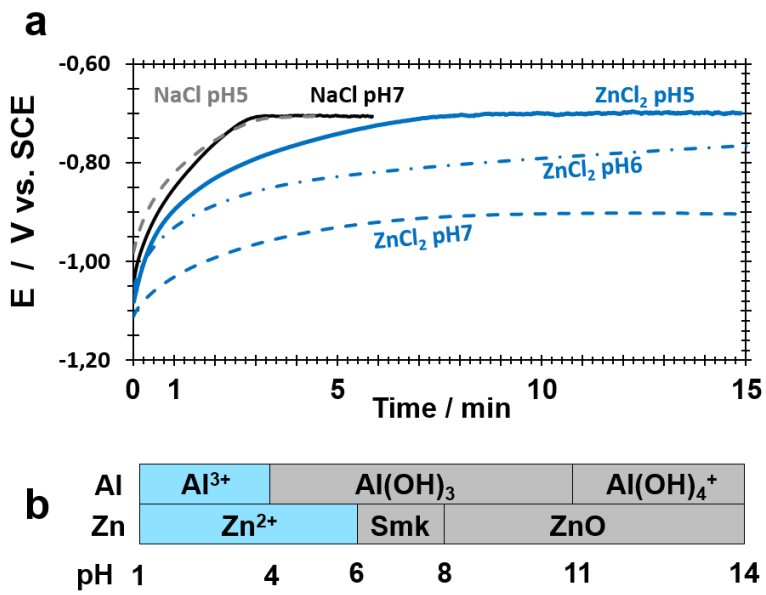


Figure 6 (a) Potentiel en circuit ouvert de l'aluminium pur en fonction du temps dans une solution aqueuse de NaCl 0,172 M ou $ZnCl_2$ 0,086 M à pH 5 à 7 (ajusté avec une solution aqueuse de NaOH 1 M). (b) Espèce prédominante simulée contenant Al / Zn

L'activation de l'aluminium par le zinc le rend plus protecteur pour l'aluminium mais augmente également le couplage galvanique avec toutes les autres phases composant les revêtements. Si et Al_3FeSi_2 sont deux de ces phases et leur potentiel de corrosion est d'environ -0,4 V vs. SCE. Les expériences de couplage révèlent que les courants développés sont en effet plus élevés lorsque Si ou Al_3FeSi_2 sont couplés à Al(Zn) à la place de l'aluminium pur et sont du même ordre de grandeur. Mg_2Si et Zn_2Mg sont censés avoir un potentiel de corrosion inférieur à Al et Al(Zn) et être protecteurs de l'acier. Le comportement de Mg_2Si est plus ambigu, quand il est couplé avec Al ou Al(Zn) son potentiel évolue rapidement vers une valeur moins négative (Fig. 7) et dans le cas du couplage Al(Zn), le potentiel Mg_2Si atteint -0.5 V vs. SCE. Après des expériences de couplage, l'analyse de surface du Mg_2Si révèle la présence d'oxyde de silicium.

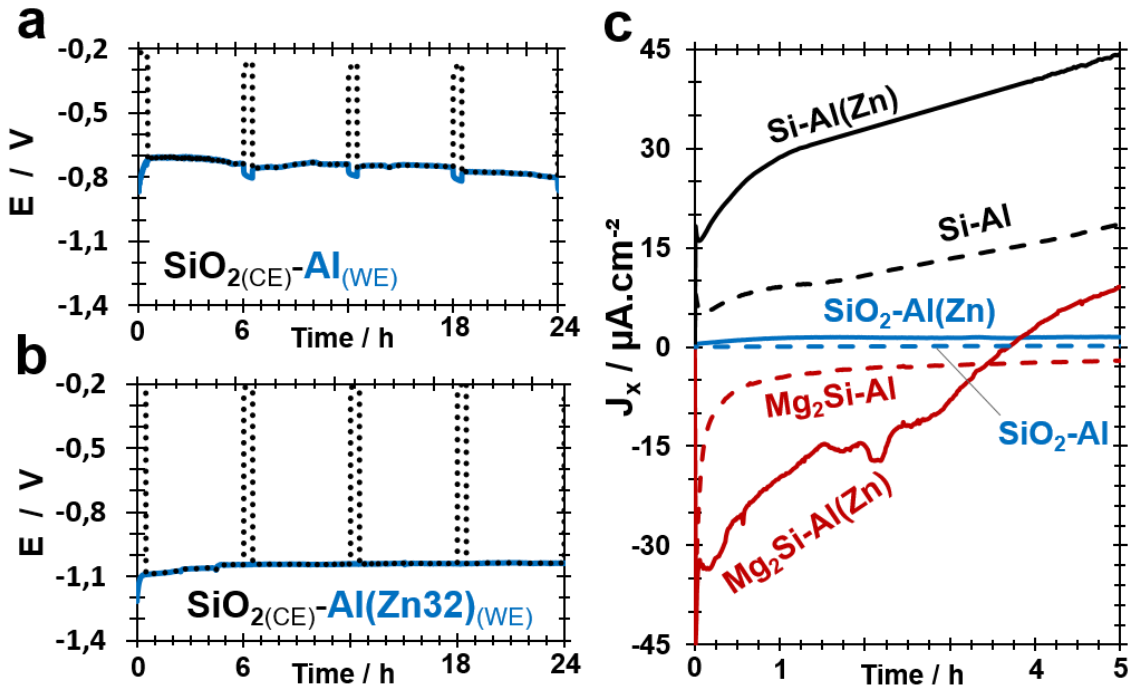


Figure 7 : Potentiels libres de phases pures pendant les essais de couplage pour (a) SiO_2-Al et (b) SiO_2-Al (Zn32) dans une solution aqueuse de NaCl 0,172 M. (c) Courant de couplage entre les phases contenant du silicium et Al ou Al (Zn32) dans une solution aqueuse de NaCl 0,172 M.

SiO_2 a été synthétisé pour vérifier la différence de comportement électrochimique entre Si et SiO_2. Le courant initial et le courant final de couplage avec SiO_2 sont systématiquement plus faibles qu'avec Si ou Mg_2Si. Le couplage SiO_2 avec la matrice Al est moins critique que le couplage Si. Cependant, il est incertain que le SiO_2 formé après la corrosion de Mg_2Si et que le SiO_2 formé après que le traitement thermique de Si aient la même structure.

5 Effet protecteur des produits de corrosion des revêtements anticorrosion AlSi(ZnMg) pour les aciers haute résistance.

Les tests de corrosion sur tranches en milieu chlorure confirment l'impact important de l'alliage de zinc sur le pouvoir sacrificiel des revêtements. Ce gain en termes de pouvoir sacrificiel s'accompagne d'une forte dissolution du revêtement (figure 3) due au couplage galvanique assurant la protection cathodique de l'acier. On remarque également que l'intermétallique AlFeSi n'est pas consommé même après dissolution de la matrice du revêtement ce qui signifie que cette phase ne protège pas cathodiquement l'acier. Des produits de corrosion semblables à des plaquettes sont visibles sur les deux revêtements AlSiZn et AlSiZnMg. L'ajout de magnésium dans la composition du revêtement réduit sa consommation

par rapport aux revêtements AlSiZn et les produits de corrosion formés à la surface de l'acier sont plus fins et semblent plus couvrants.

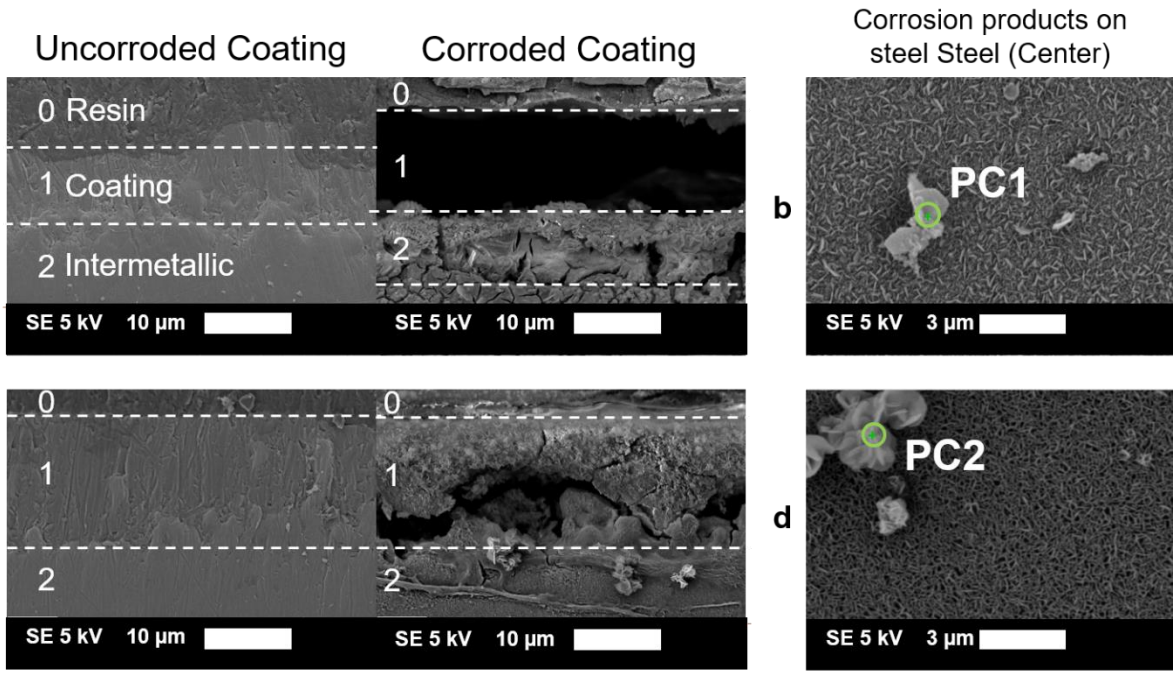


Figure 8 : Les images électroniques secondaires d'arrêtes coupées d'aciers revêtus d' (a) AlSiZn et (b) AlSiZnMg après 48h d'immersion dans une solution aqueuse NaCl 1 % massique à pH initial 7. 0: résine; 1: Revêtement; 2: Intermétallique.

L'analyse EDS sur la surface de l'acier au centre des arrêtes coupées révèle une différence dans la composition des produits de corrosion. Avec le revêtement AlSiZn, les produits de corrosion sont principalement des Al-Zn LDH tandis que les produits de corrosion pour le revêtement AlSiZnMg sont des Al-Mg LDH. Le fait que des produits de corrosion soient présents sur l'acier, supposé cathodique dans ce système, laisse penser que les produits de corrosion se forment préférentiellement ou plus facilement en présence d'ions hydroxydes dans la solution. Cette hypothèse est cohérente avec les observations dans nos travaux précédents où les produits de corrosion sont plus nombreux sur les phases cathodiques. Les doubles hydroxydes lamellaires LDH à base de Al-Mg (Hydrotalcite) sont les produits les plus protecteurs observés dans nos expériences.

L'effet de ces produits de corrosion sur le courant d'oxygène est visible dans l'expérience électrochimique de polarisation. En effet, suite à la seconde polarisation cathodique des revêtements, le courant d'oxygène pour le revêtement AlSiZnMg est quatre fois moins intense que pour le revêtement AlSiZn. Des expériences utilisant la technique SVET ont été effectuées

pour obtenir des informations sur la distribution des zones anodiques et cathodiques et leur évolution dans le temps.

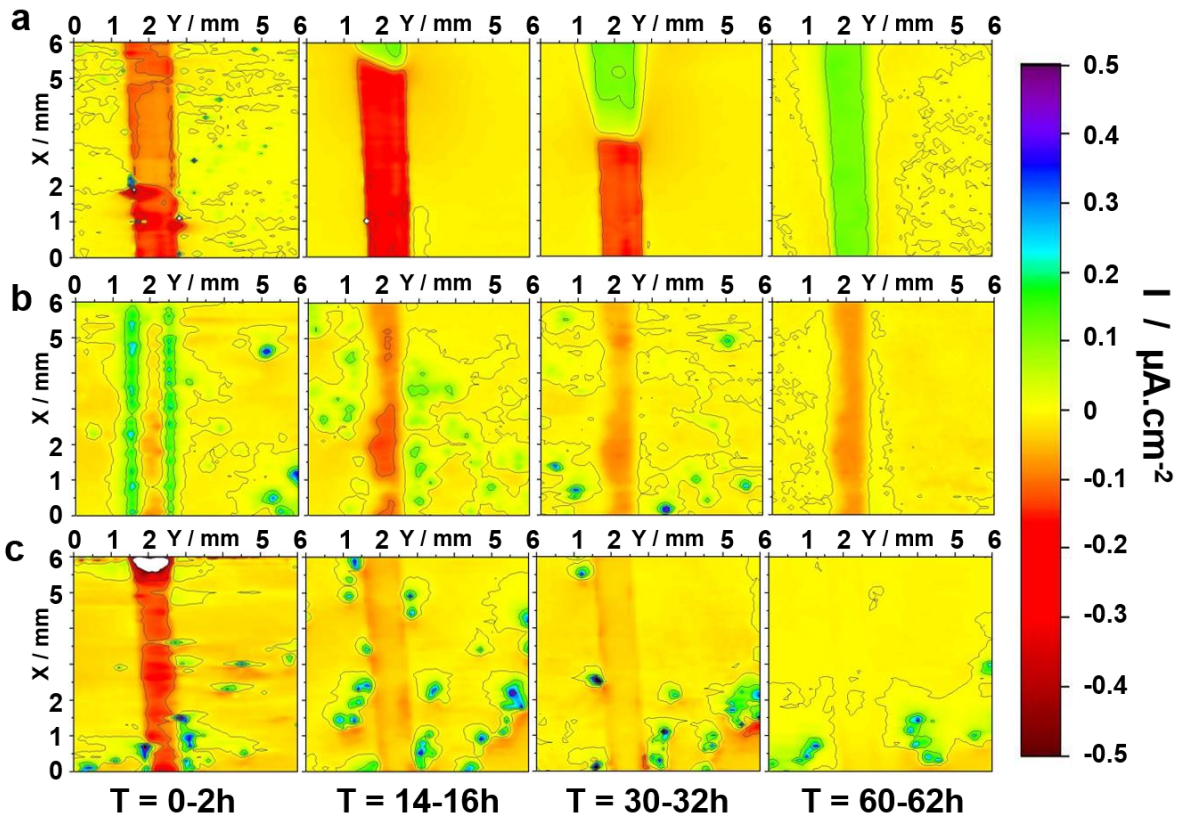


Figure 9 : Cartographie par électrode vibrante en continu d'aciers revêtus par (a) AlSi (b) AlSiZn et (c) AlSiZnMg (rayés) dans NaCl 100 mg.L^{-1}.

Les revêtements AlSiZn et AlSiZnMg présentent des réactivités différentes. Pour le revêtement AlSiZn, au stade initial de la corrosion, la surface et les rayures sont légèrement cathodiques (Fig. 9), l'activité anodique est maintenue par les bordures de la rayure. Quant au revêtement AlSiZnMg, toute la surface est légèrement anodique avec une activité locale plus élevée et la rayure est fortement cathodique. De plus, l'activité cathodique dans la rayure diminue et disparaît presque après 60 h d'expérience tandis que l'activité anodique diminue également. Ceci montre à la fois l'activation du Zn pour les deux revêtements et le retour de la protection barrière grâce à la formation de produits de corrosion avec Mg.

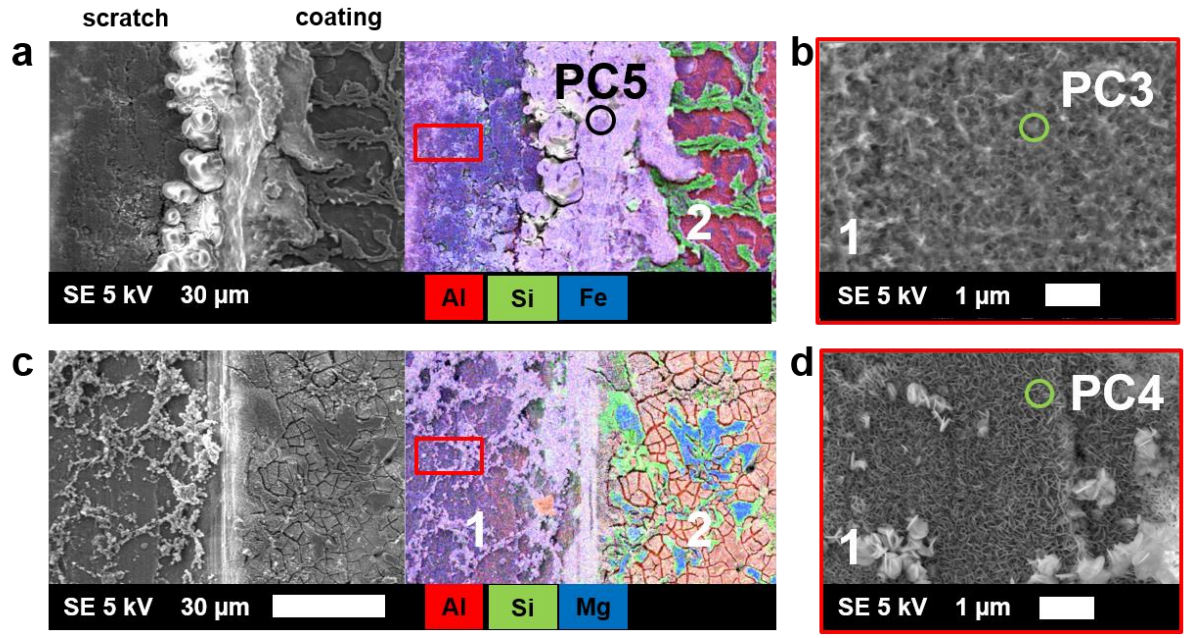


Figure 10 : Imagerie d'électrons secondaires et élémentaires EDS correspondant pour des aciers revêtus par (a) AlSiZn, (b) AlSiZnMg (rayés). 1: À l'intérieur de la rayure; 2: En dehors de la rayure.

Sur l'expérience SVET présentée sur la figure 9, l'activité cathodique dans la rayure pour AlSiZn augmente avec le temps alors qu'elle diminue pour AlSiZnMg, ce qui confirme l'efficacité des produits de corrosion formés sur les revêtements AlSiZnMg. Sur la figure 10, présentant les images en MEB des échantillons après SVET (Fig.9), on observe que l'hydrotalcite se forme sur les revêtements AlSiZnMg, alors que seul l'oxyde de fer est présent pour AlSiZn. On peut en conclure que les produits de corrosion AlSiZnMg se forment aussi dans des milieux moins concentrés.

6 Conclusions et perspectives

Ce travail démontre que le comportement en corrosion des revêtements AlSi peut être amélioré par la dépendance au Zn et au Mg et que les effets bénéfiques de ces deux éléments sont complémentaires. Il montre également que les mécanismes de corrosion des revêtements AlSi(ZnMg) peuvent être expliqués par une combinaison des comportements électrochimiques individuels des phases pures qui les composent et de l'impact des produits de corrosion sur la réactivité des revêtements. En prenant en compte les effets des produits de corrosion, il devient possible de corréler la composition des revêtements et la microstructure à leurs propriétés anticorrosion finales. Les revêtements AlSi, AlSi, AlSiZnMg ont leur propre mécanisme et comportement de corrosion.

Le revêtement AlSi présente un comportement de passivation typique avec une fine couche d'oxyde à la surface et une corrosion localisée semblable à des piqûres. Le revêtement AlSiZn montre une forte dissolution sélective autour des inclusions de silicium engendrée par l'activation de l'aluminium par le zinc contenu dans la solution solide de la matrice. Le comportement de corrosion de Al(Zn) peut s'expliquer par la somme des comportements de ses phases pures. Le potentiel de la solution solide Al(Zn) est inférieur (de 200 mV) à celui de l'aluminium pur dans un environnement chloré en raison de l'effet de zinc sur l'aluminium. Al(Zn) permet la protection cathodique de l'acier par couplage galvanique. Ce nouveau pouvoir sacrificiel entraîne de nouveaux couplages galvaniques avec les différentes phases présentes dans le revêtement. En effet, les aiguilles de silicium pur présentes dans les revêtements à base de AlSi et la couche intermétallique d'AlFeSi à l'interface revêtement/acier sont des phases fortement cathodiques qui vont provoquer une corrosion prématurée et sélective de la matrice autour d'elles. Malgré la prise en compte de toutes les phases, du comportement électrochimique des revêtements AlSiZn, les différences entre revêtements AlSiZn et AlSiZnMg restent inexplicables. Les nouvelles phases apportées par l'alliage de magnésium (Mg_2Si et Zn_2Mg) ont un potentiel de corrosion plus faible, pouvant créer un couplage galvanique encore plus important car Si pur et AlFeSi intermétallique sont toujours présents.

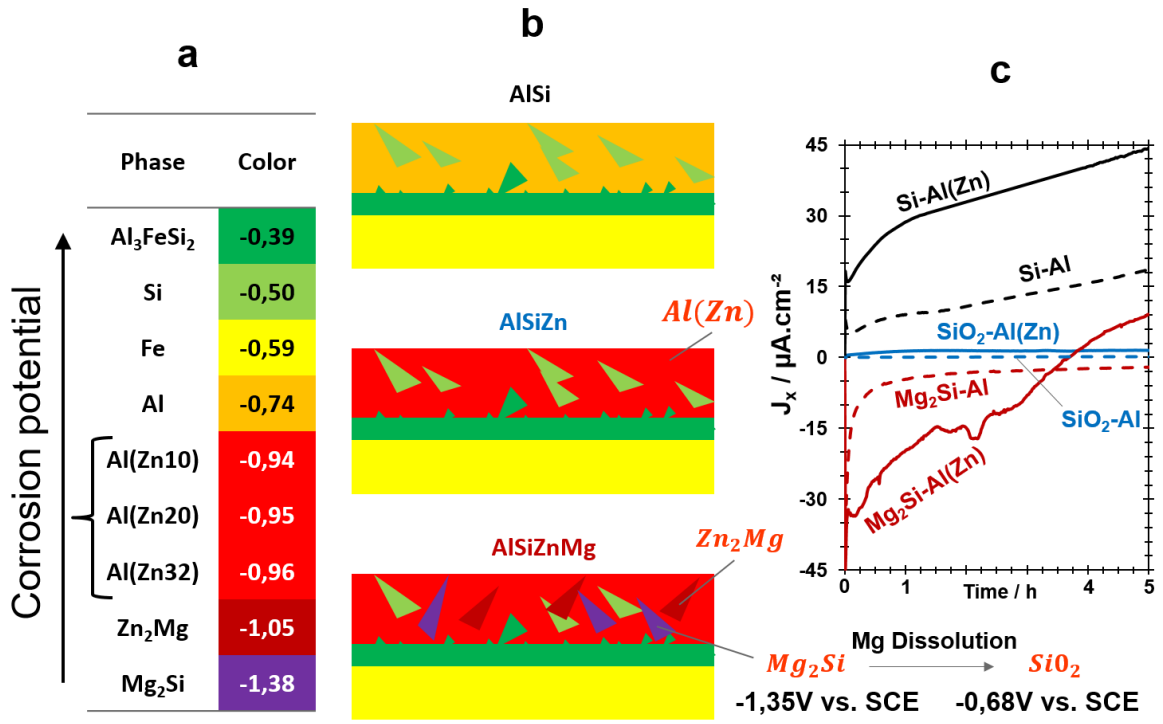


Figure 11 : (a) Phases triées par potentiel de corrosion dans une solution aqueuse de NaCl 1 % massique. De Si en vert clair (-0,170 V vs. SCE) à Mg_2Si en violet (-1,35 V vs. SCE). (b) Schéma des microstructures de AlSi, AlSiZn et AlSiZnMg avec échelle de couleur. (c) Courant de couplage galvanique entre Si et Al ou Al(Zn32) dans une solution de NaCl 1 % massique.

Grace aux multiples effets du magnésium, la résistance à la corrosion des revêtements AlSiZnMg est nettement plus performante que celle des revêtements AlSiZn. Mg_2Si présente dans la microstructure AlSiZnMg est sélectivement dissoute et forme du SiO_2. Ce SiO_2 a un potentiel de corrosion élevé mais ne provoque pas autant de corrosion micro-galvanique que les aiguilles en Si. Le magnésium libéré dans la solution a deux effets principaux. Il empêche le pH d'augmenter avec la précipitation de $Mg(OH)_2$ et il apporte les conditions ioniques favorables pour former des produits de corrosion protecteurs.

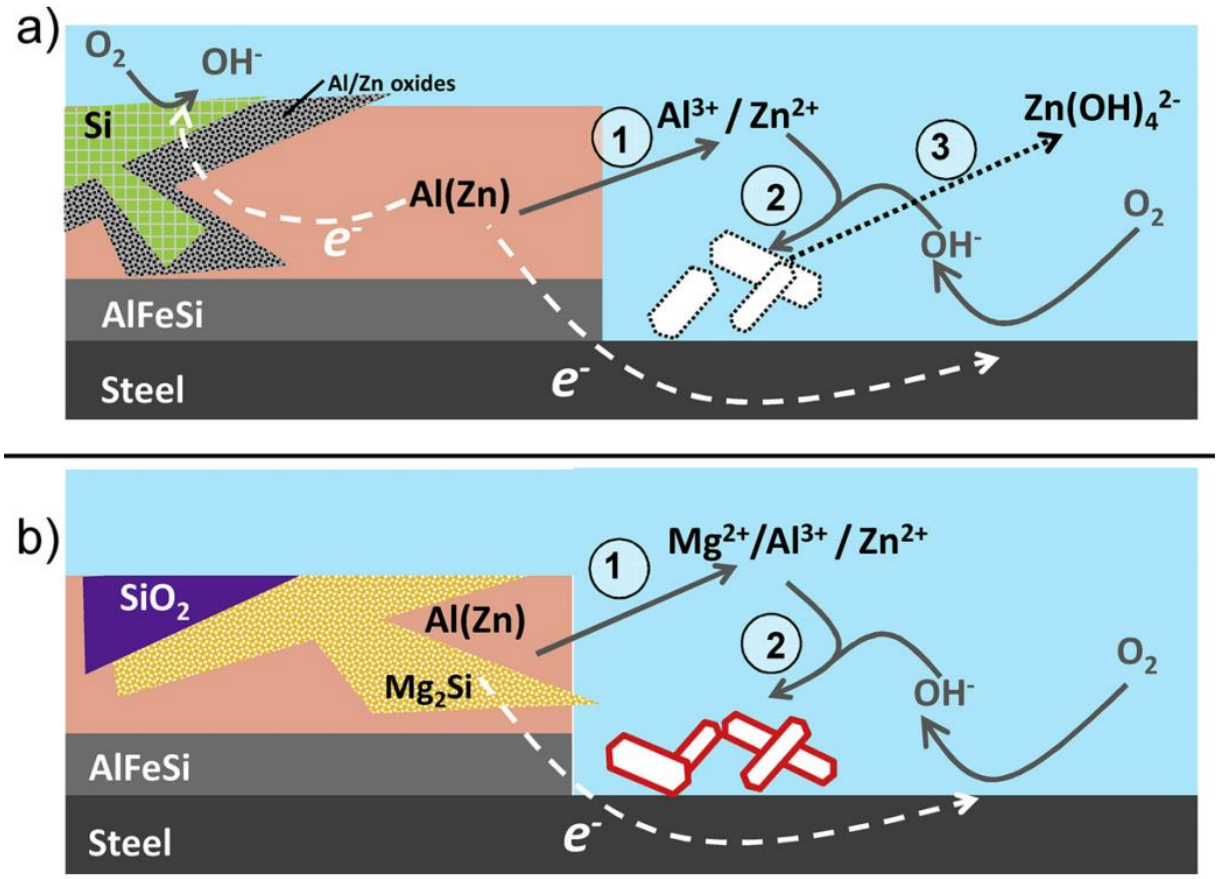


Figure 12 : Représentation schématique des mécanismes de corrosion et de protection proposés dans le cas d'aciers revêtus par (a) AlSiZn et (b) AlSiZnMg en présence du défaut allant jusqu'à l'acier.

Les produits de corrosion formés sur AlSiZn sont différents selon les conditions d'essai. Dans les environnements à base de chlorure, les revêtements AlSiZn formeront des oxydes de fer ou ZnO pour les tests de corrosion des revêtements rayés, simonkolleïte pour les essais de corrosion des revêtements non rayés, Al-Zn LDH pour les tests de corrosion des arêtes coupées. Pour AlSiZnMg, les produits de corrosion observés contiennent toujours de la LDH à base de Mg-Al.

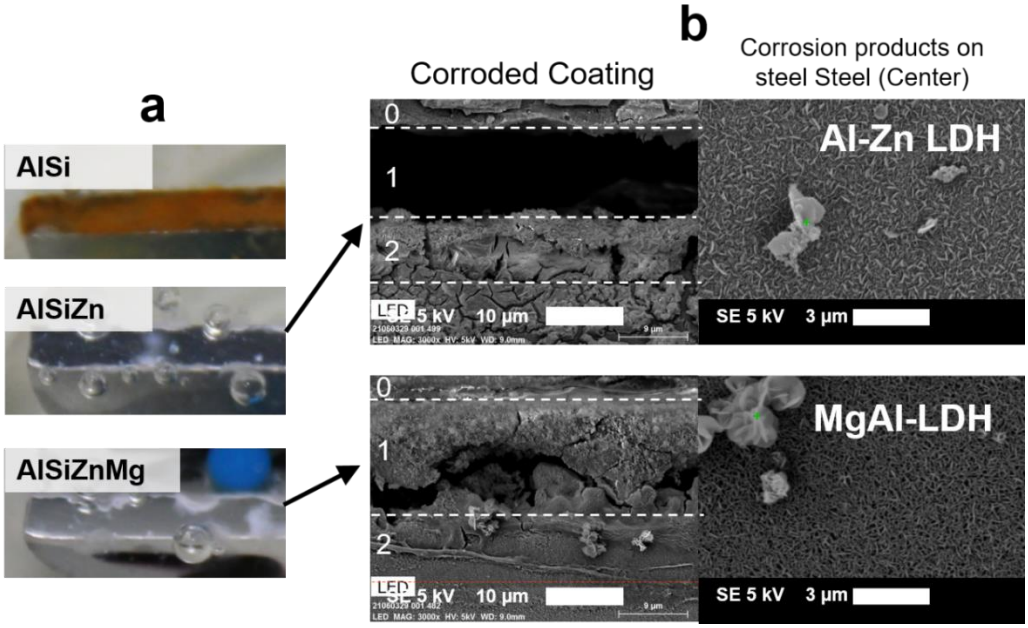


Figure 13 : (a) Aspect des arêtes de coupe typiques des revêtements AlSi, AlSiZn, AlSiZnMg après 48h d'immersion dans une solution aqueuse de NaCl 1 % en masse à pH initial 7. (b) Imagerie en électrons secondaires de bord coupés d'aciers revêtus par AlSiZn et AlSiZnMg après 48h d'immersion dans une solution aqueuse de NaCl 1 % en masse à pH initial 7. 0: résine; 1: Revêtement; 2: Intermétallique.

L'effet des produits de corrosion sur la réactivité des revêtements est différent entre les revêtements AlSiZn et AlSiZnMg. Le LDH à base de Al-Mg réduit considérablement le courant d'oxygène et ralentit les réactions de corrosion dans les zones cathodiques. Les phases Mg_2Si et Zn_2Mg très actives rendent les revêtements AlSiZnMg plus actifs que AlSiZn au stade de la corrosion initiale mais les produits de corrosion réduisent rapidement l'activité générale à un niveau acceptable alors que l'activité de AlSiZn reste trop élevée.

RÉSUMÉ

Les revêtements AlSi, aujourd'hui largement utilisés dans l'industrie automobile, offrent une bonne protection barrière mais aucune protection cathodique à l'acier. Pour améliorer leur pouvoir sacrificiel, l'ajout de Zn et de Mg a récemment été avancé. Cette thèse vise à comprendre les mécanismes de protection anticorrosion et à expliquer les différences significatives de résistance à la corrosion observées entre des aciers revêtus par des revêtements AlSi, AlSiZn ou AlSiZnMg. Pour corréler la composition et la microstructure au comportement en situation de corrosion, des essais électrochimiques et des tests de corrosion ont été effectués sur des revêtements modèles avec et sans rayures à l'acier. Afin de détecter une possible dissolution sélective et d'identifier les produits de corrosion, la composition des électrolytes a été analysée après tests et les surfaces et sections ont été caractérisées par diffraction des rayons-X, spectroscopie Raman et microscopie électronique. La passivation du revêtement AlSi entraînant l'absence de protection sacrificielle a été confirmée. L'action sacrificielle des revêtements AlSiZn a été expliquée par la formation d'une solution solide d'aluminium avec du zinc soluble, empêchant la passivation de celui-ci. Sur la base d'expériences électrochimiques avec les phases pures et leurs combinaisons dans des tests de couplages électrochimiques, il a été démontré que le couplage galvanique de AlZn avec des intermétalliques Si et AlSiFe cathodiques est responsable de la corrosion prématurée de la matrice Al(Zn). En utilisant l'électrochimie locale et la microscopie, nous avons compris que des courants cathodiques locaux élevés à l'intérieur du revêtement provoquaient une augmentation rapide du pH et une dissolution des produits de corrosion de Zn. L'effet de l'alliage de Mg sur la résistance à la corrosion s'est révélé multiple. Tout d'abord, le Si, présent dans AlSiZn sous forme d'aiguilles de silicium pur, est allié au magnésium dans les revêtements AlSiZnMg pour former un intermétallique Mg_2Si moins nocif pour la consommation de la matrice Al(Zn). Deuxièmement, grâce à la libération de Mg^{2+} pendant la corrosion, l'augmentation du pH est limitée aux environs de 10 empêchant la dissolution des produits de corrosion de Zn. En même temps, de nouveaux produits de corrosion (doubles hydroxydes lamellaires) ont été détectés en présence de Mg. L'électrochimie globale et locale a confirmé que les produits de corrosion contribuaient à la diminution de la vitesse de corrosion du revêtement et de l'acier nu dans les défauts artificiels.

MOTS CLÉS

Corrosion atmosphérique ; Revêtements métalliques pour l'acier ; AlSiZnMg; Produits de corrosion ; Mécanismes de corrosion ; Dissolution sélective

ABSTRACT

AlSi coatings, widely used in automotive industry, offer good barrier but no sacrificial protection to steel. To improve sacrificial protection, Zn and Mg alloying was recently proposed. This PhD aimed to understand mechanisms of anticorrosion protection of steel by these new AlSi(Zn,Mg) coatings and to explain the significant differences in corrosion resistance observed between AlSi, AlSiZn and AlSiZnMg coated steels. To correlate the composition, microstructure and corrosion behaviour, electrochemical and corrosion tests were made on model coatings with and without artificial scratches up to the steel and on pure phases detected in the coatings and their combinations. In order to detect selective dissolution and to identify the corrosion products, solution composition after the tests was analysed and surfaces and cross sections were characterized before and after the tests by X-ray diffraction, Raman spectroscopy and electron microscopy. The AlSi passivation resulting in the absence of sacrificial protection was confirmed. The sacrificial action of AlSiZn coatings was explained by formed Zn solid solution in Al matrix preventing Al passivation. On the basis of electrochemical experiments with pure phases and their electrochemically coupled combinations, it was demonstrated that galvanic coupling of AlZn with cathodic Si and AlSiFe intermetallic is responsible for the premature corrosion of the Al(Zn) matrix. Using local electrochemistry and time lapse microscopy, it was understood that high local cathodic currents inside the coating caused rapid pH increase and dissolution of Zn corrosion products. The effect of Mg alloying on corrosion resistance was shown to be multiple. First, Si, present in AlSiZn as Si needles, in AlSiZnMg was bounded into Mg_2Si intermetallic, less harmful for AlZn consumption by galvanic coupling. Secondly, thanks to Mg^{2+} release during corrosion, the pH increase was limited to the values around 10 preventing the dissolution of Zn corrosion products. At the same time, new corrosion products (layered double hydroxides) were detected in presence of Mg. Global and local electrochemistry confirmed that the corrosion products contributed in decrease of corrosion rate of both, the coating and the naked steel in artificial defects.

KEYWORDS

Atmospheric corrosion; Metallic coatings for steel; AlSiZnMg; Corrosion product; Corrosion mechanisms; Selective dissolution